AD_____

Award Number: DAMD17-03-2-0021

TITLE: Molecular Genetic and Gene Therapy Studies of the Musculoskeletal System

PRINCIPAL INVESTIGATOR: Subburaman Mohan, Ph.D.

CONTRACTING ORGANIZATION: Loma Linda Veterans Association for Research & Education
Loma Linda CA 92357-1000

REPORT DATE: February 2007

TYPE OF REPORT: Annual

PREPARED FOR: U.S. Army Medical Research and Materiel Command
Fort Detrick, Maryland 21702-5012

REPORT DOCUMENTATION PAGE

Form Approved
OMB No. 0704-0188

1. REPORT DATE *(DD-MM-YYYY)*	**2. REPORT TYPE**	**3. DATES COVERED** *(From - To)*
01-02-2007	Annual	09 Sep 05 - 31 Jan 07

4. TITLE AND SUBTITLE
Molecular Genetic and Gene Therapy Studies of the Musculoskeletal System

5a. CONTRACT NUMBER

5b. GRANT NUMBER
DAMD17-03-2-0021

5c. PROGRAM ELEMENT NUMBER

6. AUTHOR(S)
Subburaman Mohan, Ph.D.

E-Mail: subburaman.mohan@va.gov

5d. PROJECT NUMBER

5e. TASK NUMBER

5f. WORK UNIT NUMBER

7. PERFORMING ORGANIZATION NAME(S) AND ADDRESS(ES)

Loma Linda Veterans Association for Research & Education
Loma Linda CA 92357-1000

8. PERFORMING ORGANIZATION REPORT NUMBER

9. SPONSORING / MONITORING AGENCY NAME(S) AND ADDRESS(ES)
U.S. Army Medical Research and Materiel Command
Fort Detrick, Maryland 21702-5012

10. SPONSOR/MONITOR'S ACRONYM(S)

11. SPONSOR/MONITOR'S REPORT NUMBER(S)

12. DISTRIBUTION / AVAILABILITY STATEMENT
Approved for Public Release; Distribution Unlimited

13. SUPPLEMENTARY NOTES

14. ABSTRACT
The proposed research projects focuses on bone health, including relevance to the musculoskeletal system in battlefield performance and in battlefield injury. We have utilized state-of-the-art molecular genetic and gene therapy technologies to address fundamental questions in bone biology with particularly emphasis on attempting to clarify gene function for those genes that are involved in digit tip regeneration, bone size, skeletal repair and anabolic response to mechanical loading. The molecular genetic approaches have utilized various knockout mouse models and whole genome microarray analysis for evaluation of gene functions. The gene therapy approaches have utilized various viral and non-viral vectors to transfer gene of interest to treat localized and systemic skeletal deficits. We have successfully accomplished nearly all of the objectives proposed for the past year. The four core facilities funded by this project have contributed enormously to the success of our research activities. Our research activities during the past year have lead to 5 publications and 2 abstracts. We believe that our successful completion of proposed studies will provide a foundation of knowledge 1) that will allow the identification of genes that are involved in regulating skeletal repair, regeneration, and/or as well anabolic response to mechanical stress and 2) that will provide proof of principles in animal models for successful gene therapy applications to accelerate endosteal bone formation and healing of skeletal injuries.

15. SUBJECT TERMS
Mechanical strain, quantitative trait loci analysis, microarray analysis, osteoblasts, signaling pathways, bone formation

16. SECURITY CLASSIFICATION OF:			**17. LIMITATION OF ABSTRACT**	**18. NUMBER OF PAGES**	**19a. NAME OF RESPONSIBLE PERSON**
a. REPORT	**b. ABSTRACT**	**c. THIS PAGE**			USAMRMC
U	U	U	UU	223	**19b. TELEPHONE NUMBER** *(include area code)*

Table of Contents

Page

PROJECT 1

PRINCIPAL INVESTIGATOR: David J. Baylink, M.D.

TITLE: Studies on Genetic Regulation of Digit Tip Regeneration

I. GENERAL INTRODUCTION

This proposal is divided into three sections: A) Molecular Genetic Projects, of which there are four projects. B) Gene Therapy Projects, of which there are three projects; and C) Support Service Facilities, of which there are four projects. Each of the above projects has an introduction .

Our goals for the first 12-months of this funding period for each of the technical objectives, as well as our progress for each of the technical objectives, are described below. The progress report for each project is organized according to the outline provided by the office of the U.S. Army Medical Research and Material Command.

A. MOLECULAR GENETICS PROJECTS

PROJECT 1 PRINCIPAL INVESTIGATOR: David J. Baylink, M.D.

TITLE: Studies on Genetic Regulation of Digit Tip Regeneration

Introduction

Our long-term goal in this study is to identify the genes involved in bone and soft tissue regeneration and to evaluate the functions of those genes. Such genes are particularly relevant to identifying one's risk for and prevention of stress fractures, as well as the risk of fractures from battlefield injuries and to corresponding gene therapy treatment for such fractures.

Recently, we and others have demonstrated that the MRL mouse, as opposed to several other inbred strains of mice, show regeneration of ear hole punches. This is a genetically controlled phenomenon and in our study we found 10 different QTL gene loci responsible for the difference in healing between the SJL and MRL mouse. More recently, it has been shown that the MRL mouse is capable of cardiac muscle regeneration. Based on these observations, we have proposed earlier to study digit tip regeneration in a series of inbred strains of mice in an attempt to identify good and poor digit tip regenerators in order to eventually identify the genes responsible for good and poor bone regeneration. In this regard, we found that amputated digit tip healed significantly faster in MRL mice compared to DBA and C57BL/65 inbred strains of mice.

Whole genome microarray studies using healing digit tip from fast healer MRL/MpJ (MRL) and poor healer C57BL/6J (B6) have revealed that a number of genes were differentially expressed between fast healer and poor healer strains. We have selected two genes, namely formin2 and EphA4, for our further studies based on the following rationale. We selected formin2 because formin1, another member of forming gene family, is involved in skeletal development. We selected EphA4 because recent studies have shown that this gene plays an important role in nerve regeneration. Nothing is known about the role of either formin2 or EphA4 in bone. We have therefore proposed studies to evaluate the role of formin2 and EphA4 in bone.

Body

1. Technical Objectives

Our specific objectives during the first 12 months of this continuation grant period are as follows:

1) To continue to characterize mice lacking formin2 and EphA4 in digit tip regeneration. To this end, we will continue to breed heterozygous EphA4 knockout mice obtained from Jackson Laboratories to generate homozygous knockout and corresponding control mice. New born pubs will be used for digit tip regeneration studies. Regeneration rates will be determined by Faxitron X-ray, microCT and histology.

2) To evaluate the skeletal phenotype of formin2 knockout and EphA4 knockout mice. We will evaluate areal bone density in knockout and control mice by PIXImus at week 3, 6, 9 and 12 weeks of age. We will measure bone size and volumetric bone density at 12 weeks of age after sacrifice.
3) To evaluate the biological role of formin2 and EphA4 in regulating osteoblasts, we will initiate studies to overexpress sense or antisense constructs (or siRNAs) using appropriate vectors and determine the effects on proliferation, differentiation and apoptosis in mouse osteoblasts.
4) To identify signaling pathways by which formin2 and EphA4 regulate osteoblasts, we will generate knockout and control mice and extract RNA from bones for whole genome microarray studies.

Our specific objectives during the final 3 months of this project as follows:

1) To analyze phenotype data from formin2 and EphA4 knockout mice and write up the results for publication.
2) To continue the studies on overexpression of sense or antisense constructs (or siRNAs) using appropriate vectors and determine the effects on proliferation, differentiation and apoptosis in mouse osteoblasts.

2. Progress on Technical Objectives

Technical Objective 1: To continue to characterize mice lacking formin2 and EphA4 in digit tip regeneration. To this end, we will continue to breed heterozygous EphA4 knockout mice obtained from Jackson Laboratories to generate homozygous knockout and corresponding control mice. New born pubs will be used for digit tip regeneration studies. Regeneration rates will be determined by Faxitron X-ray, microCT and histology.

EphA4 Mutant Mice. Knockout mice of EphA4 are not commercially available. However, a strain of mice with a spontaneous mutation of EphA4 is available from Jackson Laboratories. Two heterozygous breeding pairs of mice with a spontaneous mutation of EphA4 were obtained from Jackson Laboratories. The EphA4 mutant mice bred but homozygous mutant offspring were found to be not very viable. Thus, not enough mice could be obtained for regeneration studies and these studies were undertaken with FMN2 knockout mice.

FMN2 Knockout Mice. FMN2 knockout mice were obtained from Dr. Philip Leder (Department of Human Genetics, Harvard Medical School, Howard Hughes Medical Institute, Boston, MA). The mice were originally generated in inbred 129Sv mice by homologous recombination of a targeting vector with 1300 bp of the FH1 domain of FMN2 deleted and replaced by 1257 bp containing the PGK-Neo gene followed by stop codons in all three reading

frames (10). Two heterozygote FMN2 (+/-) male/female pairs were bred to generate wildtype (+/+), and knockout (-/-) pups for subsequent regeneration, bone density, bone size and bone volume studies.

FMN2 Regeneration Studies. Surgery was conducted on the pup's digit tips within 1-day of birth. The neonatal mice were anesthetized with 5% Halothane mixed with O2 5L/min. The right front 3rd and 4th digit tips were amputated, with the left side as uncut controls. Since the level of amputation is very important to subsequent regrowth capabilities, all surgery was performed under a microscope and a scalpel was used to dissect the digit tips as accurately as possible at the mid-point of the third phalanges. The accuracy of digit tip surgery and amounts of tissue dissected were documented and measured by capturing images of the digits both before and after surgery. Both left (uncut) and right (cut) paw X-ray images were taken at 0, 7, 14, 21, and 28 days post surgery with a Faxitron MX-20 X-ray. In order to insure that regrowth results were not influenced by differences in mouse size, the data was normalized by dividing right cut growth measurements by left uncut growth measurements. Figure 1 shows the results of the regeneration studies. Knockout FMN2 mice appear to have slightly appeared regeneration. However, these regrowth percentages did not reach statistical significance. This is likely due to measurement variations implicit in manual measurement methods.

Figure 1. Percent Digit Tip Regrowth in FMN2 Knockout and Wildtype Mice. FMN2 knockout mice display slightly less regeneration than wildtype mice. The difference did not reach statistical significance however.

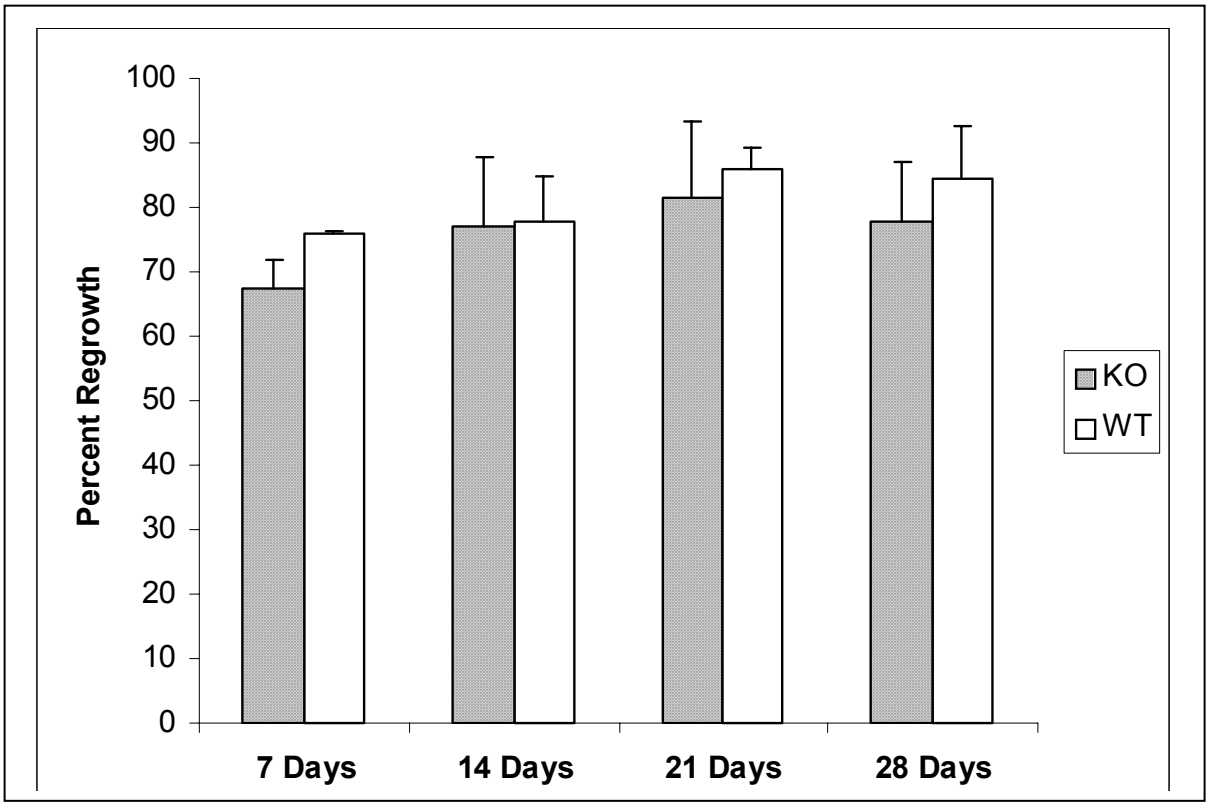

Technical Objective 2: To evaluate the skeletal phenotype of formin2 knockout and EphA4 knockout mice. We will evaluate areal bone density in knockout and control mice by PIXImus at week 3, 6, 9 and 12 weeks of age. We will measure bone size and volumetric bone density at 12 weeks of age after sacrifice.

Bone Measurements

Volumetric bone mineral density (vBMD) and geometric parameters of femurs were determined by peripheral quantitative computed tomography (pQCT) (Norland Medical Sytems). The resolution limit of this instrument is approximately 70 microns. Calibration of pQCT was performed daily with a defined cone phantom standard. Analysis of the pQCT scans was performed using Bone Density Software version 5.40 (Norland Medical Systems). Total bone mineral density (total BMD) and geometric parameters were estimated with Loop analysis. The threshold was set at 230-630 mg/cm^3. Femur bone parameters were measured and averaged for three scans at mid-diaphysis. The longitudinal lengths of femurs were measured with a caliper. Statistical analyses of bone parameters were done using Statistica software (Statsoft Inc).

FMN2 Knockout Mouse Phenotypes

Knockout (-/-) and wildtype (+/+) FMN2 mice were measured for bone size and volumetric BMD at 12 weeks by peripheral quantitative computed tomography (pQCT) The studies of knockout FMN2 mice find that they have decreased femur cortical thickness and total bone density and increased endosteal circumference of femurs in comparison to wildtype FMN2 mice.

Table 1. Bone Phenotypes Measured by pQCT. Shown are mean total weight and bone size and density measurements for FMN2 knockout and wildtype mice. FMN2 knockout mice exhibit significantly reduced femur cortical thickness due to an increase in femur endosteal circumference.

Unadjusted Phenotypes	**FMN2 (+/+) (n = 9)**	**FMN2 (-/-) (n = 7)**
Body weight (g)	24.1 +/- 1.7	21.1 +/- 1.4
Length (mm)	14.2 +/- 0.93	14.5 +/- 0.90
vBMD (mg/cm3)	884.5 +/- 44.3	850.0 +/- 27.8
Periosteal Circumference (mm)	4.28 +/- 0.23	4.04 +/- 0.29
Endosteal Circumference (mm)	2.29 +/- 0.35	2.44 +/- 0.16
Cortical Thickness (mm)	0.32 +/- 0.06	0.25 +/- 0.02

FMN2 knockout mice were found to have significantly decreased cortical thickness caused by apparent changes in periosteal and endosteal circumference compared to control mice. This contributes to a 6% reduction in vBMD in FMN2 knockout femurs ($p = 0.04$). The mechanisms that cause these femur phenotypes could be either increased bone resorption (osteoclast cells) and/or decreased bone formation (osteoblast cells).

EphA4 Mutant Mice. Areal bone density and weight in EphA4 mutant and control mice was measured by PIXImus at week 3, 6, 9 and 12 weeks of age. EphA4 knockout mice were found to be significantly smaller in size at all time points. This size phenotype also led to significantly reduced BMD. Figure 1 shows these results. At 12 weeks of age bone measurements were also undertaken by pQCT. Table 2. shows these results. In summary, EphA4 mutatn mice are significantly smaller in size and have reduced total BMD. However, the pQCT measurements find no significant differences in any bone phenotype between mutant and wildtype EphA4 mice.

Figure 1A. Body weight of EphA4 mutant and wildtype mice. EphA4 knockout mice are significantly smaller at all time points in comparison to wildtype mice.

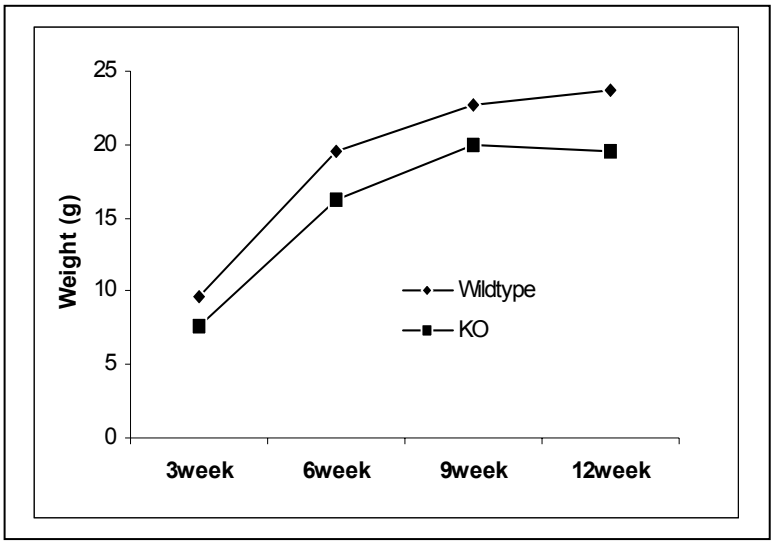

Figure 1B. Bone mineral density (BMD) of EphA4 mutant and wildtype mice. EphA4 knockout mice have reduced BMD in comparison to wildtype mice at all time points measured.

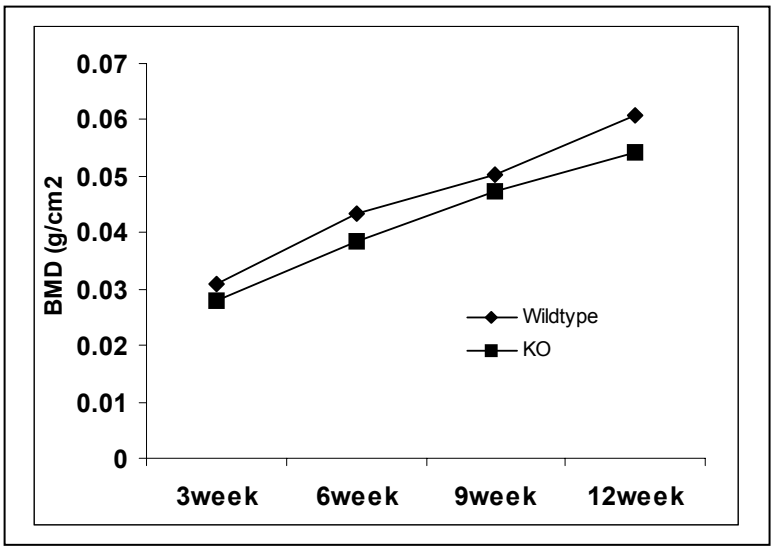

Table 2. EphA4 Bone Phenotypes Measured by pQCT. Shown are all bone phenotypes measured by pQCT for EphA4 mutant and wildtype mice. No significant differences were found in any of the bone measurements.

	TOT_CNT	TOT_DEN	TOT_ATT	CRTSUB_CNT	CRTSUB_DEN	CRTSUB_ATT
EphA4 Wildtype (N=16)	1.289	812.521	1.223	1.276	1003.556	1.453
EphA4 Knockout (N=12)	1.192	815.553	1.226	1.170	998.961	1.448
T-Test	0.274	0.941	0.941	0.221	0.832	0.832

	TRAB_CNT	TRAB_DEN	TRAB_ATT	TOT_A	TRAB_A
EphA4 Wildtype (N=16)	0.019	64.790	0.300	1.579	0.314
EphA4 Knockout (N=12)	0.026	98.431	0.348	1.459	0.294
T-Test	0.283	0.138	0.163	0.065	0.576

These data suggest that the phenotype of reduced BMD of EphA4 mutant mice is almost entirely due to reduced body size. This suggests that EphA4 influences overall growth and is not influencing primarily bone biology. In contrast, FMN2 mutant mice display significantly decreased femur cortical thickness caused by apparent changes in periosteal and endosteal circumference. Thus, primary bone osteoblast cells in the in vitro studies focused on the FMN2 knockout and control mice.

Technical Objective 3: To evaluate the biological role of formin2 and EphA4 in regulating osteoblasts, we will initiate studies to overexpress sense or antisense constructs (or siRNAs) using appropriate vectors and determine the effects on proliferation, differentiation and apoptosis in mouse osteoblasts.

Real Time PCR Expression of FMN2

To determine the cell types that contribute to the observed skeletal phenotype in the FMN2 knockout mice, we measured expression levels of FMN2 by real time RT-PCR using RNA from MC3T3-E1 (osteoblast-like) and RAW264.7 (osteoclast-like) cell lines. We found that MC3T3-E1 but not RAW264.7 cells express FMN2 transcript. This suggests that FMN2 likely functions through osteoblast cells in bone formation. Additional studies were undertaken to confirm that FMN2 acts in bone formation by treating MC3T3-E1 cells with Wnt3a, a bone formation stimulation protein. RNA was extracted from the Wnt3A treated cells and reverse transcribed with oligo (dT) primers and Superscript II reverse transcriptase (Invitrogen) to produce cDNA. Real-time PCR was done using the SYBR Green PCR Core Reagents Kit (Applied Biosystems). The gene expression levels FMN2 were normalized to housekeeping gene TBP5 using the comparative Ct method. These studies found that treated of MC3T3 osteoblast-like cells with Wnt3A significantly increased the expression of FMN2 by 2.7 fold.

Table 3. Treatment of MC3T3 osteoblast-like cells with Wnt3A, a bone formation stimulator, increased the expression of FMN2 by 2.7 fold ($P<0.01$).

RNA Sample	Ct FMN2	Ct TBP5	Delta Ct	Delta Ct to Untreated Control	Relative Amount of RNA to Untreated Control
MC3T3-E1	36.37 +/- 0.55	26.47 +/- 1.01	9.9	0	1
MC3T3-E1 + Wnt3A	33.42 +/- 0.44	24.95 +/- 0.22	8.47	-1.43	2.69
RAW264.7	40 (No amplification)	27.32 +/- 0.63	NA	NA	NA

These studies indicate that FMN2 is expressed by cells of osteoblast lineage but not by cells of osteoclast lineage. This suggests that FMN2 acts primarily through bone formation and not bone remodeling. Also, the RNA Expression studies suggest that FMN2 may be involved in the WNT signaling pathway. In order to clarify the mechanisms through which FMN2 functions we undertook primary cell culture studies of FMN2 wildtype and knockout osteoblast cells.

Alkaline Phosphatase (ALP) Differentiation Assays

Osteoblasts mature from progenitor cells that reside in the bone marrow. During osteoblast differentiation from progenitor cells, alkaline phosphatase (ALP) upregulation occurs. Thus a marker for the differentiation activity of osteoblast cells is the upregulation of ALP. Calvarial cells are primary comprised of osteoblast cells and calvarial cells undergo natural differentiation when cultured. Thus for in vitro studies FMN2 knockout and wildtype primary cells, osteoblasts were isolated from calvaria of 4-week old knockout and wildtype mice.

FMN2 knockout and wildtype calvaria cells were harvested from 28-day-old fetal mice and were digested in a solution containing 0.1% collagenase and 0.05% trypsin at 37°C. After 10-minute digestion, the solution was discarded, and a new enzyme solution was added to the sediment and re-digested for 10-20 min. Isolated cells were maintained in a-MEM containing 10% calf serum and antibiotics at 37°C in a humidified atmosphere consisting of 5% CO2 in air. The medium was then changed into a-MEM with 2% FCS. 48 h after incubation, cells were washed with phosphate-buffered saline twice, and cell lysates were extracted with 0.05% Triton X-100. ALP activity in cell lysates was measured at 0, 1, 2, 3, 4, and 5 hours. FMN2 knockout osteoblast cells were found to have reduced ALP activity at all time points except time 0. Figure 2 shows that ALP activity was reduced at these time points for osteoblasts derived from FMN2 knockout mice in comparison to wildtype control mice.

Figure 2. ALP Activity in FMN2 wildtype and knockout osteoblast cells. Knockout FMN2 osteoblasts show significantly reduced ALP activity at 1, 2, 3, 4 and 5 hours ($P<0.01$). This indicates that differentiation of FMN2 knockout osteoblasts is reduced in comparison to wildtype FMN2 osteoblasts.

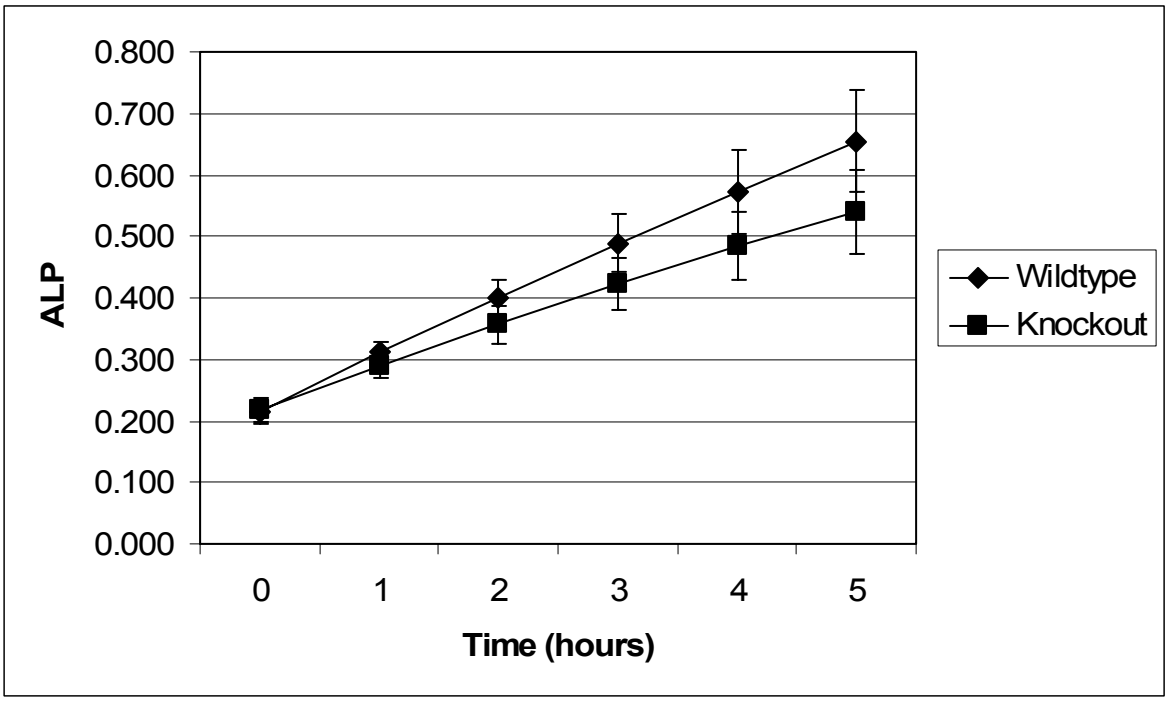

Cellular Proliferation BrdU Assays

Evaluation of cell cycle progression through measuring cellular proliferation is useful for determining the mechanisms through which mutated genes act. A well-established method to measure proliferation is the use of bromodeoxyuridine (BrdU), a thymidine nucleotide analog. BrdU is incorporated into newly synthesized DNA strands of actively proliferating cells. Following denaturation of double stranded DNA, BrdU is detected immunochemically allowing the assessment of the population of cells which are actively synthesizing DNA. Thus to measure FMN2 wildtype and knockout osteoblast proliferation we undertook colorimetric proliferation enzyme-linked immunosorbent assays (ELISA) for the detection of bromodeoxyuridine incorporation into newly synthesized DNA of cells. BrdU (Exalpha Biologicals, Inc.) was incorporated into DNA in calvarial osteoblast cell cultures for 1 hour. Washed and fixed in paraformaldehyde, the cultures were incubated with mouse anti BrdU monoclonal antibody which was detected by a secondary antibody and then conjugated with peroxidase marking the cells actively synthesizing DNA. The amount of BrdU was quantified with a microplate spectrophotometer at a wavelength of 450 nm with reference at a wavelength of 570 nm. Monolayer cultures without BrdU incorporation were used as a negative control. Figure 3 shows that cellular prolifereation was also reduced in osteoblasts derived from FMN2 knockout mice in comparison to wildtype control mice.

Figure 3. Cellular Proliferation in FMN2 wildtype and knockout osteoblast cells. Knockout FMN2 osteoblasts show significantly reduced proliferation in comparison to wildtype FMN2 osteoblasts ($P<0.01$).

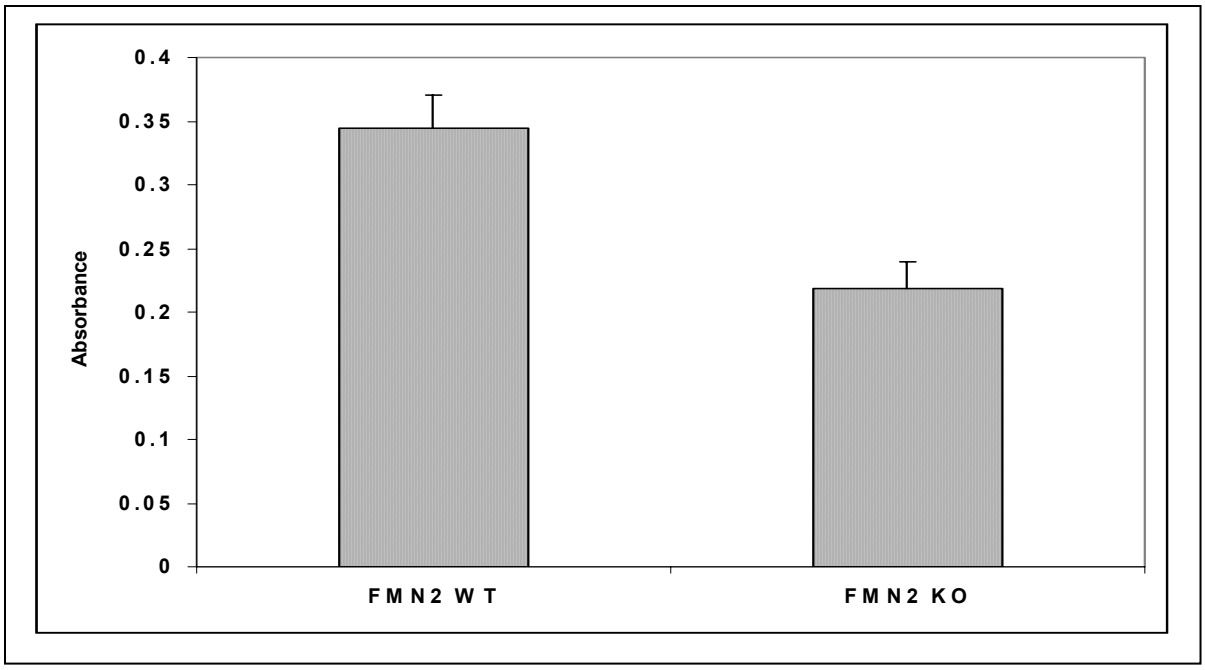

Mineralized Bone Nodule Formation Assay

In vitro studies of primary cell cultures of calvarial cells were undertaken to examine bone formation capabilities of FMN2 knockout and wildtype osteoblast cells. FMN2 knockout and wildtype calvarial cells were plated at a density of 7 × 106 cells/90-mm per plastic tissue culture dish in α-MEM containing 10% calf serum, 100 U/ml penicillin, and 100 μg/ml streptomycin. Culture media were changed every 2 days for 6 days and then switched to mineralization media by adding 50 μg/ml ascorbic acid and 10 mM β-glycerophosphate. Ater 30 days, cells were washed with PBS, followed by fixation in ice cold 70% ethanol for at least 1 h. Ethanol was removed, and cells were rinsed with water and stained with 40 mM alizarin red (pH 4.2) for 10 minutes at room temperature. Stained cells were further processed by five rinses with water, followed by a 15-minute wash in PBS with rotation to reduce nonspecific alizarin red stain. The area and the number of bone nodules stained were measured with the use of computerized image analyzer software and the percent area of the plates covered with bone nodules calculated. The results show that knockout FMN2 osteoblasts show significantly reduced bone nodule formation in comparison to wildtype FMN2 osteoblasts.

Figure 4. Bone nodule formation in FMN2 wildtype and knockout osteoblast cells. Knockout FMN2 osteoblasts show significantly reduced bone nodule formation in comparison to wildtype FMN2 osteoblasts (P<0.03).

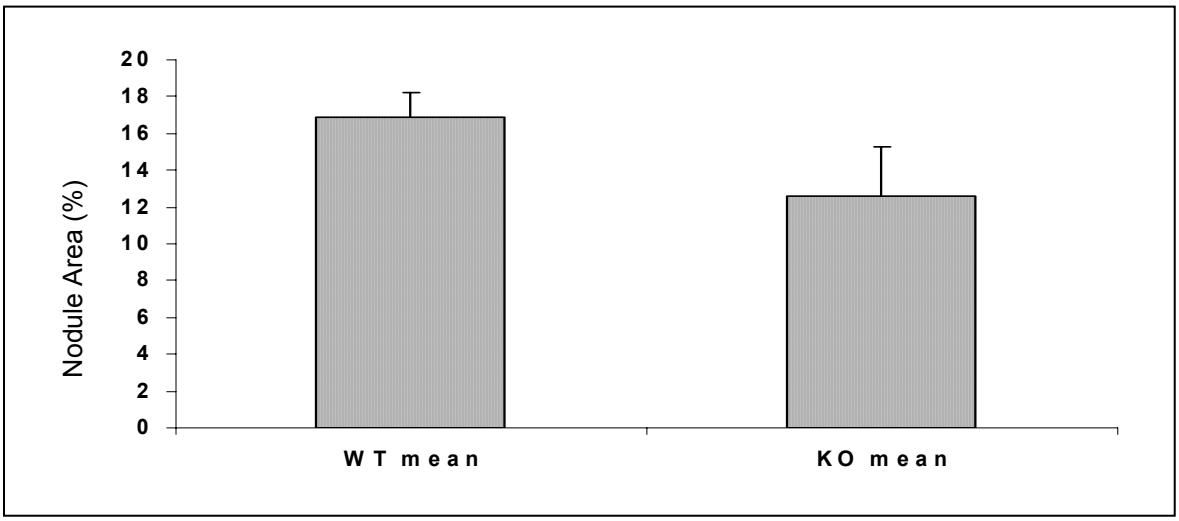

Technical Objective 4: To identify signaling pathways by which formin2 and EphA4 regulate osteoblasts, we will generate knockout and control mice and extract RNA from bones for whole genome microarray studies.

FMN2 Knockout and Wildtype Microarray Expression Analysis. Whole genome microarray analysis examines the expression analysis of all known genes in a single experiment. By comparing the expression levels of all genes in wildtype and mutant cells can give clues to a genes function and pathway. Thus, we undertook whole genome microarray expression analysis of FMN2 knockout and wildtype cells in order to determine the molecular functions and pathways of the FMN2 gene. Total RNA was isolated from mouse calvarial osteoblast cells and bones using Trizol followed by RNAEasy column purification (Qiagen). Custom oligonucleotide slides were spotted with ~38,000 70mer oligonucleotides that represent the mouse geneome (MEEBO set) obtained from Illumina. A Q-Array2 robot (Genetix) was used for spotting. A total of 250 ng RNA was used to synthesize double stranded cDNA using the Low RNA Input Fluorescent Linear Application Kit (Agilent). The slides were scanned using an 4200A Genepix scanner (Axon). Expression analysis of microarray experiments was performed with GeneSpring software (Agilent) using the raw intensity data generated by ImaGene software. Local background-subtracted total signal intensities were used as intensity measures, and the data was normalized using per spot and per chip LOWESS normalization. Genes that were significantly differentially expressed between wildtype and knockout FMN2 osteoblast cells were determined by utilizing a one-sample Student's t-test to test whether the mean normalized expression level for the gene is statistically different from 1.0. To characterize and classify the function of genes significantly differentially expressed in FMN2 knockout and wildtype osteoblast cells, genes were then classified according to their biological process Gene-Ontology (GO) category. Table 3 lists genes significantly downregulated in FMN2 knockout osteoblast cells and Table 4 lists genes significantly upregulated in FMN2 knockout osteoblast cells.

Table 3. Genes significantly ($p < 0.05$) downregulated in FMN2 knockout primary osteoblast cells in comparison to wildtype primary osteoblast cells.

Gene Name	Normalized ratio	P-value	Description	Gene Ontology Biological Process
Postn	0.41	0.009	Periostin, osteoblast specific factor	cell adhesion
Igfbp5	0.46	0.002	Insulin-like growth factor binding protein 5	regulation of cell growth
Lrrc15	0.47	0.001	Leucine rich repeat containing 15	
Crabp1	0.50	0.003	Retinoic acid binding protein I	transport
Ccl8	0.60	0.009	Chemokine (C-C motif) ligand 8	chemotaxis; signal transduction
Fbn1	0.61	0.004	Fibrillin 1	
Egfl6	0.62	0.009	EGF-like-domain, multiple 6	
D15Ertd781e	0.62	0.022	TBC1 domain family, member 22a	
H2-T22	0.63	0.026	Histocompatibility 2, T region locus 22	MHC class I; defense response
Kif2c	0.63	0.030	Kinesin family member 2C	microtubule-based movement
Lpl	0.64	0.000	Lipoprotein lipase	lipid catabolism; lipid metabolism
Pdzrn3	0.66	0.028	PDZ domain containing RING finger 3	intracellular signaling cascade
Plac8	0.66	0.029	Placenta-specific 8	biological_process unknown
Gsta3	0.66	0.015	Glutathione S-transferase, alpha 3	
Csrp2	0.67	0.001	Cysteine and glycine-rich protein 2	cell differentiation; development
D330027H18Rik	0.67	0.005	RIKEN cDNA D330027H18 gene	
Epc2	0.67	0.019	Enhancer of polycomb homolog 2	
9530025L08Rik	0.69	0.037		
1300017K07Rik	0.69	0.040	Threonine aldolase 1	
Nvl	0.70	0.013	Nuclear VCP-like	
Dhrs6	0.70	0.036	Dehydrogenase/reductase member 6	biological_process unknown
5730523P12Rik	0.71	0.002		
Evc2	0.71	0.022	Ellis van Creveld syndrome 2 homolog	
BC043944	0.71	0.035	CDNA sequence BC043944	
Slc27a3	0.72	0.013	Solute carrier family 27	fatty acid metabolism; lipid metabolism; lipid transport
A430060F13Rik	0.72	0.045	RIKEN cDNA A430060F13 gene	
H2-T10	0.72	0.039	Histocompatibility 2, T region locus 10	MHC class I; defense response
1810054O13Rik	0.73	0.026	Transmembrane protein 86A	
6720460K10Rik	0.73	0.025		
Suox	0.73	0.001	Sulfite oxidase	electron transport
Sp7	0.73	0.008	Trans-acting transcription factor 7	osteoblast differentiation; regulation of transcription from Pol II promoter
5730596B20Rik	0.73	0.022	RIKEN cDNA 5730596B20 gene	

Snapap	0.74	0.015	Synaptosomal-associated protein 25 binding protein	exocytosis; synaptic vesicle exocytosis
Bach2	0.74	0.030	BTB and CNC homology 2	regulation of transcription, DNA-dependent
Il17f	0.74	0.048	Interleukin 17F	
BC023892	0.74	0.028	cDNA sequence BC023892	
4930546E12Rik	0.74	0.039		
Phgdhl1	0.74	0.031		
IGHV1S1	0.74	0.050	Ig H-chain V-region 186-1	
BC034664	0.75	0.023	CDNA sequence BC034664	electron transport
Thbs2	0.75	0.008	Thrombospondin 2	cell adhesion
Scd2	0.75	0.008	Stearoyl-Coenzyme A desaturase 2	fatty acid biosynthesis; lipid biosynthesis
Trim59	0.75	0.012	Tripartite motif-containing 59	regulation of transcription, DNA-dependent
Hoxd8	0.75	0.003	Homeo box D8	development; organogenesis; pattern specification; regulation of transcription, DNA-dependent
1810020D17Rik	0.75	0.008	RIKEN cDNA 1810020D17 gene	
Mrgprb4	0.75	0.009	MAS-related GPR, member B4	G-protein coupled receptor protein signaling pathway
AI173486	0.75	0.033	RIKEN cDNA 1500015A07 gene	
1110013I04Rik	0.75	0.040		
A430057M04Rik	0.75	0.019	RIKEN cDNA A430057M04 gene	
Fgf3	0.75	0.025	Fibroblast growth factor 3	cell proliferation; induction of an organ; regulation of cell cycle; signal transduction
Gpr74	0.75	0.033	G protein-coupled receptor 74	G-protein coupled receptor protein signaling pathway
4930511H11Rik	0.76	0.013	RIKEN cDNA 4930511H11	
Armcx2	0.76	0.023	Armadillo repeat containing, X-linked 2	
Slc30a9	0.76	0.029	Solute carrier family 30	protein biosynthesis
Col5a1	0.76	0.048	Procollagen, type V, alpha 1	cell adhesion
Gas1	0.77	0.010	Growth arrest specific 1	cell cycle arrest; programmed cell death
2610034H20Rik	0.77	0.045	De-etiolated homolog 1 (Arabidopsis)	ubiquitin cycle
Cga	0.77	0.023	Glycoprotein hormones, alpha subunit	
2310047D07Rik	0.77	0.004	RIKEN cDNA 2310047D07 gene	
AK052220	0.77	0.011	Periostin, osteoblast specific factor	
0610009C03Rik	0.77	0.019	WD repeat domain 57	
Gars	0.78	0.001	Glycyl-tRNA synthetase	glycyl-tRNA aminoacylation; protein biosynthesis; regulated secretory pathway; tRNA aminoacylation for protein translation
Uchl3	0.78	0.049	Ubiquitin thiolesterase	protein deubiquitination; ubiquitin cycle; ubiquitin-

				dependent protein catabolism
1700001E16Rik	0.78	0.035	Decapping enzyme, scavenger	
D930050H05Rik	0.78	0.006	Kelch-like 20 (Drosophila)	cytoskeleton organization and biogenesis
2900046L07Rik	0.78	0.019		
Erbb3	0.79	0.012	v-erb-b2 erythroblastic leukemia viral oncogene homolog 3	cellular physiological process; heart development; peripheral nervous system development; protein amino acid phosphorylation; regulation of cell cycle
9530013L04Rik	0.79	0.025		
9030607L20Rik	0.79	0.049		
Tns	0.79	0.021		
AW125391	0.79	0.028	Radical S-adenosyl methionine domains 1	
Cnbp2	0.79	0.021	Cellular nucleic acid binding protein 2	electron transport
Amh	0.79	0.039	anti-Muellerian hormone	gonad development; gonadal mesoderm development; urogenital system development
Qscn6l1	0.79	0.005	Quiescin Q6-like 1	
Hmgn2	0.79	0.024	High mobility group nucleosomal binding domain 2	DNA packaging
1810009M01Rik	0.79	0.028	RIKEN cDNA 1810009M01 gene	
Sort1	0.79	0.016	Sortilin 1	carbohydrate metabolism; endocytosis
Tna	0.79	0.041	C-type lectin domain family 3	skeletal development
Siat8c	0.80	0.019	sialyltransferase 8C	protein amino acid glycosylation
2900073F20Rik	0.80	0.033		
BC009118	0.80	0.045	CDNA sequence BC009118	
Phf10	0.80	0.018	PHD finger protein 10	regulation of transcription, DNA-dependent
AI450757	0.80	0.021	Splicing factor, arginine/serine-rich 12	mRNA processing; nuclear mRNA splicing, via spliceosome

Table 4. Genes significantly ($p < 0.05$) upregulated in FMN2 knockout primary osteoblast cells in comparison to FMN2 wildtype primary osteoblast cells.

Gene Name	Normalized ratio	P-value	Description	Gene Ontology Biological Process
Cugbp2	1.20	0.020	CUG triplet repeat	mRNA processing; mRNA splice site selection; nuclear mRNA splicing, via spliceosome
Nap1l1	1.20	0.050	Nucleosome assembly protein 1-like 1	nucleosome assembly

App	1.21	0.008	Amyloid beta (A4) precursor protein	apoptosis; cell adhesion; endocytosis; extracellular matrix organization and biogenesis
C530043A13Rik	1.21	0.046	RIKEN cDNA C530043A13 gene	
Atp6v1a1	1.22	0.004	ATPase, isoform 1	ATP biosynthesis; ATP synthesis coupled proton transport; ion transport
Ccrl2	1.23	0.049	Chemokine (C-C motif) receptor-like 2	G-protein coupled receptor protein signaling pathway
Rpl10	1.23	0.049	Ribosomal protein 10	protein biosynthesis
Pgam1	1.23	0.050	Phosphoglycerate mutase 1	glycolysis; metabolism
Fkbp8	1.24	0.043	FK506 binding protein 8	cell fate specification; dorsal/ventral pattern formation; eye morphogenesis (sensu Mammalia); protein folding; smoothened signaling pathway
2010319C14Rik	1.24	0.003	Phosphatidylinositol glycan, class X	
Prrx1	1.24	0.043	Paired related homeobox 1	development; regulation of transcription, DNA-dependent
E430002N23Rik	1.24	0.037		
Ppia	1.25	0.005	Peptidylprolyl isomerase A	protein folding
Hmga1	1.25	0.000	High mobility group AT-hook 1	DNA packaging; chromosome organization and biogenesis (sensu Eukaryota); regulation of transcription, DNA-dependent; spermatogenesis
Tessp2	1.25	0.030	Testis serine protease 2	
Stc1	1.25	0.020	Stanniocalcin 1	calcium ion homeostasis; monovalent inorganic anion homeostasis; protein amino acid phosphorylation
B930082K07Rik	1.26	0.011		
Rps7	1.26	0.037	Ribosomal protein S7	protein biosynthesis; ribosome biogenesis
9530076L18	1.27	0.034		
NC004605	1.27	0.046	mVI036803	
4930563A19Rik	1.27	0.039		
S100a4	1.28	0.035	S100 calcium binding protein A4	
Lig4	1.28	0.001	Ligase IV, DNA, ATP-dependent	DNA recombination; DNA repair; DNA replication; cytokinesis; single strand break repair
Thbd	1.28	0.000	Thrombomodulin	blood coagulation; embryonic development; negative regulation of coagulation; pregnancy
D15Ertd621e	1.28	0.048	DNA segment, Chr 15 expressed	
Adm	1.28	0.008	Adrenomedullin	neuropeptide signaling pathway
Hspa5	1.29	0.012	Heat shock 70kD protein 5	ER-overload response; protein folding; response to unfolded protein

5930435M05Rik	1.29	0.050		
Rps26	1.30	0.032	Ribosomal protein S26	protein biosynthesis
A330102K04Rik	1.30	0.050	RIKEN cDNA A330102K04 gene	
Crim1	1.30	0.007	Cysteine-rich motor neuron 1	regulation of cell growth
AK038963	1.30	0.035	Lectin, galactose binding, soluble 8	
V1rd15	1.30	0.007	Vomeronasal 1 receptor, D15	G-protein coupled receptor protein signaling pathway
Ercc6	1.32	0.032	Excision repair cross-complementing	pyrimidine dimer repair; response to oxidative stress; transcription-coupled nucleotide-excision repair
Pafah1b1	1.32	0.034	Platelet-activating factor acetylhydrolase	acrosome formation; cell migration; cytokinesis; mitosis; neuroblast proliferation; neurogenesis; neuronal migration; retrograde axon cargo transport
AU067695	1.33	0.013	TRNA splicing endonuclease 2	mRNA processing; tRNA processing
Kcnrg	1.33	0.036	Potassium channel regulator	
Mapk9	1.33	0.049	Mitogen activated protein kinase 9	protein amino acid phosphorylation
Gababrbp	1.34	0.049	Gamma-aminobutyric acid receptor binding protein	biological_process unknown
Rnf10	1.34	0.013	Ring finger protein 10	
Rad1	1.35	0.042	RAD1 homolog (S. pombe)	DNA repair
AU021034	1.35	0.038	Expressed sequence AU021034	
Ribc2	1.36	0.041	RIB43A domain with coiled-coils 2	biological_process unknown
Mia1	1.36	0.035	Melanoma inhibitory activity 1	cell-matrix adhesion; extracellular matrix organization and biogenesis
Gnb3	1.36	0.039	Guanine nucleotide binding protein	G-protein coupled receptor protein signaling pathway; signal transduction
A930027G11Rik	1.37	0.042		
Rab22a	1.37	0.046	RAB22A, member RAS oncogene family	protein transport; small GTPase mediated signal transduction
4930519F16Rik	1.37	0.023	RIKEN cDNA 4930519F16 gene	
LOC238771	1.37	0.037	Similar to Metaxin 1	
4930515G01Rik	1.37	0.009	RIKEN cDNA 1100001D10 gene	
2010300F17Rik	1.38	0.004		
Cxcl5	1.38	0.003	Chemokine (C-X-C motif) ligand 5	chemotaxis; immune response; inflammatory response; signal transduction
Slpi	1.39	0.042	Secretory leukocyte protease inhibitor	
Serpinb2	1.39	0.049	Serine proteinase inhibitor, clade B	
4933436E23Rik	1.40	0.001		
1700061N14Rik	1.41	0.034		
Dio3	1.42	0.014	Deiodinase	

4933430F16Rik	1.42	0.041	RIKEN cDNA 4933430F16 gene	
1190002H09Rik	1.43	0.048	RIKEN cDNA 1190002H09 gene	
AK081844	1.43	0.002		
Ddx3y	1.43	0.047	DEAD (Asp-Glu-Ala-Asp) box polypeptide	
1100001I19Rik	1.43	0.004	RIKEN cDNA 1100001I19 gene	
Gm1960	1.44	0.003	Gene model 1960, (NCBI)	
Timm22	1.45	0.034	Translocase of inner mitochondrial membrane 22	intracellular protein transport
Sertad2	1.45	0.011	SERTA domain containing 2	regulation of transcription, DNA-dependent
Sprrl9	1.47	0.006	Small proline rich-like 9	
Pigt	1.48	0.026	Phosphatidylinositol glycan, class T	
Cdc42ep3	1.48	0.030	CDC42 effector protein	
Sqrdl	1.48	0.001	Sulfide quinone reductase-like (yeast)	electron transport
2900016D05Rik	1.49	0.005	RIKEN cDNA 2900016D05 gene	
Sdpr	1.51	0.008	Serum deprivation response	
Serping1	1.54	0.005	Serine peptidase inhibitor, clade G	blood coagulation; complement activation; complement activation, classical pathway
Tm4sf1	1.54	0.003	Transmembrane 4 superfamily member	
Odd1	1.57	0.029	Odd-skipped related 1	
Atp1a1	1.60	0.030	ATPase, Na+/K+ transporting, alpha 1	cation transport; metabolism; monovalent inorganic cation transport; potassium ion transport; sodium ion transport
S100a8	1.61	0.025	Calgranulin A	Chemotaxis
Akr1c18	1.61	0.004	Aldo-keto reductase family 1	progesterone metabolism
B430201A12Rik	1.65	0.006	RIKEN cDNA B430201A12 gene	
1700009P13Rik	1.67	0.036	RIKEN cDNA 1700009P13 gene	
Lcn2	1.70	0.035	Lipocalin 2	Transport
Efemp1	1.73	0.008	Epidermal growth factor-containing fibulin-like extracellular matrix protein 1	cell adhesion
Cxcl2	1.74	0.006	Chemokine (C-X-C motif) ligand 2	chemotaxis; immune response; inflammatory response; signal transduction
Psca	1.81	0.033	Prostate stem cell antigen	
2610028F08Rik	1.89	0.005	R-spondin 2 homolog	protein amino acid phosphorylation; transmembrane receptor protein tyrosine kinase signaling pathway
Esm1	2.02	0.022	Endothelial cell-specific molecule 1	regulation of cell growth
Ssxb1	2.08	0.016	Synovial sarcoma, X member B	regulation of transcription, DNA-dependent
Aqp1	2.29	0.020	Aquaporin 1	transport; water transport

Our specific objectives during the final 3 months of this project as follows:

1) To analyze phenotype data from formin2 and EphA4 knockout mice and write up the results for publication.
2) To continue the studies on overexpression of sense or antisense constructs (or siRNAs) using appropriate vectors and determine the effects on proliferation, differentiation and apoptosis in mouse osteoblasts.

A presentation describing the results of the FMN2 knockout mouse studies was presented at the American Society for Bone and Mineral Research, 28th Annual Meeting in September 2006 in Philadelphia, Pennsylvania Also, a paper describing the digit tip regeneration phenotypes of MRL mice is currently in press in the journal Wound Repair and Regeneration. In vitro studies on primary osteoblasts are also ongoing.

3. Key Research Accomplishments

Subproject 1:

1) Formin-2 (FMN2) knockout mice have significantly reduced femur cortical thickness and total bone mineral density and significantly increased femur endosteal circumference.

2) EphA4 mutant mice have reduced total BMD due primarily to reduced body size and weight.

3) FMN2 was found to be expressed in osteoblast-like MCT3T cell line but not in osteoclast-like RAW264.7 cell line.

4) FMN2 was found to be increased in expression in Wnt3A treated MCT3T osteoblast cell line, suggesting that FMN2 is in the Wnt signaling pathway.

5) Knockout FMN2 osteoblasts show significantly reduced ALP activity in comparison to wildtype FMN2 osteoblasts at 1, 2, 3, 4 and 5 hours ($P<0.01$). This indicates that differentiation of FMN2 knockout osteoblasts is reduced in comparison to wildtype FMN2 osteoblasts.

6) Knockout FMN2 osteoblasts show significantly reduced proliferation in comparison to wildtype FMN2 osteoblasts ($P<0.01$).

7) Knockout FMN2 osteoblasts show significantly reduced bone nodule formation in comparison to wildtype FMN2 osteoblasts ($P<0.03$).

8) Microarray expression analysis of find that periostin (POSTN) and IGF Binding Protein 5 (IGFBP5) are significantly downregulated in FMN2 knockout osteoblasts (as well as other genes).

9) These studies suggest that FMN2 is expressed in bone primarily in osteoblast cells; that FMN2 is influenced by WNT signaling; that FMN2 is important in osteoblast differentiation and proliferation; and that FMN2 is important in bone formation.

5. Reportable Outcomes

Presentations:

RB Chadwick, LM Bu, Y Hu, Y Zhu, DJ Baylink, S Mohan. Formin-2 Knockout Mice Exhibit Reduced Femur BMD and Cortical Thickness. American Society for Bone and Mineral Research, 28th Annual Meeting, Sept 15-19, 2006, Philadelphia, PA

Publications:

RB Chadwick, LM Bu, Y Hu, Y Zhu, DJ Baylink, S Mohan. Digit Tip Regrowth and Differential Gene Expression in MRL/Mpj, DBA/2 and C57BL/6 Mice. Wound Repair and Regeneration, in press, 2007.

Conclusions

In conclusion, Formin-2 (FMN2) knockout mice have been found to have significantly reduced femur cortical thickness and total bone mineral density and significantly increased femur endosteal circumference. Members of the formin gene family have been implicated in the WNT signaling pathway which is known to initiate growth and regulate cell differentiation in a number of tissues [1, 2]. Also, bone formation has been shown to be activated by WNT signaling in osteoblast stem cells by promoting osteoblastic differentiation and proliferation [3, 4].

Our in vitro studies of FMN2 knockout osteoblast cells find that they demonstrate reduced differentian and proliferation capacities in comparison to wildtype FMN2 osteoblast cells. These findings further support the hypothesis that FMN2 is important gene involved in differentiation, proliferataion and bone formation. The data also indicates that FMN2 is involved in the WNT signaling pathway.

Our microarray expression studies find that Periostin (POSTN) is significantly downregulated in FMN2 knockout osteoblast cells. POSTN is a secreted protein that is highly expressed in developing osteoblast cells and is thought to function by supporting cellular adhesion. Periostin has also been shown to be present at the osteogenic fronts of calvarial bones and studies have shown that POSTN is upregulated by TGF-b and WNT3 [5, 6]. Our expression studies of WNT3 treated osteoblast-like MC3T3 cells have found that FMN2 is upregulated. However, microarray expression studies of FMN2 knockout osteoblasts find that POSTN is downregulated when FMN2 is mutated. Thus, our current hypothesis is that FMN2 is most likely downstream of WNT3 and upstream of POSTN. Future studies will be undertaken to confirm or disprove this hypothesis.

References

[1] Habas R, Kato Y, He X. WNT/Frizzled activation of Rho regulates vertebrate gastrulation and requires a novel Formin homology protein Daam1. Cell. 2000; 107(7):843-54.
[2] Church VL, Francis-West P. WNT signalling during limb development. Int. J. Dev. Biol. 2002; 46: 927-936.

[3] Gong Y, Slee RB, Fukai N, Rawadi G, Roman-Roman S, Reginato AM, Wang H, Cundy T, Glorieux FH, Lev D, Zacharin M, Oexle K, Marcelino J, Suwairi W, Heeger S, Sabatakos G, Apte S, Adkins WN, Allgrove J, Arslan-Kirchner M, Batch JA, Beighton P, Black GC, Boles RG, Boon LM, Borrone C, Brunner HG, Carle GF, Dallapiccola B, De Paepe A, Floege B, Halfhide ML, Hall B, Hennekam RC, Hirose T, Jans A, Juppner H, Kim CA, Keppler-Noreuil K, Kohlschuetter A, LaCombe D, Lambert M, Lemyre E, Letteboer T, Peltonen L, Ramesar RS, Romanengo M, Somer H, Steichen-Gersdorf E, Steinmann B, Sullivan B, Superti-Furga A, Swoboda W, van den Boogaard MJ, Van Hul W, Vikkula M, Votruba M, Zabel B, Garcia T, Baron R, Olsen BR, Warman ML; Osteoporosis-Pseudoglioma Syndrome Collaborative Group. LDL receptor-related protein 5 (LRP5) affects bone accrual and eye development. Cell 2001; 107: 513-523.

[4] Bain G, Muller T, Wang X, Papkoff, J. Activated beta-catenin induces osteoblast differentiation of C3H10T1/2 cells and participates in BMP2 mediated signal transduction. Biochem. Biophys. Res. Commun. 2003; 301: 84-91.

[5] Haertel-Wiesmann M, Liang Y, Fantl WJ, Williams LT. Regulation of cyclooxygenase-2 and periostin by Wnt-3 in mouse mammary epithelial cells. J Biol Chem. 13;275(41):32046-51, 2000.

[6] Horiuchi K, Amizuka N, Takeshita S, Takamatsu H, Katsuura M, Ozawa H, Toyama Y, Bonewald LF, Kudo A. Identification and characterization of a novel protein, periostin, with restricted expression to periosteum and periodontal ligament and increased expression by transforming growth factor beta. J Bone Miner Res. 14(7):1239-49, 1999.

PROJECT 2

PRINCIPAL INVESTIGATOR: Apurva Kumar Srivastava, Ph.D.

TITLE: Sensitizer Screening to Enhance Detection of Enu-Induced Mutant Phenotypes

Project 2: Sensitizer Screening to Enhance Detection of ENU-Induced Mutant Phenotypes

Introduction

In the present study, we propose to employ mouse models in which genes that have been previously implicated to play a critical role in the development and maintenance of musculoskeletal tissues have been knocked out. By using mice with mutation in a gene known to affect musculoskeletal phenotypes, we propose to sensitize a classical ENU mutagenesis screening system (1), and thereby increase the recovery of mutants by discovering genes that have subtle effects on musculoskeletal phenotype. The principle for increased sensitivity of recognition is synergism between the unknown ENU mutation and the known knock out gene (2-4). One of the important requirements for the success of our approach involving sensitizer screen to identify novel mouse mutants for musculoskeletal phenotypes relates to which knockout mouse models are selected for ENU mutagenesis screens. In this regard, it is now widely accepted that IGF-I (5) and TGF β (6) are two critical regulatory molecules that regulate growth and development of musculoskeletal tissues and that deficiencies in these two growth factors contribute to impaired growth and maintenance. Furthermore, IGF-I and TGF β have been implicated in mediating the effects of many systemic and local factors that regulate musculoskeletal system. Therefore, we employed *lit/lit* mouse where *lit* allele results in a nonfunctional growth hormone related hormone receptor (GHRHR). These mice are IGF-I deficient. The Smad2 is a key molecule for TGF β signaling pathway in bone cells, the homozygous smad2 knockout mice are lethal but heterozygous smad2 mice survive and appear to have normal musculoskeletal phenotype. We have used these models to screen for musculoskeletal phenotypes based on the hypothesis that ENU induced mutation will exhibit greater effect on the musculoskeletal phenotype under reduced dosage of IGF-I and TGF-β.

Body

Technical Objectives

To identify the mouse mutants with musculoskeletal phenotypes in the F1 progeny of ENU treated male mice mated with IGF-I deficient *lit/lit* and TGF β deficient Smad2 knockout female mice compared to their respective wild type female mice.

To achieve the above technical objective, we have proposed the following specific objectives during the final 12 months of this study.

a) Breed knockout females with wild type ENU treated males to generate approximately 100 F1 progeny for each lit/lit and Smad2 mutant. Breed wild type females with ENU treated males to produce 100 F1 control progeny.
b) Perform musculoskeletal screens at 10 weeks of age in the F1 progeny to measure bone mineral content, bone density, bone size, muscle size and fat content using PIXImus and pQCT instruments. Perform biochemical measurements of bone turnover in the serum samples.
c) Begin to confirm the mutant phenotypes by backcrossing the mutant mice with lit/lit or Smad2 knockout mice, as appropriate.

Progress on Specific Objectives

We used two mouse models for our sensitized screen. The first model involves mice carrying a mutation in growth hormone (GH) releasing hormone receptor (denoted '*lit*' allele) resulting in GH deficiency, low IGF-I expression, and reduced growth. The second mouse model lacked *smad2*, signal transducer for TGF-beta, an important bone growth factor. The *smad2*-/- mice are lethal, but *smad2*-/+ mice exhibit normal growth. Designs of these sensitized screens have been described in **Figures 1 & 2**.

Specific Objective 1.

In the current reporting period, we focused our efforts and resources on the interesting phenotypic deviants that we already identified in the previous grant periods. We believed that it was imperative to focus our resources on further phenotypic characterization and follow-up of these phenotypic deviants as compared to screening of new F1 mice. Therefore, we did not generate any new F1 progeny as proposed in Specific Objective 1 instead we generated large number of F1 mice from backcrossing the phenotypic deviants identified earlier with Wild type (WT) lit/+ or smad2+/- mice.

The phenotypic deviants that were followed-up for further breeding are described under four different lines in **Table-1**. Out of four phenodeviant lines, one line (line 14104) was in lit/+ background and three lines (lines 1665CM, 1665DF & 2195) were in smad2+/- background. Accordingly, mice from the line 14104 were bred with WT mice carrying lit/+ genotype and mice from lines 1665CM, 1665DF & 2195 were bred with WT mice carrying smad2+/- genotype. For breeding we introduced one affected male/female mice with 2-3 WT lit/+ (B6) or smad2+/- (B6) mice. Once a mating was successful, pregnant mice are separated and placed separately to give birth to F1 littermates. AT 3-week, mice were weaned, male and female were separated into separate cages and screened as described in Specific Objective 2. In addition to phenotype screening, all mice were genotyped between 3-week and 16-week age for presence of 'lit' or 'smad2' allele to calculate number of mice that carry both mutant and 'lit' or 'smad2' alleles. However, only phenotype distribution was used for separating the mutants from their unaffected littermates for further breeding. To avoid potential breeding of an un-affected progeny, we mainly bred extreme scoring mice for generating affected progeny in subsequent breeding. We generated 399 mice from four lines indicated in **Table-1** and from breeding WT lit/+ or smad2+/- mice.

Specific Objective 2

We screened total of 335 F1 mice for dominant mutations from four lines described in **Table-1**. The screening was performed under anesthesia. All F1 mice were screened at 10-week of age for body weight, bone mineral density (BMD), bone mineral content (BMC), bone size, lean mass, and fat mass using dual energy X-ray absorptiometry (DEXA) instrument. In addition, volumetric BMD and bone size parameters such as bone area, total area, marrow area, periosteal circumference, endosteal circumference, and cortical thickness were determined in-vivo using peripheral quantitative computed tomography (pQCT) imaging system. In addition to 10-week screening, several litters of mice were also screened at 3-week, 6-week, and 16-week to obtain

longitudinal data. A phenotype was considered heritable if approximately 50% of mice show expected directional changes. From the data obtained so far, we confirmed heritability of line 14104 in both +/+ genotype and lit/+ genotype. Although we obtained several affected mice from breeding of lines 1665DF and 2195, however, since the smad2 KO mice is not in 100% B6 background, several generations of breeding will be required to confirm heritable mutation.

Specific Objective 3

The phenotypic characterization of three lines (14104, 1665DF, and 2195) was extensively studied and progress made during current reporting period is described in this section.

Mutant Line 14104 – The 14104 mice was identified in our previous year screen involving lit/+, which is in 100% B6 background. The 14104 mice have 30-40% decreased (**Figure-4**) cross-sectional area of both midshaft tibia and femur. The lower bone cross-sectional area is a result of approximately 20% decrease in periosteal circumference in both male and female 14104 mice. The mutation is inherited as an autosomal dominant trait. We have generated >100 progeny from four generations of breeding, out of these, approximately 40% of mice were classified as mutants, which is close to expected 50% ratio. The 14104 mice have approximately 8-12% lower body weight (**Figure-5**) as compared to non-affected littermates. However, the decreased bone size phenotype is much greater and present in 3-week old mice when body weight differences are not apparent. In addition, the bone size difference is >20% even after the adjustment for body weight. This suggests that differences in bone size in mutant mice are not complemental to lower body weight. Interestingly, the endosteal circumference is 40%-50% decreased in the 14104 mice (**Figure-6**), which could indicate a corrective mechanism in response to reduced bone strength.

In-Vivo Bone Size Phenotype: The *in-vivo* analysis of bone size phenotype performed by pQCT at midshaft tibia between 3-16-week of age (n=34-74) as described previously showed that bone cross-sectional area and periosteal circumference were 20-30% lower in affected mice, as compared to control littermates (LM) (**Table-2**) or WT *lit*/+ mice (Figure-3). The mean Z-score calculated for cross-sectional area (CSA) for affected 14104 mice and non-affected littermates was -5.7±0.8 and -0.2±0.9, respectively. Interestingly, femurs and tibia from the 14104 mutant mice showed 40-50% reduced endosteal circumference in both male and female as compared to non-affected LM (n=11-34) or WT mice. This decrease in endosteal circumference was greater (>20%) in female 14104 mice. The decreased endosteal circumference could indicate increased endocortical bone formation as a compensatory mechanism in response to decreased bone strength and this could explain a slight increase in vBMD observed in the 14104 female mice. In summary, bone size phenotype in the 14104 mice occurs during early postnatal growth period and is maintained during rapid pubertal growth period.

Ex-Vivo Bone Size Phenotype: To confirm the *in-vivo* measurement, we performed bone size measurement using pQCT in bone excised from 6-week (n=16) and 12-16 week (n=17) old mice. The excised tibia and femur were scanned at 9-different slices covering the entire length (distance between slices were determined by 11% of the length). Data from excised femur and tibia from the 6-week old 14104 mice (n=7) and the non-affected littermate controls (n=10) showed that mean cross-section area was 15-45% lower, periosteal perimeter was 19-29% lower, and endosteal perimeter was 6-38% lower over the entire length of bone in the male and female

14104 mice. In addition to pQCT, we analyzed excised femurs (n=3 per group, 6- & 12-week age) by μCT, the data is shown in **Figure-7**. Thus, both pQCT and μCT analysis of excised bones confirms the phenotype observations made by the *in-vivo* pQCT measurements.

Histological Examination of Bone Size: To determine if a decrease in the bone formation rate may contribute to decreased bone area in mutant mice, bones were dual labeled at a 10-day interval using calcein and animals were sacrificed at 12-weeks of age. After second tetracycline injection, femur and tibia were isolated and cleared of surrounding tissues. To measure bone formation and resorption, a location 1 mm proximal to the midshaft was marked on the femur with a pencil. A 5 mm segment of the femur midshaft was cut from the bone starting at the mark and going distally. The samples were fixed in 10% formalin for 4 hours, rinsed in PBS, and then partially decalcified (6 hours) in 10% EDTA in the cold. The samples were infiltrated in glycol methacrylate and embedded vertically with the midshaft end down. The samples were sectioned with a Jung microtome and the first 1 mm of material discarded until the mid point of the shaft was reached. Sections were prepared for analysis by staining for ALP and tartrate resistant acid phosphatase (TRAP). Total ALP and TRAP covered surfaces were measured using the Osteomeasure system equiped with a digitizing tablet (Osteometrics, Atlanta, GA and color camera (Sony, Japan).

The cross-section area measured by histology was 34-43% lower in the 14104 mice (n=4) as compared to the control mice (n=2). In addition, the other bone size parameters were consistent with the *in-vivo* and *ex-vivo* bone size data from pQCT (details not shown). Measurement of calcein labels on bone surfaces by histomorphometry revealed a 25% lower bone formation rate at periosteal surfaces in the 14104 mice (n=4) as compared to WT mice (**Figure-8,** since BFR is adjusted for bone surface data from male and female mice were combined). As expected, there was an increase in the bone formation rate in the 14104 mice at the endosteal surface. However, the differences were not statistically significant probably due to small number of replicates.

Biomechanical Properties: The breaking load for femurs from 14104 and control mice was measured by three-point bending using an Instron DynaMight Low-Force Testing System (Instron Corporation**,** Norwood, MA). The results are shown in **Figure-7D,** indicated that the breaking load was 30% lower in mutant mice.

Biochemical Bone Markers: The bone formation marker osteocalcin was 20% lower (p=0.021) in 14104 mice (131±59 ng/ml) as compared to normal littermates (163±81 ng/ml), which indicates an overall decrease in osteoblast activity. Although the BFR at endosteum is increased, contribution from the periosteum could be several folds higher and therefore result in a systemic decrease in osteocalcin levels.

In-vitro Phenotypic Characterization of Cell Function in the 14104 Mice: To study the cellular mechanism of increased bone density in the 14104 mutant, we isolated the periosteal osteoblasts from femur and tibiae of normal and 14104 mutant mice and propagated them in culture for in vitro phenotypic characterization. In brief, the mice were euthanized with CO_2 and decapitated. Soft tissues were removed from femur and tibia without scraping off the bones so that periosteal cells were not lost at this point. Femur and tibia were placed separately in 50 ml falcon tubes

containing sterile PBS, and subsequently in culture dish containing 10 ml of DMEM/antibiotics and the left over muscles were removed from the bones. The periosteal cells were extracted from bone by collagenase digestion for 90 minutes at 37^{o}C. Cells were counted and plated at a density of 10^{6} cells per dish and grown with 10% FBS/α-MEM/antibiotics. Periosteal osteoblasts at passage 2-3 were used to study cell proliferation, differentiation, and apoptosis. These characteristics cells from mutant mice were compared with cells isolated in identical manner from age and sex matched wild type mice.

Cell Proliferation Assay:

Cell proliferation was studied using (3H)-thymidine incorporation and results were confirmed by uptake of Almar Blue dye during cell proliferation. **Figure-9** shows the proliferation rates of periosteal osteoblasts isolated from femur and tibiae of female 6-week-old 14104 and normal littermate mice. Both proliferation assays indicate that there was a significant decrease in the basal cell proliferation as well as cell proliferation under stimulated conditions in cells from 14104 mice as compared to the cells from control mice.

Differentiation Assay: Cell differentiation was measured by observing changes in the alkaline phosphatase activities using PNPP as substrate. Our preliminary studies on osteoblast like cells from 14104 mice have indicated that the basal specific activity of alkaline phosphatase was 7-29% lower ($p=0.17$) in cells from the 14104 mice (Mean±SD, 0.533± 0.035 mU/mg protein) as compared to WT mice (0.656±0.077 mU/mg protein) (details not shown).

In summary, our preliminary characterization of the mutant mice using various imaging techniques, histology, biochemical indicators, cell function, and biomechanical properties indicates that mutation decreases bone size and strength by regulating bone formation. The proliferation and differentiation assay could provide a valuable tool in selecting candidate genes (that are involved in regulating cell differentiation) and to test function of candidate gene(s) for future studies.

Line 14104 Mapping

To identify the chromosomal location of the 14104 mutation, we generated F1 mice by breeding 14104 mutant mice with C3H/HeJ and DBA/J strains of mice. In the current reporting period, we have generated 22 F1 mice (Table-1). We performed screening of these F1 mice for bone size phenotype at 3-week and 6-week age and our preliminary data shows that the bone size phenotype is expressed in both C3H/HeJ and DBA/J background. Thus, we believe that both these strains could be used for mapping the chromosomal location of the 14104 mutation.

Mutant Line 1665CM – The phenodeviant 1665CM had 18% high body weight and 13% higher total body bone density measured by DEXA (Dual Energy X-ray Absortiometry), as compared to control smad2/+ mice. The body weight adjusted bone density was not significantly higher in mutant mice. Breeding of line 1665CM mice with the WT smad2/+ mice only produced three mice. Therefore, this line was discontinued.

Mutant Line 1665DF – Mutant line 1665DF was identified in the smad2/+ strain of mice. The phenodeviant had 23% high body weight and 17% higher total body bone density measured by DEXA (Dual Energy X-ray Absortiometry), as compared to control smad2/+ mice. The body weight adjusted bone density was 4-8% higher in 16-week old 1665DF mutant mice ($p<0.05$ vs control smad2/+ mice). We believe the mutant mouse has a high growth as well as high BMD

phenotype. In the current reporting period, we bred the 1665DF phenodeviant with smad2/+ mice and generated 122 progeny. We have screened 72 F1 progeny at 16-week and we observed that only 14 mice showed high BMD phenotype (**Figure-10**). There is indication that as mutations are diluted as we bred several generations. If we continue to see decreased phenotypic effects upon further breeding of the affected mice with WT smad2+/- mice will discontinue this line.

Mutant Line 2195 – Mutant line 2195 was identified in the smad2/+ strain of mice. In the current reporting period, we bred the 2195 phenodeviant with smad2/+ mice and generated 41 progeny. We have screened 32 F1 progeny at 16-week and we observed and observed that >50% mice showed the expected phenotype (**Figure-11**). The phenodeviant had 10-20% low body weight (Z-score was <-3.0) and 18-20% lower total body bone area measured by DEXA (Z-score of <-3.0), as compared to control mice. The total body bone density was marginally lower (1-4% lower) in 16-week old 2195 mutant mice vs control mice. We believe the mutant mouse has growth defects that also affect bone size. This line could be bred for few more generations to confirm mutation.

Table – 1. Number of mice generated, mice screened for various phenotypes, and number of mice introduced to inheritance testing.

Phenotypic Deviant Mice Lines or WT Mice	Mice Generated in the Current Reporting Period
14104	147
14104 DBA/C3H	22
1665DF	122
1665CM	3
2195	41
WT lit	31
WT Neo	30

Mice listen in this table includes mice with genotype +/+ and mice that are not yet genotyped.

Table-2. Percent difference in 14104 mice as compared to control littermates in various phenotypes measured in-vivo by pQCT at midshaft tibia.

Age (Week)	No of Mice	Sex	CSA	CSA Adj.	PC	EC	BMC
3	n=16	Male	-30	-24	-16	-36	-16
	n=15	Female	-34	-32	-19	-41	-18
6	n=10	Male	-35	-27	-19	-37	-30
	n=11	Female	-41	-32	-23	-45	-33
10	n=15	Male	-37	-29	-21	-37	-29
	n=16	Female	-38	-30	-21	-44	-22
16	n=7	Male	-40	-33	-23	-42	-37
	n=13	Female	-38	-29	-21	-54	-31

All differences in CSA (cross-sectional Area), CSA Adj. (cross-sectional area adjusted with body weight), PC (periosteal Circumference), EC (Endosteal Circumference), BMC (Total Bone Mineral Content), and Bone Area had $p<0.0001$

Figure-1. The sensitized screen design to identify mutations affecting growth hormone pathway. The 'lit' allele denotes GHRHR mutant allele and is identified by genotyping the F1 progeny by a RT-PCR based SNP assay. All progeny with lit/+ genotype were candidate for sensitized mutations. For clarity, the wild type alleles are denoted as two separate symbols '+' and 'wt' for 'lit' locus and ENU mutant 'm' locus, respectively.

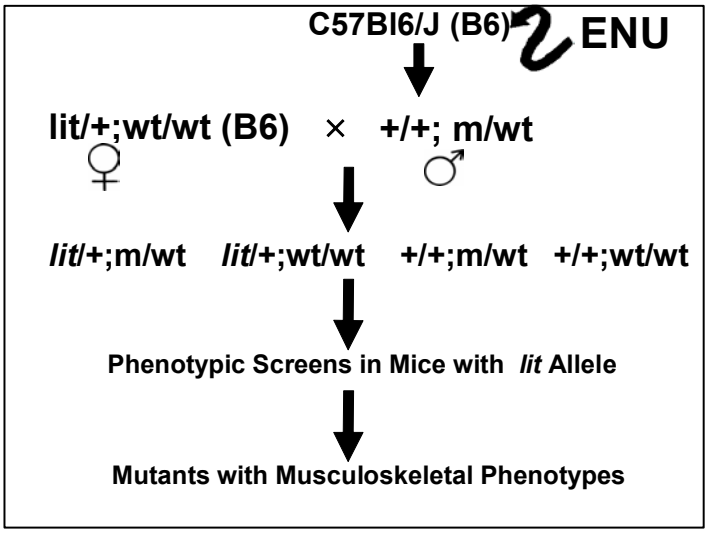

Figure-2. The sensitized ENU screen to identify mutants involved in TGF-β pathway. The 'neo' allele denotes that smad2 gene is absent and is replaced by a neomycin resistant gene cassette. We have designed primers that are specific for the neomycin resistant gene cassette and genotyped all progeny to demonstrate absence of single copy of smad2. All phenodeviants that have neo/+ background are candidates for sensitized mutations. For clarity, the wild type alleles are denoted as two separate symbols '+' and 'wt' for 'neo' locus and ENU mutant 'm' locus, respectively.

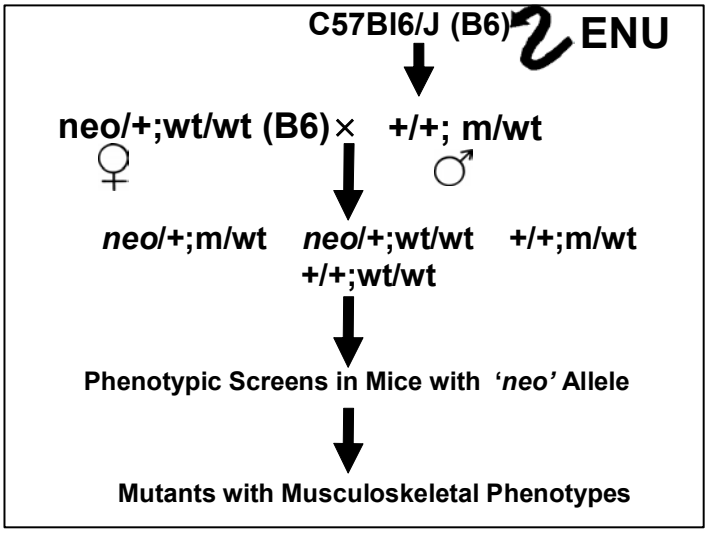

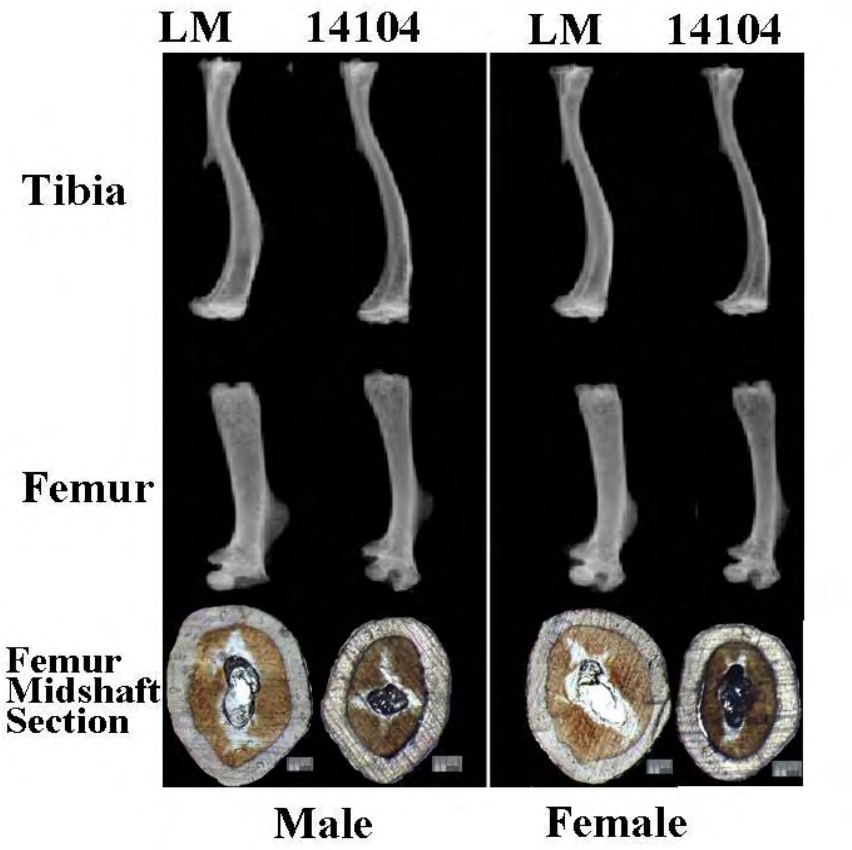

Figure-3. Bone size phenotype of one of the mutant identified in sensitized screen involving growth hormone deficient lit/- mice. The X-ray images of tibia and femurs from the 12-week old 14104 mutant mice are shown along with their non-affected littermates (LM). The 14104 mice have significantly slender bones with 17-23% lower periosteal circumference and 30-40% lower cross-sectional area ($p<0.001$) as compared to the LM. In mutant mice, the average body weight and bone lengths were marginally lower by 10-12% (Figure-1) and 2-7% (p=NS), respectively. Cross section image of mid-shaft femur is taken from histological analysis.

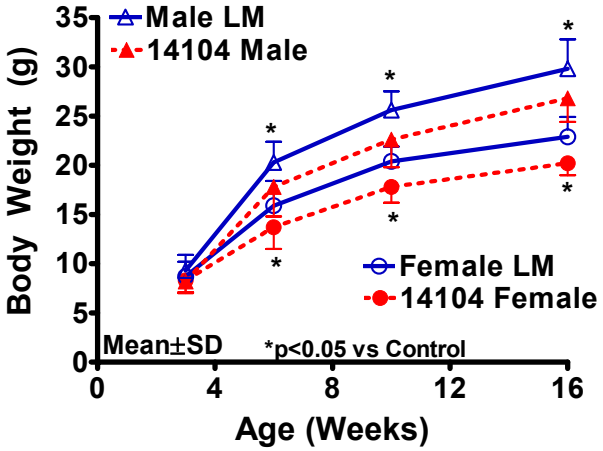

Figure-4. Body weight of 14104 mutant mice (n=6-16) and their normal littermates (n=7-20) between 3-16 weeks of age. The 14104 mutant mice showed 10-12% lower body weight (statistically significant for 6-16 week old mice) as compared to 30-40% lower bone size. Changes in bone size in the 14104 mice occur during early postnatal growth period (during or before 3-week age) when differences in body weights were not apparent. This would suggest that interaction between the mutant gene and GH/IGF-I pathway is specific for skeletal tissues.

Figure-5. The figure shows that there is uniform reduction in bone area across the entire length of the femur of 6-week old mutant mice (14104) as compared to normal littermates (Control). Bone area was measured along nine slices covering the entire length of the excised femur using pQCT. The mutation causes 30-40% lower bone area ($p<0.05$ *vs* control) as compared to control mice. Slices 1, 8 & 9 were omitted due to large variation.

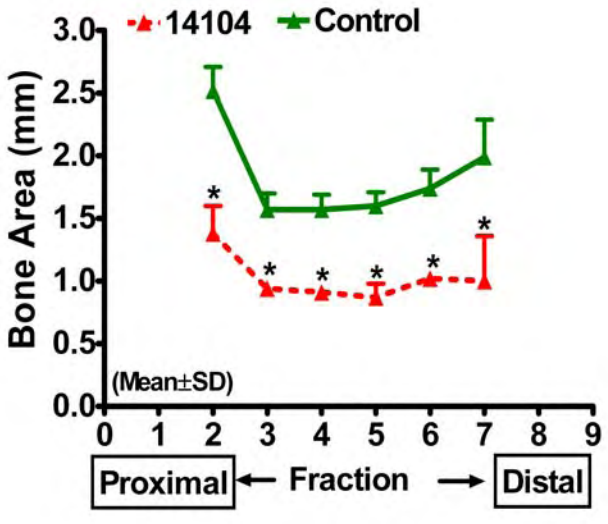

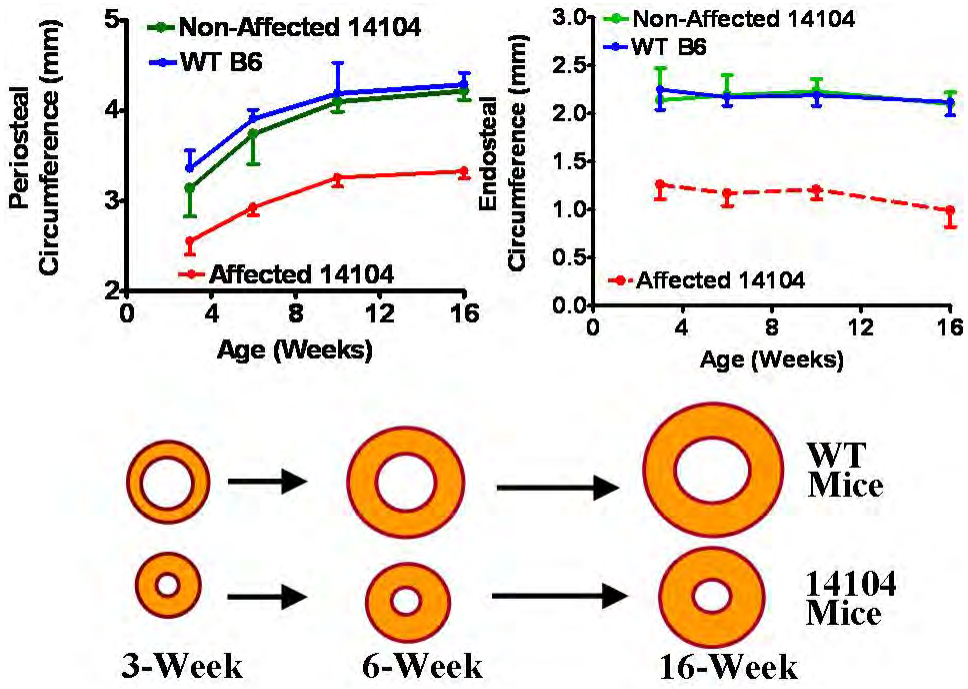

Figure-6. Longitudinal data on periosteal (PC) and endosteal circumference (EC) at mid-shaft tibia of female 14104 mutant mice as compared to littermates and WT lit/+ B6 mice (n=7-32, all differences were highly significant). The bottom illustration shows how these differences in PC (-20%) & EC (-40%) affects the cross-sectional area resulting in decreased size but increased cortical thickness relative to bone size. Interestingly, these data show that decrease in PC and EC occur during early postnatal development, thus, suggesting that 14104 gene is and important determinant of periosteal expansion in which the thickness of the cortical bone is fashioned according to a predetermined genetic plan.

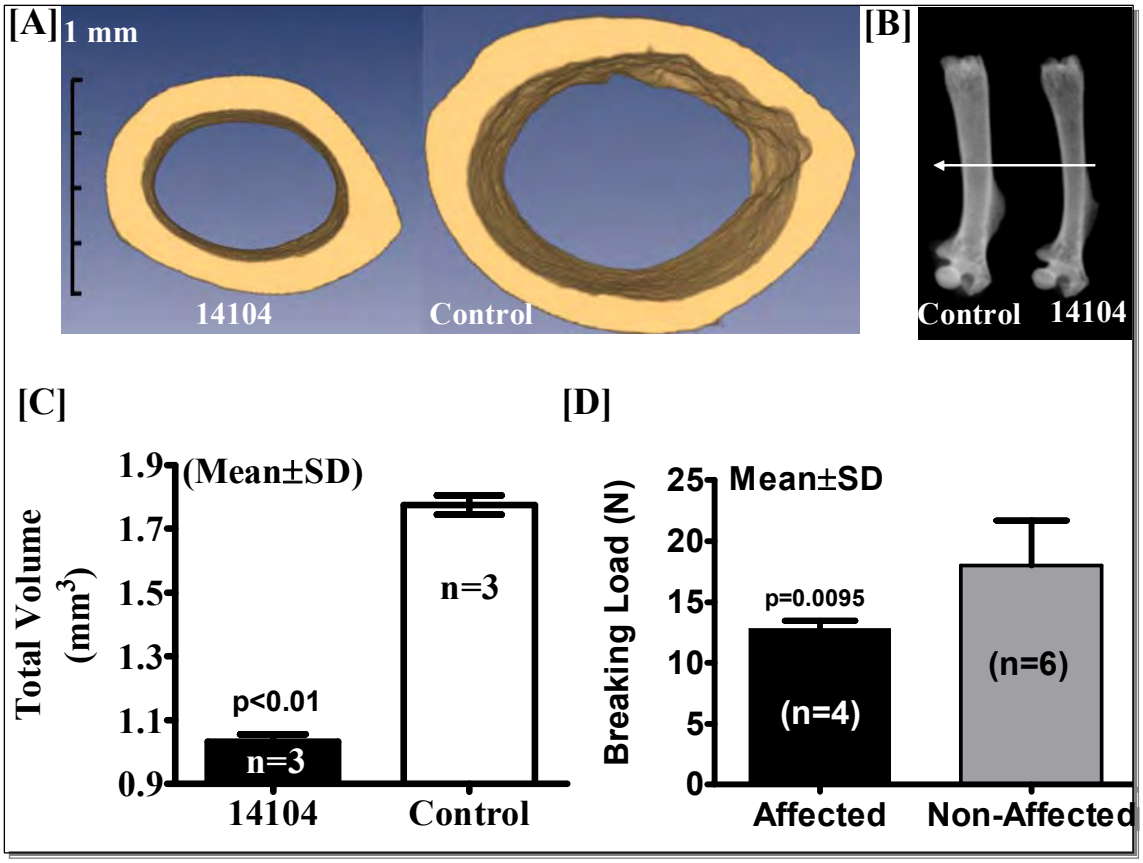

Figure-7. Cortical bone parameters computed from μCT measurements at midshaft femurs from mutant (14104) and littermates (control). A. Mutant mice have about 30% lower bone size as compared to control mice. B. The X-ray image of femur from mutant and control mice shows significantly slender bones with 17-23% lower periosteal circumference through entire length. C-D. The total volume [C] and bone volume measured by μCT were >30% lower, respectively, as compared to control. The breaking load [D] measured at midshaft femur was 29% lower in 14104 mice as compared to femurs from control mice.

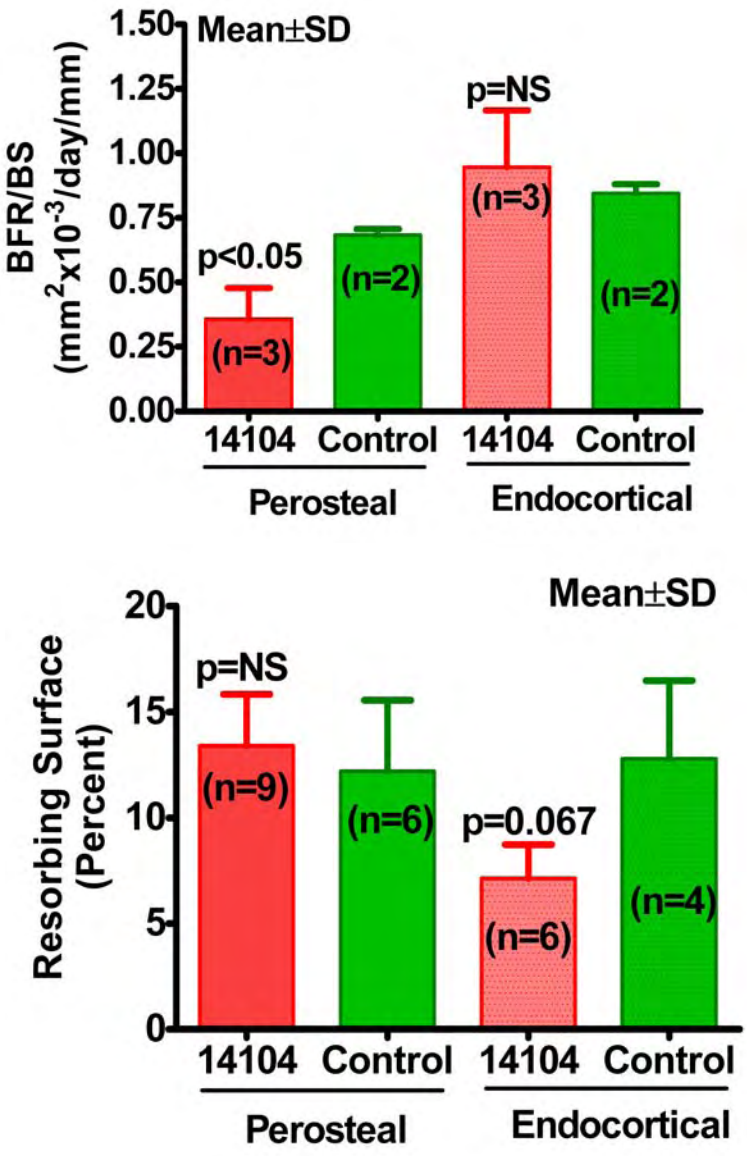

Figure-8. To determine if a decrease in the bone formation rate or increased bone resorption rate may contribute to decreased bone area in mutant mice, bones were dual labeled at a 10-day interval using calcein and mice were sacrificed at 12-weeks of age. Bone formation rate (BFR) measurement were corrected for total bone surface. The resorbing surface were measured in midshaft humerus by measuring TRAP labeled surface naphthol ASTR phosphate (Sigma) as substrate and counterstained with toluidine blue. The TRAP labeled surface is adjusted for total bone surface. (**A**) The decreased periosteal perimeter appears to be due to significantly reduced bone formation rate (-25%) per bone surface (BFR/BS). (**B**) In contrast, the decreased endosteal perimeter or reduced marrow area appears to be due to decreased bone resorption (-49%) at endosteal surface. (Control=Non-Affected Littermates of 14104 mutant mice) Since both BFR and resorbing surface measurements were adjusted for total bone surface, data from male and female mice were combined.

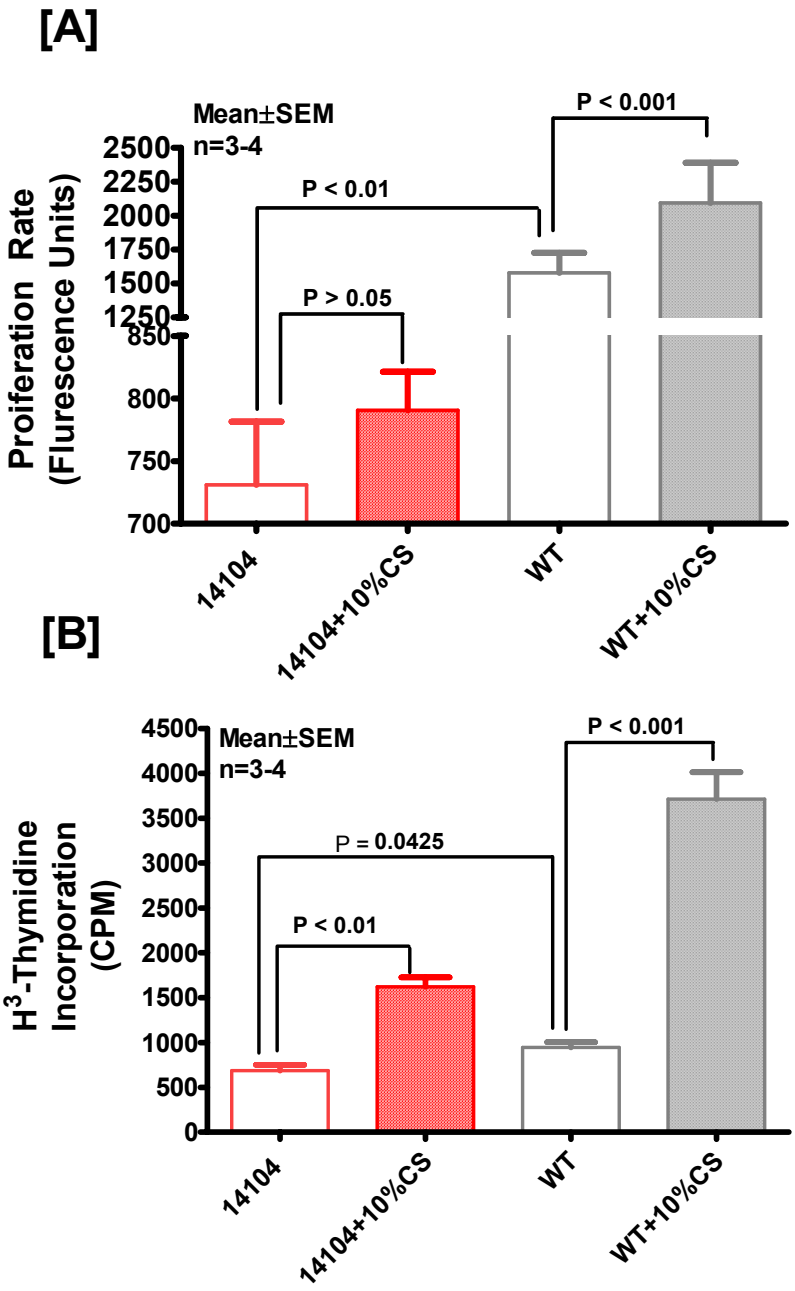

Figure-9. Basal proliferation rate of periosteal osteoblasts isolated from femur and tibia of 10-week-old B6 wild type and 14104 mutant male and female mice. Equal number of cells was seeded in 96-well plate (Almar Blue) and 24-well plate (Thymidine Incorporation) and grown in absence or presence of 10% calf serum (CS) for 48 hours. These preliminary data indicates that cell proliferation was significantly decreased in osteoblasts isolated from mutant mice as compared to controls.

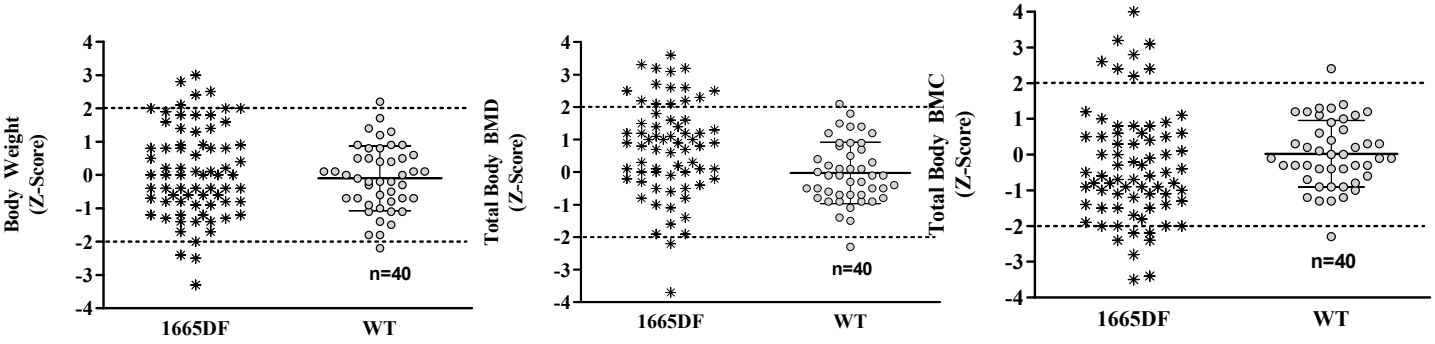

Figure-10. Phenotype data from 16-week old mutant progeny generated from backcross of a mutant mouse, 1665DF, identified in sensitized screening in Smad2/+ background. The progeny from 1665CM mutant shows 20% high body weight phenotype. In addition to body weight, the mutant progeny have 15-16% higher total body BMD (B) and 20-25% higher total body BMC (C). Each data point represents one mouse and both affected and non-affected littermates are shown under 1665DF progeny. The horizontal line indicates 2SD cut-off for identifying mutant mice from non-affected littermates. WT=Wild Type (smad2/+) (data shown as Mean±SD).

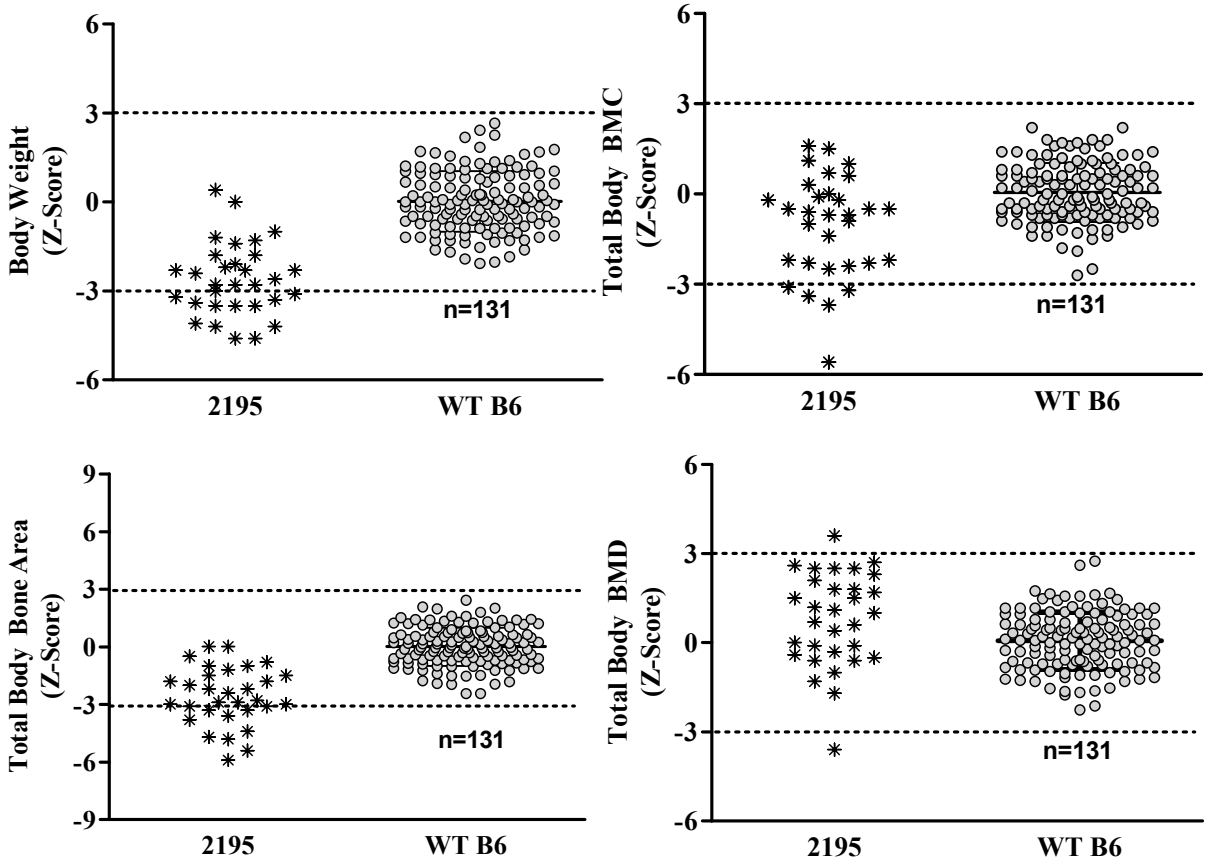

Figure-11. Phenotype data from 16-week old mutant progeny generated from backcross of a mutant line 2195. The progeny from 2195 mutant shows 20% low body weight phenotype. In addition to body weight, the mutant progeny have 15-16% lower total body BMD (B) and 20-25% lower total body BMC (C). Each data point represents one mouse and both affected and non-affected littermates are shown under 2195 progeny. The horizontal line indicates 3SD cut-off for identifying mutant mice from non-affected littermates. WT=Wild Type B6 (data shown as Mean±SD).

Key Research Accomplishments

- We maintained a breeding colony of *lit*/+ mice and Smad2/+ mice to have a continuous supply of *lit*/+ and Smad2/+ mice for breeding with ENU injected B6 males. We generated 61 mice from WT breeding.
- We bred four phenotypic deviant lines with wild type *lit*/+ or Smad2+/- mice and generated a total of 335 mice.
- We have screened 335 F1 mice generated from breeding four phenotypic deviant lines with wild type *lit*/+ or Smad2+/- mice.
- We observed that two phenodeviants in smad2/+ background require further breeding to dilute the background genetic effects.
- We have performed extensive characterization of a mutant line, 14104, identified earlier in the lit/+ background. The mutation is robustly inherited and stable. The 14104 mutant with presumably single gene mutation accounts for relatively very large effect size, a 30-40% lower cross-sectional area at mid-shaft tibia, and femur. We have demonstrated that changes in bone size in the 14104 mice occur during early postnatal growth period and bone size is only marginally affected by body size. We have shown that the decreased periosteal perimeter is accompanied by greater decrease in endosteal perimeter. Thus, the cortical thickness is not decreased in the same proportion. We have identified that mutant gene reduces bone formation rate at periosteum and that the osteoblasts cell function is altered. Since, bone size is a key determinant of bone strength and elucidation of a gene that determines 30-40% of bone size will be an important milestone in understanding genetic component of fracture risk.
- The phenotypic deviants described above represent single gene mutations, and therefore, provide interesting mouse model to identify genes that are involved in the genetic regulation of growth and musculoskeletal phenotypes.

Reportable Outcomes

Abstracts

1. **Srivastava AK**, Mohan S, Baylink DJ. A Sensitized ENU Screening System to Discover Modifier Genes by Utilizing Mouse Models Deficient in Genes Regulating Skeletal Tissues**.** 28th Annual Meeting of American Society for Bone and Mineral Research, 2006.
2. **Srivastava AK**, Mohan S, Baylink DJ. Identification of Mutant with a Large Decrease in Bone Size Identified in a Sensitized ENU Screen using Growth Hormone Deficient 'Little' Mouse. 28th Annual Meeting of American Society for Bone and Mineral Research, 2006.

Conclusions

1) Using two pathways involving IGF-I growth hormone axis and TGF-β signaling pathway, we have generated mutations with musculoskeletal phenotypes.
2) We bred *lit*/+ mice and heterozygous Smad2+/- mice to three musculoskeletal phenotypic deviants (identified in previous years) and generated F1 mice for characterization. Since, we have focused on follow-up of phenotypic deviants observed in previous years; we have not screened any new additional F1 mice produced from ENU injected male. However, in the follow-up backcrosses, we have generated and screened more than 300 mice; therefore, we have accomplished our main goal of screening 200 F1 mice in the 'Specific Objective-1a.'

3) We have generated 61 F1 mice by breeding WT lit/+ and WT smad2/+ mice.
4) We have performed musculoskeletal screens at 10 weeks of age in the F1 progeny to measure bone mineral content, bone density, bone size, lean mass and fat content using PIXImus and pQCT instruments. Therefore, we have accomplished our main goal of the 'Specific Objective-1b.'
5) We bred one phenodeviant identified in previous year screen in backcross to test inheritability of the mutation. We generated more 41 progeny from backcross and our preliminary data indicate that phenotype is inheritable. Therefore, we accomplished our goals for final objective 'Specific Objective-1c.'

References

1. Srivastava AK, Mohan, S, Wergedal JE, Baylink DJ. A Genome-wide Screening of N-Ethyl-N-nitrosourea Mutagenized Mice for Musculoskeletal Phenotypes. Bone, 33, 179-191, 2003.
2. Go MJ and Tsakonas SA. A genetic screen for novel components of the Notch signaling pathway during Drosophila bristle development. Genetics 150:211-220, 1998.
3. Carrera P, Abrell S, Kerber B, Walldorf U, Preiss A, Hoch M, Jackle H. A modifier screen in the eye reveals control genes for Kuüppel activity in the Drosophila embryo. Proc. Natl. Acad. Sci. 95:10779-10784, 1998.
4. Satterthwaite AB, Willis F, Kanchanastit P, Fruman D, Cantley LC, Helgason, Humphries RK, Lowell CA, Simon M, Leitges M, Tarakhovsky A, Tedder TF, Lesche R, Wu H, and Witte ON. A sensitized genetic system for the analysis of murine B lymphocyte signal transduction pathways dependent on Bruton's tyrosine kinase. Proc. Natl. Acad. Sci. 97: 6687-6692, 2000
5. Attisano, L. and J.L. Wrana, Signal transduction by the TGF-beta superfamily. Science, 296(5573): 1646-7, 2002.
6. Donahue, L.R. and W.G. Beamer, Growth hormone deficiency in 'little' mice results in aberrant body composition, reduced insulin-like growth factor-I and insulin-like growth factor-binding protein-3 (IGFBP-3), but does not affect IGFBP-2, -1 or -4. J Endocrinol, 136(1): 91-104,1993.

PROJECT 3

PRINCIPAL INVESTIGATOR: Subburaman Mohan, Ph.D.

TITLE: Development of Transgenic Approaches Using BAC Clones to Identify Candidate Genes for Musculoskeletal Phenotypes

Project 3: Development of Transgenic Approaches Using BAC Clones to Identify Candidate Genes for Musculoskeletal Phenotypes

Introduction

The primary goal of our studies is to localize chromosomal regions and subsequently identify genes responsible for various musculoskeletal phenotypes including bone density, bone size, fracture repair and soft tissue regeneration, and evaluate the molecular function of these genes. In our previous studies, we have made significant progress on the identification of quantitaive trait loci (QTL) in several mutant and inbred mouse strains that are associated with phenotypes of small bone size, high bone density, anabolic response to mechanical loading and soft tissue regeneration. However, these regions contain dozens of intact genes with a large piece of genomic DNA in several overlapping bacterial artificial chromosomes (BACs) and are still difficult to clone by more time-consuming, expensive positional cloning strategies. An alternate approach for identifying these disease-causing genes that is both feasible and efficient is to transfer the unknown genes from the QTL regions into the bone cells *in vitro* for a high throughput functional screening. The aim of this project is to develop a viral and non-viral gene transfer systems to deliver candidate genes as large as 150-kb into bone cells for functional studies. In the past 12 months and additional 3 months of this continuation grant, we optimized and validated a non-viral gene transfer system to express the coding sequence of test genes in the bone cells

Our specific objective during this grant period is to validate a non-viral gene transfer system for functional testing of candidate genes in vitro. Our progress in this specific objective is given below.

Body

1. Technical Objectives

In order to deliver the candidate genes that have been identified in our whole-genome microarray screening and quantitative trait loci (QTL) studies for functional testing, we developed a non-viral gene transfer system to express the coding sequence of test genes in the bone cells. We established this gene transfer strategy for the following reasons: 1) Some of our test genes may contain large introns (>100 kb), such that the size of the intact gene, including introns and exons, could be beyond the limitation of the HSV packaging capacity (e.g. >150 kb); 2) The bacterial artificial chromosome (BAC) clone containing the entire candidate gene may not be available in the mouse genome databases; and 3) The BAC clone may encode multiple, alternatively-spliced variants with diverse functions from a single gene. To validate the non-viral gene transfer system, we modified the construct of pHGCX containing a CMV promoter in front of multiple cloning sites (MCS) by inserting a small CMV intron from pmaxGFP (Amaxa Inc., Gaithersburg, MD) into the corresponding sites of SnaB1 and NheI sites of pHGCX to generate a new expression vector driven by CMV promoter/intron (Figure 1). We amplified the complete coding sequence of osterix (Osx) from a mouse bone cDNA library by polymerase chain reaction (PCR) using specific primers with an overhang of Flag sequence at the 5' end of the forward primer. The PCR product of Flag-Osx was cloned into pCR2.1 to generate pCR2.1/Flag-Osx using a TA cloning kit (Invitrogen, Carlsbad, CA). The Flag/Osx fusion gene was then released from pCR2.1/Flag-Osx, and subcloned into the BamH1

and XhoI sites of modified pHGCX to generate pHGCX/Flag-Osx that also contains a green fluorescence protein (GFP) (Figure 1).

We believe that unlike BAC clone, plasmid DNA can be transferred into bone cells by chemical transfection or electroporation. Therefore, we optimized a protocol of "Nucleoporation" technique to deliver the transgenes into nuclei of MC3T3-E1 cells, by utilizing a commercial "Nucleofection buffer" (Amaxa Inc) and "Gene Pulser" (Biorad). Briefly, 10^6 MC3T3-E1 cells were resuspended in 100 μl of nucleofector buffer T containing 5 μg of pHGCX/Osx/flag plasmid DNA. The cells were then transferred into a 2-mm gap width electroporation cuvette, and electroporated at 160 V for 20 milliseconds, using a Gene Pulser. After electroporation, the cells were transferred into prewarmed αMEM medium containing 10 % fetal bovine serum, 2 mM L-glutamine, 100 units/ml penicillin and 100 μg/ml streptomycin in 6-well plate, and cultured in a humidified 37 ^{0}C incubator with 5% CO_2. Twenty four hours after transfection, the cells were lysed in a lysis buffer containing 50 mM Tris-HCl (pH8.0), 150 mM NaCl, 0.1% SDS, 1% Triton X-100, 1 x Phosphatase Inhibitor, and 1 x Protease Inhibitor cocktail (Sigma, ST. Louis, MO) 24 hours after transfection. An aliquot of 30 μg cellular protein was separated on a 10% SDS-polyacrylamide gel and transferred to nitrocellulose. The membrane was incubated at 4 ^{0}C overnight in a buffer containing 5% dry skim milk, 150 mM NaCl, 50 mM Tris-HCl (pH 8.0), and 0.05% Tween-20. Immunoblotting was performed in the same buffer containing 0.2 μg/ml antibody against Flag (Sigma) or GFP (Santa Cruz, CA) at room temperature for 1 hour. Specific proteins were detected using appropriate secondary antibodies and Enhanced Chemiluminescence's Plus Western blotting detection system (Amersham Pharmacia Biotech UK Limited, Buckinghamshire, England). The cells in a parallel plate were trypsinized 24 hours post transfection and analyzed by fluorescence-activated cell sorter (FACS) (BD Biosciences, San Lose, CA) to assess the transfection efficiency. Another 6-well plate of cells was fixed in 0.05% glutaraldehyde for alkaline phosphatase (ALP) staining 3 days after transfection (4).

Our studies demonstrated that twenty-four hours after electroporation, the GFP reporter gene was expressed in most of MC3T3-E1 cells transfected with either pHGCX (Fig 2A) or pHGCX/Flag-Osx (Fig 2B). Flow cytometry analyses revealed more than 94% of the osteoblast cells transfected with the pHGCX or the pGHCX/Fla-Osx plasmid expressed GFP (Fig 2C & D). We have repeated the experiments and found that the efficiency of nucleoporation is reliable. The variation in transfection efficiency was less than 1%, and the viability of electroporated cells were more than 90%. In comparison with our previous data, the efficiency of gene transfer by nucleoporation was approximately 10% higher than that of a viral delivery system mediated by a HSV-amplicon in mouse preosteoblast cells (5). The transgene expression of GFP and Flag-Osx was easily detected in the cells transfected with pHGCX/Flag-Osx by utilizing Western blot with specific antibodies against Flag and GFP (Fig 2E). The pHGCX/Flag-Osx transfected cells expressed high levels of Flag-Osx fusion protein. As expected, the Flag-Osx fusion protein was undetectable while the expression of GFP was present in the cells transfected with pHGCX (Fig 2E). To assess osteoblast differentiation in the cells expressing the Osx transgene, we carried out an ALP staining 3 days after transfection (Fig 3). Approximately 20% of the osteoblast cells overexpressing Osx were differentiated and exhibited positive ALP-staining (Fig 3A). In contrast, less than 1% ALP-positive cells were seen in the control cells overexpressing GFP only (Fig 3B).

Our studies indicated that non-viral gene transfer of nucleoporation can efficiently deliver plasmid DNA directly into the nuclei of preosteoblast cells. The transgene is consistently active and

visible for more than 5 days, although the intensity of the GFP reporter becomes weaker with the culture time. A high level of transgene expression of GFP and Osx in the transfected cells was visual as early as 4 hours after electroporation and mediated cell differentiation, validating the application of nucleoporation technology for functional studies of candidate genes. Although the protocol provided in this study is specific to MC3T3-E1 cells, the system can be applied to other types of cells by modifying pulse time, voltage, and nucleofection buffer. In general, an electroporation with a low-voltage and prolonged pulse time can be applied to primary cells while a high-voltage and short pulse time should be considered for immortalized cell lines. Large cells require a low-voltage pulse.

In vivo testing of candidate genes in a transgenic mouse is time-consuming and expensive, requiring the injection of a DNA fragment into fertilized eggs and the examination of mouse phenotypes. Therefore, it would be more efficient to use *in vitro* cell models via viral or non-viral gene transfer approaches to test candidate gene function before initiating *in vivo* transgenic studies. Although infectious viral transduction medicated by a HSV amplicon provides an alternative approach, the intensive work of purifying viral particles and potential contamination of viral particles limits its wide use. The studies provided here demonstrate that cloning the cDNA of an unknown gene into the pHGCX expression vector can be accomplished within a week. By utilizing this approach, a candidate gene search in a QTL region is cheaper, safer, and faster once an appropriate cell model and end points for candidate gene function are determined. Our data also indicates that it is feasible to use the Gene Pulser for nucleofection once the conditions of pulse voltage and time are optimized. In addition, nucleoporation overcomes the limitation of infectious BAC (iBAC) technology to allow testing of the genes that iBAC cannot apply (1-3). In this regard, our data demonstrate that nucleoporation in MC3T3-E1 cells can be used as another gene transfer system for high throughput screening to identify genes important for osteoblast cell differentiation.

In conclusion, we have successfully established another non-viral gene transfer system for functional testing of candidate genes in our QTL regions. We believe that the approaches of viral and non-viral transgene delivery are useful for our future studies.

Figure 1

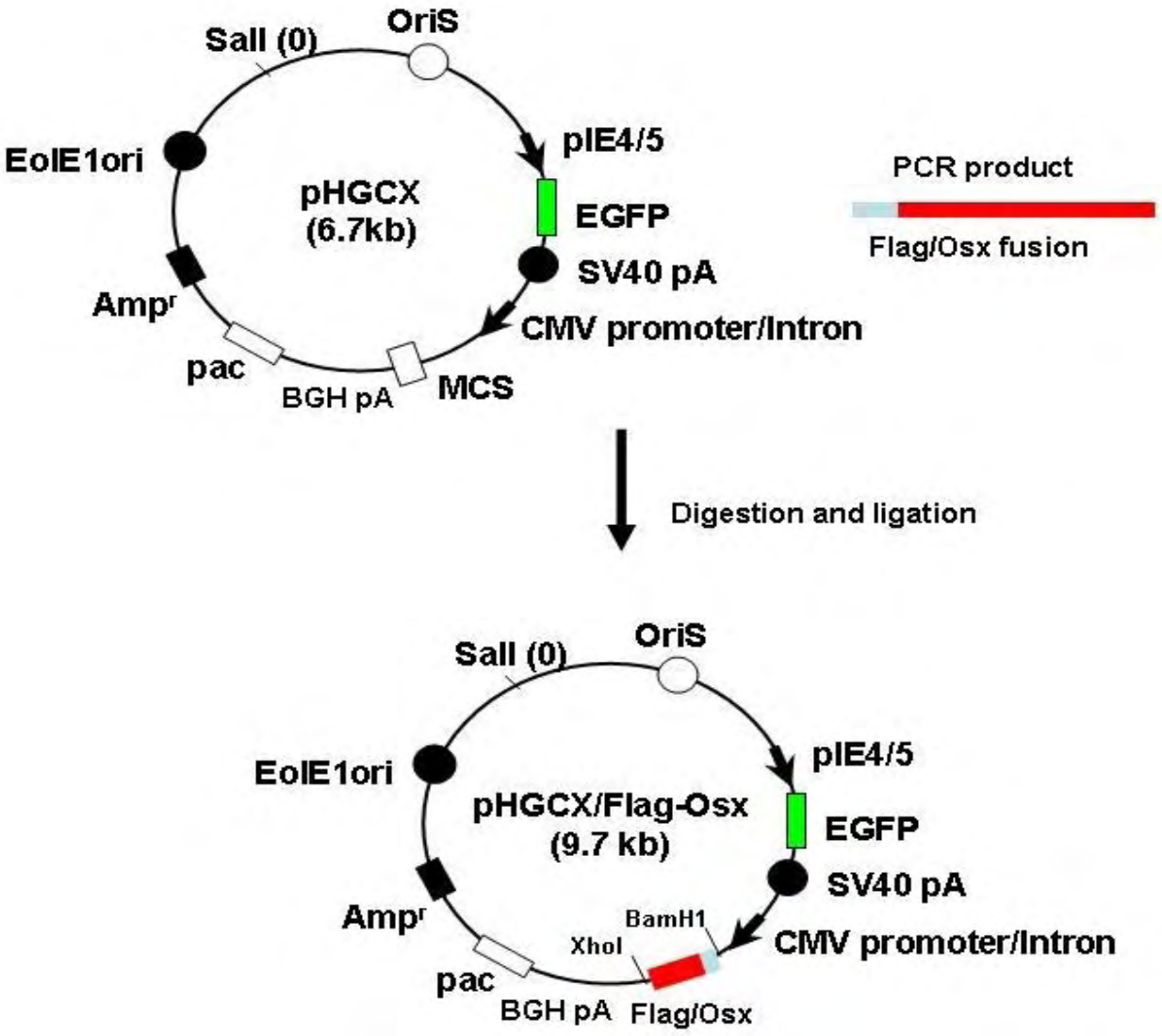

Figure 1. A schematic diagram of pHGCX/Flag-Osx construction. The PCR product of mouse osterix (Osx) coding sequence tagged with Flag is inserted into the BamH1 and XhoI sites downstream of the CMV promoter/intron of pHGCX plasmid to generate an expression vector of pHGCX/Flag-Osx.

Figure 2

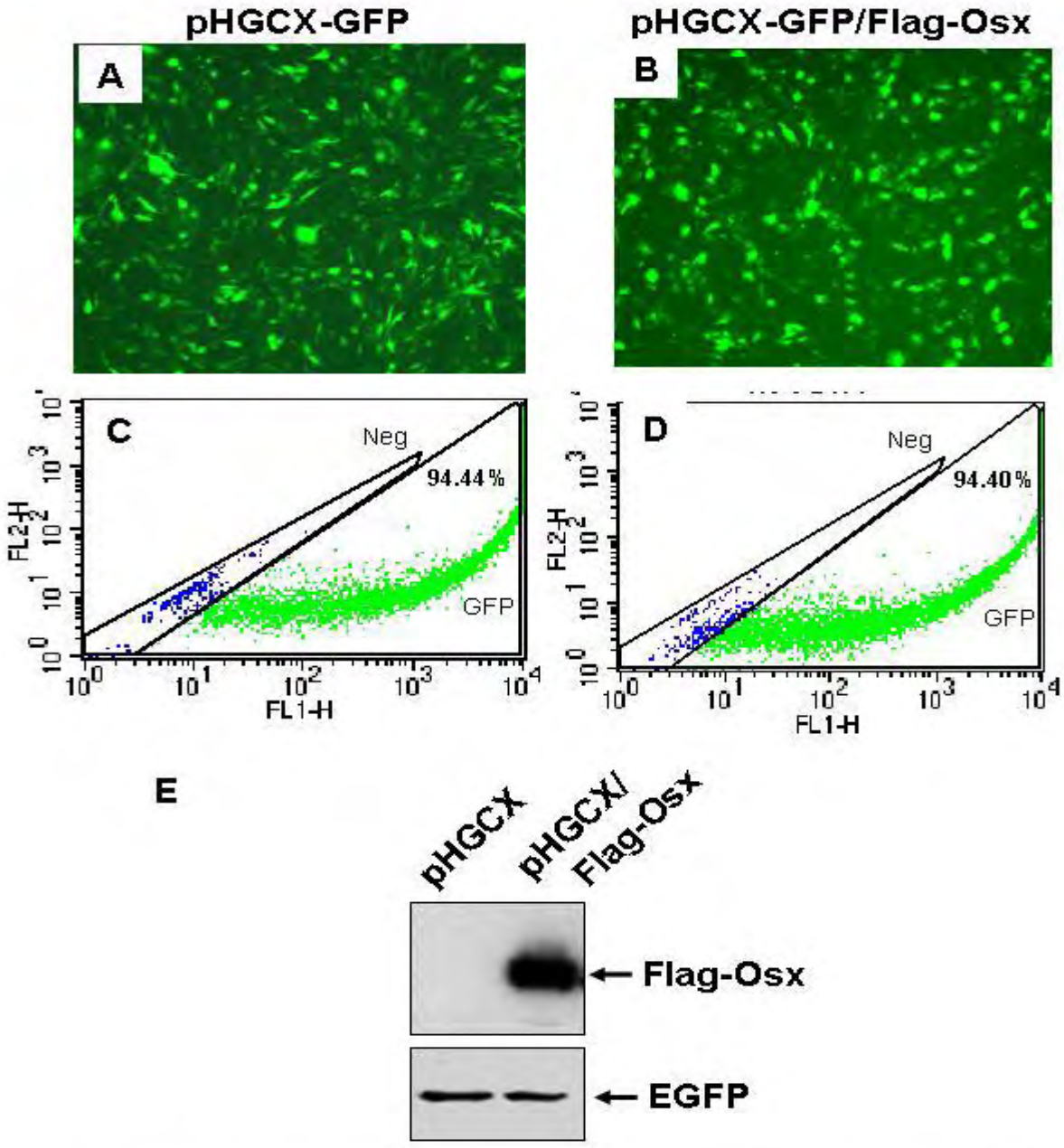

Figure 2. Transgene expression in MC3T3-E1 cells transfected by nucleoporation. **A & B**: GPF expression in MC3T3-E1 cells transfected with pHGCX and pHGCX/Flag-Osx, respectively; **C & D**: Representative data of flow cytometric analysis in the cells transfected with pHGCX and pHGCX/Flag-Osx, respectively; **E**: Flag-Osx and GFP protein expression in MC3T3-E1 cells transfected with pHGCX and pHGCX/Flag-Osx, respectively, detected by Western blot.

Figure 3

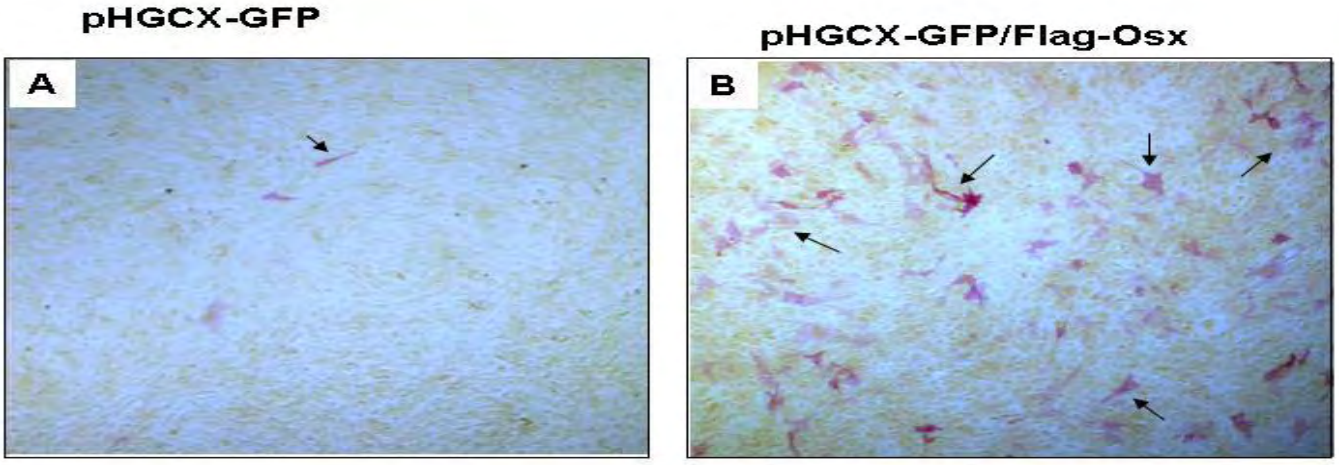

Figure 3. Alkaline phosphatase (ALP) staining of differentiated MC3T3-E1 cells (x 40 images). MC3T3-E1 cells are subjected for ALP staining 72 hours after transfection. **A**: the cells transfected with pHGCX control plasmid; **B**: the cells transfected with pHGCX/Flag-Osx. Arrows indicate the ALP-positive cells.

Key Research Accomplishments:

- Have validated cost-effective, safer non-viral deliver approaches, and established that the expression of coding sequences of candidate gene can compensate for the limitation of infectious BAC gene transfer.

Reportable Outcomes:

1. Xing W, Baylink D, Kappor A and Mohan S. A platform of high-efficiency non-viral gene transfer in mouse osteoblast cells in vitro. Molecular Biotechnology 34(1):29-35, 2006

2. Xing W, Baylink D, Kesavan C and Mohan S. HSV-1 Amplicon-Mediated Transfer of 128-kb BMP-2 Genomic Locus Stimulates Osteoblast Differentiation *in vitro* Biochem Biophys Res Commun 319(3): 781-6, 2004

3. Xing W, Baylink D, Kesavan C and Mohan S. Transfer of 128-kb BMP-2 Genomic Locus by HSV-Based Infectious BAC Stimulates Osteoblast Differentiation: A Platform for Functional Genomic Studies. *ASBMR-2004, 19 suppl 1: S150, 2004*

Conclusions

- We have successfully cloned the complete coding sequence of candidate genes into pHGCX expression vector, and deliver the transgenes into osteoblast cells with high efficiency by utilizing either viral HSV amplicon system or non-viral "Nucleoporation" approach.
- The osteoblast cells containing transgenes express high level of proteins for functional studies.
- Transfer of the coding sequence of candidate genes into bone cells provides an alternative approach for functional studies when the infectious BAC technique is not applicable.

References:

1. Cortes, M. L., Bakkenist, C. J., Di Maria, M. V., Kastan, M. B., and Breakefield, X. O. HSV-1 amplicon vector-mediated expression of ATM cDNA and correction of the ataxia-telangiectasia cellular phenotype. Gene Ther 10*:*1321-7; 2003.
2. Lenz, P., Bacot, S. M., Frazier-Jessen, M. R., and Feldman, G. M. Nucleoporation of dendritic cells: efficient gene transfer by electroporation into human monocyte-derived dendritic cells. FEBS Lett 538*:*149-54; 2003.
3. Wade-Martins, R., Saeki, Y., and Antonio Chiocca, E. Infectious delivery of a 135-kb LDLR genomic locus leads to regulated complementation of low-density lipoprotein receptor deficiency in human cells. Mol Ther 7*:*604-12; 2003.
4. Wergedal, J. E., and Baylink, D. J. Characterization of cells isolated and cultured from human bone. Proc Soc Exp Biol Med 176*:*60-9; 1984.
5. Xing, W., Baylink, D., Kesavan, C., and Mohan, S. HSV-1 amplicon-mediated transfer of 128-kb BMP-2 genomic locus stimulates osteoblast differentiation in vitro. Biochem Biophys Res Commun 319*:*781-6; 2004.

PROJECT 4

PRINCIPAL INVESTIGATOR: Henry J. Klamut, Ph.D.

TITLE: The Application of Transgenic Mice to Assess Gene Function in Mechanical Loading and In Bone Fracture Healing Models

Project 4: The Application of Transgenic Mice to Assess Gene Function in Mechanical Loading and in Bone Fracture Healing Models

Introduction

Bone formation in response to exercise or injury requires the coordinated interactions of a number of molecular pathways of gene expression. However, a more complete understanding of gene expression in bone formation and fracture repair requires definitive proof of the functional significance of the genes that regulate the molecular pathways. In this regard the analysis of mice engineered to be deficient in the expression of a particular gene-of-interest (i.e., knockout mice) is especially valuable. The study of knockout mice provides conclusive evidence of the functional significance of particular genes in the development and repair of bone. The use of knockout mice in studies of bone development and repair will eventually help to elucidate the regulation of their molecular regulatory pathways, and suggest therapeutic strategies and gene candidates to augment or accelerate bone formation and repair.

We have utilized knockout mice to determine the effect the absence of expression a particular gene of interest has on bone formation in response to mechanical loading and in fracture repair. Not only will the examination of bone formation and repair characterize the functional effects of the knockout gene deficiency in each case, but subsequent examination of the expression of other genes in these knockout mouse tissues will help to define the regulatory networks that modulate the observed knockout phenotype. Ultimately, this approach will further the understanding of gene regulation in skeletal tissues and suggest additional gene candidates for therapeutic alternatives in bone formation and healing.

Body

Technical Objectives

Our original Technical Objectives were as follows:

Technical Objective 1: The functional significance of a gene of interest on bone formation will be identified by characterizing the skeletal phenotype in mice deficient in that gene (i.e., knockout mice) in response to mechanical loading of the bone by exercise.

Our Specific Objectives were as follows:

1. to complete the identification of phenotypic differences between 3 strains of knockout mice and wild-type control mice by peripheral quantitative computed tomography (pQCT), micro-CT measurements, histological examination and molecular marker expression of the bone response to mechanical loading.
   The Specific Objectives for this continued reporting period is listed below. (see 12-month timeline #1, serpine and #3, #4 and #5 for Ephrin B-1, and 3-month timeline #2 for Ephrin B-1, below).
2. to apply microarray technology to study gene expression in the loaded bones of the one strain of knockout mice that exhibited the greatest phenotypic differences in bone response to mechanical loading.

Technical Objective 2: The functional significance of a gene of interest on bone formation in response to injury will be identified by characterizing the skeletal phenotype in mice deficient in that gene (i.e., knockout mice) during fracture healing.

Our Specific Objectives for fracture repair were as follows:

1. to complete the identification of phenotypic differences between 3 strains of knockout mice and wild-type control mice by X-ray examination, pQCT measurements, micro-CT measurements and histological examination of the fracture callus tissues (see the timeline for 12-month period #2 serpine, below).
2. to apply microarray technology to study gene expression in the fracture tissues of the one strain of knockout mice that exhibited the greatest phenotypic differences in fracture healing. This analysis continues from the previous reporting period.

Timelines

Our specific objectives during the **first 12 months** of this continuation grant period are as follows:

1) To characterize the skeletal phenotype of mice lacking plasminogen activator/inhibitor gene (serpine) and corresponding control mice by using PIXImus, PQCT and histology.
2) To introduce femoral fracture in the knockout and control mice and evaluate new bone formation by pQCT at different times after initiation of fracture. We will initiate histology studies to identify the cell types that are affected in the knockout mice during fracture repair.
3) To obtain breeding pairs of loxP Ephrin-B1 mice from our collaborator, Dr. Philippe Soriano at Fred Hutchinson Cancer Center, Seattle and establish a colony.
4) Breed loxP Ephrin-B1 mice with type I collagen cre mice to generate cre positive loxP homozygous experimental and cre negative loxP homozygous control mice.
5) To characterize the skeletal phenotype of mice lacking Ephrin-B1 specifically in osteoblasts using PIXImus, pQCT and histology.

Our objectives during the **final 3 months** of the continuation grant are as follows:

1) To complete histology studies in mice lacking plasminogen activator/inhibitor and control mice
2) To evaluate the effects of four point bending in Ephrin-B1 conditional knockout mice.

B. Description of Knockout Mouse Strains

To obtain direct experimental evidence to evaluate functional importance of candidate genes in fracture repair and mechanical loading, we have proposed to use transgenic mouse models lacking a gene of interest. The rationale for focusing on knockout mouse models for functional studies is based on widely accepted view in the scientific community that knockout mouse models represent an ideal system for conclusively demonstrating the functional significance of a gene of interest.

Table 1. Knockout (KO) Mice with Phenotypes for Mechanical Loading and Fracture Studies

Gene	JAX[1] Stock #	Genotype[2]	Phenotype
Leptin	0632	B6-*Lep* ^{ob}	NIDDM, obese, delayed wound healing
Bax	2994	B6.129X1-*bax* ^{tm1Sjk}	delayed apoptosis, organ defects (gonads)
Serpine	2507	B6.129S2-Serpine1^{tm1Mlg}/J	enhanced wound healing, fibrinolysis
Ephrin B-1	None	B6.loxP Ephrin-B1	regulator of osteoblast cell functions

1: JAX, The Jackson Labs
2: The wild-type control strain genotype is C57BL/6 (B6).

a) Leptin Knockout (Obese, *ob/ob*) Mice:

Leptin, a 16 kDa protein, expressed predominantly in adipose tissue, functions as a hormone that keeps the brain apprised of the amount of body fat and regulates carbohydrate metabolism (4). This mouse is also a model for non-insulin dependent (NIDDM, Type 2) diabetes (Table 1). Other functions related to bone formation include:

i) Stimulating osteoblastic differentiation and mineralization of bone matrix (5).
ii) Stimulating the development of the periosteal envelope in growing bone (6).
iii) Bone formation increases by peripheral leptin administration and decreases by third ventricle leptin infusion in *ob/ob* mice (7). The systemic versus local effects of leptin on the fat and bone cell lineages are not well characterized, though osteoblasts do have leptin-specific receptors (8).

The heterozygous ob/ob knockout breeder mice were purchased from the Jackson Labs and bred in our animal facility. Because of the character of recessive inheritance, only ¼ of pups were expected to be homozygous. The homozygous mice were identified by both the obese phenotype and PCR-based genotyping for the ob mutation.

b) Bax Knockout Mice:

Bax, the Bcl-2-associated X protein and a member of the Bcl-2 protein family, binds to Bcl-2 to form a heterodimeric complex. It functions to oppose Bcl-2 and promote apoptosis. The Bax/Bcl-2 ratio controls the apoptosis frequency in each cell (reviewed in 9). Both genes are expressed in cartilage and bone cells in the rat. Apoptosis has a major impact on skeletal development and remodeling, and is essential for the elimination of osteoblasts during skeletal development. The frequency of osteoblast apoptosis controls osteoblast lifespan and bone formation during the postnatal life (10).

Heterozygous breeder mice were purchased from the Jackson Labs and bred in our animal facility. These mice display a lymphoid hyperplasia and male germ cell death due to Bax deficiency (11). Only ¼ of all pups were expected to be homozygous mice, and all mice were identified by PCR-based genotyping for the Bax gene deletion. There is no obvious Bax mouse phenotype.

c) Serpine Knockout Mice:

The fibrinolytic system has been claimed to play a very important role in a variety of biological phenomena and wound healing, such as maintenance of vascular patency, inflammation, embryogenesis, angiogenesis and tissue remodeling processes. Activation of plasminogen by tissue-type plasminogen activator (t-PA) is believed to be required for these functions. However, specific plasminogen activator inhibitor (PAI-1; Protease Nexin-1, PN-1) appears to be the primary physiological inhibitor for this fibrinolytic system. Theoretically, the removal of PAI-1 should result in more or faster plasminogen activation and enhance the process of fibrin-specific clot lysis, promoting healing after fracture or other tissue injury (reviewed in 12).

Homozygous breeder mice (PAI-1 deficiency), in which the Serpine-1 gene is disrupted (1), were purchased from the Jackson Labs and bred in our animal facility. The homozygous mutants have a mild hyperfibrinolytic state but normal hemostasis. There is no obvious serpine knockout mouse phenotype. The genotype of all breeders and pups was identified by PCR-based genotyping for the serpine-1 gene deletion.

d) LoxP-Ephrin B-1 (Conditional) Knockout Mice:

In our continuation studies, we have chosen to identify the role a new genes, Ephrin B-1, in fracture repair and mechanical loading. We have chosen Ephrin B-1 since this gene is differentially expressed in bone in response to four-point bending, and since Eph-ephrin signaling has been implicated in the regulation of many critical events during development in a number of tissues including bone (2). Specifically, disruption of Ephrin-B1 resulted in perinatal lethality associated with a range of skeletal phenotypes including abnormal skeletal patterning (3). We propose to conditionally disrupt Ephrin B-1 in osteoblasts and evaluate its role in bone formation in response to mechanical loading. Such conditional knockouts are generated when the LoxP-Ephrin B-1 gene is established in an animal and bred to an animal with a combination of a promoter from a gene of interest (in our case a bone-specific collagen) and Cre, an endonuclease that excises sequences between Loxp sites. In this way the activation of the collagen promoter in bone expresses Cre and results in the tissue-specific excision of Ephrin B-1 gene with LoxP. This conditional knockout technique is well refined and produces tissue (i.e., bone)-specific knockouts, yet avoids the pre-, peri- and post-natal mortality and morbidity that often accompany more conventional, global gene knockout approaches.

C. Progress on Technical Objectives

Technical Objective 1:

Mechanical loading determines both the mechanical density and the architecture of bone. In this study, we used knockout mice to identify and characterize the functional effects of exercise-induced bone formation in mice deficient for a gene-of-interest previously implicated in bone growth or development, or in wound healing (Table 1, “Leptin”, “Bax”, “Serpine” and “Ephrin

B-1" knockout, or KO, mice). The phenotypic response to mechanical loading in the leptin KO mouse was correlated to pQCT and molecular measurements of bone formation.

Specific Objective 1: to complete the identification of phenotypic differences between 3 strains of knockout mice and wild-type control mice by peripheral quantitative computed tomography (pQCT), micro-CT measurements, histological examination and molecular marker expression of the bone response to mechanical loading.
The Ephrin B-1 knockout mouse strain was examined for fracture healing during the 12-month continuation period, when the Specific Objectives are:

1) To obtain breeding pairs of loxP Ephrin-B1 mice from our collaborator, Dr. Philippe Soriano at Fred Hutchinson Cancer Center, Seattle and establish a colony.
2) Breed loxP Ephrin-B1 mice with type I collagen cre mice to generate cre positive loxP homozygous experimental and cre negative loxP homozygous control mice.
3) To characterize the skeletal phenotype of mice lacking Ephrin-B1 specifically in osteoblasts using PIXImus, pQCT and histology.

The Ephrin B-1 knockout mouse strain was also examined during the final 3-month continuation period, when the third Specific Objective of that period is:

3) To evaluate the effects of four point bending in Ephrin-B1 conditional knockout mice.

Findings

Leptin Knockout Mice:

As reported previously, when the loading routine is normalized for bone size, the absence of leptin expression does indeed affect the cortical and total bone mineral content and bone mineral density in response to mechanical loading.

These differences were too subtle to be observed by an examination of the bone histology and histomorphometry. Micro-CT measurements were not attempted, both because of the success of the pQCT measurements and the lack of availability of the micro-CT instrument.

Bax Knockout Mice:

There were statistically significant differences in the response of only very few of the bone parameters in the Bax knockout mice as compared to the wild-type control mice applied at 6N loading and described in the previous reporting period. By pQCT measurements, however, the leptin knockout mice produced a more dramatic response to mechanical loading and were chosen for microarray analysis of gene expression induced by mechanical loading.

Serpine Knockout Mice:

The serpine mouse mechanical loading study has suffered from delayed purchasing and breeding. This portion of work for this strain is being transferred to the potentially very interesting Ephrin B-1 knockout mouse. It is expected to be conducted during the next 12 months.

Ephrin B-1 Knockout Mice:

We have received a breeding pair of EphrinB-1 loxp mice whose exons 2-5 of the EphrinB-1 gene were flanked by loxp sites from Dr. Philippe Soriano at Fred Hutchinson Cancer Center, Seattle (2) and started to expand the breeding of this transgenic loxp mouse line. To generate

osteoblast-specific conditional knockout mice, we first crossed homozygous EphrinB-1/loxp females with B6 males that express Cre recombinase under the control of type 1-alpha-2 collagen promoter to generate Cre positive EphrinB-1/loxp hemizygous males. We then bred the homozygous loxp females with Cre positive loxp hemizygous males to generate Cre positive homozygous/hemizygous loxp mice and Cre negative homozygous/hemizygous loxp mice for our experiments. The Cre positive loxp mice will be used as experimental mice for bone fracture and mechanical loading and the Cre-negative loxp mice from the same litter will be set up as control mice.

Mice carrying the conditional allele of EphrinB-1 are genotyped by PCR on tail DNA using the following primers: 5'-tggccttacacccgcttaag-3, 5'-agcagtggggtagtgactacc-3'. The PCR product of loxp is 500 base pairs, and the PCR product of wild-type allele of EphrinB-1 is 250 base pairs. We expected to generate Cre positive loxp homozygous females (25%), Cre negative loxp homozygous females (25%), Cre positive loxp hemizygous males (25%) and Cre negative loxp hemizygous males (25%) from the above breeding scheme.

Unfortunately, our preliminary data of breeding showed that lease than 5% of pups were Cre-positive loxp homozygous females. Therefore, we hypothesize that some of the Cre positive homozygous females may die prior to birth because of X chromosome-linked mutation of EphrinB-1 gene. We will examine this possibility in our future studies. *At this time this breeding problem has prevented the completion of the Specific Objective.*

In the interim, we are expanding the EphrinB-1 osteoblast-specific knock out mouse line. Once we have enough numbers of experimental knock out mice and corresponding control mice, we will characterize the skeletal phenotypes by using PIXImus, pQCT and histology. We will perform four-point bending analysis in We will perform four-point bending in conditional knockout mice once we have enough numbers of EphrinB-1 knockout mice (10 weeks old, males and females). Microarray examination of gene expression in EphrinB-1 knockout mice and control mice can then follow successful mechanical loading analysis.

Specific Objective 2: to apply microarray technology to study gene expression in the loaded bones of the one strain of knockout mice that exhibited the greatest phenotypic differences in bone response to mechanical loading.

This Specific Objective was completed for the leptin knockout mice. The analysis is ongoing, and preliminary summary of the numbers of genes in leptin mice exhibiting statistically significant differences in response to loading is presented below (Table 2).

Table 2. Gene Counts: Leptin KO Loading Microarray Gene Swap						
Dyes	**Total Genes**					
	All			2-fold difference		
	Up	Down	Total	Up	Down	Total
Cy5	1013	128	1141	141	55	196
Cy3 Swap	497	312	810	105	65	170
Dyes	**Known Genes**					
	All			2-fold difference		
	Up	Down	Total	Up	Down	Total
Cy5	905	82	987	98	29	127
Cy3 Swap	443	275	719	74	47	121
Dyes	**Unknown Genes**					
	All			2-fold difference		
	Up	Down	Total	Up	Down	Total
Cy5	108	46	154	43	26	69
Cy3 Swap	54	37	91	31	18	49
n=5, 3 females, 2 males						

Up to approximately 1000 known and unknown genes displayed changes in gene expression in response to mechanical loading. In this regard, the unknown genes are of particular interest, as they comprised approximately 10% of the total number of genes with expression changes and suggest a complex regulation of bone formation. The accuracy of the measurement was checked using the "dye swap" approach and seems to provide similar data in each case, but especially for the genes with greater than 2-fold changes in expression. The Cy3 analysis did seem to be less sensitive, however.

The microarray analysis continues, but this strain presents challenges in procedures due to sensitivity to anesthesia produced by its obesity. Moreover, the interpretation of gene expression is complicated by the diabetes that accompanies such weight gain. The phenotypic analysis of the leptin KO mouse strain provided valuable information. As reported below, the phenotypic analysis of the mechanical loading data revealed sex-related differences in bone size that were pursued in a study that was recently concluded. The microarray data in the male and female mouse tibias that underwent mechanical loading will be examined separately to attempt to identify sex-specific molecular markers of bone formation in this bone. Additionally, the mechanical loading analysis in the Ephrin B-1 KO mouse will be undertaken and microarray analysis of bone formation genes conducted should the phenotypic results suggest that this gene affects loading.

Additional Findings in Leptin Knockout Mice:

During the analysis of the leptin KO mouse phenotype, sex-related differences in the size of the femur were observed that were not observed in the tibias during the mechanical loading analysis. Androgen action is primarily anabolic, while the estrogens act mainly through the suppression of resorption. Because the sex hormones are influenced by body fat accumulation

and distribution (reviewed in 19), these findings suggest interactions with regulators of body fat, such as leptin. A study of this connection between sex-related bone size in leptin KO and wild-type mice was pursued. The initial results reported previously, but only recently completed. *This entire study represents an important description of sex-specific differences in bone size and is in addition to that described in the original Technical Objectives.*

The initial phenotypic comparison of body weight, total body fat and total lean body mass was performed on male and female mice at 10 weeks of age. Each study group contained at least 12 animals and was described in a previous report.

Bone parameters in male and female mice were compared at 12 weeks of age (Figure 1). The midpoint of the femoral diaphysis was analyzed by peripheral quantitative computerized tomography (pQCT). The periosteal circumference (PC), endosteal circumference (EC), total bone mineral density (BMD), total bone mineral content (BMC) and polar moment of inertia (MOI) using an analysis threshold of 630-630. pQCT measurements of the trabecular (marrow) bone area used an analysis threshold of 570-214. Each study group contained more than 11 animals. These thresholds were designed to provide the most accurate size measurements.

The MOI is an important addition to these measurements (Figure 1F), as it estimates the adaptive bone formation around the axis of the bone that might be expected in an obese subject such as the leptin knockout mouse (12). Because the polar moment of inertia was not significantly different in the leptin KO mice and the female wild-type mice, we conclude that the sex-specific differences in bone formation were not caused by a response to the increased load in the obese subjects. In summary, male leptin knockout mice displayed reductions in several parameters of bone size; the exception was the femur lengths, which were the not significantly different between males and females of either strain. Leptin deficiency appeared to cause a sex-specific reduction in bone size.

To more conclusively demonstrate that the differences in bone size in leptin KO mice sex-related, pre-pubertal male and female leptin KO mice were compared to pre-pubertal wild-type mice to determine whether these effects could be observed in the absence of the sex hormones. The reductions in the bone size in adult male leptin KO mice would not be expected in immature mice prior to the onset of puberty and sex hormone function. In this case, the pQCT parameters were adjusted to 150-300 to detect the less mineralized bone of such young animals. As can be seen in Figure 2, the body weight (A) and total lean body mass (C) were not significantly different in leptin KO mice versus their wild-type counterparts, though the body fat (B) was increased in both genders of the leptin KO mice, even at this early time.

An examination of the bone parameters in the pre-pubertal mice was then conducted in the pre-pubertal leptin KO and wild-type mice (Figure 3). There were no significant differences in any of the bone size parameters examined in the leptin KO and wild-type males or females prior to sexual maturity. This observation indicates that the observed reductions in the femur size in the adult male leptin KO mice were indeed influenced by sex hormone function.

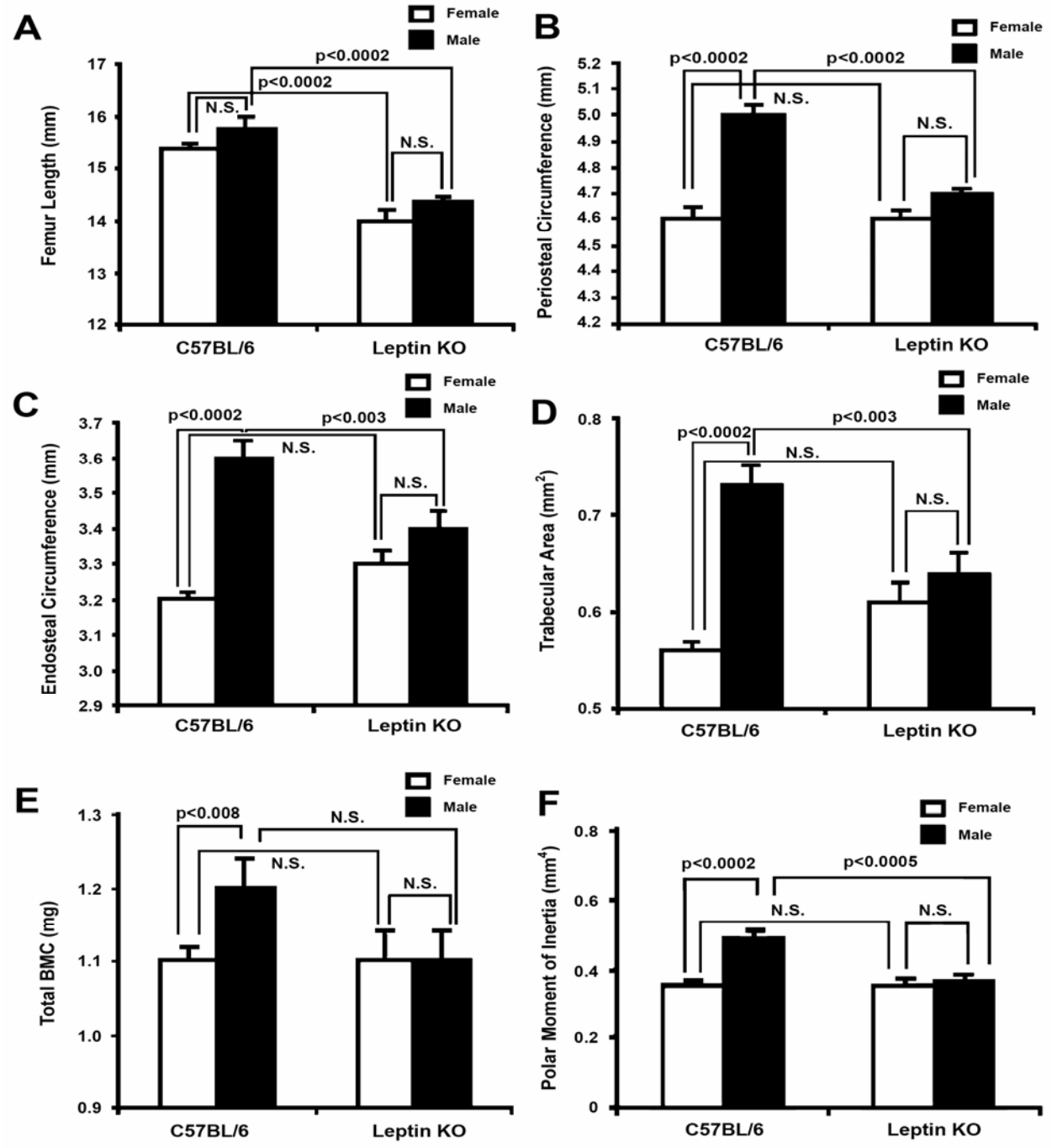

Figure 1. Summary of the phenotypic comparison of femurs from male and female leptin knockout (KO) and C57BL/6 wild-type mice. The addition of the polar moment of inertia data (F) to the previous measurements of (A) length, (B) PC, (C) EC, (D) TA and (E) total BMC completes the comparison of the sex differences for this bone. The other measurements were described in the previous reporting period. Values are expressed as mean +/- Standard Error of the Mean (SEM). Statistical analysis was performed by two-way ANOVA with a post-hoc Newman-Kuels Test. Differences were deemed significant at $p<0.05$.

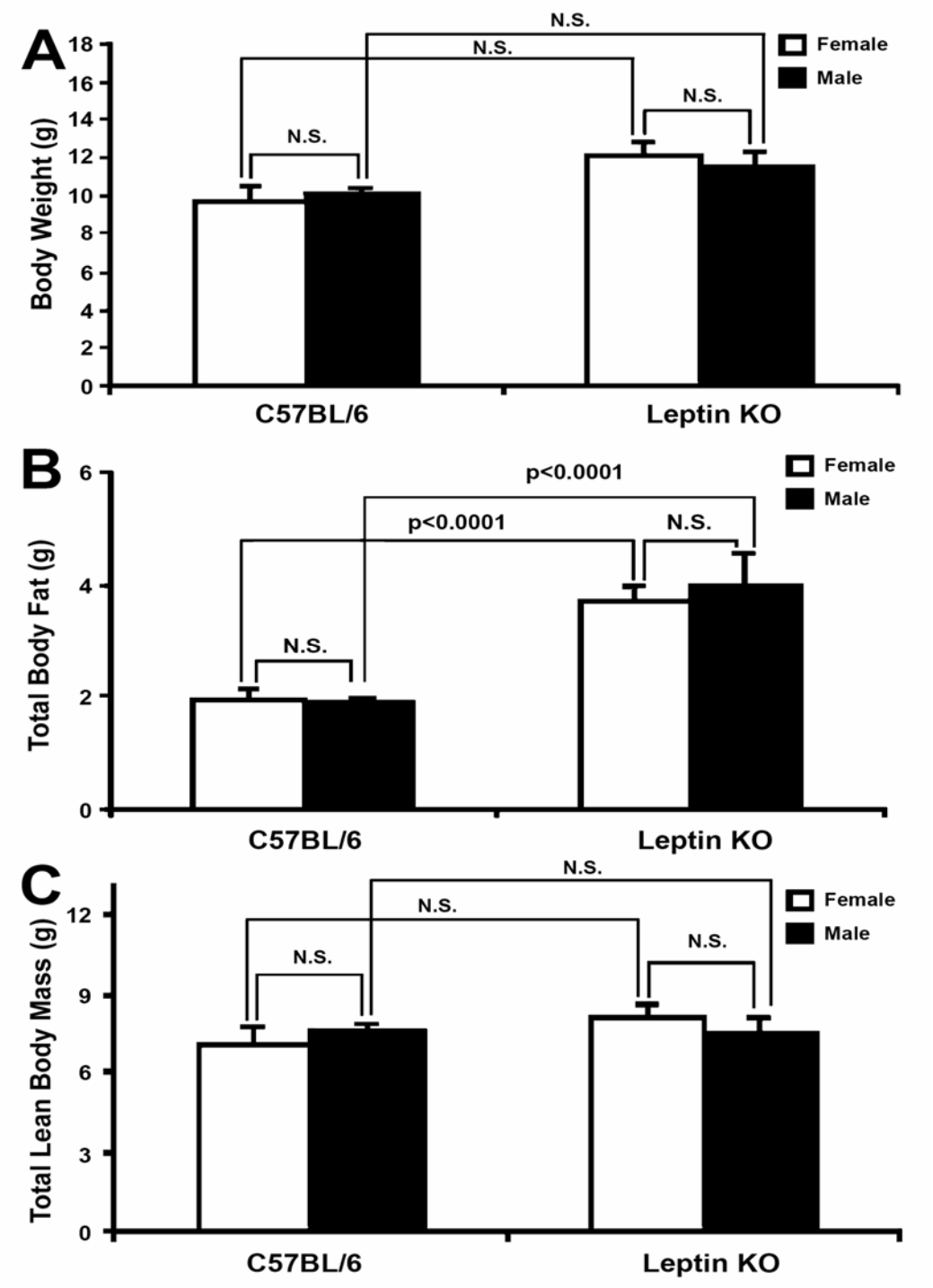

Figure 2. Phenotypic comparison of body characteristics in pre-pubertal male and female leptin knockout (KO) and C57BL/6 wild-type mice, (A) body weight, (B) total body fat and (C) total lean body mass. Values are expressed as mean +/- Standard Error of the Mean (SEM).

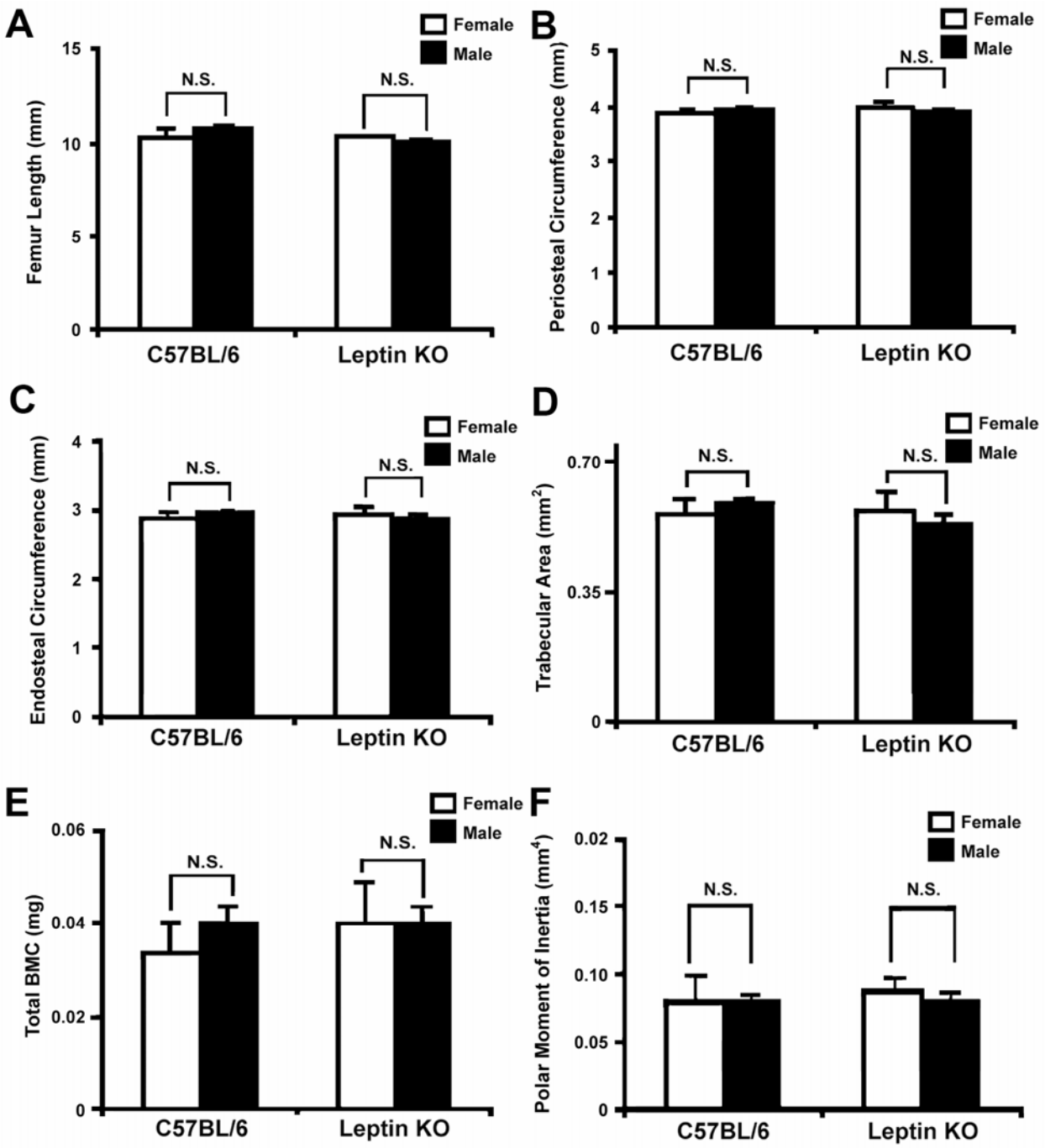

Figure 3. Summary of the phenotypic comparison of femurs from pre-pubertal male and pre-pubertal female leptin knockout (KO) and C57BL/6 wild-type mice. The measurements determined were those of the 10-week-old mice, (A) length, (B) PC, (C) EC, (D) TA, (E) total BMC and (F) polar moment of inertia. Values are expressed as mean +/- Standard Error of the Mean (SEM). Statistical analysis was performed by two-way ANOVA with a post-hoc Newman-Kuels Test. Differences were deemed significant if $p<0.05$.

Gender-specific differences in bone mass and size are suggestive of sex steroid hormone functions in bone metabolism (13). To determine whether a reduction in androgen levels might explain the effect of leptin deficiency on bone size, the circulatory levels of androgen and estrogen in male and female leptin knockout mice were more rigorously examined than in the previous report. In this case, each study group contained more than 18 animals and both testosterone and estradiol were measured in both males and females. As before, mouse sera were collected from the retro-orbital venous plexus under general anesthesia, and serum testosterone and estradiol were determined using the respective ^{125}Iodine radioimmunoassay (RIA) kits.

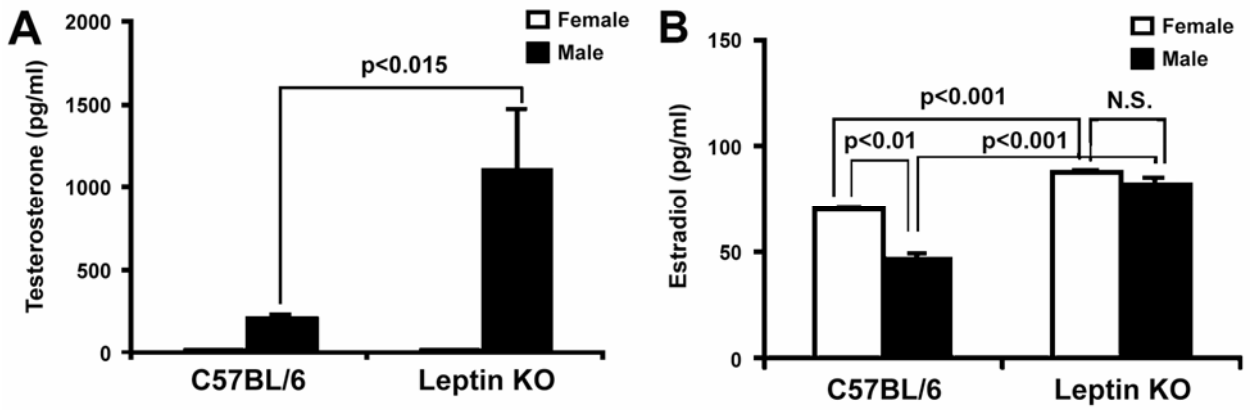

Figure 4. Comparison of serum sex hormone levels in leptin knockout (KO) and C57BL/6 wild-type male and female mice. This extension of the previous report examined each sex hormone in each gender of both strains (A) testosterone, (B) estradiol. Values are expressed as mean +/- Standard Error of the Mean (SEM). Statistical analysis was performed by two-way ANOVA with a post-hoc Newman-Kuels Test. Differences were deemed significant at $p<0.05$.

The serum testosterone levels in male leptin knockout mice were compared to C57BL/6 wild-type mice in the previous report and indicated that the loss of sex-specific characteristics in the body phenotype and bone parameters could not be attributed to a reduction in testosterone levels, but possibly to a defect in testosterone signaling (Figure 4). Estradiol levels were significantly higher in leptin knockout female mice, but the similarities in the body characteristics and femoral bone parameters between the C57BL/6 and leptin knockout female mice suggest that the effects observed in males were not estrogen-related.

We then examined androgen receptor expression in the leptin knockout mouse to determine whether androgen signaling is defective in the absence of leptin. As measured by real-time RT-PCR, we could find no significant differences in androgen receptor expression between male leptin knockout mice and male C57BL/6 wild-type mouse periosteal cells in response to testosterone stimulation in vitro. This observation remained the same, despite examining several different genes linked to testosterone function. A list of the testosterone genes examined is presented in Table 3.

Table 3. Androgen-responsive gene expression examined in response to testosterone stimulation of male leptin KO and wild-type periosteal cells in vitro

Androgen-Responsive Gene		
TFAM-A	CAMKKB	XORF43
RAB-7	NCL	SARG
NKX-3.1	SynSTK	SYTL4
HMG-20B	SIAH-BP	NGFRAP1
EAR-2	KIAA0830	Clusterin
BTG-1	BCOR	

We conclude that leptin deficiency in the male mouse resulted in a loss of several sex-specific differences in bone size that might be attributable to androgen effects on bone formation. These results contrast with previous studies that have established that leptin affects on bone formation, but have not evaluated sex differences (14). However, the molecular pathway remains difficult to elucidate, probably because of cross-talk between the components of the various intracellular signaling pathways, including the sex hormone and leptin pathways. Because of obvious implications for the interactions of bone size, obesity and sex hormone effects, we will continue to investigate this phenomenon in leptin knockout mice, especially with respect to androgen signal transduction.

Technical Objective 2:

The functional significance of a knockout gene of interest in fracture repair has been studied by a comparison of femur fracture healing in knockout mice deficient in that gene with wild-type control mice. The three knockout mouse strains examined were the Leptin KO, Bax KO and Serpine KO mice (Table 1). A description of each knockout mouse, the relevance of the phenotype to bone formation in mechanical loading and fracture repair and the results of our breeding program are provided (above).

Bone formation was measured following healing intervals that have been determined to provide characteristic landmarks of fracture callus maturation in initial experiments in wild-type mice. The phenotypic response to fracture healing in the particular strain of knockout mouse was correlated to X-ray and molecular measurements of bone formation and histologic examination of the fracture tissues. These measurements were used to determine whether the knockout gene-of-interest was functionally significant in fracture healing, and which fracture tissues were affected by the absence of its expression.

Specific Objective 1: to complete the identification of phenotypic differences between 3 strains of knockout mice and wild-type control mice by X-ray examination, pQCT measurements, micro-CT measurements and histological examination of the fracture callus tissues. This Specific Objective is the completion of the fracture studies undertaken in Bax knockout mice.

The Serpine (PAI-1) knockout mouse strain was examined for fracture healing during the 12-month continuation period, when the Specific Objectives are:

1) To characterize the skeletal phenotype of mice lacking plasminogen activator/inhibitor gene (serpine) and corresponding control mice by using PIXImus, PQCT and histology.

2) To introduce femoral fracture in the knockout and control mice and evaluate new bone formation by pQCT at different times after initiation of fracture. We will initiate histology studies to identify the cell types that are affected in the knockout mice during fracture repair.

The Serpine (PAI-1) knockout mouse strain was also examined for fracture healing during the final 3-month continuation period, when the fourth Specific Objective is:

4) To complete histology studies in mice lacking plasminogen activator/inhibitor and control mice

An extensive analysis of the phenotype of the serpine KO skeleton was performed through a pQCT comparison the femurs with wild-type femurs. In each case male mice were examined. This approach was adopted instead of the PIXImus and histology examinations because we have extensive experience with femur measurements with respect in the leptin KO mouse, and data can be most easily used to interpret the phenotype in the fracture repair model. Analysis was performed at the midshaft fracture scan (pQCT slice 5) under thresholds that rigorously identify the cortical bone (630-630). *The results of the serpine KO bone phenotype analysis that completed this Specific Objective are presented below.*

Findings

Serpine Knockout Mice:

An examination of several parameters of the femoral cortical bone revealed significant differences in the size of serpine KO mice versus wild-type mice. Specifically, the periosteal and endosteal circumferences were smaller in the serpine KO mice (Figure 5). The length of the bone was also less in the serpine KO mice (Figure 5), which is consistent with an overall size reduction and not merely a reduction in circumference in a femur of the same length as the wild-type femur.

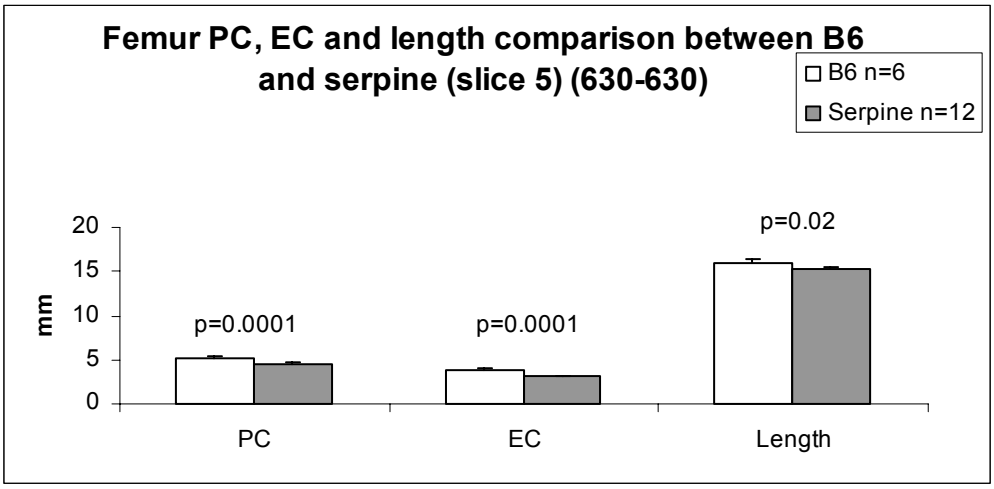

Figure 5. Comparison of femur dimensions in male serpine KO and wild-type mice. Cortical bone pQCT thresholds (630-630) were compared at a mishaft scan (slice 5). Periosteal circumference (PC), endosteal circumference (EC) and femur length were compared in 12 serpine KO and 6 wild-type mice. Data is presented as the mean +/- standard error of the mean. Statistics were performed by t-Test.

An examination of the bone mineral content and the area also revealed significant reductions in the serpine KO femur (Figure 6). These results indicate that the mineral content and the area it occupies are lower in serpine KO femurs and consistent with a smaller bone as suggested by the bone circumference measurements (Figure 4).

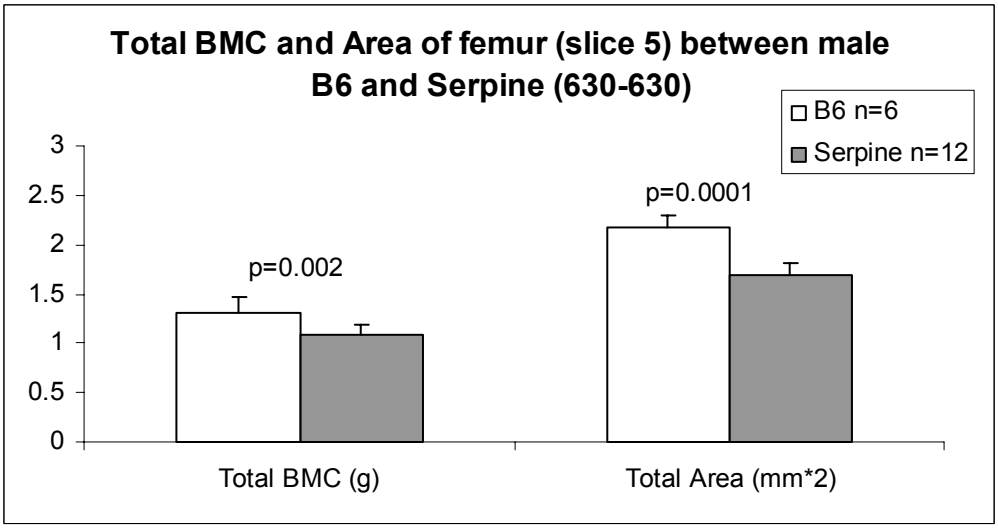

Figure 6. Comparison of femur cortical bone mineral content (BMC) and cortical area in male serpine KO and wild-type mice. Cortical bone pQCT thresholds (630-630) were compared at a mishaft scan (slice 5). BMC and area were compared in 12 serpine KO and 6 wild-type mice. Data is presented as the mean +/- standard error of the mean. Statistics were performed by t-Test.

An examination of the bone mineral density under these same pQCT thresholds revealed no significant difference between the serpine KO and wild-type mice (Figure 7). The bone mineral density measurement is consistent the bone mineral content of the serpine KO mice (Figure 7) in a smaller bone, as first suggested in the serpine KO femur circumference measurements (Figure 4).

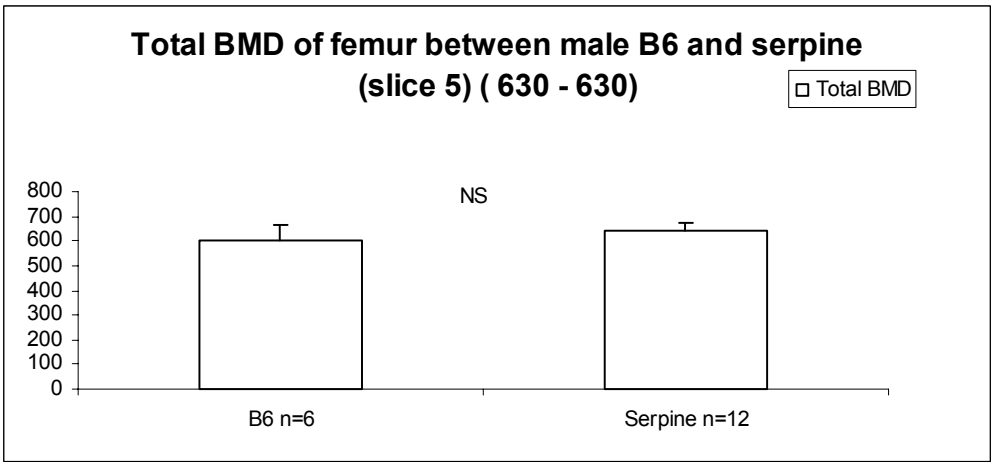

Figure 7. Comparison of femur cortical bone mineral density (BMD) in male serpine KO and wild-type mice. Cortical bone pQCT thresholds (630-630) were compared at a mishaft scan

(slice 5). BMD was compared in 12 serpine KO and 6 wild-type mice. Data is presented as the mean +/- standard error of the mean. NS, no significant difference.

An examination of the cortical polar moment of inertia (a measure of the mineralized cortical bone around the bone axis and an indicator of the torsional strength of the femur (Figure 8) confirms that the serpine mice have a smaller femur that might affect interpretations of native bone strength, as well as fracture healing. This is a critical observation, as this gene is important in extracellular matrix aspects of wound healing.

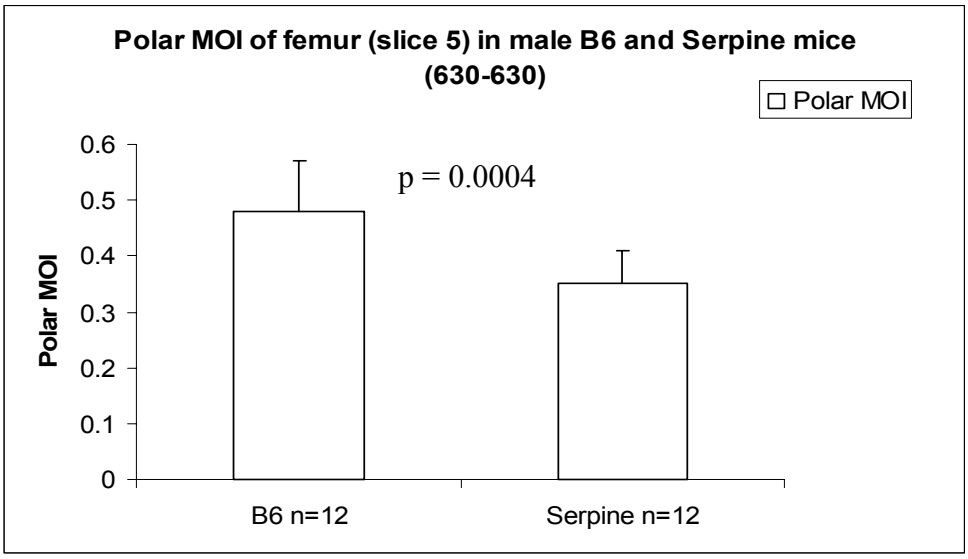

Figure 8. Comparison of femur cortical bone polar moment of inertia (MOI) in male serpine KO and wild-type mice. Cortical bone pQCT thresholds (630-630) were compared at a mishaft scan (slice 5). Polar MOI was compared in 12 serpine KO and 6 wild-type mice. Data is presented as the mean +/- standard error of the mean. Statistics were performed by t-Test.

Ephrin B-1 Knockout Mice

Ephrin B-1 KO mice await the acquisition of sufficient numbers of mice to complete the phenotypic examination, as well as the mechanical loading analysis. *This problem has not allowed us to complete the Specific Objective at this time.*

Technical Objective 2:

Specific Objective 1: to complete the identification of phenotypic differences between 3 strains of knockout mice and wild-type control mice by X-ray examination, pQCT measurements, micro-CT measurements and histological examination of the fracture callus tissues. This Specific Objective is the completion of the fracture studies undertaken in Bax knockout mice.

The Serpine (PAI-1) knockout mouse strain was examined for fracture healing during the 12-month continuation period, when the Specific Objectives are:

3) To characterize the skeletal phenotype of mice lacking plasminogen activator/inhibitor gene (serpine) and corresponding control mice by using PIXImus, PQCT and histology.
4) To introduce femoral fracture in the knockout and control mice and evaluate new bone formation by pQCT at different times after initiation of fracture. We will initiate histology studies to identify the cell types that are affected in the knockout mice during fracture repair.

The Serpine (PAI-1) knockout mouse strain was also examined for fracture healing during the final 3-month continuation period, when the fourth Specific Objective is:

5) To complete histology studies in mice lacking plasminogen activator/inhibitor and control mice

The femur fracture model that was developed in the first year of this study was again applied to the Serpine knockout mouse strain and the C57BL/6 wild-type control strain. As described previously, an intramedullary pin was surgically implanted in the femur prior to fracture and the skin incision closed. A diaphyseal fracture was produced by the three-point bending technique (15). This procedure produced fractures that were consistently transverse and midshaft, and provided a uniform basis for the comparison of the differences in fracture healing between wild-type and knockout mice.

The development of the fracture callus during healing was examined by X-ray, pQCT and histology methods. X-ray images were examined and evaluated for fracture callus size and for any evidence of improved or impaired bridging of the fracture callus; such bridging is referred to as "bony union" and is the hallmark of endochondral bone healing. For the analysis of callus development by pQCT, it was necessary to adapt the pQCT parameters to quantify soft and hard tissues of the maturing fracture callus. We therefore scanned the bone at high resolution 1 mm intervals along the length of the fracture callus. The thresholds of the pQCT analysis were adjusted so that only the lower density (noncortical) bone or soft tissue was measured. The values at each 1 mm scan interval were integrated to quantify the bone mineral content of the entire fracture callus. In this way we used pQCT data to analyze the development of the soft and hard callus and identify differences between wild-type (normal) and knockout (altered) healing in mice. The pQCT parameters and their threshold settings used to quantify the fracture callus were the:

1) bone mineral content (BMC) of the lower density fracture callus and intramedullary bone, at threshold 214-570, a measurement of the bone in the fracture callus, excluding the cortical bone.
2) cross-sectional area of the lower density fracture callus and intramedullary bone (TA), at threshold 214-570, a measurement of the cross-sectional area of the bony fracture callus, excluding the cortical bone.
3) cross-sectional area of the soft tissue and lower density fracture callus and intramedullary bone, at threshold 0-570, a measurement of the cross-sectional area of all bony and soft tissue of the fracture callus, excluding the cortical bone.

Because the C57BL/6 is the background strain on which all of these knockout mouse strains have been developed, the same C57BL/6 mice served as controls for the X-ray and pQCT analysis of all 3 knockout mouse strains. Statistical analysis was performed by least significant analysis test, and deemed significant at $p<0.05$. Micro-CT measurements were not attempted because of the unavailability of the micro-CT instrument; a micro-CT instrument is being acquired by our research group, and several fracture samples have been prepared from the leptin knockout, Bax knockout and serpine knockout at 14 days post-fracture and stored in preparation for analysis.

Findings

Serpine Knockout Mice:

The serpine knockout mouse fracture study was completed in the previous 12 months. The fracture callus was examined by pQCT as described above. Several parameters were compared by pQCT for interpretation. Groups of 6 animals were examined for each strain at each post-fracture healing interval.

Interestingly, the serpine KO mice displayed a significant increase in fracture bone mineral content at 14 and 28 days healing, but not at the intervening 21 day time (figure 9). These results suggest that the influence on fracture healing by serpine (PAI-1) is complex and might involve different regulatory processes.

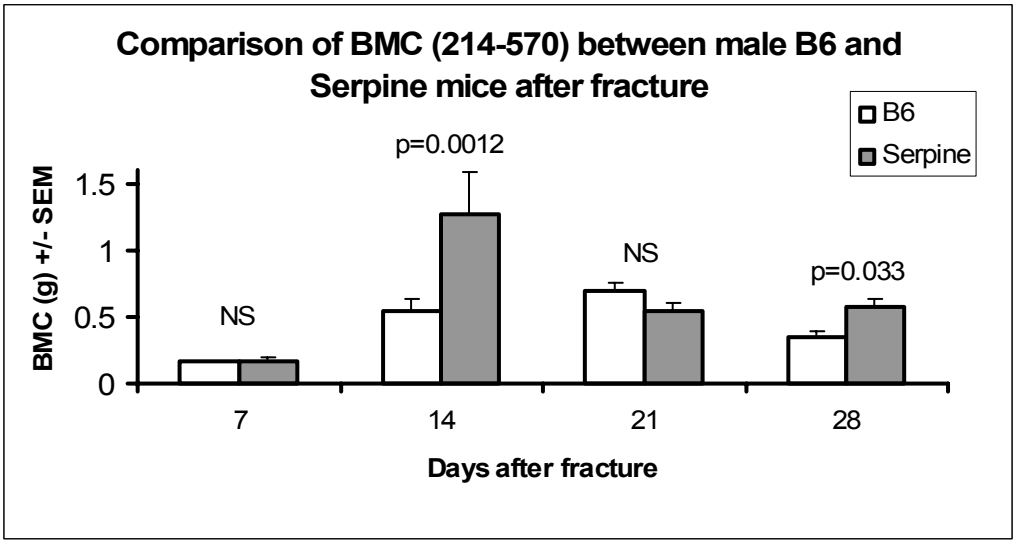

Figure 9. Bone mineral content after femoral fracture in male Serpine KO and C57BL/6 wild-type control mice. The bone mineral content of the fracture callus was significantly different at 14 and 21 days healing. Six mice from each strain were examined at each time. Data is presented as mean +/- SEM. Statistics were performed by t-Test. NS, no significant difference.

Measurements of the area of the lower density trabecular-type bone confirm the bone mineral content measurements, in that the area of callus bone is significantly greater only at 14 and 28 days healing (Figure 10). These results indicate that the bony component of the fracture callus is significantly larger at these times, but, as the bone mineral content (Figure 9) and the callus bone area have both increased, the bone mineral density has not. We have confirmed this observation using pQCT measurements of the fracture callus bone mineral density, which is not significantly different between mouse strains (data not shown).

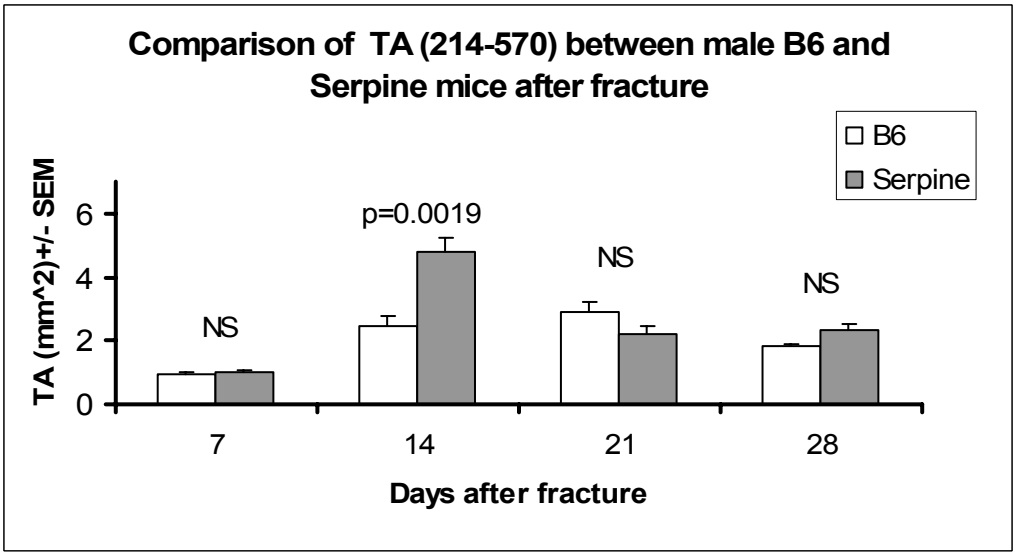

Figure 10. Area of trabecular-type bone (TA) after femoral fracture in male Serpine KO and C57BL/6 wild-type control mice. The bone mineral content of the fracture callus was significantly different at 14 and 21 days healing. Six mice from each strain were examined at each time. Data is presented as mean +/- SEM. Statistics were performed by t-Test. NS, no significant difference.

To determine whether serpine gene expression affects the total callus size (i.e., the bony callus and the soft callus components) the fracture callus was examined by pQCT using measurement thresholds that exclude the cortical bone. These results are shown in Figure 11, and demonstrate that the size of the serpine KO fracture callus was greater at 14 and 28 days healing; the greater difference at 14 days was no doubt due to a much greater quantity of soft callus tissue than that normally observed at this time. Most of the soft tissue has been replaced by bony callus at 28 days, when the difference between mouse strains in much smaller and barely significant.

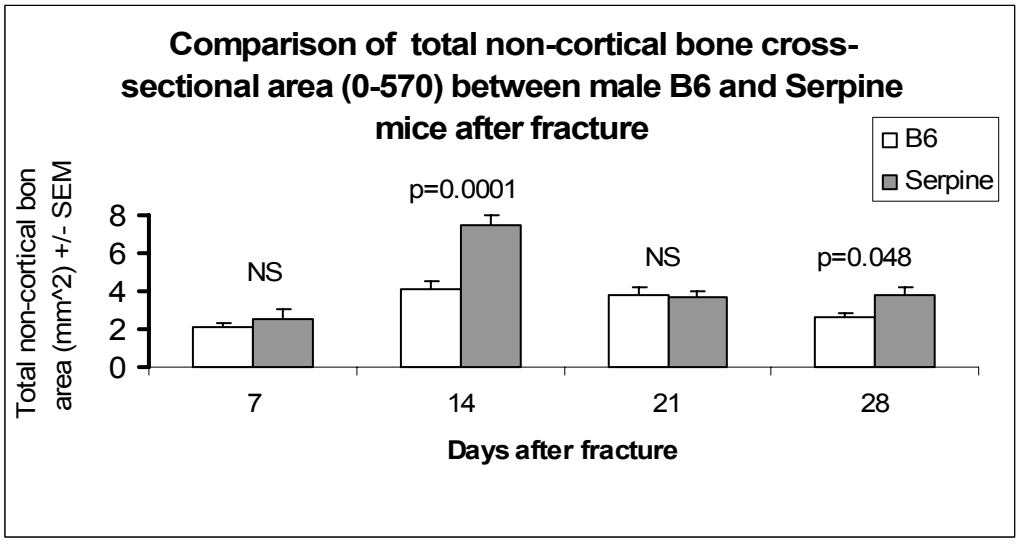

Figure 11 Area of soft tissue and trabecular-type bone (i.e., all non-cortical callus components) after femoral fracture in male Serpine KO and C57BL/6 wild-type control mice. Six mice from each strain were examined at each time. Data is presented as mean +/- SEM. Statistics were performed by t-Test. NS, no significant difference.

The effects of impaired serpine expression that were manifested at 2 different post-fracture healing times confirm the qualitative X-ray observations from the previous report, and we have pursued an analysis of the 14 day interval because the difference is quite large and expected to produce observable results by other histology techniques. An examination of the fracture callus cartilage at this time has also revealed large changes in the fracture callus at this time. Figure 12shows a view of the fracture cartilage for the entire callus at 14 days post-fracture, and qualitatively demonstrates that the fracture cartilage appears to make a large contribution to the serpine callus (Figure 12) at this time.

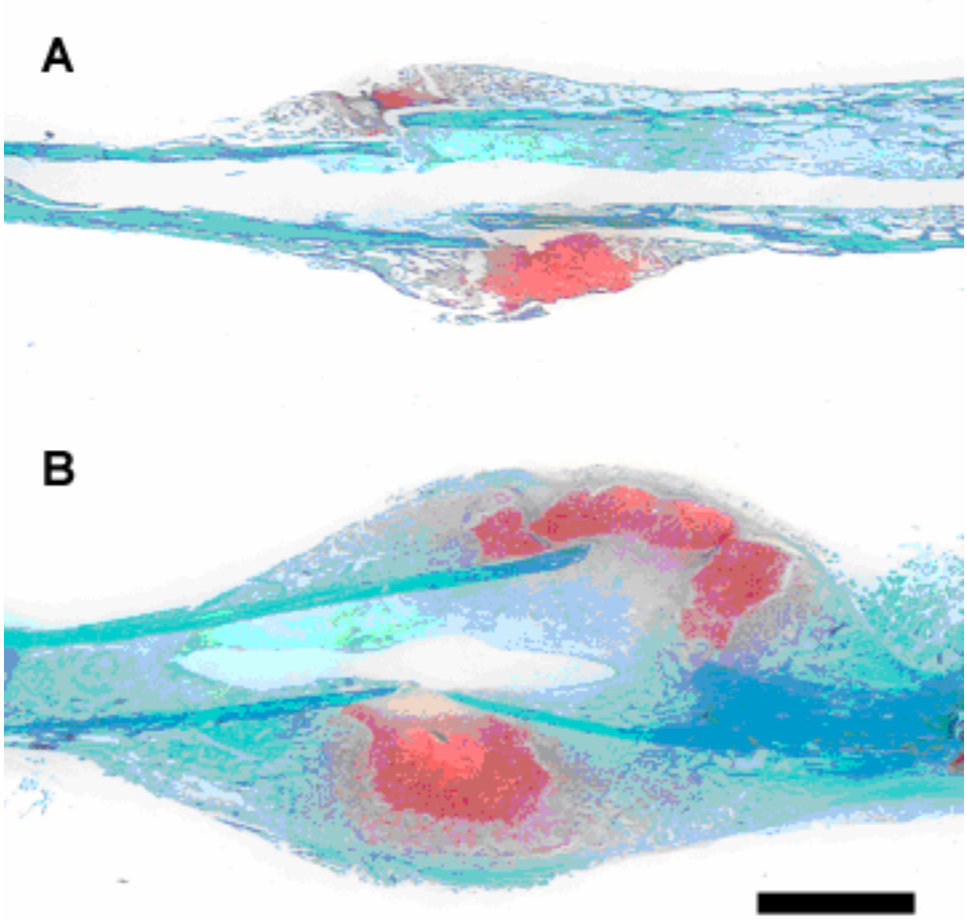

Figure 12 gobal view of the fracture callus comparing cartilage formation at 14 days in (A) wild-type and (B) serpine KO mice. The cartilage stains red by Safranin-Orange, and the non-cartilage components stain with the methyl green counterstain. Scale bar = 2 mm.

Quantification of the cartilage by histomorphometric analysis of Safranin-Orange stains (Figure 13) was performed to confirm the qualitative observations in Figure 12. In this case, duplicate sections were collected from more than 3 fracture calluses from each strain of mouse and measured at 7, 14 and 21 days. The duplicate sections were not adjacent to one another and therefore more representative as they are derived from different areas of the fracture callus. It was found that the serpine KO fracture calluses had significantly more cartilage than their wild-type counterparts at 14 days (and close to significance at the other times), and that this difference was quite large. These results suggest that serpine gene expression is an important regulator of fracture chondrogenesis at 14 days healing.

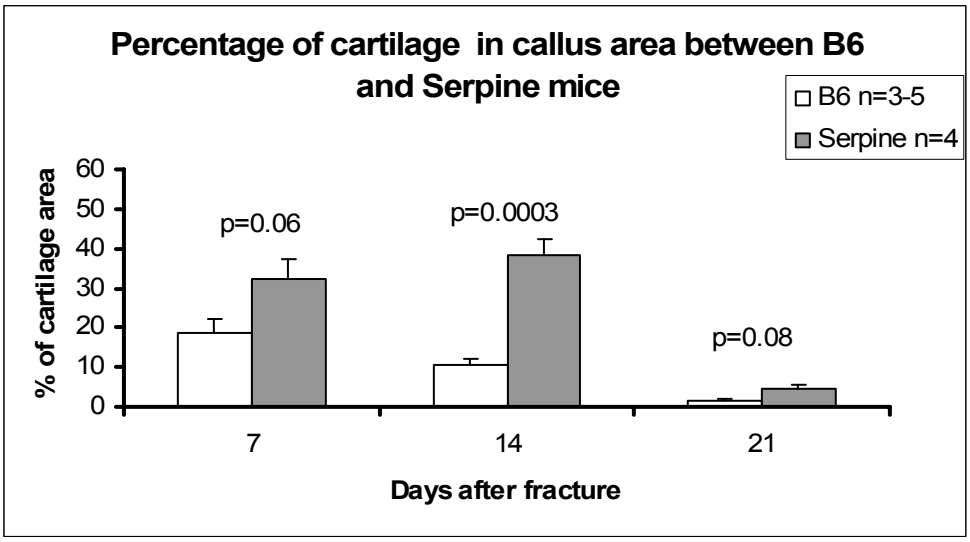

Figure 13. Histomorphometric analysis of the cartilage area in wild-type and serpine KO mice during fracture healing. More than 3 different fractures were measured for each mouse strain, and duplicate sections were counted; each of the duplicates was taken from a different plane of the callus and the measurements are representative of different areas of the callus. Data is presented as mean +/- standard error of the mean. Statistics were performed by t-Test.

A higher magnification examination of the serpine KO fracture histology at 14 days post-fracture using a conventional stain again shows the cartilage when compared to the wild-type fracture at the same time (Figure 14). However, the serpine KO fractures also exhibit a layer of bone immediately under the periosteum that is not typical of the normal pattern of callus cartilage conversion to bone that eventually produces the bony union of healing observed in wild-type mice. This cartilage turnover at this time is highly suggestive of some molecular pathway that more efficiently mineralizes the cartilage at the perimeter of the fracture callus. It was also evident in the global view of cartilage formation in Figure 14. While we have no explanation for this observation at this time, we intend to investigate this aspect of serpine KO fracture healing further using in vitro techniques.

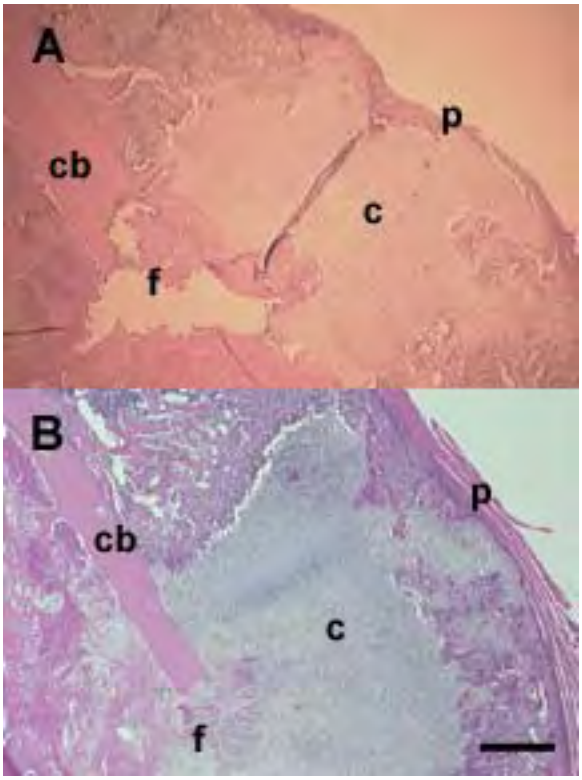

Figure 14. Hematoxylin and eosin stain of fracture callus sections at 14 days healing. (A) C57BL/6 wild-type control mouse, (B) serpine KO mouse. The cortical bone (cb), cartilage (c), fracture (f) and periosteum (p) are visible in each panel. More cartilage is visible in the serpine KO fracture, and callus bone has developed under the periosteum, a pattern seen also in Figure 10 (B) and one that is not typical of wild-type fracture healing. (A) was presented in a previous report as the control section for comparison to Bax KO and leptin KO fracture healing at this time. Scale bar = 0.50 mm.

The pattern of fracture healing that produces bone around the perimeter of the fracture callus cartilage is suggestive of enhanced callus strength. We therefore examined the strength of the serpine fracture callus at 14 days post-fracture by torsional mechanical testing. An analysis of fracture strength in comparison to wild-type mice reveals that the serpine KO calluses displayed a higher ultimate force to failure than their wild-type counterparts (Figure 15). In this case, the ultimate force from each fracture was normalized to that obtained from torsional testing of the unfractured contralateral femur from each animal, and presented as the percentage fractured force versus unfractured force for each animal. This approach accounted for the smaller size of the serpine KO femurs observed in the Specific Objective for this continuation period. Therefore, not only does serpine gene expression regulate the type of the fracture callus tissues, it also regulates the normal pattern of callus development that produces a stronger fracture callus even at 14 days post-fracture, a very early time in bony callus tissue development. It is probable that the absence of the serpine (PAI-1) inhibition of the plasminogen activators has accelerated cartilage replacement with bone at the perimeter, and the mechanism of this action certainly warrants further investigation.

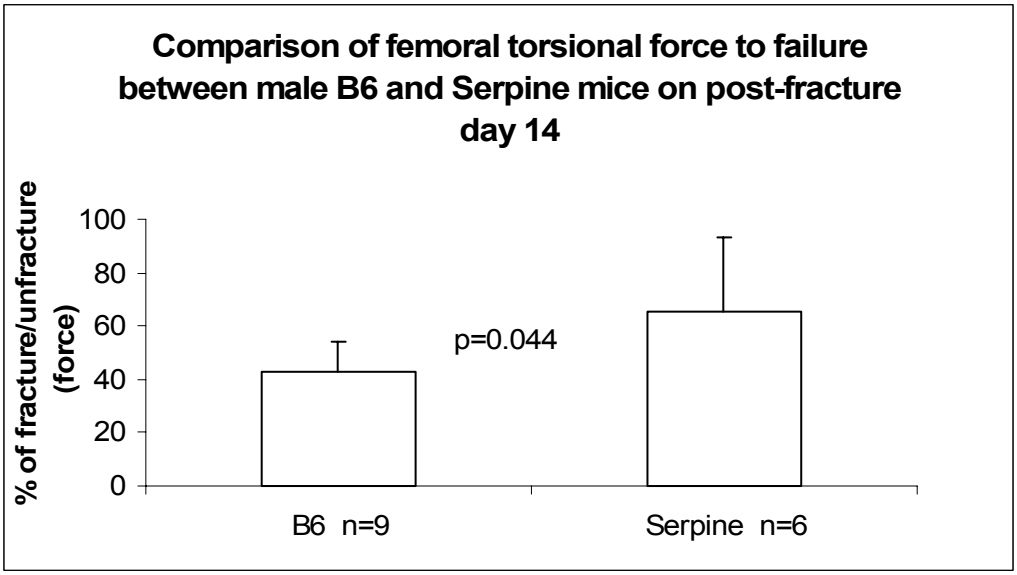

Figure 15. Torsional mechanical testing of male serpine KO and wild-type mice at 14 days post-fracture. Nine wild-type and 6 serpine KO mice were examined. Data is presented as mean +/- SEM. Statistics were performed by t-Test.

In summary, the serpine KO fracture healing analysis has yielded interesting results that might have significant implications for fracture therapy. *With the exception of the micro-CT analysis, we have completed the Specific Objectives for the analysis of fracture repair in this mouse strain.* We have produced serpine KO and wild-type mouse fractures, harvested the fractured femurs and stored them for analysis by micro-CT when our research group obtains the instrument. We nevertheless intend to follow these studies with additional investigations.

Bax Knockout Mice

To date, more than 30 homozygous mice at the age of 12 weeks have been used for fracture repair study and analyzed by X-ray and pQCT. These results were presented in the previous report, but because a close examination of the Bax KO mice fracture results revealed changes in fracture bone mineral content, trabecular-type bone area and total non-cortical callus area produced significant increases in each parameter at both the 14 and 28 day post-fracture intervals, the analysis has continued. This analysis uses both histology and molecular techniques to attempt to elucidate the mechanism for the apparently complex Bax gene regulation of healing that produced the enhanced fracture callus bone mineral content and trabecular-type bone area in Bax KO fractures at both 14 and 28 days.

Initially, we attempted to visualize the apoptotic phenotype of the Bax cells in the fracture callus histology. This study was undertaken to determine whether Bax-mediated apoptosis was operative in the fracture. Figure 13 shows the results of TUNEL staining of the fracture callus at 14 days post-fracture, when the greatest effects Bax gene deficiency were observed in fracture healing by pQCT. Because the original description of this model determined apoptosis to occur primarily in the bone marrow, we examined intramedullary bone marrow cells in the fracture callus, as well as fracture cartilage, where apoptosis would be expected to be important. There were no significant differences in apoptotic cells of fractured femurs between Bax KO and B6

control mice. To explain the bigger callus and more BMC in Bax KO mice, we are examining the cartilage area change in both fractured femur from healing day 7 to 28 by Safranin-O stain and histomorphometric quantification.

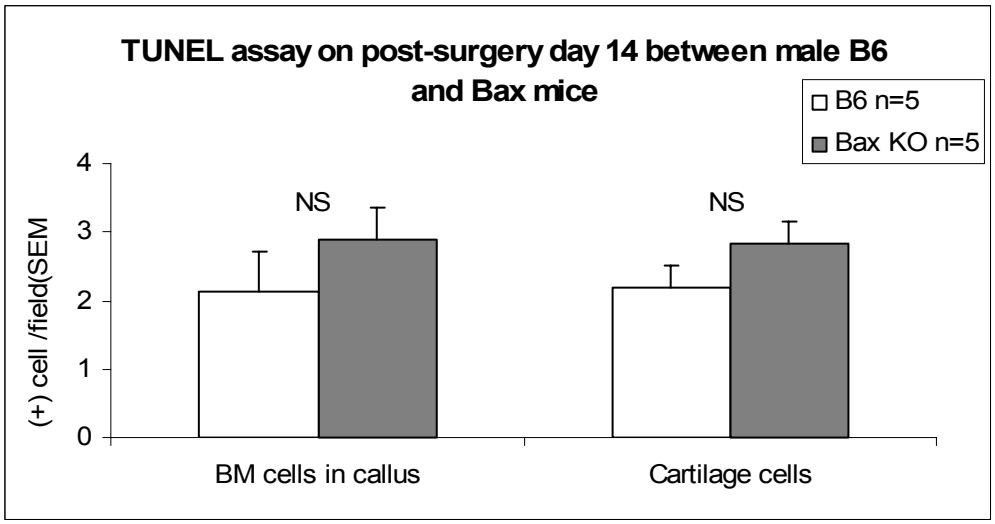

Figure 16. TUNEL assay for apoptosis on sections of fractured femurs in Bax KO mice and B6 control mice at 14 days post-fracture. Five fractures were analyzed from Bax and wild-type mice. Multiple sections were examined for each fracture. Callus intramedullary bone marrow (BM) cells and callus cartilage cells were examined. Data is presented as mean number of TUNEL-positive cells per field +/- standard error of the mean. Statistics were performed by t-Test. NS, no significant difference.

The results of the TUNEL Assay comparison in Bax KO and wild-type fractures at 14 days post-fracture indicate that there are very few apoptotic cells per field and the frequency of apoptosis is very low (Figure 16). The original description of these mice required a challenge to elicit a measurable apoptotic response in the bone marrow, so it is possible that Bax-mediated apoptosis does not affect fracture repair; rather Bax might act directly on the fracture callus at 14 and 28 days through proliferative effects.

To further attempt to relate Bax gene regulation of fracture histology, we quantified the area of fracture cartilage relative to the total cartilage area, as was done in the serpine KO mice. Histomorphometry was used to evaluate the Safranin-Orange-stained cartilage. In Figure 17, it can be seen that the cartilage area was significantly greater in Bax KO mice at 7 (approximately 3-fold) and 14 days post-fracture (approximately 2-fold), and almost negligible at 21 and 28 days. Cartilage cell density measurements (the number of cells/area) were found not to be significantly different between the two strains (data not shown). This observation suggests that the larger cartilage area is not caused through an increase in cell proliferation, but that the absence of Bax gene expression might increase bone formation and reduce bone remodeling through other mechanisms. The observation that Bax expression produces a larger fracture callus early in fracture healing (14 days), and late in fracture healing (28 days) but not at the time between these two post-fracture times suggests that Bax might have different functions during early and later fracture repair. The absence of observable apoptosis given such differences in the fracture callus bone and cartilage is difficult to interpret, however.

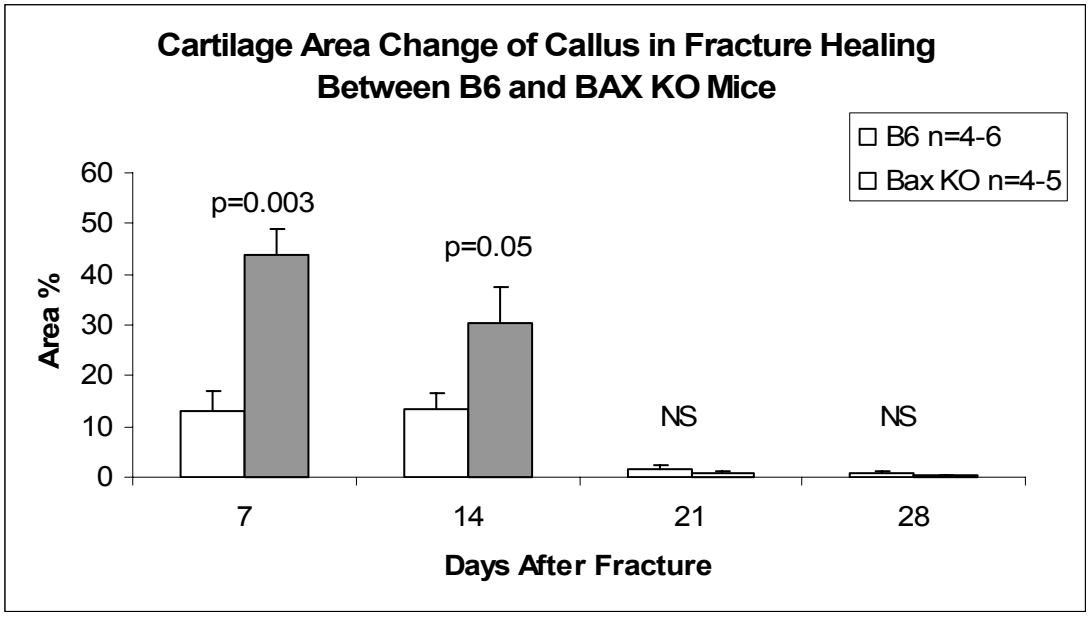

Figure 18. Histomorphometric analysis of the cartilage area in wild-type and Bax KO mice during fracture healing. Between 4 and 6 different fractures were measured for each mouse strain, and duplicate sections were counted; each of the duplicates was taken from a different plane of the callus and the measurements are representative of different areas of the callus. Data is presented as mean +/- standard error of the mean. Statistics were performed by t-Test.

Osteoclast number and activity also play an important role in bone healing, in particular through bone remodeling. To examine this problem, we determined identified osteoclasts in the fracture callus through staining by tartrate-resistant acid phosphatase (TRAP). Figure 18 compares TRAP staining in wild-type fractures at 28 days healing with Bax KO fractures at 28 days healing. It appears that the Bax KO mouse fractures have more osteoclasts in the fracture tissue.

The numbers of osteoclasts were counted from TRAP-stained sections from Bax KO and wild-type fractures at weakly intervals during healing, from 7 through 28 days. In Figure 19, it can be seen that the osteoclast number is significantly greater in Bax KO fractures than the wild-type fractures at both 21 days (approximately 20 per mm versus 15 per mm) and at 28 days (approximately 15 per mm versus 10 per mm). The increased number of osteoclasts at these later healing times is consistent with an increased resorption of the callus that might be required to remove much of the larger callus from 14 days healing. This might explain the larger callus at 28 days healing, but not at 14 days healing. Though we have not yet identified the effect of Bax expression at to two different times of fracture healing, we will continue to examine Bax KO fracture histology.

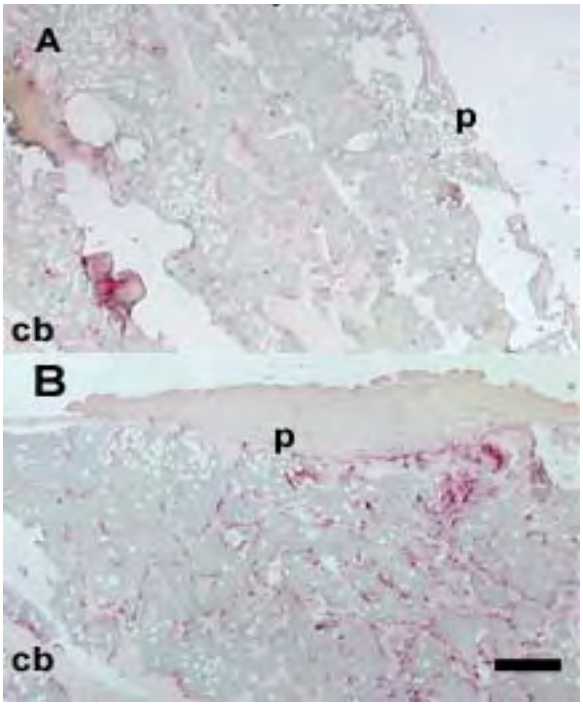

Figure 18. TRAP stain of fracture callus sections at 14 days healing. (A) C57BL/6 wild-type control mouse, (B) Bax KO mouse. The cortical bone (cb) and periosteum (p) are visible in each panel, and the fracture site is outside the lower left of each panel. More osteoclasts are visible in panel, and the fracture site is outside the lower left of each panel. More osteoclasts are visible in Bax KO fracture. Scale bar = 0.50 mm.

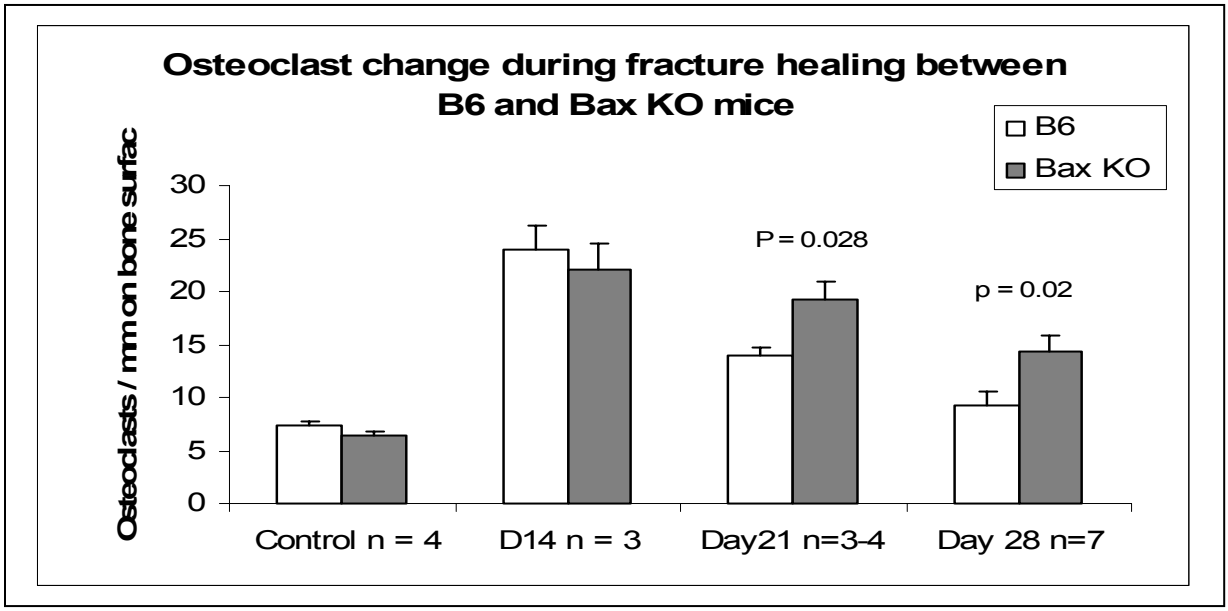

Figure 19. Histologic determination of the numbers of fracture callus osteoclasts in wild-type and Bax KO mice during healing. Between 3 and 7 different fractures were measured for each mouse strain, and multiple sections were counted; each of the duplicates was taken from a different

plane of the callus and the measurements are representative of different areas of the callus. Data is presented as mean +/- standard error of the mean. Statistics were performed by t-Test.
In summary:

1) Bax knockout mouse fractures developed more cartilage during early fracture healing.
2) The additional cartilage area in the Bax knockout mouse callus is not due to augmented cell proliferation and number, but a difference of cell size that might be expected during chondrocyte maturation.
3) There are more osteoclasts on the callus trabecular-type bone surface in the callus of Bax knockout mice at a later healing stage, consistent with enhanced remodeling.
4) No significant difference in apoptotic cells was found between Bax knockout and B6 control mice as had been expected. This result is quite interesting and implies that Bax gene expression is redundant or that Bax might have other functions in wound healing.

With the exception of the micro-CT analysis, we completed the Specific Objective for the analysis of fracture healing in the Bax knockout mice. Additionally, we have extended the histologic analysis of Bax KO fracture repair to cartilage and osteoclast determinations that have yielded more information. As our micro-CT becomes available, we will analyze Bax femur fractures that we have prepared and stored.

Leptin Knockout Mice

As previously reported, at no time during fracture healing did the leptin knockout mice display any significant changes in the bone content or cross-sectional area of the bony tissue or total tissue. The leptin knockout mice also display additional conditions, such as diabetes, that contributed to fracture healing. *This portion of the technical Objective was achieved, except for the micro-CT examination.* Our research group is expecting micro-CT instrumentation shortly, and as it becomes available, leptin knockout fracture calluses at 14 days post-fracture that we have harvested and stored will be examined to obtain a higher resolution measurement of healing. These results will also be examined in light of the sex-specific differences in unfractured femur size observed in these mice and discussed above.

Specific Objective 2: to apply microarray technology to study gene expression in the fracture tissues of the one strain of knockout mice that exhibited the greatest phenotypic differences in fracture healing.

Microarray analysis provides a powerful tool for the characterization of global gene expression in fracture repair (16). This study used whole genome microarray gene analysis to identify the genes expressed in fracture repair of the Bax knockout mouse femur at 14 days healing, when the pQCT data indicated, and subsequent histology data confirmed, that the Bax knockout fracture callus displays altered healing as compared to the wild-type C57BL/6 wild-type control. The repertoire of expressed genes regulating Bax KO healing would be expected to differ greatly from controls at this time, so the 14 day fracture callus was chosen for an analysis of global gene expression in fracture repair.

Total RNA was compared by microarray analysis of 14 day fracture calluses from 5 individual male Bax knockout mice and 5 individual C57BL/6 knockout mice. The individual pairs of samples were hybridized and analyzed separately. The RNA from each fracture callus was labeled with Cy3 or Cy5 dye and hybridized to our in-house mouse gene chip that contained approximately 28,000 unique mouse gene targets. Analysis was performed using (Agilent)

Genespring software and changes in expression between the Bax knockout fracture callus and the C57BL/6 callus deemed significant at $p<0.05$. During this reporting period we have confirmed the expression of several gene candidates by real-time PCR, to confirm the previous X-ray and current histology observations of Bax KO fracture cartilage development and to elucidate the regulatory pathways of Bax KO fracture healing. For these purposes, real-time PCR analysis of gene expression was compared in RNA preparations from healing Bax KO and wild-type fractures at 14 days post-fracture, as well as at 7 days post-fracture, prior to the observed histology but when the genes that regulate the pathways that produce the observed effects should be expressed.

Findings:

The previous report described the numbers of genes expressed and the Bax-related (i.e., mitochondrial apoptosis) genes expressed as determined by microarray analysis. Briefly, 5,458 genes displayed significant changes in expression, of which approximately 15% were unknown genes or expressed sequence tags (ESTs). These results indicate that Bax effects on fracture repair are complex and that many of the regulating genes remain to be elucidated. Surprisingly, approximately equal numbers of known and unknown genes were up-regulated and down-regulated, possibly a result Bax-related interactions with other molecular pathways of fracture repair.

Surprisingly, real-time PCR confirmations of Bax-related gene expression from the microarray data were successful, yet they failed to define changes in the mitochondrial apoptotic pathway that would compensate for Bax gene deficiency and produce the observed effects on fracture healing when the expected reduction in apoptosis was not observed. This study examined the Bcl-2 and Bcl-XL ratios that might be expected to be altered in response to Bax deficiency and restore the balance in apoptosis. Likewise, the expression several other mediators of mitochondrial apoptosis, among them Bad, Bak, Bok, could not explain the apparent lack of Bax deficiency on fracture apoptosis. An exception was the up-regulated expression of Biklk (Bik-like), another mitochondrial apoptotic regulator that binds and inhibits both Bcl-2 and Bcl-XL (17); Biklk was confirmed by real-time PCR to be up-regulated approximately 2-fold, suggesting that its expression compensated for the absence of Bax in promoting apoptosis and reduced the severity of the Bax knockout phenotype and its effect on fracture healing.

The examination of the genes regulated was therefore extended to several other categories of genes that might be expected to affect:

(1) fracture chondrogenesis, the major effect that was observed
(2) cell proliferation versus differentiation

The microarray data has been categorized and tabulated to facilitate the examination of genes related several processes and is presented in Appendix A:

Appendix A1: structural genes
Appendix A2: apoptosis genes
Appendix A3: cartilage regulation genes
Appendix A4: transcription factor genes
Appendix A5: other genes

Real-time PCR measurements compared Bax KO mouse fracture gene expression to C57BL/6 (wild-type) mouse fracture gene expression. Initially, cartilage-related gene expression was examined at 7 days, during early chondrogenesis and at 14 days, during later chondrogenesis, and when the differences in Bax gene healing were observed by pQCT and histology. The collagen genes Col 2α1, a marker for prehypertrophic chondrocytes, Col9α1, a marker for all chondrocytes, and Col10α1, a marker for hypertrophic chondrocytes were examined to determine the degree of cartilage development. The chondrocyte regulatory genes identified with slight differences in expression in the microarray analysis at 14 days were also examined. These genes included Sox-6, Frizzled (Fzd) and Max binding inhibition transcription factor (Mitf).

The results are presented below for the 7 day post-fracture measurements (Figure 20). In this convention, greater gene expression is identified as a greater negative difference in cycle number when normalized to the housekeeping gene. It was found that Col 2α1 and Col9α1 gene expression was up-regulated in the Bax fracture callus at 7 days healing. None of the other genes, including Col10α1, displayed significant differences in expression from the wild-type fractures. These results are consistent with an accumulation of prehypertrophic chondrocytes in early chondrogenesis in the Bax KO that mature to hypertrophy at the same rate as the wild-type chondrocytes in later chondrogenesis. The 14 day post-fracture gene expression data revealed no significant differences between mouse strains in the expression of these genes (data not shown). It appears that by this later time that some regulatory event has compensated for the uncoupled early chondrogenesis and hypertrophy.

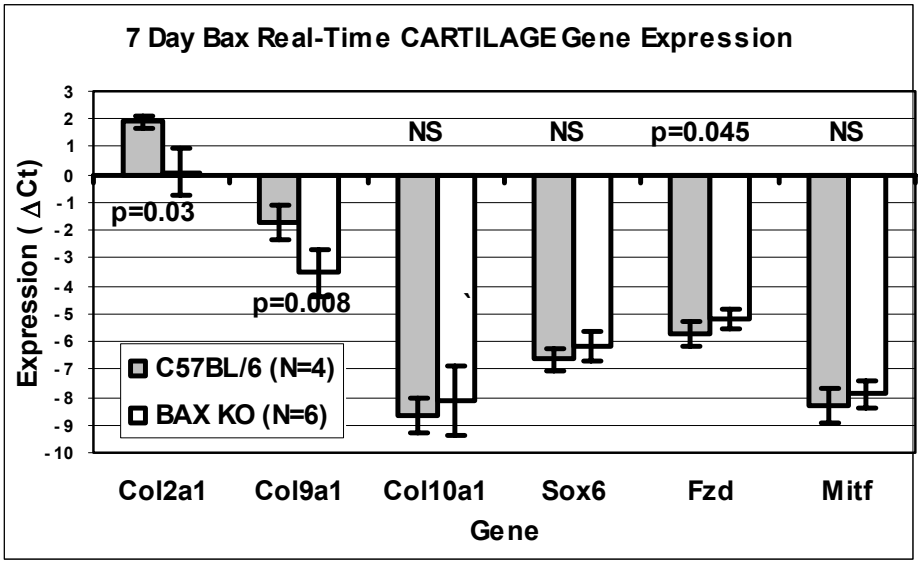

Figure 20. Real-time PCR analysis of cartilage gene expression in wild-type and Bax KO mice at 7 days post-fracture. RNA from between 4 or 6 different fractures were measured for each mouse strain. Data is presented as mean +/- standard deviation. Greater gene expression is identified as a greater negative difference in cycle number (ΔCt) relative to the cyclophilin housekeeping gene, defined as zero ΔCt. Statistics were performed by t-Test. The collagen structural genes are Col2α1, Col9α1 and Col10α1. The collagen regulatory genes are Sox-6, Frizzled (Fzd) and Max binding inhibition transcription factor (Mitf). NS, no significant difference.

To further characterize Bax KO fracture cartilage development, gene expression was measured in Bax KO and wild-type fracture calluses at 7 days and 14 days post-fracture. These studies attempted to identify possible interactions that balance cartilage proliferation, maturation and apoptosis. They included genes that might regulate p53 control pathways of proliferation and apoptosis (p53, p21, Inhibitor of Apoptosis-2, IAP-2; 18) cartilage condensation (Sox-9) and hypoxia (Hypoxia-inducible Factor-1α, HIF-1α; 19). Preliminary results in the few genes that have been examined to date are presented below; the comparison of gene expression between the Bax KO and wild-type mouse strains is presented below in Figure 21 (7 days post-fracture) and Figure 20 (14 days post-fracture).

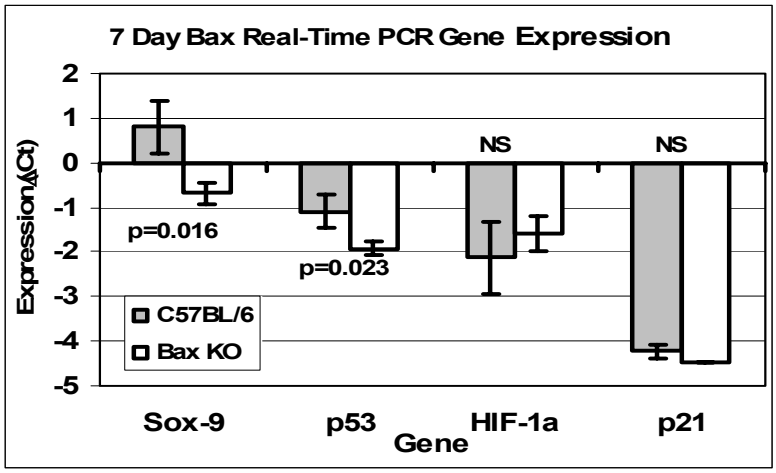

Figure 21. Real-time PCR analysis of cartilage gene expression in wild-type and Bax KO mice at 7 days post-fracture. RNA from 3 different fractures was measured for each mouse strain. Data is presented as mean +/- standard deviation. Greater gene expression is identified as a greater negative difference in cycle number (ΔCt) relative to the cyclophilin housekeeping gene, defined as zero ΔCt. Statistics were performed by t-Test. HIF-1α, hypoxia-inducible factor; NS, no significant difference.

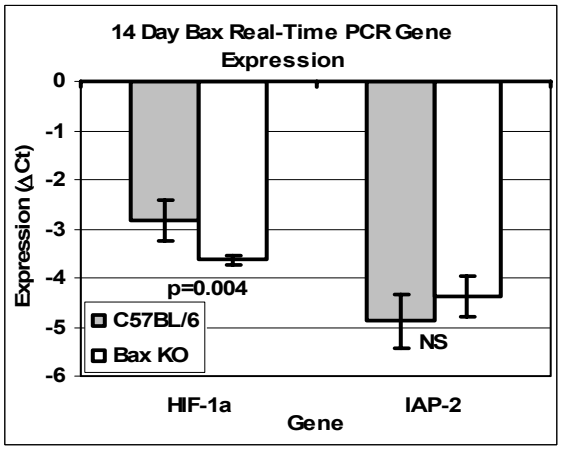

Figure 22. Real-time PCR analysis of cartilage gene expression in wild-type and Bax KO mice at 7 days post-fracture. RNA from between 3 different fractures was measured for each mouse strain. Data is presented as mean +/- standard deviation. Greater gene expression is identified as a greater negative difference in cycle number (ΔCt) relative to the cyclophilin housekeeping gene, defined as zero ΔCt. Statistics were performed by t-Test. HIF-1α, hypoxia-inducible factor; IAP-2, Inhibitor of Apoptosis-2; NS, no significant difference.

In Figure 22, it can be seen that the Sox-9 and p53 gene expression affects early (7 day) fracture callus development; Sox-9 is an early marker for chondrogenesis, while p53 might regulate a balance between cell proliferation and apoptotic regulatory pathways. Both markers reveal increased expression in Bax KO mice. None of the other markers at this time show significant differences in expression between Bax KO and wild-type fractures. This observation is interpreted as a greater degree of chondrocyte differentiation, and, by extension, a greater cartilage development. By 14 days post-fracture, HIF-1α, a component of the apoptotic regulatory pathway, displays increased expression in the Bax KO mice (Figure 20), suggesting that hypoxia-induced apoptosis might regulate Bax KO cartilage development and help to balance the initial bias toward a cartilage increase at 7 days and resolve the fracture callus. These effects at 14 days post-fracture might operate in concert with resorption at this time. However, further study of additional Bax-related genes is required to more thoroughly characterize gene expression and resolve the observed effects on Bax KO fracture repair.

Key Research Accomplishments:

1) Analysis of the response to mechanical loading for two knockout strains of mice (leptin and Bax) has been completed.
   a) The microarray analysis of molecular regulation of the loaded leptin knockout bones has suggested novel gene candidates for is currently underway.
   b) Additionally, we have obtained and are attempting to generate sufficient numbers of the Ephrin B-1 knockout mouse strain to perform this analysis and complete this study for the third knockout strain of mouse.
2) Two of proposed knockout strains of mice (the Bax knockout and serpine knockout) have been phenotypically analyzed by the fracture repair model.
   a) The analysis of the serpine knockout mice strain suggests that serpine-1 (plasminogen activator inhibitor, PAI-1) regulates cartilage formation in the fracture callus development and bone size during normal bone growth.
   b) The histological analysis of the Bax knockout mouse has been extended to more fully characterize the observed effect on fracture repair. The analysis of the regulatory pathways of gene expression identified by the microarray analysis has also been extended to better characterize several categories of genes that regulate chondrocyte proliferation and maturation, in addition to the apoptotic gene candidates.

Reportable Outcomes:

Manuscript:

1. Wang, X., C.H. Rundle, J. Wergedal, A. Srivastava, S. Mohan and K.H-W. Lau (2007) Loss of sex-specific difference in femoral bone parameters in male leptin knockout mice. Provisionally accepted for publication by *Calcified Tissue International*.

Conclusions:

1) The development and optimization the mechanical loading model of bone formation and the femur fracture model of bone repair in knockout mice allowed the analysis of the functional significance of genes of interest for bone formation in each case.

2) X-ray and pQCT analysis suggests that leptin influences bone formation in mechanical loading. Microarray data suggest that the molecular regulation of bone formation in mechanical loading is complex.
3) pQCT and serum sex steroid analysis suggests that leptin also influences the acquisition of bone size in males through sex hormone-related effects.
4) X-ray, pQCT, and histological analysis of fracture healing suggests that serpine-1 (plasminogen activator inhibitor, PAI-1) regulates components of the plasminogen axis of extracellular matrix development critical not only to fracture cartilage development, but also the size parameters of normal bone development.
5) X-ray, pQCT and histological analysis of fracture healing suggest that Bax expression influences fracture callus cartilage development and bone remodeling. Microarray analysis of fracture healing at 14 days post-fracture suggests that Bax regulation of fracture chondrogenesis is complex and not directly affected by Bax regulation of mitochondrial apoptosis, but that interacting pathways of proliferation and differentiation might ultimately produce the observed effects in Bax knockout fractures.

References:

1. Carmeliet, P., Kiekens, L., Schoonjans, L., et al. (1993). Plasminogen activator inhibitor-1 gene-deficient mice. I. Generation by homologous recombination and characterization. J. Clin. Invest. 92:2746-2755.
2. Davy, A., Aubin, J. and Soriano, P. (2004) Ephrin-B1 forward and reverse signaling are required during mouse development. Genes Dev. 18:572-583.
3. Coulthard, MG., Duffy, S., Down, M., Evans, B., Power, M., Smith, F., Stylianou, C., Kleikamp, S., Oates, A., Lackmann, M., Burns, GF. and Boyd, AW. (2002) The role of Eph-ephrin signaling system in the regulation of developmental patterning. Int. J. Dev. Biol. 46:375-384.
4. Ducy P., Amling M., Takeda S., et al. (2000). Leptin inhibits bone formation through a hypothalamic relay: A central control of bone mass. Cell 100:197-207.
5. Steppan CM., Crawford DT., Chidsey-Frink KL., et al. (2002). Leptin is a potent stimulator of bone growth in ob/ob mice. Regulatory Peptides 92:73-78.
6. Matkovic V., Ilich JZ., Skugor M., et al. (1997). Leptin is inversely related to age at menarche in human females. J. Clin. Endocrinol. Metab. 82:3239-3245.
7. Takeda S., Elefteriou F., Levasseur R., et al. (2002). Leptin regulates bone formation via the sympathetic nervous system. Cell 111:305-317.
8. Lee, Y-J., Park, J-H., Ju, S-K., et al. (2002). Leptin receptor isoform expression in rat osteoblasts and their functional analysis. FEBS Letters 528:43-47.
9. Willis, S., Day, CL., Hinds, MG., et al. (2003). The Bcl-2-regulated apoptotic pathway. J. Cell Science 116:4053-4056.
10. Mocetti P., Silvestrini G., Ballanti P., et al. (2001). Bcl-2 and Bax expression in cartilage and bone cells after high-dose corticosterone treatment in rats. Tissue & Cell 33:1-7.
11. Knudson CM., Tung KSK., Tourtellotte WG., et al. (1995). Bax-deficient mice with lymphoid hyperplasia and male germ cell death. Science 270:96-98.
12. Nelson, DA., Simpson, PM., Johnson, CC., et al. (1997). The accumulation of whole body skeletal mass in third- and fourth-grade children: Effects of age, gender, ethnicity and body composition. Bone 20:73-78.

13. Thomas, T. and Burguera, B. (2002). Is leptin the link between fat and bone mass? J. Bone Miner. Res. 9:1563-1569.
14. Hamrick MW., Pennington C., Newton D., Xie D., Isales C. (2004) Leptin deficiency produces contrasting phenotypes in bones of the limb and spine. Bone 34:376-383.
15. Bonnarens, F. and Einhorn, TA. (1984). Production of a standard closed fracture in laboratory animal bone. J. Orthop. Res. 2:97-101.
16. Hadjiargyrou, M., Lombardo, F., Zhao, S., et al. (2002). Transcriptional profiling of bone regeneration: Insight into the molecular complexity of wound repair. J. Biol. Chem. 277:30177-30182.
17. Coultas, L., Bouillet, P., Stanley, EG., et al. (2004). Proapoptotic BH-3-only Bcl-2 family member Bik/Blk/Nbk is expressed in hematopoietic and endothelial cells but is redundant for their programmed death. Mol. Cell. Biol. 24:1570-1581.
18. Greijer, AE. and van der Wall, E. (2004) The role of hypoxia inducible factor 1 (HIF-1) in hypoxia induced apoptosis. J. Clin. Pathol. 57:1009-1014.
19. Basu, A. and Haldar, S. (1998) The relationship between Bcl2, Bax and p53: consequences for cell cycle progression and cell death. Mol. Hum. Reprod. 4:1099-1109.

PROJECT 6

CO-PRINCIPAL INVESTIGATORS: Kin-Hing William Lau, Ph.D.

Susan Hall, M.D., Ph.D., MPH

Henry J. Klamut, Ph.D.

TITLE: Systemic Gene Therapy for the Skeleton

B. GENE THERAPY PROJECTS
Project 6: Systemic Gene Therapy For The Skeleton

Introduction

For this project, we propose to develop and test the efficacy of a mouse model for systemic gene therapy for massive skeletal tissue damage by means of hematopoietic stem cells (HSC) transplant. For this model, we will determine the skeletal marrow tissue and non-skeletal sites of engraftment, the quantity of short-term and long-term bone formation achieved, and the effect of the age of the recipient mice on the bone formation response. To our knowledge, our studies will be the first to use transplantation of transduced HSCs to deliver gene therapy to induce bone formation. These studies will focus on the induction of bone formation for massive skeletal injury. However, there is evidence that HSCs have the plasticity to regenerate other tissue types. Therefore, a successful HSCs-delivered gene therapy strategy for bone injury could be adapted to treat other damaged tissues, such as skin and muscle that are likely to be sustained along with massive skeletal injury, by the insertion of tissue-specific promoters to drive the therapeutic gene.

Body

1. Technical Objectives

Our specific objectives for the third 12 months were to continue and complete engraftment studies and explore mechanistic questions regarding our gene therapy murine model.

Technical Objective 1: To complete studies to determine the skeletal marrow and non-skeletal sites of engraftment in recipient mice after transplant with donor HSCs, we will

a) Transplant GFP-expressing HSCs derived from transgenic mice into myelosuppressed recipient mice and assess the short-term (8 weeks), mid-term (6 months) and long-term engraftment (1 year) in the skeletal marrow and non-skeletal sites. Engraftment efficiencies will be quantitated by measuring the percentage of GFP-expressing cells in the peripheral blood and bone marrow of the recipient mice using flow cytometry.
b) Assess the pluripotent ability of the engrafted donor cells to produce mature hematopoietic lineages (T-cell, B-cell, neutophil/granulocyte/monocyte and erythroid) by using lineage-specific immunostaining and FACs analysis of the recipients' peripheral blood.
c) Detect donor cells in non-skeletal tissues by frozen sectioning of the bone, heart, lungs, liver and spleen of the recipients and fluorescent microscopic observation.

Technical Objective 2: To complete studies to assess and quantitate the short-term and long-term bone formation achieved in mice following transplantation with HSCs transduced to express a growth factor gene we will:

a) Transduce HSC-enriched cells with an HIV-based vector expressing the BMP 2/4 gene under the control of the CMV promoter. Transgene expression will be assessed using immunohistochemical staining of the transduced cell cultures and Western blot analysis of the conditioned media
b) Transplant the transduced donor cells via tail vein into myelosuppressed recipient mice and evaluate bone formation after 8 weeks, 6 months and 10 months. Bone formation will be evaluated by measuring serum osteocalcin and alkaline phosphatase. Bone density and

cortical thickness in the host animals will also be assessed by faxitron X-ray and pQCT analysis.

NOTE: Technical Objective 3 revision approved in June, 2005.
Revised Technical Objective 3: To explore the possible mechanism(s) for why transplantation of HSC-enriched cells transduced to express BMP4 did not induce bone formation as expected.

a. To determine if silencing of the BMP2/4 transgene occurs we will, transplant donor HSCs transduced to express BMP 2/4 (or marker control gene) into myelosuppressed recipient mice and evaluate transgene expression at 8 weeks and 6 months post transplant. Transgene expression will be evaluated by real time RT-PCR in RNA extracts and PCR in DNA extracts
b. To determine if BMP2/4 interferes with engraftment of HSCs, we will transduce Sca-1^+ cells to express BMP 2/4 (or marker control gene) and transplant at 4 cell doses (500, 5000, 50,000 or 500,000 cells/recipient) into myelosuppressed recipient mice and evaluate engraftment at 4, 6, 8, 10 and 16 weeks.
c. To determine if BMP2/4 induces Sca-1^+ cell differentiation into hematopoietic lineages, we will transduce Sca-1^+ cells to express BMP 2/4 (or marker control gene) and transplant at 4 cell doses (500, 5000, 50,000 or 500,000 cells/recipient) into myelosuppressed recipient mice and evaluate the percentage of various hematopoietic lineages (T-lymphocytes, B-lymphocytes, monocytes and erythroid) at 4, 6, 8, 10 and 16 weeks. Hematopoietic lineage will be assessed by immunostaining and FACs analysis.

2. Progress on Technical Objectives

Objective 1a: To transplant GFP-expressing HSCs derived from transgenic mice into myelosuppressed recipient mice and assess the short-term (8 weeks), mid-term (6 months) and long-term (1 year) engraftment in the skeletal marrow and non-skeletal sites. The Sca-1 molecule has been implicated as a marker for hematopoietic stem cell (HSCs). In year 1, HSCs isolated from TgN-GFP donor mice were transplanted into recipient mice, and skeletal marrow and non-skeletal sites were analyzed for engraftment at various time points post-transplant. The donor TgN mouse is a transgenic strain transduced to produce the GFP marker gene. Use of this donor strain allows for the tracking of donor cells *in vivo* after transplantation.

In year 2, we repeated experiments and confirmed our results from the first year. In addition, we improved our gene therapy strategy by using a retro-orbital intravenous injection method for delivering the transduced stem cells rather than using the tail vein injection method. With the retro-orbital injection, mice are briefly anesthetized with isofluorane and injected by inserting a needle into the retro-orbital plexus and injecting the sterile cell preparation. With this method we have improved our transplantation success rate from approximately 37% to nearly 100%. In addition, the variation of the engraftment using the retro-orbital injection technique was significantly reduced, as evidenced by a 3- to 4-fold decrease in experimental coefficient of variance compared to the tail vein method. The retroorbital injection method is relatively safe to the host, as none of the mice injected by retroorbital injection have suffered adverse effects to their eyes and, in most experiments, no animal was lost due to anesthesia or other complication.

Objective 1b: Assess the pluripotent ability of the engrafted donor cells to produce mature hematopoietic lineages (T-cell, B-cell, neutophil/granulocyte/monocyte and erythroid) by using lineage-specific immunostaining and FACs analysis of the recipients' peripheral blood. Experiments were performed in year 1 and repeat experiments to confirm results were initiated in year 2 and completed in year 3. We have assessed the ability of the engrafted donor cells to produce mature hematopoietic lineages using lineage-specific immunostaining and FACs analysis of the recipients' peripheral blood. For these experiments, whole bone marrow cells from TgN (GFP+) mice were harvested by flushing tibiae and femurs with PBS using a 26g needle and syringe. Erythrocytes were removed by osmotic lysis using a solution of 155 mM NH_4Cl, 10mM $KHCO_3$ and 110μM Na_2EDTA, followed by rinsing with PBS. After osmotic depletion of erythrocytes (RBC-lyzed), the cell preparation was enriched for Sca-1 cells by incubating the cells with Sca-1 specific antibody-magnetic microbead conjugates. The mixture was then applied to an automated magnetic separation column (AutoMacs™) according to manufacturer instructions. This procedure resulted in 19-fold enrichment in Sca-1+ cells. The enriched cells were transplanted into sublethally irradiated recipient W41/W41 mice. At 5 months post transplantation, recipient peripheral blood was collected and erythrocytes were removed by osmotic lysis. The mononuclear fraction was assessed by immunostaining for expression of hematopoietic lineage surface markers and measured by FACs analysis. For this analysis, PE-fluorochrome conjugated antibodies specific for hematopoietic lineage were incubated for 30 minutes in separate tubes with the mononuclear cell fraction from each recipient mice. For T-lymphocytes (T-cells) lineage, a mixture of CD3-, CD4e-, and CD8a-specific antibodies was used. For granulocytes/monocytes/macrophages, a mixture of Mac-1- and Gr-1-specific antibodies was use. For B-lymphocytes (B-cells), a B220-specific antibody was use and for erythroid lineage cells, a Ter-119-specific antibody was used. After incubation the cells were rinsed once and resuspended in PBS and % PE positive cells were assessed by FACs analysis. Parallel tubes were processed using PE-conjugated isotype non-specific antibodies and FACs results were adjusted to account for non-specific binding. In addition, the total engraftment (%GFP positive cells) was assessed. Table 1 shows the mean ± SD for each cell lineage type in mice transplanted with Sca-1+ cells 5 months after transplantation. Cells that were PE+ and GFP+ were of donor origin, while cells that were PE+ but GFP– were considered of recipient host origin. No significant difference in contribution of T-lymphocyte lineage was observed between host (14.7%) and donor (11.8%) origin. In contrast, donor cells contributed a larger percentage than host cells to the macrophage-monocyte-neutrophil lineage (22.9 vs. 6.9%; $p < 0.001$) and B lymphocytes (22.9 vs. 6.9%; $p < 0.01$). The erythroid hematopoietic compartment was made up exclusively of cells of donor origin. These results are comparable with the relative distribution of cells of hematopoietic lineage in peripheral blood of control mice reported by Morel et al. (Hematologic recovery in mice transplanted with bone marrow stem cells expressing anti-human immunodeficiency virus genes. *Human Gene Ther.* 10:2779-2787, 1999). Morel reported for control mice: Gr1+ (granulocytes) ~17% , Mac1+ (macrophages) ~26%,B220 (b-cells) ~ 55% and CD3+ (t-cells ~22%) Thus, the results indicate that our Sca-1+ cell transplantation strategy leads to multilineage hematopoietic cell engraftment.

TABLE 1

	Total % PE^+ mean (st.dev.)	% PE^+ & GFP^- mean (st. dev.)	% PE^+ & GFP^+ mean (st.dev.)
T-cells	19.4 (5.8)	14.7 (3.0)	11.8 (4.4) ^{ns}

Mac/Mono/Gr	32.2 (25.7)	6.9 (3.5)	22.9 (5.8) **
B-cells	21.4 (6.7)	11.6 (5.2)	22.9 (7.2) *
Erythroid	4.8 (3.8)	Non-detectable	5.4 (2.8)

Table 1: Independent t-test comparisons of % PE^+ & GFP^- (host) vs. % PE^+ & GFP^+ (donor): NS = non-significant, * $p< 0.01$, ** $p<0.001$, St. Dev. = Standard Deviation of Mean. Results are shown as mean ± SD. For this analysis, W41/W41 mice were transplanted with GFP-expressing Sca-1 cells isolated from TgN-GFP mice. Five months after transplantation, erythrocyte-lyzed cells from recipient mice were incubated with PE-conjugated antibodies specific to various hematopoietic lineages: T lymphocytes (T-cells), macrophages, monocytes and granulocytes (Mac/Mono/Gr), B lymphocytes (B-cells) and erythroid lineage cells. The percentage of each hematopoietic cell lineage in peripheral cells was determined with a FACSCalibur System. Cells positive for PE but negative for GFP were considered of recipient host origin, while cells positive for PE and positive for GFP were considered of donor.

Objective 1c: To determine the skeletal marrow and non-skeletal sites of engraftment in recipient mice after transplant with donor HSCs, we will assess the presence of donor cells in non-skeletal tissues will be accomplished by frozen sectioning of the heart, lungs, liver and spleen of the recipients and fluorescent microscopic observation. Experiments were performed in year 1 and initiated in year 2 to assess the presence of donor cells in non-skeletal tissues. Over the past year, the heart, lungs, liver, kidneys, spleen and bone marrow cavities of the recipients mice transplanted with Sca-1+ enriched cells from TgN (GFP+) mice were harvested 6 months post transplantation. Tissue specimen were prepared by frozen sectioning and examined for the presence of GFP+ donor by fluorescent microscopy. Frozen sectioning of bone tissue revealed severe autofluorscence from the surface of the bony tissues in both control and GFP-transplanted mice. Due to this technical difficulty valid comparisons could not be made. However, FACs analysis of the bone marrow of the GFP-transplanted mice indicated that 30-50% of the bone marrow cells in the recipients were GFP+, indicating that Sca-1+ cells of donor origin are capable of homing and establishing long term engraftment in the bone marrow cavity of the recipients. Small numbers of GFP+ cells (~1-2 cells per 10x magnification field) were observed within the blood vessels of the heart, lungs, liver and kidneys of the recipient mice. However, no donor-derived cells were observed in the parenchymal tissue of these organs, suggesting that no significant engraftment of donor Sca-1+ cells occurs in these tissues. In contrast, as seen in Figure 1, increased GFP fluorescence was observed in the spleens of GFP+ cell transplanted recipients (right panel) compared to nontransplanted control mice (left panel). These data suggest that intravenously injected donor cells home and engraft within the spleen and represent a potential for unwanted side effects. However, recent studies have demonstrated that the degree of spleen engraftment after transplantation can be vastly lowered by infusing cells from donors of an age different that that of the recipient. **(**Liang, et. al., Effects of aging on the homing and engraftment of murine hematopoietic stem and progenitor cells, *Blood* 2005, Vol. 106, No. 4, pp. 1479-1487). Nevertheless, our results indicate that future studies evaluating the safety of hematopoietic stem cell-delivered gene therapies will require the assessment of effects on the spleen as well as the targeted tissues.

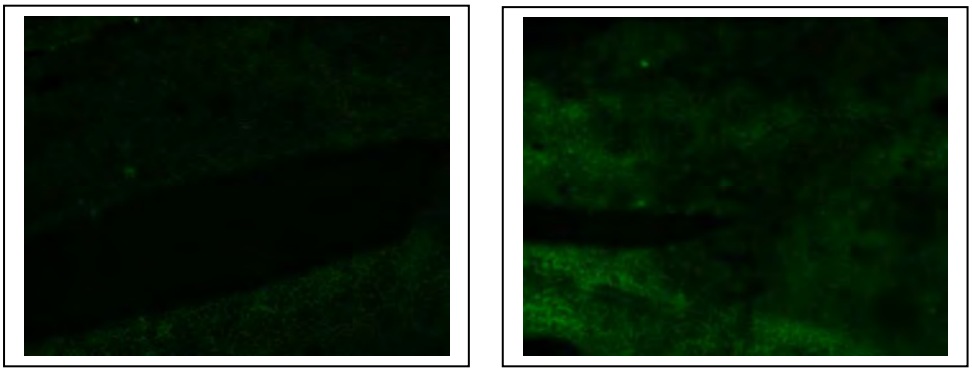

Figure 1: Photomicrographs of frozen sections (5µm thickness) of the spleens from a representative non-transplanted W41/W41 control mouse (left panel) and a representative mouse injected 6 months prior with hematopoietic stem cell enriched cells from a GFP+ donor mouse.

<u>Technical Objective 2</u>: To assess and quantitate the short-term and long-term bone formation achieved in mice following transplantation with HSCs transduced to express a growth factor gene.

a. **Transduce HSC-enriched cells with an HIV-based vector expressing the BMP 2/4 gene under the control of the CMV promoter.**
b. **Transplant transduced donor cells via tail vein into myelosuppressed recipient mice and evaluate bone formation after 8 weeks, 6 months and 10 months.** In year 1 and 2, we performed the experiments described in Objective 2. Sca-1^+ cells were transduced to express the BMP4 transgene and transplanted into recipient mice. As previously reported this strategy did not result in large increases in bone formation as expected. Briefly, Sca-1^+ cells from TgN donor mice were transduced with either a marker gene (b-gal) or BMP2/4 transgene lentiviral based vectors and transplanted preconditioned W^{41}/W^{41} recipient mice. At several time points post-transplant, engraftment was assessed and after 6 months bone formation parameters were measured in the two groups. No significant differences in engraftment levels between the groups was observed at any time point. Serum skeletal alkaline phosphatase (AP), a bone formation biochemical indicator was measured. Serum AP levels were elevated in the BMP2/4-treated group (32 U/ml) compared to the control group (29 U/ml), but this difference did not reach statistical significance. Bone formation parameters (total bone mineral density (BMD), trabecular BMD, cortical BMD, cortical thickness, endosteal circumference or periosteal circumference) of femurs from the mice were also determined. No significant differences were observed in total BMD or endosteal circumference between the BMP2/4-transplanted mice and controls. Trabecular BMD was significantly increased ($p < 0.05$) in mice in the BMP2/4 treatment group compared to control mice (0.312 mg/cm^3 vs. 0.266 mg/cm^3, respectively). These data suggested that overexpression of the BMP2/4 transgene increased trabecular BMD levels compared to controls. Furthermore, although not statistically significant, the BMP2/4 mice had higher serum AP, total BMD and smaller endosteal circumference. We acknowledge that these results should be interpreted with caution. Results from experiments performed in year 1, showed no significant differences in bone formation parameters between controls and BMP2/4-treated mice. We suspect that one potential reason for this discrepancy may be the wide variation in transgene expression between recipient mice. It is also possible that the level of transgene expression may be insufficient to produce effects of a sufficient magnitude to be detected at the power level achieved by the experimental design. Finally, although BMP4 is a well-established promoter of bone formation in many animal models, it is possible that overexpression of this protein may adversely affect stem cell engraftment and/or hematopoietic differentiation. As a result of these experimental results, our Technical Objective 3 below was revised to explore these and other possible mechanisms underlying our observed results.

<u>Revised Technical Objective 3</u>: To explore the possible mechanism(s) for why transplantation of HSC-enriched cells transduced to express BMP4 did not induce bone formation as expected.

a) **To determine if silencing of the BMP2/4 transgene occurs we will, transplant donor HSCs transduced to express BMP 2/4 (or marker control gene) into myelosuppressed recipient mice and evaluate transgene expression at 8 weeks and 6 months post transplant. Transgene expression will be evaluated by real time RT-PCR in RNA**

extracts and PCR in DNA extracts In year 3 we have initiated experiments to examine whether silencing of the BMP2/4 transgene occurs after transplantation into recipient mice. In the first set of studies, preconditioned W41/W41 recipient mice were each injected with 350,000 Sca-1+ cells from GFP+ donor mice that were transduced to express either the b-gal marker (control) gene, modified bone morphogenic protein (BMP2/4) gene or the human growth hormone (hGH) gene. At 8 weeks post transplantation, peripheral blood was collected from the recipient mice and DNA and RNA was extracted from the mononuclear cells fractions. Real time PCR (reflecting successful insertion of the transgene into the donor cells and successful engraftment of donor cells) and real time RT-PCR (reflecting transgene expression) was performed on the DNA and RNA isolates, respectively and results of these analyses are displayed in Tables 2 and 3.

	mean DNA ratio (st. dev)	
cells transplanted	**hGH /cyclophillin**	**BMP4 /cyclophillin**
b-gal-transduced	**0.00 (0)**	**0.00 (0)**
hGH-transduced	**1.16 (0.44) ***	**0.00 (0)**
BMP2/4-transduced	**0.00 (0)**	**0.02 (0.01) ***

Table 2. Real time PCR analysis of mononuclear blood cells 8 weeks post transplantation from recipient mice transplanted with Sca-1+ cells transduced to express b-galactosidase (b-gal-transduced), human growth hormone (hGH-transduced) or bone morphogenic 2/4 (BMP2/4-transduced) genes. DNA quantities (pg) were determined for hGH and BMP4 transgenes and cyclophillin housekeeping gene using specific primers and standard curves. Ratios were calculated by quantity of DNA of specific gene divided by quantity of cyclophillin DNA. ANOVA * p-value < 0.0001

	mean RNA ratio (st. dev)	
cells transplanted	**hGH /cyclophillin**	**BMP4 /cyclophillin**
b-gal-transduced	**0.00 (0)**	**0.00 (0)**
hGH-transduced	**4.15 (3.32) ***	**0.00 (0)**
BMP2/4-transduced	**0.00 (0)**	**0.05 (0.03) ****

Table3. Real time RT-PCR analysis of mononuclear blood cells 8 weeks post transplantation from recipient mice transplanted with Sca-1+ cells transduced to express b-galactosidase (b-gal-transduced), human growth hormone (hGH-transduced) or bone morphogenic 2/4 (BMP2/4-transduced) genes. DNA quantities (pg) were determined for hGH and BMP4 transgenes and cyclophillin housekeeping gene using specific primers and standard curves. Ratios were calculated by quantity of DNA of specific gene divided by quantity of cyclophillin DNA. ANOVA * p-value < 0.002, ** p-value < 0.0002

As seen in Table 2, as expected, hGH DNA was detected in the peripheral mononuclear blood cells of mice transplanted with Sca-1+ cells expressing this transgene but not of mice in the b-gal and BM2/4 groups and BMP4 protein was only detected in mice transplanted with cells transduced to express the BMP4 gene, suggesting that donor cells were successfully transduced

and successfully engrafted recipient mice. Comparison of the amount of DNA relative to the housekeeping gene (cyclophillin) suggests that cells transduced with the hGH vector were more efficient in transduction and/or engraftment than donor cells transduced with the BMP2/4 vector. However, because different primers specific for each transgene were employed in these studies, it is difficult to determine the degree to which primer efficiency may have affected the analysis. Therefore, future studies include the design of a primer specific to our retroviral vector and measure the level of DNA present in cell extracts from recipient mice. This approach will eliminate differences in primer efficiencies between the different transgenes and allow for more accurate comparisons. Measurements of RNA expression levels as reported in Table 3 are consistent with the DNA data, as reflected by higher relative levels of hGH mRNA compared to BMP4. At this time the cause for the differential DNA and RNA levels observed between different transgenes are unknown but will be explored in more detail in planned studies. Future studies also will include measurement of DNA and RNA levels in these recipient mice at later a later time point (6 months post transplantation) to determine if levels change over time. In addition, we have repeated this transplant experiment to confirm our results.

b. To determine if BMP2/4 interferes with engraftment of Sca-1$^+$ cells we will: transduce Sca-1$^+$ cells transduced to express BMP 2/4 (or marker control gene) and transplant at 4 cell doses (500, 5000, 50,000 or 500,000 cells/recipient) into myelosuppressed recipient mice and evaluate engraftment at 4, 6, 8, 10 and 16 weeks.

c. To determine if BMP2/4 induces Sca-1$^+$ cell differentiation into hematopoietic lineages. Transduce Sca-1$^+$ cells transduced to express BMP 2/4 (or marker control gene) and transplant at 4 cell doses (500, 5000, 50,000 or 500,000 cells/recipient) into myelosuppressed recipient mice and evaluate the percentage of various hematopoietic lineages (T-lymphocytes, B-lymphocytes, monocytes and erythroid) at 4, 6, 8, 10 and 16 weeks. Hematopoietic lineage will be assessed by immunostaining and FACs analysis.

Mice have been transplanted and the experiments will be performed as described above in Objective 3b and 3c.

Key Research Accomplishments for year 3

- We have repeated enrichment and transplantation experiments and confirmed that we can consistently achieve high enrichment of Sca-1$^+$ cells, high transplantation success and high, stable engraftment of Sca-1$^+$ cells for up to 40 weeks.
- We have demonstrated that transplantation of donor Sca-1+ cells (5 months post transplantation) leads to long term and multilineage hematopoietic cell engraftment.
- We have determined that the bone marrow cavity and the spleen are the primary sites of engraftment of the Sca-1+ donor cells after transplantations. In contrast, the liver, heart, kidneys and lungs demonstrate insignificant engraftment of these cells.
- We have performed transduction experiments using the BMP2/ transgene and confirmed that we can successfully transduce Sca-1$^+$ cells using a retroviral-based vector. However, overexpression of BMP2/4 resulted only in small increases in bone formation. We have

demonstrated that while BMP2/4 transduced cells successfully engraft, the level of BMP4 DNA and RNA present in the recipient mice is much lower than observed with other transgenes such as hGH. These data suggest that one mechanism contributing to the lack of effect on bone formation observed with BMP2/4 in previous studies is likely insufficient therapeutic levels of the transgene after engraftment.

Reportable Outcomes

None

Conclusions

In our systemic gene therapy subproject, we can achieve consistently high yields of highly enriched hematopoietic progenitor cells from donor mice. Transplantation of these cells into preconditioned recipient mice results in consistently high, stable engraftment in the skeletal and splenic tissues, with minimal engraftment in non-skeletal tissues of the recipient animal. We have successfully transduced the hematopoietic progenitor cells using retroviral-based vectors which overexpress BMP2/4 or hGH. Transplantation with donor cells retrovirally transduced to express BMP4 did not produce large increases in bone formation in recipient mice as expected. This lack of response may be the result of insufficient dose levels of the therapeutic protein. Future work is planned to explore this and other the potential mechanism(s) of action that may explain these results

PROJECT 7

PRINCIPAL INVESTIGATOR: Kin-Hing William Lau, Ph.D.

TITLE: Study of Synergistic Growth Factors in Skeletal Gene Therapy

Sub-Project 7: Study Of Synergistic Growth Factors In Skeletal Gene Therapy

Introduction:

Skeletal gene therapy strategies utilizing a single osteogenic growth factor have been shown to be effective in stimulating bone formation and enhancing bony repair (1-4). There are recent studies suggesting that combination of two growth factor genes produced significant synergistic osteogenic effects (5). This observation provides a strong rationale for development of gene therapy-based strategies employing two or more osteogenic growth factor genes for repair of bone injuries or to treat bone-wasting maladies. Accordingly, synergistic gene therapies would not only provide significantly greater osteogenic effects, but would also allow the use of significantly lower dosages of the growth factor genes. The use of lower dosages not only would reduce the costs of the therapy and could also potentially reduce undesirable side effects due to high doses of growth factors. Consequently, the long-term objective of this sub-project was to develop a safe and effective combination ex vivo gene therapies to deliver locally in bone two or more osteogenic genes for repair of skeletal injuries. The immediate objectives were: 1) to assess the feasibility of a combination ex vivo skeletal gene therapy strategy to locally express in bone two osteogenic genes acting synergistically to promote healing of a large skeletal defect, 2) to identify an appropriate combination pair of osteogenic growth factor genes that would produce synergistic enhancement of bone formation, and 3) to determine the optimal conditions for the synergistic combination gene therapy. The original objective was to evaluate the therapeutic potential of primary bone marrow-derived stromal cells overexpressing Cox-2 and VEGF in the mouse critical-sized calvarial defect model. Because our work during the past two years have shown that Cox-2 and VEGF did not synergistically interact with each other to promote healing of the critical-sized calvarial defect (summarized in Section II.2.A.3 below), we shifted our focus to investigate the potential interaction between BMP-4 and VEGF (see Section II.2.A.4) and between BMP-4 and Cox-2 (see Sections II.2.B.1 and II.2.B.2). We also initiated work to test other osteogenic growth factors, such as FGF-2 and growth hormone.

Body:

1. Technical Objectives:

The specific technical objectives of year one were:

1) To prepare MLV-based retroviral vectors expressing the Cox-2 and VEGF genes, and to characterize transgene expression levels following transduction of primary bone marrow derived stromal cell cultures (MSCs) in vitro;

2) To evaluate the impact of transcplantation of MSCs expressing Cox-2 and VEGF on the rate and quality of healing of critical-size mouse calvarial defects in vivo.

The specific technical objectives of the year two and current reporting year were:

3) To optimize the dose and time of growth factor combinations with regard to bone formation time and bone quality;

4) To initiate studies aimed at determining the molecular mechanism of bone formation by osteogenic growth factors.

To facilitate the readers' understanding of our overall progress in the context of each Technical Objective, we will first briefly summarize our past progress made during the first two years of funding. We will then describe in details the progress made during the current reporting period. In general, our work thus far supports the notion that this novel therapeutic approach is technically feasible and can significantly enhanced bone regeneration in the mouse calvarial defect model. On the other hand, during the course of our investigation, we have also encountered unexpected difficulties, which we will summarize in Section 2.C below. Specifically, our studies disclosed an interesting, but totally unexpected, observation with respect to the combination use of Cox-2 and BMP4 genes in the marrow stromal cell-based ex vivo gene therapy strategy to repair a critical-sized calvarial defect in mice. In this regard, while we have demonstrated that Cox-2 synergizes with BMP4 in promoting osteoblastic differentiation of mouse marrow stromal cells in vitro, enhanced Cox-2 transgene expression in the mouse calvarial defect model in vivo, not only did not synergistically enhance, but in fact markedly suppressed, the bone formation effects of BMP4. These unexpected, but also highly interesting results, are the focus of this current report.

2. Progress towards Technical Objectives:

A. Summary of Progress Made During the Past Funding Years.

1. Adaptation of the rat critical-sized calvarial defect model in mice. A prerequisite for this project is a reliable bone repair model for use to test the feasibility of the combination gene therapy strategies. In this regard, we have previously established a rat critical-sized calvarial defect model and utilized this model to assess the therapeutic efficacy of ex vivo MLV-based BMP4 gene therapy to promote bone regeneration in the rat (1). A bone defect is defined to be of critical size when healing does not occur spontaneously over an extended period of time. Such defects are ideal for testing the bone regenerating activity of novel therapeutic modalities such as growth factor gene therapy. The critical-sized calvarial defect model has an important advantage over critical-sized bony defects involving limbs or the spinal column. The calvarial model does not require surgical stabilization of the defects, and test compounds can easily be inserted into the calvarial defect and held tightly in place after suturing of the skin. However, one of our long-term goals was to understand molecular mechanisms leading to the synergistic enhancement of bone regeneration by investigating the bone regeneration and repairing processes in response to single or combination gene therapy strategies in transgenic mice in which the candidate gene is deleted or overexpressed. Thus, we sought to adapt the rat critical-sized calvarial defect model in mice to produce a mouse critical-sized calvarial defect model for the proposed work. Therefore, a significant effort has been put forth in our group to establish a reliable mouse critical-sized calvarial defect model.

Briefly, a 5-mm circular defect was carefully created (without damaging the highly vascularized dura mater) using a diamond-based dental burr in the calvaria of adult C57BL/6J mice. This defect, by definition, did not heal by itself over extended observation period (as long as 8 weeks). A piece of gel foam impregnated with mouse bone marrow-stromal cells, transduced with MLV-based expressing a bone growth factor gene (e.g., BMP4) or a β-galactosidase (β-gal) control gene, was placed in the calvarial defect. New bone formation within the bony defect was then detected by X-ray, quantitated with DEXA, and confirmed with bone histology. In this mouse model, defects implanted with BMP-4 expressing stromal cells showed healing and robust new bone formation that completely filled the hole within 4 weeks. In

contract, defects implanted with gel foams without cells or with cells expressing the β-gal control gene showed no appreciable bone formation. Therefore, we have successfully established a mouse critical-sized calvarial defect model for use in this project.

2. Progress toward Technical Objective #1: preparation of MLV-based retroviral vectors expressing the Cox-2 and VEGF genes, and to characterize transgene expression levels following transduction of primary bone marrow derived stromal cell cultures in vitro. We chose MLV-based vectors for our work because we have extensive experience with these vectors (6) and because these retroviral vectors have been shown to transduce effectively human and rodent bone marrow stromal cells. The rationale for choosing VEGF and Cox-2 as the initial test gene combination was because these two genes have been shown to have both osteogenic and angiogenic actions: both of which are essential for bony regeneration and bone repair.

There are at least five forms of VEGF (VEGF-A, -B, C-, D, and placental growth factor, PlGF). Since VEGF-A is the major and the most studied form, and since it has shown to stimulate bone formation and is also the most strongly associated with angiogenesis, the human VEGF-A was chosen as the test gene in this project. There are nine major VEGF-A isoforms (VEGF-A_{121}, -A_{145}, -A_{148}, -A_{162}, -A_{165}, -A_{165b} (an endogenous inhibitory isoforms that binds to VEGFR2 with similar affinity to VEGF-A_{165} but does not activate it), -A_{183}, -A_{189}, and -A_{206}). Because VEGF-A_{165} has been shown to synergize with BMP-4 to promote bone formation (5), we chose VEGF-A_{165} for investigation. The human VEGF-A_{165} was cloned by PCR, and an MLV-based vector expressing the human VEGF-A_{165} was constructed as a similar strategy described for the MLV-BMP2/4 vector (6). In contrast, Cox-2 is an inducible gene and its mRNA is highly unstable because, like most inducible genes, the Cox-2 mRNA contains numerous AU-rich elements (AREs) in its 3' untranslated region (3'-UTR); AREs have been shown to be responsible for mRNA instability and degradation (7). The half-life of unmodified Cox-2 mRNA is therefore extremely short, which would limit production of the Cox-2 protein. Accordingly, we modified the human Cox-2 transgene to improve mRNA stability and protein translation by a) removing the large majority of the ARE-containing 3'-UTR and b) replacing the native Kozak sequence of human Cox-2 gene with an optimized Kozak sequence (8). An MLV-based vector expressing the modified human Cox-2 gene was again constructed as described previously (6). MLV-based vectors expressing BMP4, FGF-2, and β-gal and green fluorescence protein (GFP) control genes in the same viral backbone were also produced and used in this study as control and as alternative osteogenic genes for comparison. In these vectors, expression of the trangene is under control of a constitutively active, potent CMV promoter.

To characterize transgene expression levels following transduction of primary bone marrow derived stromal cell cultures with these MLV vectors in vitro, primary mouse bone marrow stromal cells were transduced two to three times with MLV vector expressing each of the test osteogenic gene at a multiplicity of infection (MOI) of 10-20 over 36 hrs as previously described (6). This "2- or 3-hit protocol over 26 hrs would ensure that cells are actively proliferating and undergo at least one cell division in the presence of the retroviral vector, which is absolutely essential for MLV transduction as MLV would transfect only proliferating cells. Indeed, this transduction protocol led to >90% transduction efficiency in primary mouse marrow stromal cells. As measurements of transgene expression, the human VEGF-A_{165}, Cox-2, or BMP4 protein levels were measured in conditioned media (CM) as well as in cell extracts by

both ELISA and Western immunoblot assays over a 4-week period. The VEGF-A level in the CM of transduced cells assayed by a specific ELISA was 250 to 500 ng/10^6 cells/24 hrs 7 days after transduction. Because of the modification of Cox-2 gene, cells transduced with Cox-2 expressing virus also led to high (600 to 1,200 ng/10^6 cells/24 hrs) and sustained secretion of Cox-2 protein. Cells transduced with MLV-BMP4 were also shown to secrete in their CM high levels (100 to 200 ng/10^6 cells) BMP4 protein. The biological functional activity of VEGF was confirmed by increased angiogenesis in vivo and that of Cox-2 was confirmed by increased PGE_2 formation in transduced cells in vitro. Consequently, we have now successfully accomplished our Technical Objective 1.

3. Progress toward Technical Objective #2: Evaluation of the impact of transplantation of mouse marrow stromal cells expressing Cox-2 and VEGF-A_{165} on the rate and quality of healing of critical-sized mouse calvarial defects in vivo. To evaluate the impact of transplantation of mouse marrow stromal cells expressing Cox-2 and VEGF-A on the healing of the critical-sized calvarial defect, a gelatin matrix scaffold (Gel-foam) cut to fit the calvarial defect was impregnated with 1 x 10^6 transduced cells expressing Cox-2, VEGF-A, BMP4 (positive control), or GFP control gene each alone or in combination overnight. The Gel-foam impregnated with transduced cells was then transplanted to the critical-sized calvarial defect. Recipient mice receiving Gel-foam without cells were also included as an untreated negative control. New bone formation (assessed by X-ray and DEXA) was measured 14 days post-tranplantation to assess the efficacy of bone regeneration of the transgene. During the initial phase of healing of calvarial defects, osteoblasts (or precursors) at the margin of the defect proliferate and differentiate rapidly, migrate towards the center of the wound and establish formation and mineralization of the bone matrix along the wound periphery until the entire defect is filled up with newly formed bone. This bone regenerating activity is thought to be stimulated by growth and differentiation factors that are released locally in response to the injury. Failure to close the critical-sized defect is believed to result from a deficiency in the level or persistence of local bone growth factor production (9). Accordingly, it is anticipated that transplantation of marrow stromal cells (which contain osteoblast precursors) expressing a suitable osteogenic factor in the defect would promote repair of the defect. In this regard, we have clearly demonstrated that transplantation of BMP4 expressing marrow stromal cells in the rat critical-sized calvarial defect promoted complete healing of the defect (1).

As predicted, there was no evidence for new bone formation in the defects receiving untreated Gel-foam or those transplanted with control cells expressing the GFP control gene. There was also no new bone formation in control defects transplanted with untransduced marrow stromal cells. Conversely, as in the rat critical-sized defect model, transplantation of mouse marrow stromal cells expressing BMP4 yielded a complete regeneration of the defect after 14 days. Surprisingly and intriguingly, there was also no clear evidence for significant new bone formation in defects receiving cells expressing Cox-2 or VEGF-A_{165} alone or in combination. Transduction of mouse marrow stromal cells with our MLV-Cox-2 virus led to significant increase in PGE_2 production and alkaline phosphatase (ALP) activity in the transduced cells and the in vivo administration of the same MLV-Cox-2 vector promoted fracture repair in the rat femoral fracture model. Thus, the lack of bone regenerating effect of the Cox-2 expressing cells was not due to production of inactive Cox-2. Subsequent analysis of Cox-2 mRNA levels within the defect indicates that the lack of a bone formation effect was also not due to expression of

Cox-2 in transduced cells within the defect. Similarly, there was strong evidence for a massive increase in blood vessel formation in the defects receiving cells expressing VEGF-A_{165}, indicating that there were sufficient amounts of functional VEGF-A produced within the treated defects over the course of treatment. Thus, the lack of bone formation effects of the VEGF-A in this model was not due to insufficient expression of VEGF-A or inactive VEGF-A protein. Histological analysis of the defects confirmed the results of the X-ray and DEXA bone density analyses. The absence of a bone formation response with VEGF-A therapy alone was not entirely surprising as a previous study showed that transplantation of messenchymal stem cells expressing VEGF-A alone in a segmental defect model not only did not enhance bone formation, but actually slightly inhibited bone formation, although the VEGF-A and BMP4 combination markedly enhanced the bone formation response of BMP4 (5). What was surprising is that the Cox-2 treatment did not produce a bone formation response in this calvarial defect model, given the fact that the same MLV-Cox-2 vector markedly enhanced bone formation and fracture repair in the femoral fracture model and that Cox-2 and PGE_2 treatments have been shown to promote bone formation in a number of in vivo and in vitro models. Our current efforts focus on determining the potential reasons for the absence of a bone formation response in the calvarial defect model by the Cox-2 therapy (see below). Regardless of the reason for the lack of a bone formation response for the VEGF-A or Cox-2 therapy in our model, this study clearly indicates that the combination gene therapy of VEGF-A and Cox-2 would not produce synergistic response in repairing calvarial defects in mice.

Inasmuch as the results of our work were unexpected and largely of negative nature, we have nevertheless completed all of the proposed work of Technical Objective #2.

4. Progress toward evaluation of the effects of transplantation of mouse marrow stromal cells expressing VEGF-A and/or BMP4 on the rate and quality of healing of critical-sized mouse calvarial defects in vivo. Since our overall objective is to develop a synergistic gene transfer-based therapeutic strategy for enhancing bone healing and repair, we have modified our Technical Objectives to identify a more suitable pair of synergistic osteogenic growth factor genes for evaluation. We next decided on testing the possibility that either Cox-2 or VEGF-A might synergize with and enhances the bone formation effect of BMP4 in the mouse critical-sized calvarial defect model. We first examined the potential synergistic effects between BMP4 and VEGF-A, since it has previously been reported that VEGF-A when given in the ratio of 1:5 with BMP4 produced a synergistic enhancement of bone formation in a rat segmental defect model compared to BMP4 ex vivo gene therapy alone (5).

To test whether VEGF-A would synergize with BMP4, defects transplanted were with 4 x 10^5 cells of BMP4 expressing mouse marrow stromal cells, 1 x 10^5 cells of VEGF-A expressing cells, alone or in combination (BMP-4:VEGF-A in 1:4 ratio). As expected, BMP4 treatment produced a significant increase in bone formation, while VEGF-A treatment had no significant bone formation effect compared to control defects with no cells or transplanted with GFP expressing control cells. However, contrary to what was reported for the rat segmental defect model, the BMP4 and VEGF-A combination regiment did not produce a large synergistic enhancement in new bone formation. On the contrary, quantitative bone mineral density (BMD) measurements by DEXA revealed that the combination therapy produced a significant 20% reduction in BMD compared to BMP4 treatment alone 4 weeks after transplantation. However,

the VEGF-A treatment led to a massive increase in highly vascularized, soft tissue. When the total material density of both hard and soft tissues over the defect were measured by X-ray and the Alpha Innotech light imaging system, quantified by the Chemi-Imager 4400 software, the BMP4/VEGF-A combination therapy produced a dose-dependent (with respect to the number of VEGF-A expressing cells) decrease compared to BMP4 treatment alone. Our results are very different from that of Peng et al. (5), which reported synergistic enhancement of bone formation and healing of segmental defects in the long bones by muscle stem cell-expressed VEGF and bone morphogenetic protein-4. Potential explanations for the differences seen in our studies and their study include, but are not limited to, the use of different bony defect model (calvarial defect model vs. long bone segmental defect), the different vehicle (marrow stromal cells vs. muscle stem cells), or the cell dosages. Regardless of the reasons, our data confirm that the ex vivo BMP4 gene therapy can effectively repair the mouse critical-sized calvarial defect. However, the presence of VEGF expressing cells did not synergistically enhance the bone formation response of BMP4 in this model.

Cox-2 (Cyclooxygenase 2, also known as Prostaglandin H synthase) has been shown to be a potent osteogenic factor that stimulates bone formation in a large number of models, including fracture repair. Cox-2 is the enzyme that mediates the conversion of arachidonic acid to PGH_2, which is the key rate-limiting step of prostaglandin biosynthesis, including PGE_2. PGE_2 has been established to be a potent bone formation agent. Accordingly, it has been generally assumed that the osteogenic action of Cox-2 is in part mediated through PGE_2. Cox-2 as well as PGE_2 are both potent stimulators of osteoblast proliferation. In addition, Cox-2 is a potent angiogenic factor, which is also required for osteogenesis. In contrast, BMP4 is a potent differentiation agent of osteoblasts and is believed to stimulate bone formation primarily through osteoblast differentiation. Consequently, there is a good rationale to believe that Cox-2 and BMP4 could act synergistically to promote bone formation. Consequently, a majority of our efforts during the current reporting year and the past year have focused on the combination treatment of Cox-2 and BMP4 to promote healing of mouse calvarial defects. The results of our preliminary work in this area during the past year and the current reported period will be reported together in the following section in order to give readers a more comprehensive picture of our progress in this area as a whole.

B. Detailed Summary of Progress Made During the Current Reporting Year.

1. Progress toward Technical Objective #3: evaluation of the effects of transplantation of mouse marrow stromal cells expressing Cox-2 and BMP4 on the healing of critical-sized mouse calvarial defects in vivo and optimization of the dose and time of growth factor combinations with regard to bone formation and bone quality. To evaluate if BMP4 and Cox-2 would synergize with each other to promote healing of the critical-sized calvarial defect in the mouse, we transplanted gel-foam impregnated with a sub-maximal amount of (1×10^5) mouse marrow stromal cells expressing BMP4 with or without 9×10^5 Cox-2 expressing cells, 9×10^5 Cox-2 expressing cells plus 1×10^5 GFP expressing cells, or 1×10^6 GFP expressing control mouse marrow stromal cells. The healing was allowed to proceed for 4 weeks, and bone mineral density over the defect site was determined with Faxitron. Figure 1 shows that defects treated with BMP4 expressing cells alone significantly increased the mineral density over the defect area and brought it back to ~70% of the BMD of the normal calvaria. Conversely, defects receiving Cox-2 expresing cells at the test dose not only did not increase, but slightly reduced the mineral density

over the defect site compared to control defects receiving the GFP expressing cells. Most importantly, defects receiving the BMP4 and Cox-2 combination treatment not only did not show an enhancement of, but in fact completely suppressed the bone formation response of BMP4 in this bone healing model. This experiment has been repeated three times, with combination of different numbers of BMP4 or Cox-2 cells. However, because of the differences in viral titers, transduction efficiencies, growth rate of transduced mouse marrow stromal cells, etc., the amounts of BMP4 and/or Cox-2 protein produced by the same number of transduced cells could vary in different experiments. Thus, the absolute values of changes in mineral density varied from experiment to experiment. However, the suppression of the BMP4 bone formation response in this defect model was reproducible and seen in every repeat experiment. The suppression of bone formation response of BMP4 by Cox-2 was confirmed with histology (data not shown). Consequently, these findings not only did not support a synergistic enhancement between BMP4 and Cox-2 gene therapy, at least at the test dose, in bone formation with the mouse calvarial defect model.

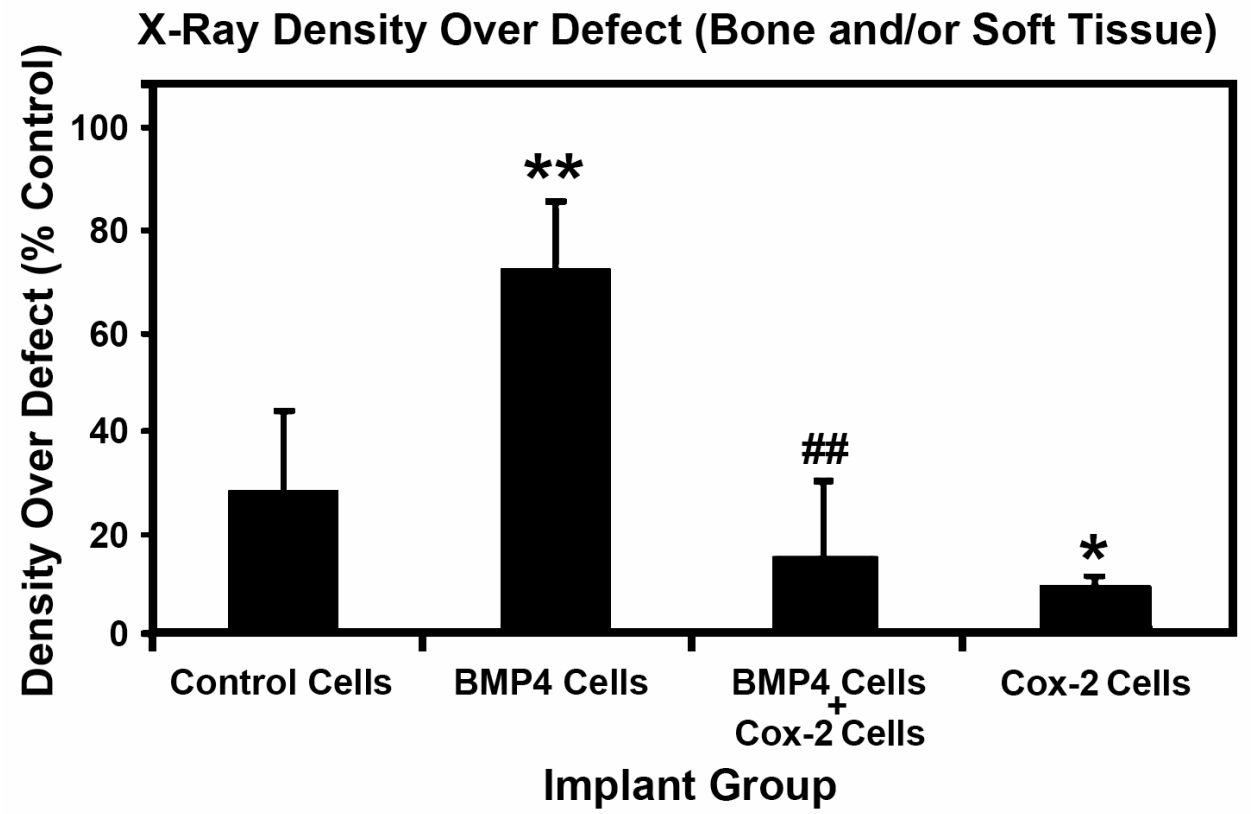

Figure 1: Tissue Density in mouse critical-sized calvarial defects after 4 weeks with BMP-4 and Cox-2 ex vivo gene therapy. Mouse critical-sized (5-mm i.d.) calvarial defects were implanted with gel-foam impregnated with 1 x 10^6 GFP expressing primary mouse marrow stromal cells alone (Control Cells), 1 x 10^5 BMP4 expressing cells plus 9 x 10^5 GFP control cells (BMP4 Cells), 9 x 10^5 Cox-2 expressing cells plus 1 x 10^5 BMP expressing cells (BMP4 Cells + Cox-2 Cells), or 9 x 10^5 Cox-2 expressing cells plus 1 x 10^5 GFP expressing control cells (Cox-2 Cells). The healing was allowed to proceed for 4 weeks. The animals were then sacrified and calvaria were dissected free of other tissues. X-ray images of the calvariae were taken with Faxitron and analyzed with the Alpha Innotech light imaging system. Values are average ± S.D.

from 4 animals per test group. *$p<0.05$; and **$p<0.01$ compared with Control cells group, $^{\#\#}p<0.01$ compared with BMP4 cells group.

The previous report indicates that the synergy between BMP4 and VEGF-A was dose-dependent and was related to the relative ratio between BMP4 expressing stem cells and VEGF-expressing stem cells (5). To investigate if the synergy between BMP4 and Cox-2 might also be dependent of the relative ratio of BMP4- and Cox-2-expressing cells, we treated calvarial defects with two different ratios of BMP4- and Cox-2-expressing cells (i.e., 1:1, 1:5, and 1:10). Similar suppression of the bone formation response of BMP4 by Cox-2-expressing cells was seen in treatments with either ratio, although the higher ratio group (i.e., 1:9 ration of BMP4:Cox-2) appeared to show a smaller suppression (data not shown). Therefore, our in vivo work with the mouse critical-sized calvarial cefect model yielded a surprising observation in that the combination Cox-2 ex vivo gene therapy with BMP4 ex vivo gene therapy not only did not produce a synergistic enhancement in the bone healing response, but it unexpectedly suppressed the bone formation response of the BMP4 gene therapy. Although it was our intention in the Technical Objective #3 to optimize the combination gene therapy, we feel that it would be important to determine the mechanistic reason(s) for the suppression prior to further experimentation to optimize this combination therapy. Once we have determined potential molecular mechanisms by which Cox-2 acts to suppress BMP4 in the healing of the calvarial defect, we will then continue to optimize the combination therapy. We should also emphasize that these two growth factors, which act on different phases of bone formation, could have different optimal time- and/or dose-dependent kinetics, which need extensive optimization in order to obtain the synergistic effect.

2. Progress toward Technical Objective #4: Initiation of work to determine molecular mechanism of bone formation by osteogenic growth factors. Specifically, to gain molecular insights into molecular mechanism(s) whereby Cox-2 suppresses the bone formation response of BMP4 in the mouse calvarial defect model. During the current reporting year, we focused our efforts on the determination of potential mechanistic reasons for the negative interaction between Cox-2 and BMP4 gene therapy, primarily with in vitro approaches (Technical Objective #4).One of the possibilities that we have considered is that Cox-2 (or its anabolic product, PGE_2) might not produce a synergistic interaction with BMP4 on osteoblast activity, even evidence in the literature strongly supports such a synergy. As an initial test for this possibility, we treated primary mouse marrow stromal cells with 200 ng/ml recombinant BMP4 protein, 10 μM PGE_2, or the combination of the two effectors, along with the solvent control, for 7 days. Cell extracts were then prepared by extracting each treated cell culture with 0.1% Triton X-100. The alkaline phosphatase (ALP) activity, which is a well-accepted marker of osteoblast differentiation, was measured. As previously shown repeatedly that BMP4 is a potent stimulator of osteoblast differentiation, the BMP4 treatment alone led to ~8-fold increase in ALP activity (Fig. 2). Also as previously reported, the PGE_2 treatment alone also yielded a ~2-fold increase. Most significantly, the PGE_2 and BMP4 combination produced a significantly larger increase in ALP than BMP-4 alone. Similar results were obtained after 3 days, rather than 7 days, of incubation (data not shown). These results were highly reproducible and were seen in two separate repeat experiments. These findings indicate that PGE_2 can act synergistically with BMP-4 in promoting osteoblast differentiation in vitro, and as such are entirely consistent with the contention that the product of Cox-2, PGE_2, and BMP-4 can act synergistically to stimulate bone formation.

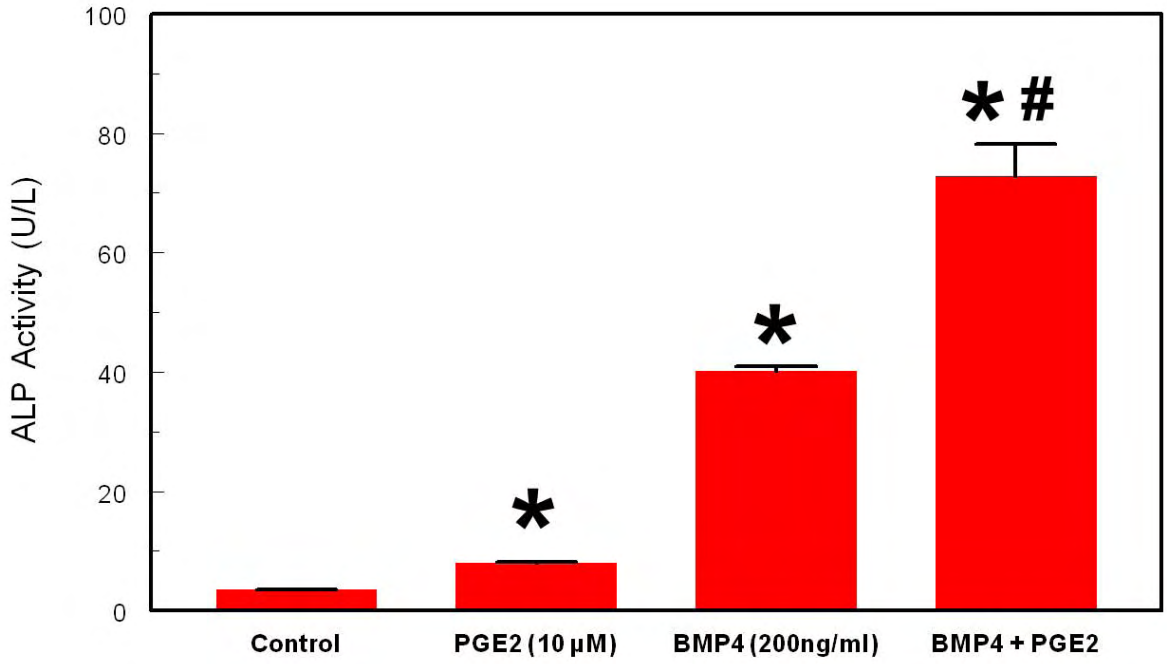

Figure 2. Synergistic stimulation of ALP expression in primary mouse marrow-derived stromal cells by prostaglandin E_2 (PGE_2) and BMP4 in vitro. Primary mouse marrow-derived stromal cells were plated in 6-well culture plates. Twenty-four hrs after plating, PGE_2 (10 µM), recombinant human BMP4 (200 ng/ml), each alone or in combination were added to replicate cultures (n = 6 per group). Cell medium were changed every 3 days, and cell extract was prepared by exacting each cell layer with 1 ml 0.1% Triton X-100. The ALP activity in each extract was then assayed with 10 mM p-nitrophenylphosphate (pH 10.3). Results are shown as average ± S.D. *$p<0.05$, compared to the vehicle control, and $^{\#}p<0.05$, compared with BMP4 alone.

We cannot rule out the unlikely possibility that the MLV transduction process might alter the primary marrow-derived stromal cells so that the transduced cells could respond to these two osteogenic factors differently than untransduced cells to added effectors. Consequently, we next tested whether co-culture of Cox-2-expressing mouse marrow stromal cells with BMP4-expressing cells in 1:1 ratio would also produce a similar synergistic enhancement in ALP activity compared to BMP4 group alone. Also, to assess whether the effects were dose-dependently related to cell density, three different cell densities (i.e., 50,000 cells, 25,000 cells, or 10,000 cells) were tested. After 3- or 7-days of incubation, the ALP activity of each culture was measured as described above. As expected, Figure 3 shows that BMP4-expressing cells showed a significant increase in ALP activity after 7 days in culture compared to GFP-expresing control cells. The BMP4-mediated increase in ALP expression appeared to be proportional to the number of BMP4-expressing cells plated. Conversely, Cox-2-expressing cells had no significant increase in cellular ALP expression. However, when the same number of BMP4-expressing cells were co-cultured with Cox-2-expressing cells, the increase in ALP expression was significantly greater than those with BMP4-expressing cells alone, supporting a synergistic enhancement between BMP4 and Cox-2 on ALP expression in the transduced cells. The synergistic interaction

was seen in each test cell density. Similar synergistic interactions were seen after 3 days of incubation (data not shown). Based on these in vitro findings, we do not believe that the observed suppressive effect of Cox-2 expression on the bone healing action of BMP4 in the calvarial defect model was a result of the lack of synergistic interaction between the two effectors.

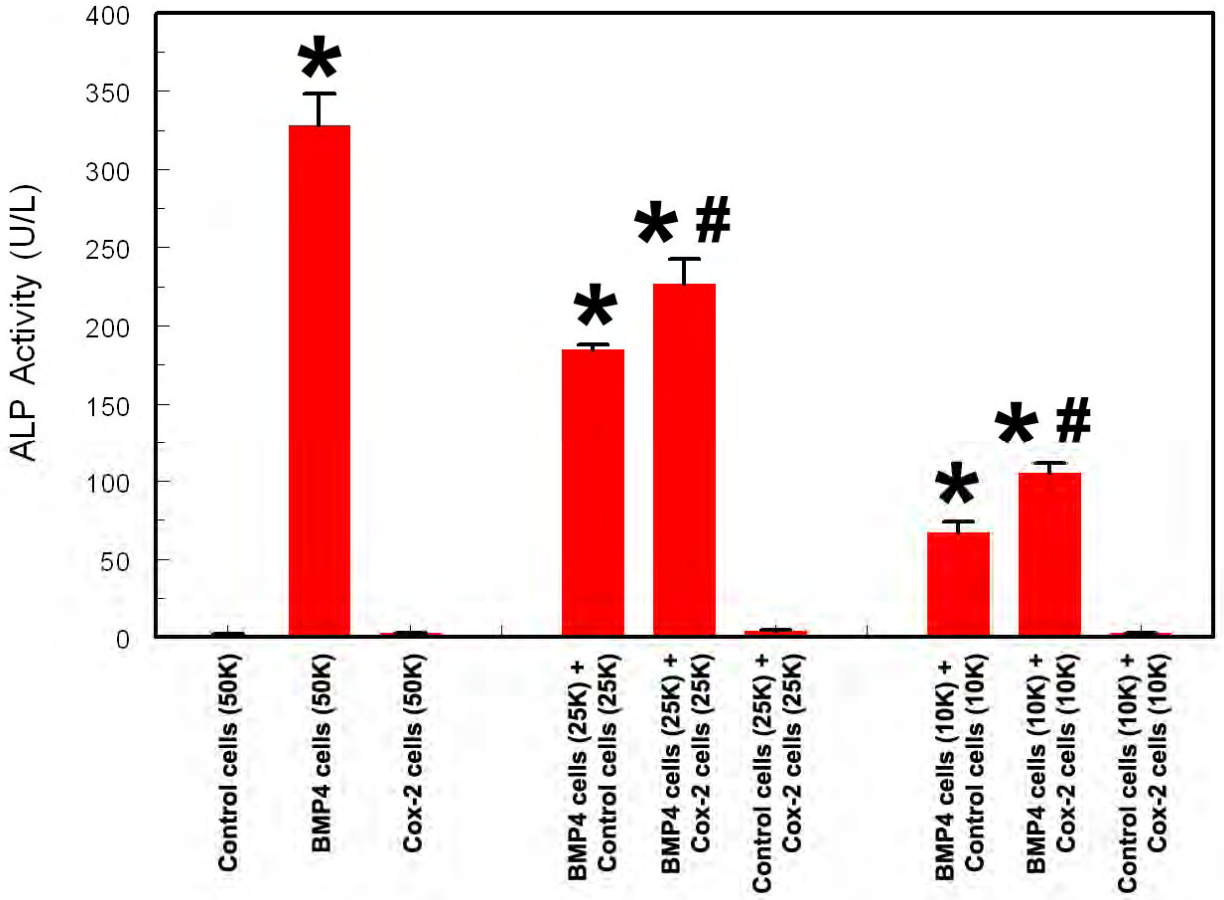

Figure 3. Synergistic interaction of BMP4-expressing mouse marrow-derived stromal cells and Cox-2-expressing mouse marrow-derived stromal cells in enhancing ALP expression in vitro. Various numbers (i.e., 50,000, 25,000, or 10,000) of BMP4-expressing mouse marrow stromal cells, Cox-2-expressing mouse marrow stromal cells, or GFP-expressing control cells, were plated alone or in combination in 6-well plates. Cell medium was changed every three days, and each layer was extracted with 1 ml of 0.1% Triton X-100. ALP activity was then assayed. Results are shown as mean ± S. D. (n = 6 per group). *$p<0.05$ compared to GFP-expressing control cells. #$p<0.05$, compared to each corresponding BMP4-expressing cell group.

Healing of the bony defect not only involves the proliferation and activation of osteoblastic cells, but also involves recruitment and migration of osteoblastic cells to the wound site. Accordingly, another possible explanation for the suppressive effects of Cox-2 on the bone healing response of BMP4 may involve a suppression of migration of osteoblastic cells to the center of the wound to establish formation and mineralization of the bone matrix along the wound periphery until the entire defect is filled up with newly bone. Consequently, as a

preliminary testing of this interesting possibility, we measured the effect of expression of BMP4 or Cox-2 on cell migration using an in vitro cell migration assay. In this assay, 1 x 10^6 untreated or each test transduced cells were plated in the bottom of the transwell. The number of cells migrated to the membrane from day 3 to day 14 were then measured. Table 1 summarizes the results of this preliminary experiment.

Table 1. Effect of BMP4 or Cox-2 expression on migration of the transduced mouse marrow stromal cells. Results are shown as average ± S.D. (n = 3 per group).

Cells	Cells Migrated to the membrane (x 10^5 cells)	P value*
Untreated cells	4.17 ± 0.10	n.s.
GFP-expressing cells	3.68 ± 0.48	---
BMP4-expressing cells	5.89 ± 0.47	<0.05
Cox-2-expressing cells	4.37 ± 0.55	n.s.

* P values are comparison between the test group and the GFP-expressing control cells.

This preliminary experiment suggests that expression of BMP4 significantly increased the migration of transduced marrow stromal cells. In contrast, expression of Cox-2 also appeared to slightly (but did not reach statistically significant level due to the small sample size) increased the migration of mouse marrow stromal cells compared to GFP-expressing cells. These findings support the contention that each of these two effects also possesses cell migration promoting activity. This preliminary experiment did not address the issue whether Cox-2 expression would suppress the BMP4-mediated cell migration, which will be done in our future experiment. However, since both agents appeared to promote cell migration, we do not believe the possibility that Cox-2 suppressed BMP4-induced cell migration is a very likely explanation for the suppression effect of Cox-2 on BMP4-induced bone healing.

Because the bone formation response of BMP4 was suppressed in the presence of Cox-2 expression, one of the possibilities is that the amounts of BMP4 produced by BMP4-expressing cells was reduced in response to Cox-2 or the number of BMP4-expressing cells was decreased in response to Cox-2. Thus, we next tested whether co-expression of Cox-2 in the milieu of Gel-foam could suppress BMP4 gene expression by performing an in vitro experiment in which we impregnated gel foam with BMP4 expressing primary mouse marrow stromal cells alone or in combination with Cox-2-expressing cells at 1:1 or 1:9 ratios. The total number of transduced cells in each Gel-foam strip was 2 x 10^6 cells. GFP-expressing cells were added in each treatment group to make up the total number of transduced cells. The cells were incubated in 2 ml of culture medium, which was sufficient to cover the entire Gel-foam. At day 1 and day 4, respectively, a set of three replicate Gel-foam of each group was rinsed with phosphate-buffered saline, and bisected. Total RNA was then extracted from each sample with a commercial RNA extraction kit. Each RNA sample, after confirmation of quality, was reversed transcribed to cDNA. The human BMP4 mRNA transcript levels was then measured using a primer set that was specific for human BMP4 by real-time RT-PCR using the SybrGreen assay method and the relative level was calculated by the ΔCT method and reported as relative percentage of its endogenous GAPDH transcript levels. The results are shown in Figure 4. These results illustrate two important points. First, there was a time-dependent decrease in BMP4 mRNA transcript level even in Gel-foam containing BMP4-expressing cells, suggesting that there might be a rapid cell death (or BMP4 gene silencing) in BMP4-expressing cells when impregnated within Gel-

foam. Second and more importantly, this time-dependent decrease in BMP4 transcript levels was enhanced by the presence of Cox-2-expressing cells in an apparent dose-dependent manner. Although these in vitro data must be confirmed in vivo situation, these preliminary data nevertheless raise the interesting possibility that Cox-2 may either promote BMP4 gene silencing or death of BMP4-expressing cells.

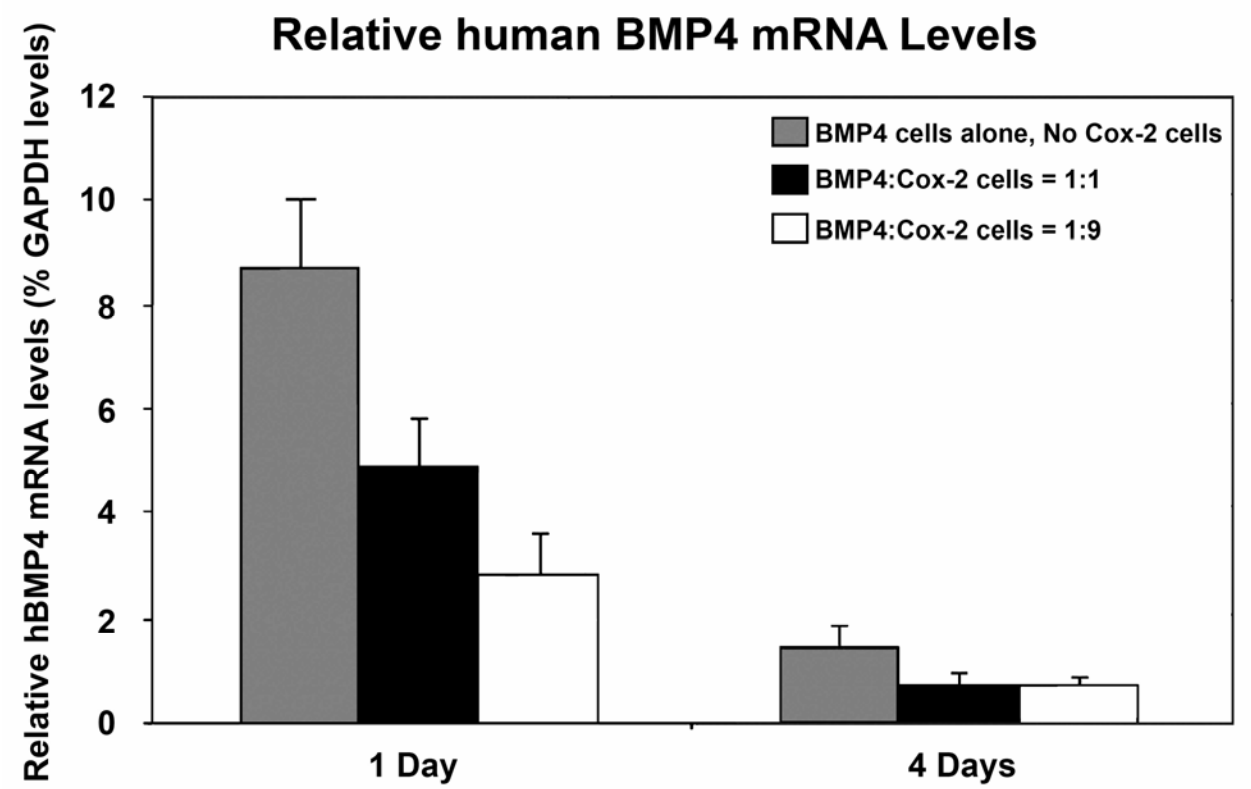

Figure 4. Effects of Cox-2 expression on the expression of BMP4 transgene level in transduced mouse marrow stromal cells in vitro. Gelfoam strips of 5 x 10 mm in size were impregnated with 2 x 10^5 mouse marrow stromal cells expressing BMP4 in combination with Cox-2-expressing cells in either 1:1 or 1:9 ratios, or with the same ratios of GFP-expression cells. The Gelfoam of each test group had a total of 2 x 10^6 transduced cells. Each gel-foam was plated incubated in wells of 6-well plates containing 2 ml of growth medium. After 1 day or 4 days in culture, the strips were washed briefly with phosphate-buffered saline, cut in half, and the total RNA was isolated. Each RNA sample was then reverse-transcribed to cDNA, and the relative levels of human BMP4 transgene transcript was determined by real-time RT-PCR using a primer set that is specific for human BMP4, which would not recognize endogenous mouse BMP4 transcript. Each relative level was normalized against respective GAPDH transcript level, also performed with real-time RT-PCR. Relative human BMP4 expression level was determined by the ΔCT method using a QuantiTech SybrGreen PCR assay kit and is reported as percentage of endogenous GAPDH transcript level. Results are shown as average ± SD from three Gel-foams per group. Each real-time RT-PCR assay was done in triplicate on a MJ Research Opticon real-time PCR system.

As an initial test of the possibility that Cox-2 expression might reduce the BMP4-expressing cells, we also measured the relative levels of incorporation of the human BMP4 expression vector into the host chromosome of the remaining transduced mouse marrow stromal cells in the aforementioned experiment after 14 days of incubation. We found that even in Gel-foam strips impregnated with BMP4-expressing cells without Cox-2 expressing cells, the genomic levels of human BMP4 gene in the host cells was barely detectable (by PCR-based assay). Co-incubation with the Cox-2-expressing cells did not significantly alter the relative levels of genomic incorporation of the human BMP4 transgene (data not shown). However, because of the high variation of the assay, and because of the relatively low levels of genomic incorporation, we do not have high confidence with these results. Consequently, although our preliminary data do not support the possibility of Cox-2-induced reduction of BMP4-expressing cells under our experimental conditions, we cannot rule out this interesting possibility.

In addition to stimulating bone formation, Cox-2 induces a number of physiologically important biological actions. Among the various biological actions of Cox-2, Cox-2 is a well-known, potent pro-inflammatory agent. Several pro-inflammatory cytokines, such as TNFα, IL-1 and IL-6, can inhibit bone formation. Therefore, the possibility that the suppressive effects of Cox-2 might suppress the bone formation response of BMP4 in part through its pro-inflammatory cytokine pathways cannot be ruled out. Our future work will attempt to address this possibility. Finally, there is strong evidence that many of Cox-2 biological actions are of biphasic nature. We also cannot rule out the possibility that the suppressive effect might be a result of too high of a dosage of Cox-2-expressing cells. Consequently, we plan to re-examine if there is potential synergy with reduced dosages of Cox-2-expressing cells in our future work.

Key Research Accomplishments:

1. A murine critical-sized calvarial defect model has been established and was used in our ex vivo skeletal gene therapy studies to promote bony healing.
2. MLV-based retroviral vectors expressing BMP-4, VEGF-A_{165}, Cox-2 or a control gene (β-galactosidase or GFP) have been constructed and produced.
3. Bone marrow stromal cells have been transduced (with >90% transduction efficiency) with MLV-based growth factor vectors (BMP-4, VEGF-A_{165}, Cox-2) and gene expression determined over 4 weeks in culture by Western blot or ELISA. The growth factor proteins produced were functionally active in vitro and in vivo.
4. The mouse calvarial critical defect model has been developed. Bone marrow stromal cells expressing BMP-4 were implanted and healing has been observed within 4 weeks. Net bone formation in implants was quantitated by dual X-ray absorptiometry and bone quality was evaluated by histological methods.
5. As expected, BMP4 single gene therapy produced significant increase in bone density measured by pQCT. Surprisingly, neither VEGF-A_{165} nor Cox-2 single gene therapy significantly increased bone formation. VEGF therapy promoted blood vessel formation but not bone formation.
6. Cox-2 and VEGF combination gene therapy produced no synergistic or enhancing effects on bone regeneration in the mouse calvarial defect model.
7. VEGF and BMP-4 combination gene therapy also did not yield synergistic interaction in promoting bone regeneration, but increased blood vessel and soft tissue formation.

8. Very surprisingly, Cox-2 not only did not synergize with BMP-4, but also completely suppressed the bone formation effect of BMP-4 in this mouse calvarial defect healing model. The inhibitory effect of Cox-2 was dose-dependent.
9. In vitro studies suggested that Cox-2 did not appear to have an inhibitory effect on BMP-4 gene expression or the survival of the transduced marrow stromal cells.
10. BMP-4 enhanced alkaline phosphatase expression in marrow stromal cells, Cox-2 or PGE2, a product of Cox-2, not only did not inhibit, but significantly enhanced, the stimulatory effects of BMP-4 on alkaline phosphatase expression in these cells in vitro.
11. We are now working on the molecular mechanism whereby Cox-2 to suppress the bone formation effect of BMP-4 in the mouse calvarial defect model.
12. Because we have evidence that FGF-2 promote bone formation in the endosteal bone formation model, we may test the synergistic effects between FGF-2 and Cox-2.

Reportable Outcomes:

There are not yet any reportable outcomes at this time.

Conclusions:

1. The mouse calvarial critical bone defect model has been developed for the evaluation of growth factor genes expressed *ex vivo* in bone marrow stromal cells.
2. This model is being used to test combination of growth factors that may be synergistic and promote bone healing more efficiently than a single growth factor.
3. A surprising finding of the inhibitory action of Cox-2 on BMP-4 led us to conclude that the choice of osteogenic growth factors is an important issue, since it appears that certain osteogenic growth factor (e.g., Cox-2) might have antagonistic effects on other osteogenic factor (e.g., BMP-4).
4. Cox-2 (or PGE_2) synergistically enhanced the anabolic response of BMP4 in the stimulation of osteoblastic differentiation of mouse marrow stromal cells. Thus, the suppressive effects of Cox-2 on the BMP4-induced bone formation are not likely due to a lack of synergy between the two effectors.
5. Cox-2 expression appeared to suppress the BMP4 expression in a dose-dependent manner in vitro, suggesting that Cox-2 may promote BMP4 gene silencing and/or death of BMP4-expressing mouse marrow stromal cells.

References:

1. Gysin R, Wergedal JE, Sheng MH-C, Kasukawa Y, Miyakoshi N, Chen S-T, Peng H, Lau K-HW, Mohan S, and Baylink DJ (2002) *Ex vivo* gene therapy with stromal cells transduced with a retroviral vector containing the BMP4 gene completely heals critical size calvarial defect in rats. *Gene Therapy* 9:991-999.
2. Rundle CH, Miyakoshi N, Kasukawa Y, Chen S-T, Sheng MH-C, Wergedal JE, Lau KHW, and Baylink DJ (2003) *In vivo* bone formation in fracture repair induced by direct retroviral-based gene therapy with BMP-4. *Bone* 32:591-601.
3. Zhang XS, Linkhart TA, Chen S-T, Peng H, Wergedal JE, Guttierez GG, Sheng MH-C, Lau K-HW, and Baylink DJ (2004) Local *ex vivo* gene therapy with bone marrow stromal cells expressing human BMP4 promotes endosteal bone formation in mice. *J Gene Med* 6:4-15.

4. Klamut HJ, Chen S-T, Lau K-HW, and Baylink DJ (2004) Progress toward skeletal gene therapy. *Crit Rev Eukaryotic Gene Expression* 14:89-136.
5. Peng H, Wright V, Usas A, Gearhart B, Shen H-C, Cummins J, and Huard J (2002) Synergistic enhancement of bone formation and healing by stem cell-expressed VEGF and bone morphogenetic protein-4. *J Clin Invest* 110:751-759.
6. Peng H, Chen S-T, Wergedal JE, Polo JM, Yee J-K, Lau K-HW, and Baylink DJ (2001) Development of an MFG-based retroviral vector system for high secretion of functionally active human BMP-4. *Mol Therapy* 4:95-104.
7. Cok SJ, and Morrison AR (2001) The 3'-untranslated region of murine cyclooxygenase-2 contains multiple regulatory elements that alter message stability and translational efficiency. *J Biol Chem* 276:23179-23185.
8. Lida Y and Masuda T (1995) Quantification analysis of translation initiation signal sequences in vertebrate mRNAs. *Nucleic Acids Symp Ser* (34)**:**103-104.
9. Krebsbach PH, Mankani MH, Satomura K, Kuznetsov SA, Gehron Robey P (1998) Repair of craniotomy defects using bone marrow stromal cells. Transplantation 66:1272-1278.

PROJECT 8

PRINCIPAL INVESTIGATOR: Donna D. Strong, Ph.D.

TITLE: Nuclear Targeting of Transposon-Based Plasmid Vectors for Gene Therapy

Project 8: Nuclear Targeting of Transposon-Based Plasmid Vectors For Gene Therapy

A. TECHNICAL OBJECTIVE. Develop and test a novel nonviral protein expression vector for use in gene therapy. The plasmid will contain DNA sequences to a) increase movement of the plasmid DNA into the nucleus and thus increase transfection efficiency and expression levels; and b) produce a transposase to increase stable vector DNA integration into genomic DNA, thus increasing long term transgene expression.

Introduction

Our primary research objective is to develop improved nonviral plasmid vectors for *in vivo* applications in hard and soft tissues by incorporating into a single vector a nuclear entry sequence to increase transfection efficiency and a transposon to increase long term transgene expression. Plasmid vectors will provide a safer, less expensive and more easily manufactured reagents for gene delivery compared to viral vectors, but have not been widely used for *in vivo* applications because of several different cellular barriers to *in vivo* transfection and transgene expression. These barriers include plasmid entry into the cell, subsequent entry into the nucleus, and for long term expression, stable transgene integration into genomic DNA. After entering cells, traditional plasmids enter the nucleus during mitosis, so transfection efficiency is dependent on active cell proliferation. We and others have identified nuclear entry DNA sequences, such as the virally derived SV40 DTS, that enhance nuclear entry of plasmid DNA and increase *in vivo* transfection efficiency and transgene expression levels even in non-proliferating cells (1-7). Traditional plasmid DNA integrates into genomic DNA randomly and with low efficiently. To improve efficiency of integration, we have also developed a plasmid vector that expresses a mammalian transposase, *Sleeping Beauty*, (SBT) and incorporates the gene of interest but not the transposase within a transposon. The transposase facilitates transgene integration into AT-rich regions of genomic DNA, resulting in high levels of long term expression (8-12). No single plasmid vector has been developed that incorporates both a nuclear entry sequence and transposon with transposase expression. We propose that our enhanced plasmid expression vectors will significantly increase transfection efficiency and transgene integration, resulting in higher levels of long term therapeutic gene expression *in vivo* than are possible with existing nonviral gene therapy vectors. Our studies are designed to prepare novel plasmid vectors with nuclear entry activity, a transposon/transposase and either a marker gene or the BMP-2/4 therapeutic gene. We will show that cells expressing BMP-2/4 from a nonviral vector can produce BMP-2/4 at levels as well as cells expressing BMP-2/4 from an MLV vector. We will show that both vector/cell systems stimulate bone formation *in vitro* and *in vivo*.

Objectives Years 1-3:

Specific Objective 1. Initiate studies to compare effectiveness of SV40DTS/SBT BMP-4 plasmid and MLV BMP-2/4 viral vector in stimulating osteoblast differentiation in cultured rat MSCs and osteoblasts.

Specific Objective 2. Initiate studies to compare bone formation induced by rat MSCs transduced *in vitro* with SV40DTS/SBT-BMP-2/4 plasmid or MLV BMP-2/4 viral vectors *in vivo* in a rat subcutaneous implant model.

Body

A. Summary of progress. Previous progress included preparation of plasmid vectors that included the red fluorescent protein (RFP) marker gene or the Bone Morphogenic Protein (BMP)-2/4 therapeutic gene, the sleeping beauty transposon (SBT), and the SV40 DTS nuclear entry sequence. We prepared pPrince Charming (pPC) vector-based constructs by PCR to reduce the size and remove the Neo selection cassette. We showed that in rat and human osteoblast-like cells that the pPC based vector transfected cells with a higher efficiency than the parental pPC vector. We introduced the SV40DTS into pPC-based plasmid vector (pARSS, Figure 1) vectors and prepared and tested BMP-2/4 vectors (pABSS, Figure 1) by replacing the BP3-NLS-RFP with the BMP-2/4 coding region.

Transfection of rat marrow stromal cells (rMSCs) and rat calvarial osteoblasts (rCobs) with Effectene (Qiagen) and the pARSS vector resulted low levels (1-5%) transfection efficiency and in long term expression of nuclear RFP *in vitro* (4 weeks). After transfection, transgene expression was stable, dividing cells expressed the transgene and colonies of cells expressing the transgene were observed in culture. Long term expression of more than 2-3 days was not observed with vectors that did not have the sleeping beauty transposon. Transfection of C2C12 cells with the pABSS caused cells to transdifferentiate and produce ALP activity and transfection

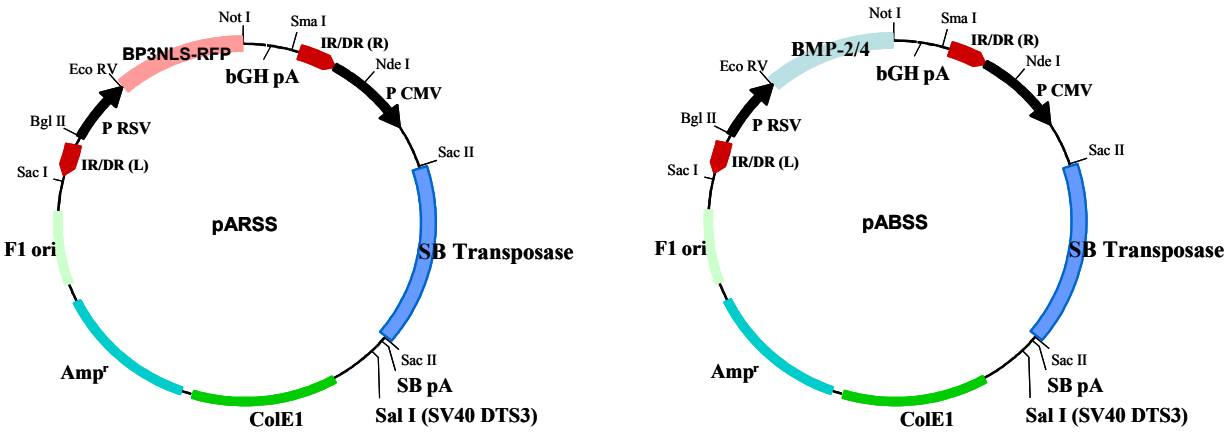

Figure 1. **Sleeping Beauty transposon/nuclear entry based plasmid vectors.** The plasmid vectors for gene delivery contain the Sleeping Beauty (SB) Transposon and transposase (SBT) and the nuclear localization signal from the SV40 virus. pARSS contains a red fluorescent protein (RFP) marker protein and the pABSS vector contains a hybrid BMP-2/4 transgene. A pARS control vector that contains BP3NLS-RFP and the SB Transposase but not the SV40DTS3 has also been prepared.

with pABSS stimulated a significant increase in ALP activity in cultured rCobs.

Since the last progress report (October 2005), we found that BD Biosciences collagen and ceramic scaffolds treated with fibronectin reproducibly sustained growth of MLV-GFP transduced rMSCs moreso than OPLA scaffolds *in vitro*. More total RNA was isolated from the rMSC-collagen scaffolds and more osteopontin was produced than by rMSCs attached to the two other scaffolds, reflecting maturation of rMSCs into active osteoblasts on the fibronectin-coated collagen scaffold. We tested rMSC-covered scaffolds *in vivo*. Specifically, we studied the longevity of retrovirally transduced GFP producing marrow stromal cells in the collagen, ceramic and OPLA scaffolds in a Fischer344 rat implant model.

While we found that GFP expressing rMSCs survived on the collagen matrix for two to three weeks *in vitro*, we found that the majority of GFP-expressing rMSCs were gone from the scaffolds within one week *in vivo*. In addition, GFP producing cells could not be found adjacent to the collagen scaffold within one week *in vivo* suggesting a rapid loss of GFP expressing cells from the implant but not into the surrounding tissue area. In addition we found that the collagen and OPLA matrices were degraded and disappeared within two weeks *in vivo*. These results led us to consider the use of alternative scaffold material and immunocompromised mice for future implant studies.

We also studied the cellular content (GFP-expressing rMSCs) of the collagen and ceramic scaffolds in detail. After loading collagen and ceramic scaffolds with GFP-cells and growing them *in vitro* for 7-14 days, the scaffolds were fixed with buffered formalin and sectioned. We found that GFP-rMSCs formed a layer on the scaffold surface but did not penetrate into the scaffold interior. This was true of both collagen and ceramic scaffolds. Similar results have been reported by others. For example, mineralization measured and quantitated by μCT only occurred on the surface of collagen disks implanted with mouse myoblasts expressing osteoinductive trangenes *in vitro* (13-15). Our results and the results of others prompted us to consider using a different, more readily populated matrix material to support growth of rMSCs or rCObs in three dimensions. Preliminary studies with PuraMatrix-hydrogel (BD Biosciences, Bedford, MA) resulted in growth of cells throughout the matrix and led us to consider using PuraMatrix hydrogel-based or a similar Extracel-LG hydrogel-based (Glycosan Systems, Salt Lake City, UT) matrix for continuing studies.

One of the main objectives of our work was to develop an efficient transfection protocol to introduce our plasmid vectors into rat marrow stromal cells or osteoblasts, to study osteoinductive transgene expression *in vivo* and compare the ability of plasmid transfected cells with retrovirally transduced cells to stimulate bone formation *intro* and *in vivo.* We developed plasmid vectors with the SV40DTS and Sleeping beauty transposon with marker and BMP-2/4 transgenes to increase transfection efficiency in vivo and in nontransformed cells and to be incorporated into the genome for long term stable expression. We tested Nucleofector (Amaxa) based transfection reagents for plasmid delivery into rMSCs and rCObs based on high transfection efficiencies achieved with mouse MSCs and MC-3T3-E1 osteoblasts by other investigator's. Amaxa's Nucleofector T kit produced transfection efficiencies of 70-90% in MC-3T3 osteoblasts and mMSCs. We tested the ability of Amaxa's T kit to transfect rMSCs and rCobs. The T kit transfected rMSCs with efficiencies up to 20% however 90% of the cell population did not survive at the voltages required to achieve higher efficiencies. rCobs were not transfected at high efficiency with the T kit using a variety of voltages, pulses and DNA concentrations. However, we found that Amaxa's fibroblast kit transfected osteoblasts with 10-30% efficiency and that 30-50% of the cells survived. rMSCs, on the other hand, transfected with low (1-5%) efficiency and that the voltages required for even low efficiency transfection reduced cell survival to 10% or less. These results led us to consider using direct electroporation of rMSCs while in scaffold materials for our continued studies.

Finally, we discovered that co-expression of Cox-2 and LMP-1 with BMP-2/4 of the three transgenes increased alkaline phosphatase activity in rMSCs and rCobs indicating increased differentiation of both cell populations *in vitro*. Because increased differentiation should lead to increased bone formation *in vivo*, in our continuing studies, we would like to co-express Cox-2 and LMP-1 with BMP-2/4 to increase the osteoinduction/bone formation capacity of BMP-2/4 in our implant model after transgene delivery.

B. Detailed Progress

1) Preparation and analysis of rMSC populated scaffolds *in vitro*. Collagen and ceramic supports were pre-coated with fibronectin by adding 100 ul of a 100 ug/ml solution to each dry scaffold in wells of a 24 well plate. The scaffold absorbed this solution completely. The scaffolds were incubated 1 hour before adding cells. Cells were trypsinized and filtered through a 40 μM nylon sieve (BD Bioscience) counted and added to each well as 400,000 cells in 1 ml. This number of cells just covered the surface of the scaffold. After 3 hours, 1 ml more media was added and the cultures were incubated with media changes for 7-21 days prior to analysis or implantation. Scaffolds were moved to new 6 well plates when cells began to populate the bottom of the tissue culture dish. Before implanting, the scaffolds were examined by epifluorescence microscopy and GFP cells were observed on the surface of the scaffold (Figure 2). Cells grew and expressed GFP for 14 days. At 21 days, the number of GFP expressing cells on the surface were reduced (Figure 2), therefore cells on scaffolds were implanted within 7-14 days of culture for in vivo studies. The number of cells on the interior of the scaffolds (collagen and ceramic). Very few cells were found at one, two or three weeks on the scaffold interior on either material. Figure 2 shows a representative illustration of GFP on the cellular interior at three weeks which is indicative of early time points as well.

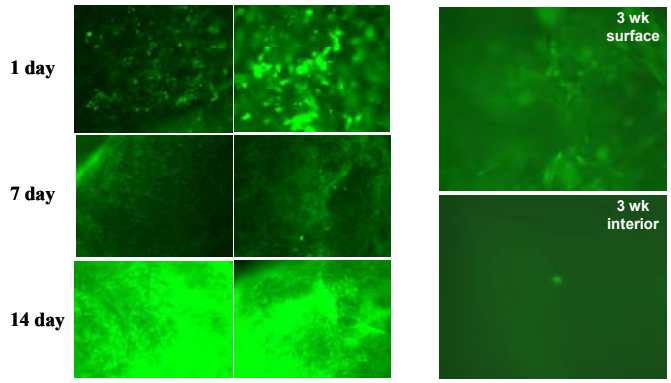

Figure 2. **GFP-rMSC growth on collagen scaffold *in vitro*.** Left panel: rMSCs were seeded on scaffolds and grown for 7-14 *days in vitro* before implantation. Fluorescent microscopy was used show GFP expression on collagen scaffolds. More cells were visible on the cell surface at day 14 compared to day 1 and 7. Right panel: rMSCs remaining on the surface and inside the collagen scaffold after 21 days in culture.

When rMSCs were grown on ceramic scaffolds, cells expressing GFP grew well on the matrix surface for up to two weeks. At three weeks there was a reduction in GFP-expressing cells on the matrix surface and very few GFP-expressing cells on the interior. Inspections of the matrix interior at one and two weeks resulted in similar cell numbers in the matrix interior (data not shown).

These experiments led us to consider the use of other matrix materials that would better support growth of cells on the matrix interior. Because cells grew well on the exterior of the matrix we conducted several implant surgeries to

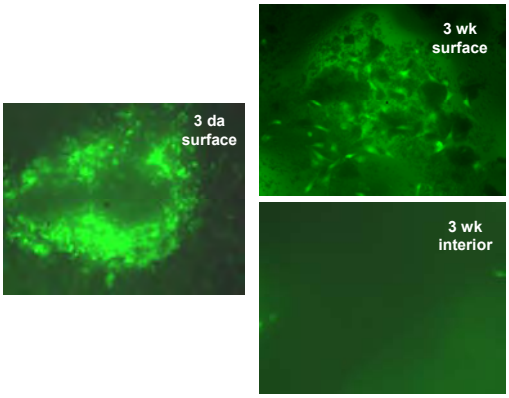

Figure 3. **Growth of rMSC-GFP on ceramic scaffolds *in vitro*.** rMSCs from Fischer 344 inbred rats were transduced with an MLV-GFP vector and seeded onto ceramic scaffolds. GFP expressing cells were grown for 3 weeks *in vitro* and the scaffold exteriors were inspected by fluorescent microscopy after 3 days and 3 weeks and the interiors were inspected at 3 weeks.

determine if GFP-expressing cells would survive on our inbred rat model.

2.) Growth of rMSCs expressing GFP on scaffolds *in vivo***.** rMSCs were grown on collagen and ceramic scaffolds for 3-7 days *in vitro* as described in section 4a) and implanted under the skin in inbred Fischer 344 rats. GFP expression in cells on the scaffold was assessed by epifluorescent microscropy and cell survival/bone formation was assessed by histology from 7-14 days after implantation of the matrix.

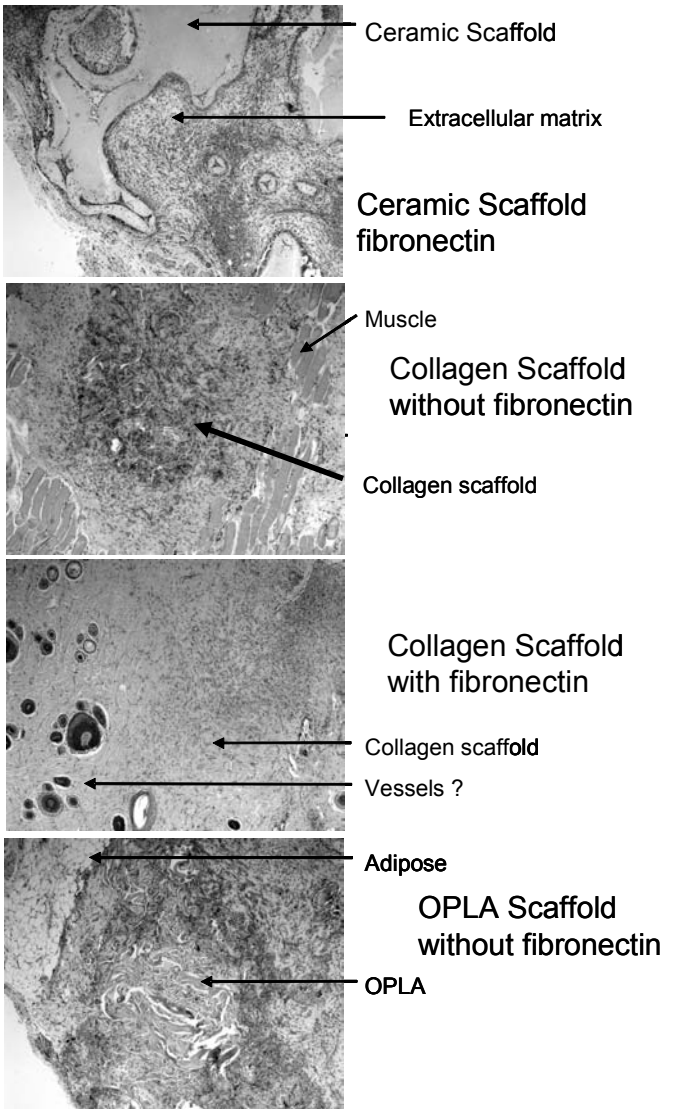

Figure 4. **Growth of MLV-GFP-rMSCs on scaffolds *in vivo.*** MLV-GFP transduced rMSCs were grown on scaffolds (ceramic, collagen and OPLA) with or without coating with fibronectin for one week and then implanted subcutaneously in rats for 16 days. Implants were removed, cells visualized with fluorescent microscopy, then scaffolds were fixed, sectioned and stained with H& E.

i). Rat skin implant surgery. Fischer 344 rats, 13 weeks old, were anesthetized with ketamine and xylazine and four 0.8-1.2 cm incisions were made on the shaved back skin. Blunt dissection with a small hemostat was used to create a small pocket to the lateral side of each incision, then one scaffold (collagen, ceramic or OPLA containing rMSC-GFP cells) was inserted into each pocket. The incisions were closed with 3 stitches (3-0 non-resorbable) and the rats were allowed to recover in plastic cages on a warm pad before return to normal housing. Rats were monitored hourly until normal feeding was observed.

ii.) Analysis of implanted scaffolds. Initial implant experiments with rMSCs to assess whether collagen scaffolds and attached cells would induce a significant inflammatory reaction in the host rat tissues were negative. After 14 days, the rats were euthanized with CO_2 and the implants were dissected out and placed in PBS on ice. There were no indication of an inflammatory reaction in the implant sites. Because syngenic cells were used and implant scaffolds did not elicit an inflammatory reaction, a rMSC rejection raction was not anticipated.

Collagen, ceramic and OPLA scaffolds containing rMSCs grown for one week *in vitro* and were implanted as described. The scaffolds were removed at 7-14 days after implantation.

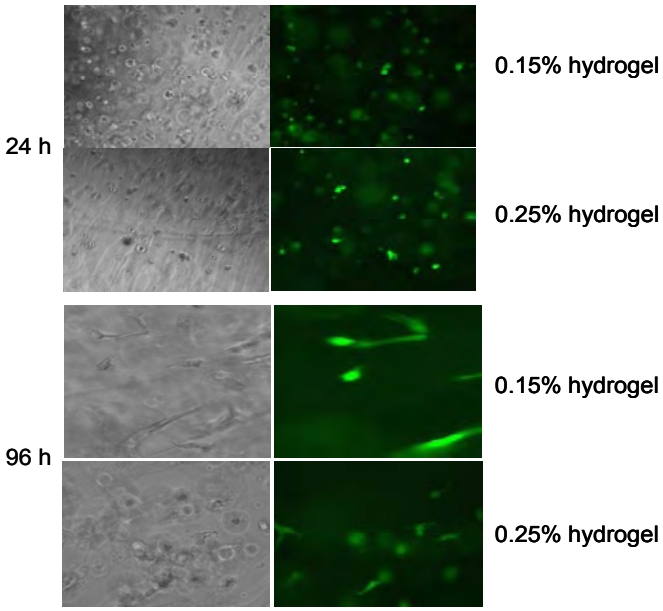

Figure 5. **MLV-GFP rMSCs in hydrogel prepared by the drop method**. rMSCs were grown for 24 hours in DMEM/10%FBS and media was replaced with media containing either 0.15% or 0.25% PuraMatrix that was dropped onto the adherent cells. Cells were grown culture for 24 or 96 hours and GFP

Collagen and OPLA scaffolds were resorbed into the surrounding tissues by 14 days but could be identified at 7 days but were infiltrated with blood vessels with 10-30% of the scaffold remaining. The collagen scaffolds were also tightly incorporated into the overlying skin dermis layer and had some blood vessel growth. Krebsbach's group reported (16) that blood vessels and marrow elements invaded gelfoam scaffolds (collagen based) that were loaded with mouse MSCs. The collagen scaffolds were not eroded in the immunocompromised mouse model that this group used.

Only a few GFP positive cells were found on the scaffold surface and inside the scaffold (Figure 4).We found that very few GFP-expressing cells were visible on the surface or inside the matrices after 7 days in any of the matrices. GFP expressing cells could not be identified in the surrounding tissues. After fluorescent microscopy, the implants were fixed in 10% buffered formalin overnight and then sectioned to assess the cellular content in the matrix. Each of the matrix materials were populated with cells. Because these cells did not express GFP, we concluded that the cells had invaded from surrounding tissues. Blood vessels appeared to infiltrate the collagen matrix but not the other matrices.

In continued studies with the rat implant model with ceramic scaffolds, which were not eroded within 14 days *in vivo*, we found GFP rMSCs or rCobs did not remain at the surface or remain in the interior of ceramic scaffolds at 7 days.

Our results and the results of Krebsbach's group led us to consider the use of immunocompromised mice for additional *in vivo* studies.

3.) Testing alternative scaffold materials. Our studies with collagen, OPLA and ceramic scaffolds suggested that rMSC and rCob cell viability was limited *in vitro* and especially when implanted in the scaffolds *in vivo* These findings led us to test other scaffold materials to better support the growth of three dimensional cultures that would support the viability and expansion of rMSCs and rObs *in vitro* and *in vivo.*

Toward this goal, we conducted preliminary *in vitro* experiments with BD™ PuraMatrix™ Peptide Hydrogel matrix. PuraMatrix Hydrogel is a synthetic matrix that is used to create defined three-dimensional (3D) microenvironments for a variety of cell culture experiments. This material is composed of a synthetic peptide containing four repeats of Arg-Ala-Asp-Ala and was recently reported to support differentiation and mineralization of mouse embryonic fibroblasts (17-19). Under physiological conditions, the peptide component self-assembles into a 3D hydrogel that exhibits a nanometer scale fibrous structure that promotes cell attachment, but does not activate RGD-dependent integrin signaling. The gel is biocompatible and devoid of animal-derived material and pathogens and can be used in implant studies. The material can be dropped onto growing cells (drop method) or cells can be suspended with the hydrogel (encapsulation

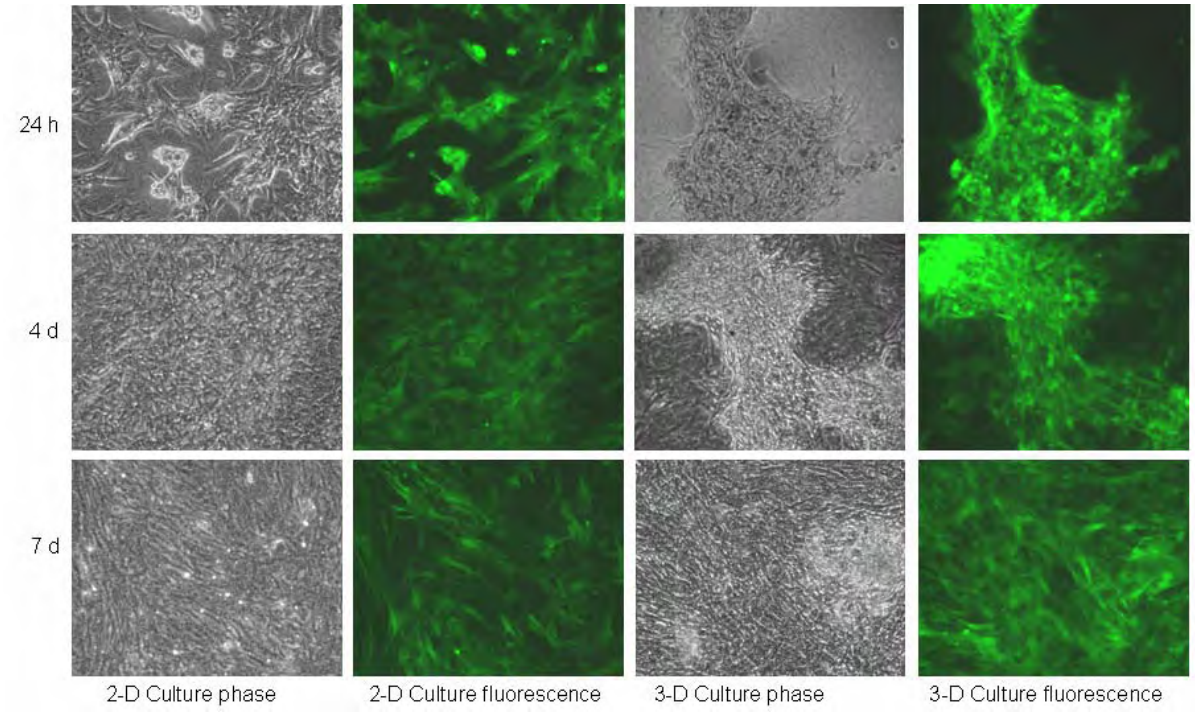

Figure 6. MLV-GFP transduced rMSCs in PuraMatrix-hydrogel. Cells were plated and grown in 2-D culture or were suspended in PuraMatrix by the encapsulation methods in wells of a 6 well plate for 24 h, 4 days or 7 days. 100,000 cells were encapusulated in 0.15% hydrogel/sucrose and dropped into the culture well. 2 ml of DMEM/10% FBS was added to the well for cell growth. Fluorescent microscopy was used to evaluate cell growth from 1-7 days.

method) and placed in a culture dish. We cultured rMSCs with different concentrations of hydrogel under both conditions. Figure 5 illustrates growth of GFP-rMSC cultures 24 and 96 hours after drop culturing. The cells did not grow well using this method and did not form three dimensional cultures. Figure 6 illustrates growth in hydrogel using the encapsulation method. MLV-GFP expressing rMSCs were grown in parallel two dimensional cultures for comparison. Cells grew into three dimensional cultures within 7 days using this method. These results indicated that hydrogel could be used as an alternative matrix to establish rMSCs with osteoinductive transgenes in the implant model.

4.) Development of transfection procedures that will efficiently transfect non-transformed cells. It is well recognized that nontransformed cells are difficult to transfect with high efficiency. Amaxa's

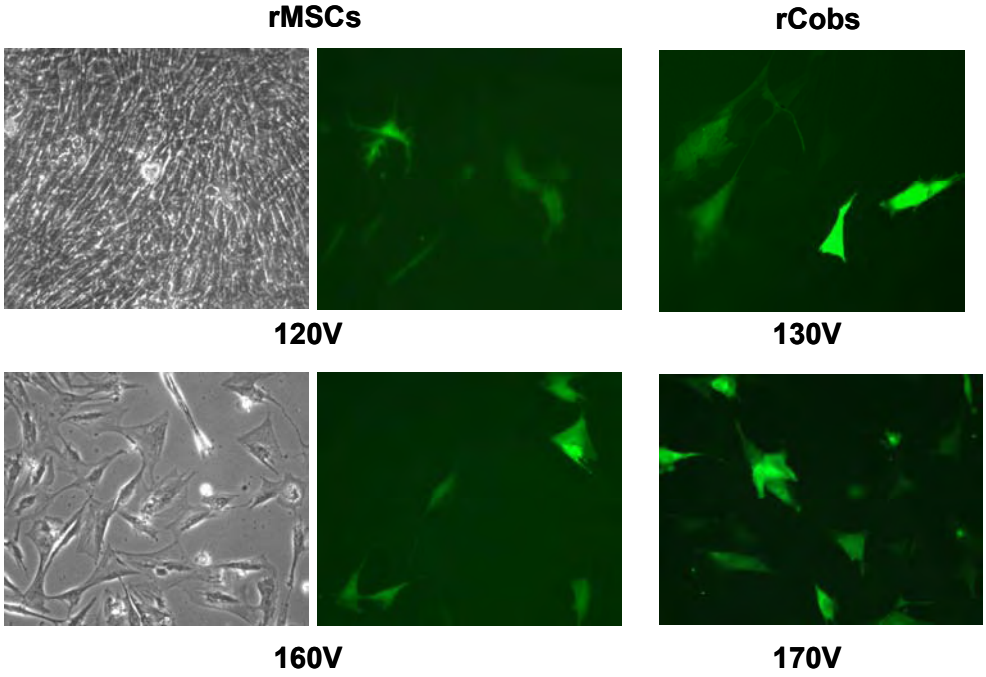

Figure 7. **Evaluation of transfection efficiency of rMSCs and rCobs with Amaxa's Nucleofector reagents.** Left and center panel: rMSCs (500,000-750,000 cells) were transfected with 2µg p*max*GFP plasmid vector using T kit nucleofector reagents. Transfection efficiency was determined by FACS analysis and was 15% using a 120V, 20ms square wave pulse. Transfection efficiency was 21% using a 160V 20 ms square vave pulse, however cell survival was 30% of that obtained with the 120V pulse. Only 30% of the cells were viable with the 120V pulse. GFP expression was evaluated by fluorescent microscopy after 48 h.
Right panel: rCobs (400,000-500,000) were transfected with 2 µg p*Max*GFP plasmid using the Nucleofector fibroblast kit. rCobs were transfected at 10V increments between 130 and 170V using a 20 ms square wave pulse. At 24 hr and 48 hr from 21-27% of the cells were transfected as determined by FACS analysis.

Nucleofector reagents have been used to transfect many nontransformed cell lines with high efficiency and members of our group have successfully transfected plasmid vectors in nontransformed mouse fibroblasts and osteoblasts with high efficiency. We tested two Nucleofector kits that worked well with mouse cells to determine if rat marrow stromal cells and osteoblasts could also be transfected with high efficiency. Our group determined that Amaxa's T kit with the pMaxGFP optimized vector transfected MC3T3 osteoblasts with 70-90% efficiency while Amaxa's fibroblast kit transfected mouse marrow stromal cells with 80% efficiency using the GenePulsar (Biorad). We tested the ability of Amaxa's T kit with the p*Max*GFP vector to transfect rMSCs. Early passage rMSCs (500,000) were transfected with 2µg of p*Max*GFP vector using the T kit using a 20 ms single square wave pulse with voltages ranging from 120-160V in a 2 mm cuvette. GFP expression was followed for 48 hours. 120V transfection provided 30% cell survival with a transfection efficiency of 15% while cells transfected at 170V resulted in 15-20% cell survival with 21% transfection efficiency. rCobs did not transfect with high efficiency with the T kit at any of the voltage conditions tried.

Early passage rCobs (500,000) were transfected with 2 µg of p*Max*GFP vector using the fibroblast kit as recommended by Amaxa. A 20ms pulse between 130-170 volts was applied.

50-70% of the cells survived and transfection efficiencies ranged from 21-34%. 160V optimally delivered plasmid DNA into rCobs with the fibroblast kit with 50% cell survival. The fibroblast kit did not deliver DNA into rMSCs using the same conditions.

After identifying Nucleofector reagents that transfected at least 20% of each cell population, transfections were conducted with pARSS, the RFP expressing plasmid vector with nuclear entry sequence SV40DTS and sleeping beauty transposon SBT (Figure 1). A dose response experiment was conducted with 2, 4 and 6 µg pARSS vector with the fibroblast kit at 170V, 20ms pulse, in rCobs. Four and six micrograms of plasmid DNA resulted in the highest transfection efficiencies. Five micrograms of plasmid DNA were used for additional experiments. Expression was monitored from 24-5 days. Transfection efficiencies ranged from 1-5% and expression continued for 3 weeks. While transfection efficiencies up to 34% could be obtained with the 3.8 kb p*Max*GFP vector provided by the manufacturer, efficiencies with our 9kb pARSS vector was much lower. Transfection of the pARSS vector into rMSCs with the T kit was less than 1% using conditions optimal for transfections with pMaxGFP (data not shown).

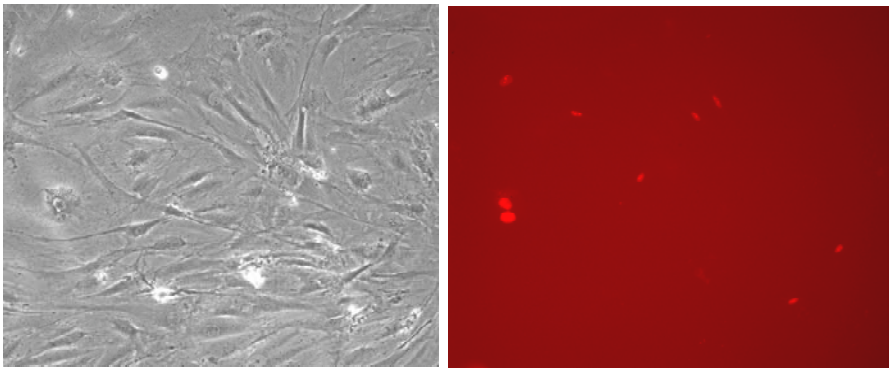

Figure 8. **Evaluation of transfection efficiency of rCobs with the pARSS vector.** 500,000 rCobs were transfected with Nucleofector fibroblast kit reagents, 5µg pARSS at 160V with a 20ms pulse in a 2 mm cuvette. Cells were cultured for three weeks and RFP expression in the nucleus was assessed by fluorescent microscopy.

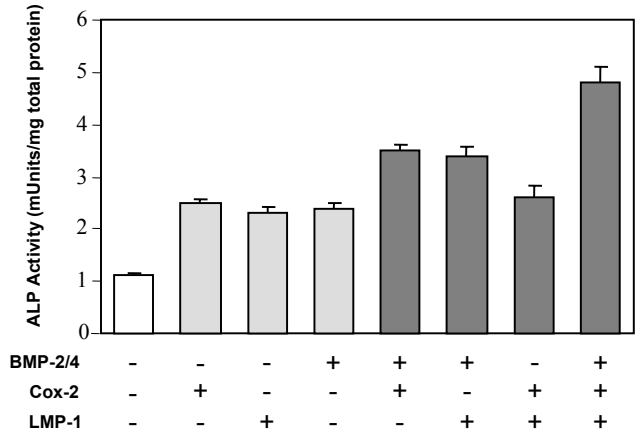

Figure 9. **Multiple transgene overexpression is superior to single transgene overexpression in stimulating ALP activity in rCobs.** To test the hypothesis that BMP-2/4 would be more osteoinductive in the presence of LMP-1 or cox-2 or both, we cocultured rCobs that had been transduced with either MLV-BMP-2/4, LMP-1 or Cox-2. Cultures were seeded in a ratio of 50:50 to test two transgenes and in a ratio of 30:30:30 to test the three transgenes. An untransduced control culture was also grown for 5 days. Cells were washed and lysed for total protein determination and for ALP activity measurements.

These disappointing results prompted us to consider electroporation experiments of cells in support materials (puraMatrix) with electrodes or directly into bone tissues *in vivo* using needle, twizzer, paddle electrodes to introduce plasmid DNA for continuation studies. We are proposing changes in the technical objectives to more effectively test our plasmid vectors.

6.) rat Calvaria Osteoblasts (rCobs) transduced with retroviral BMP-2/4, LMP-1 and Cox-2 vectors. ALP activity was not extensively increased after transduction with the MLV-BMP-2/4 (~2 fold above control in rCobs. To increase ALP activity, an indicator of bone formation in MSCs and Cobs, we tested the hypothesis that combinations of BMP-2/4, LMP-1 and Cox-2 overexpression would have synergistic effects on induction of ALP activity. Cox-2 has been shown to increase ALP activity in rCobs and LMP-1 has been shown to increase osteocalcin production in rCobs. rCob cells transduced with each of the MLV-expression vectors and were mixed in equal numbers and plated in 6 well plates (eg. LMP1 + BMP, etc). After 5 days ALP activity was determined (Figure 9). In this experiment, BMP2/4, cox-2 and LMP-1 overexpression by themselves modestly increased ALP activity above control. The combination of BMP2/4 + Cox-2 transduced cells increased ALP further in rCobs. For unexplained reasons, mixing LMP-1 transduced cells with Cox-2 expressing cells did not increase ALP activity compared to Cox-2 or LMP-1 alone. Importantly, the combination of BMP-2/4, LMP-1 and Cox-2 increased ALP activity more than any transgene alone or any transgene combination. These results led us to consider transductions or transfections with multiple transgenes (BMP-2/4, LMP-1 and Cox-2) in our continuation studies to increase bone formation *in vitro* and *in vivo.*

Key Research Accomplishemnts

- We did not find GFP-expressing rMSCs or rCobs on the collagen or ceramic scaffolds (within 7 days) after transplantation under the skin in our rat model.
- This result led us to reinvestigate the survival of rMSCs and rCobs on scaffolds *in vitro*. We found that rMSCs and rCobs do not divide and populate the interior of either the collagen or the ceramic scaffold *in vitro*.
- This result led us to investigate other scaffold materials that might support the growth of cells inside a three dimensional matrix.
- We found that PuraMatrix- a peptide based hydrogel, a novel synthethic nanofiber scaffold supported the growth of encapsulated MLV-GFP transduced rat marrow stromal cells. This matrix material could be substituted for collagen, ceramic or OPLA scaffolds to increase the number of cells delivered in our implant model.
- Gene delivery of plasmid vectors into rCobs with Nucleofector-based transfection reagents (fibroblast kit) transfected up to 34% of the cells under optimal conditions with 50% cell survival. Effectene (Qiagen) reagent provided transfection efficiencies of 1-5% in rCobs. These results prompted us to test our SV40DTS/SBT based vectors and determine transfection efficiency with Nucleofector reagents.
- The pARSS plasmid vector was delivered with up to 15% efficiency to rCobs with the fibroblast kit using the same transfection conditions as with the smaller p*max*GFP vector supplied with the kit. Red fluorescent protein was expressed for up to three weeks in the cultured cells. While long term expression was obtained with our vectors, conditions used to optimize transfection of a smaller vector (pmax GFP, 3.8 kb), might not be optimal for

the larger pARSS vector (9.8 kb). Additional studies will be required if we continue to use nucleofector reagents for transfection.

- rMSCs were transfected with the Nucleofector fibroblast kit and T kit. Cell survival varied but reached only 10% at voltages that resulted in up to 15% transfection efficiency.
- Nucleofector Kits that work with marrow stromal cells from mice do not provide the same transfection efficiencies or cell survival rates with rat cells. Nucleofector reagents cannot be used to deliver transgenes to rMSCs for *in vitro* or *in vivo* studies.
- Coexpression of Cox-2 and BMP-2/4 and LMP-1 and BMP-2/4 from MLV transduced cocultured cells increased the level of ALP activity in rCobs.
- Coexpression of Cox-2, BMP-2/4 and LMP-1 increased ALP activity in an additive manner and use of multiple transgenes should be considered for stimulation of bone formation in an implant model.

Reportable Outcomes

None at the present time.

Conclusions

- The use of ceramic and collagen scaffolds allows growth of rMSCs and rCobs only on the matrix surface and not inside. Cells that populate the scaffold surface did not survive *in vivo*. The number of cells transplanted and the survival of cells must be increased to have a successful transplant model.
- Cultured cells on scaffolds do not survive *in vivo* in Fisher 344 rats. Therefore further in vivo studies may be improved by using immunocompromised animals (NOD/SCID mice model) for implanting transfected rMSCS and rCobs or mouse MSCs and Cobs.
- Nucleofector reagents that increase transfection efficiency to 70-90% in mouse osteoblast and marrow stromal cells result in transfection efficiencies of 1-30% in cultured rat osteoblast and marrow stromal cells. This transfection efficiency is not adequate for comparison of plasmid transfected and virally transduced cultures which can be transduced with 80-90% efficiency.
- Additional studies using direct electroporation of scaffolds with cells or tissues with plasmid DNA to introduce plasmid vectors should be tested based on published studies showing that eletroporation of nuclear entry vectors into lung tissue, corneal tissue and muscle is very effective in animal models (2, 3, 20) .
- The use of combinations of transgenes (cox-2, LMP-1 and BMP-2/4) may provide a more effective osteoinductive gene therapy than BMP-2/4 transgene alone.

References

1. Dean DA, Dean BS, Muller S, Smith LC 1999 Sequence requirements for plasmid nuclear import. Exp Cell Res 253:713-722
2. Li S, MacLaughlin FC, Fewell JG, Gondo M, Wang J, Nicol F, Dean DA, Smith LC 2001 Muscle-specific enhancement of gene expression by incorporation of SV40 enhancer in the expression plasmid. Gene Ther 8:494-497
3. Dean DA, Byrd JN, Jr., Dean BS 1999 Nuclear targeting of plasmid DNA in human corneal cells. Curr Eye Res 19:66-75
4. Vacik J, Dean BS, Zimmer WE, Dean DA 1999 Cell-specific nuclear import of plasmid DNA. Gene Ther 6:1006-1014
5. Wilson GL, Dean BS, Wang G, Dean DA 1999 Nuclear import of plasmid DNA in digitonin-permeabilized cells requires both cytoplasmic factors and specific DNA sequences. J Biol Chem 274:22025-22032
6. Young JL, Benoit JN, Dean DA 2003 Effect of a DNA nuclear targeting sequence on gene transfer and expression of plasmids in the intact vasculature. Gene Ther 10:1465-1470
7. Prasad TK, Rao NM 2005 The role of plasmid constructs containing the SV40 DNA nuclear-targeting sequence in cationic lipid-mediated DNA delivery. Cell Mol Biol Lett 10:203-215
8. Ivics Z, Hackett PB, Plasterk RH, Izsvak Z 1997 Molecular reconstruction of Sleeping Beauty, a Tc1-like transposon from fish, and its transposition in human cells. Cell 91:501-510
9. Hackett PB, Ekker SC, Largaespada DA, McIvor RS 2005 Sleeping beauty transposon-mediated gene therapy for prolonged expression. Adv Genet 54:189-232
10. Liu G, Geurts AM, Yae K, Srinivasan AR, Fahrenkrug SC, Largaespada DA, Takeda J, Horie K, Olson WK, Hackett PB 2005 Target-site preferences of Sleeping Beauty transposons. J Mol Biol 346:161-173
11. Liu G, Aronovich EL, Cui Z, Whitley CB, Hackett PB 2004 Excision of Sleeping Beauty transposons: parameters and applications to gene therapy. J Gene Med 6:574-583
12. Score PR, Belur LR, Frandsen JL, Guerts JL, Yamaguchi T, Somia NV, Hackett PB, Largaespada DA, McIvor RS 2006 Sleeping Beauty-mediated transposition and long-term expression in vivo: use of the LoxP/Cre recombinase system to distinguish transposition-specific expression. Mol Ther 13:617-624
13. Gersbach CA, Byers BA, Pavlath GK, Guldberg RE, Garcia AJ 2004 Runx2/Cbfa1-genetically engineered skeletal myoblasts mineralize collagen scaffolds in vitro. Biotechnol Bioeng 88:369-378
14. Gersbach CA, Byers BA, Pavlath GK, Garcia AJ 2004 Runx2/Cbfa1 stimulates transdifferentiation of primary skeletal myoblasts into a mineralizing osteoblastic phenotype. Exp Cell Res 300:406-417
15. Gersbach CA, Le Doux JM, Guldberg RE, Garcia AJ 2006 Inducible regulation of Runx2-stimulated osteogenesis. Gene Ther 13:873-882
16. Krebsbach PH, Kuznetsov SA, Satomura K, Emmons RV, Rowe DW, Robey PG 1997 Bone formation in vivo: comparison of osteogenesis by transplanted mouse and human marrow stromal fibroblasts. Transplantation 63:1059-1069

17. Garreta E, Genove E, Borros S, Semino CE 2006 Osteogenic differentiation of mouse embryonic stem cells and mouse embryonic fibroblasts in a three-dimensional self-assembling peptide scaffold. Tissue Eng 12:2215-2227
18. Zhang S, Holmes TC, DiPersio CM, Hynes RO, Su X, Rich A 1995 Self-complementary oligopeptide matrices support mammalian cell attachment. Biomaterials 16:1385-1393
19. Leon EJ, Verma N, Zhang S, Lauffenburger DA, Kamm RD 1998 Mechanical properties of a self-assembling oligopeptide matrix. J Biomater Sci Polym Ed 9:297-312
20. Dean DA, Strong DD, Zimmer WE 2005 Nuclear entry of nonviral vectors. Gene Ther 12:881-890

PROJECT 9

DIRECTOR: David J. Baylink, M.D.

TITLE: Administrative Support Service Facility

C. SUPPORT SERVICE FACILITIES
Project 9
Progress Report – Administrative Support Service Facility

Introduction

The research proposed in this application will be performed within the Musculoskeletal Disease Center (MDC), which is a large, multi-disciplinary research center consisting of more than 70 scientific and technical staff members, including 15 senior investigators with diverse expertise and research training. Of the 70 staff members, 43, including 13 senior investigators, are currently working on the Army projects. Strong administrative support is needed for organizing, coordinating, facilitating, and monitoring the research supported by the Army projects and is absolutely essential for the success of such a large, dynamic, and expanding research program. Consequently, the primary responsibility of this Administrative Support Service Facility is to support the administrative needs of the investigators supported by this Army grant. Moreover, synergistic interactions and collaborations between the investigators of the Army grant and other investigators of the MDC, as well as other investigators at local academic institutions and research organizations, such as Loma Linda University (LLU), Loma Linda Veterans Association for Research and Education (LLVARE), Loma Linda VA Medical Center, the University of California at Riverside, and the City of Hope, would enhance the productivity of the Army projects. Accordingly, the secondary objective of this Administrative Support Service Facility is to provide and stimulate interdepartmental, interdisciplinary, and inter-institutional dialogue and to improve the existing interactions and productivity between various investigators of the local institutions and organizations in musculoskeletal research

Body

Technical Objective 1:

To continue to provide a stimulating and supportive environment for Investigators supported by the Army grant that is conducive to focusing on bench research work so that administrative responsibilities are reduced.

Our Administrative Support Staff work with the investigators on these awards to keep them apprised of ongoing budgetary issues; to facilitate supply and equipment purchasing decisions; to order supplies and equipment; to prepare manuscripts for publication; to retrieve journal articles from the library; to prepare paperwork for submission to oversight committees; to organize meetings; to help with recruitment; and to help facilitate the preparation of progress reports. Maintaining a strong administrative support team has been critical to the success of our scientists. During the second year of the award for this project, our scientists have published 7 articles and 5 abstracts. The total number of publications for our group since 2000 is 42 plus the 34 abstracts published in the past year.

Regular weekly or bi-weekly meetings are convened at which our senior investigators (Drs. Mohan, Lau, Strong) discuss scientific issues related to the fulfillment of the specific

objectives of all of our Army funded projects. In order to insure that all of the scientific work of our current Army awards remains on track and progress toward meeting the specific objectives of each of our awards is being met, these regular meetings are essential. Our current awards include: DAMD17-99-1-9571; DAMD17-01-1-0744; DAMD17-02-1-0685; and DAMD17-03-2-0021.

Technical Objectives 2:

To continue to serve as the necessary and essential Support Service in order to stimulate interdepartmental, interdisciplinary, and inter-institutional dialogue and enhance the existing interactions and productivity between various investigators of LLU, Loma Linda University Medical Center, and LLVARE in musculoskeletal research.

Weekly staff meetings are held for all Musculoskeletal Disease Center (MDC) staff. When scientific issues are presented at the MDC staff meetings, these meetings are open to other investigators from Loma Linda University (LLU) as well as other VA and LLVARE investigators. Senior Investigators give talks on new technologies and areas relevant to the Army funded projects. Likewise, MDC investigators are invited to meetings of various research groups at LLU, the City of Hope and, periodically, the University of California Riverside (UCR). We invite expert scientists from other institutions to give talks on issues relevant to our Army funded research. This sharing of ideas with investigators from other institutions has proven to be very important.

Technical Objective 3:

The Core Facility "user" committee" will continue to evaluate the service rendered by each of the support service facilities. This information will then be provided in written form to the director of the corresponding support services facilities.

The end users evaluate the performance of our Informatics/Microarray, Vector, and Phenotype Core facilities on an ongoing basis and report to the Principal Investigator if any problems in service are found. Suggestions for improvement are discussed with the individual leaders of the Support Facilities as well as at general Staff Meetings. No major problems have been reported with any of the Core Facilities in the past year.

PROJECT 10

PRINCIPAL INVESTIGATOR: Jon E. Wergedal, Ph.D.

TITLE: Phenotype Support Services

Project 10 Phenotype Services.

Introduction

The major technical objective for this phenotype support service facility will be to receive samples, perform the appropriate measurements on these samples, and then transfer all the data electronically to the corresponding investigator. Specific objectives include:

1. To assist investigators in the design of studies involving given phenotypes.
2. To perform measurements as requested by the investigators on the samples provided.
3. To follow the development of emerging technologies in the literature and at meetings and make recommendations to investigators regarding the possibility of adopting some of these new technologies in the phenotype support service facility.

Body

1. To assist investigators in the design of studies involving given phenotypes.

Project 1. Studies on Genetic Regulation of Digit Tip Regeneration.

a. Development of laminum staining for identification of basement memebrane under the epidermal cell layer. Because the disruption of the basement membrane may be an important part of limb regeneration. Therefore good methods for the demonstration of basement membranes at the regeneration site will be important. Previously we have tested several methods for determining basement membranes including immunostaining for type IV collagen, and silver staining for reticulin fibers. These methods gave variable staining for the basement membranes under the epidermal cell layer of the skin. Laminum is one of the components of the basement membrane. We have previously established that laminum immunostaining as an excellent way to outline muscle fiber bundles. Staining in digit tip samples with a 1:50 dilution of stock anti laminum antibodies (a concentration that works well with skeletal muscle samples) resulted in highly overstained digit tip samples. Further testing of lower concentrations of antibody showed that dilution of the antibody 1:600, still resulted in staining of the epithelial membrane while minimizing staining of other structures.

Project 4. The Application of Transgenic Mice To Assess Gene Function In Mechanical Loading And In Bone Fracture Healing Models

a. Transgenic mice to assess gene function in mechanical testing and bone fracture. Transgenic mice with Leptin, Bax or Serpine gene knockouts are being studied to determine the influence of these genes on mechanical testing and bone fracture. Evaluation of fracture healing is being done by pQCT densitometry and faxitron x-Ray analysis. Because fracture healing involves the addition of a cancellous bone bridge on

the periosteal surface, the thresholding parameters for the pQCT analysis have been adjusted to identify total callus and mineralized callus or bone. This threshholding is based on our previous methods study.

b. Bone samples from mice with healing fractures have been processed for bone histology and histomorphometry. Bone samples are demineralized in EDTA and embedded in paraffin. Longitudinal sections through the fracture site are prepared and stained with H&E, Van Geisen Trichrome stain, or Mason's trichrome stain. Cartilage is determined by Safranin-O staining.

Project 6. Systemic Gene Therapy for the Skelton

a. We have explored and reported on a number of technical approaches to identifying bone cells that express the green fluorescent protein (GFP) as well as osteoblastic markers such as alkaline phosphatase. These approaches have identified cells with these properties but have not been satisfactory for quantitation. A new method for identifying the osteoblastic marker, alkaline phosphatase activity has recently been introduced. This is a fluorescent method. It has the advantage that the GFP and alkaline phosphatase could both be determined fluorescently. The alkaline phosphatase substrate is ELF97. It is a naptholic phosphate ester that becomes fluorescent and insoluble when the phosphate is hydrolyzed off. Determination of phosphatase is straight forward. The ELF97 is dissolved in an alkaline buffer and the resulting substrate solution applied to the slide. With bone sections with preserved alkaline phosphatase activity activity is evident within minutes. If monitered under a fluorescent microscope, the incubation time can be optimized. The reaction is terminated by rinsing off the slide. The optimum microscope filter set required for viewing the fluorescence is different for the two agents. Comparison between GFP and alkaline phosphatase can be done by flipping between filter sets.
Studies to explore this approach are ongoing.

2. To perform measurements as requested by the investigators on the samples provided.

Subproject 1

Samples of paws from several mouse strains and several time points have been processed. Paraffin sections have been prepared and stored for future work. These sections have been used for the development of immunostaining protocols and other staining techniques.

Subproject 2.

Bone samples from mutant lines identified in the ENU screening project have been processed for bone histology and bone histomorphometery. The samples were from animals injected with fluorescent tetracycline or calcein labels so that bone formation measurements could be done. Thick cross sections of undemineralized femurs were prepared from methyl methacrylate embedded samples. Measurement of fluorescent label

lengths and separation were made. Bone formation rates at the endosteum and periosteum were calculated using standard histomorphological calculations.

Subproject 4

a. Bone Sections from Leptin Bax and serpine knockout mice have been prepared and stained. Samples include fractured and unfractured bones at various times after fracture. Samples were demineralizedin EDTA, processed in a tissue processor, embedded in paraffin and sectioned. Sections are stained for H&E, Mason's trichrome, Van Geisens, and Saffranin O. The Saffranin O stained sections were used to follow the development and loss of cartilage during fracture repair. Samples were also evaluated for bone resorption by staining for tartrate-resistant acid phosphatase an osteoclast marker. The tunnel staining method for demonstration of apoptosis has been established in the core laboratory and is being used to evaluate apoptosis in BAX knockout mice.

b. Bone density and bone geometry measurements have been made by pQCT and Faxitron X-Ray analysis to establish basal values and to follow fracture healing. The instrument threshold settings must be done carefully because of the deposition of low density "woven bone" at the fracture repair site.

Subproject 6.

a. Bone samples from mice treated with GFP labeled hematopoietic stem cells are being processed for histological evaluation in the Phenotyping laboratory. Histological processing includes both frozen and paraffin embedded sections of bone and soft tissues.

b. Bones are also being evaluated for bone formation by analysis of density and geometry by pQCT analysis.

3. To follow the development of emerging technologies in the literature and at meetings and make recommendations to investigators regarding the possibility of adopting some of these new technologies in the phenotype support service facility.

Subproject 1. We continue to review the literature and attend presentations related to wound healing.As described above we have added a method to identify the basement membrane under epithelial cells using immunostaining for laminin. This method identifies the basement membrane more clearly. The concentration of the antibody is critical and must be optimized for each batch of enzyme.
`

Development of new technologies.

a. Evaluation of new technologies includes literature review and attending lectures. We again attended the workshop "non-invasive Assessment of Trabecular Bone Microarchitecture Working Group" given at the American Society of Bone and Mineral Research Meeting in Philadelphia.

b. MicroCT.
We are continuing to monitor the development of MicroCT equipment. AS previously reported the Scanco instrument includes the determination of bone density. Other companies are adding this feature.

c. Analytical methods for generating trabecular bone parameters from microCT scans are continuing to evolve. Analytic approaches can sharpen the images obtained and reduce the scan time. This is important for in vivo scanning where radiation exposure is a limiting factor for longitudinal studies. However equipment costs remain high.

d. The FE methods for estimating trabecular bone strength from microCT measurements have been largely validated. Mechanical testing are consistent with the models generated by FE modeling techniques. This is especially important for human studies where estimates of bone strength should improve our understanding of the effect of therapeutic treatment in osteoporotic subjects.

e. MRI.
Improvement in the instrumentation for micro-MRI on small animals are continuing. These do require greater capital investment in higher field strength instruments. Clinical instruments are also improving and a few clinical studies are underway with this non-invasive technology. Attempts are also being made to get better standardization among manufacturers so that data obtained on different instruments can be compared.

PROJECT 11

PRINCIPAL INVESTIGATOR: Subburaman Mohan, Ph.D.

TITLE: Microarray/Informatics Support Services

Progress Report

Project 11. Microarray & Informatics Support Services

Introduction

As a result of the sequencing of the human and mouse genomes there has been a tremendous increase in discovery of novel genes with unknown functions. It is important to next interpret and determine the function and genetic pathways of the large amounts of sequence information now available. One powerful method of determining unknown gene function and genetic pathways is by microarray expression profiling. Microarrays (also called DNA chips) are glass or plastic substrates on to which known sequences of DNA have been synthesized or spotted. Fluorescently labeled RNA from different biological samples are hybridized to their complementary sequences on the microarrays. The resulting fluorescent intensities are quantified and data analysis performed to determine expression levels of RNA transcripts. Thus, microarrays allow for the experimental analysis of many genes in a single experiment, and one can compare expression levels of genes over several timepoints and different biological or disease conditions. Comparing these expression levels gives clues to gene function and is a very powerful method of discovery. Project 11 of this grant had the goal to upgrade and improve the microarray and informatics support services in the Musculoskeletal Disease Center. Following are the technical objectives:

Body

1. Technical Objectives:

Following are the specific objectives during the second year of the grant period:

Technical Objective 1: **To provide technical service.**

Technical Objective 2: **To provide education.**

Technical Objective 3: **To update on recent advances.**

2. Progress on Technical Objectives

Technical Objective 1: To Provide Technical Service

In the past year in order to improve the technical service of the microarray support service, we upgraded our Genetix Q-Array-2 robotic spotting pins to 50 micron silicon pins. These pins have highly precise volumetric uptakes of as little as 25 nanoliters. The pins also have the ability to print completely to dryness. Both of these advantages have greatly reduced waste of our expensive oligo spotting libraries. The use of these pins has also greatly improved the quality of our manufactured arrays. The pins make arrays with

very uniform spots and with little to no bleeding through from one spot to another. Figure 1A demonstrates an actual microarray RNA hybridization of a chip with over 38,000 spots manufactured using these new pins. Figure 1B is a magnified image of one of the 48 fields spotted by one of the 48 silicon pins.

Figure 1A. →
Microarray image of over 38,000 spotted oligos using 48 silicon pins (50 micron tip size) from Parallel Synthesis Technologies. Note the uniform printing shown in all 48 printing fields.

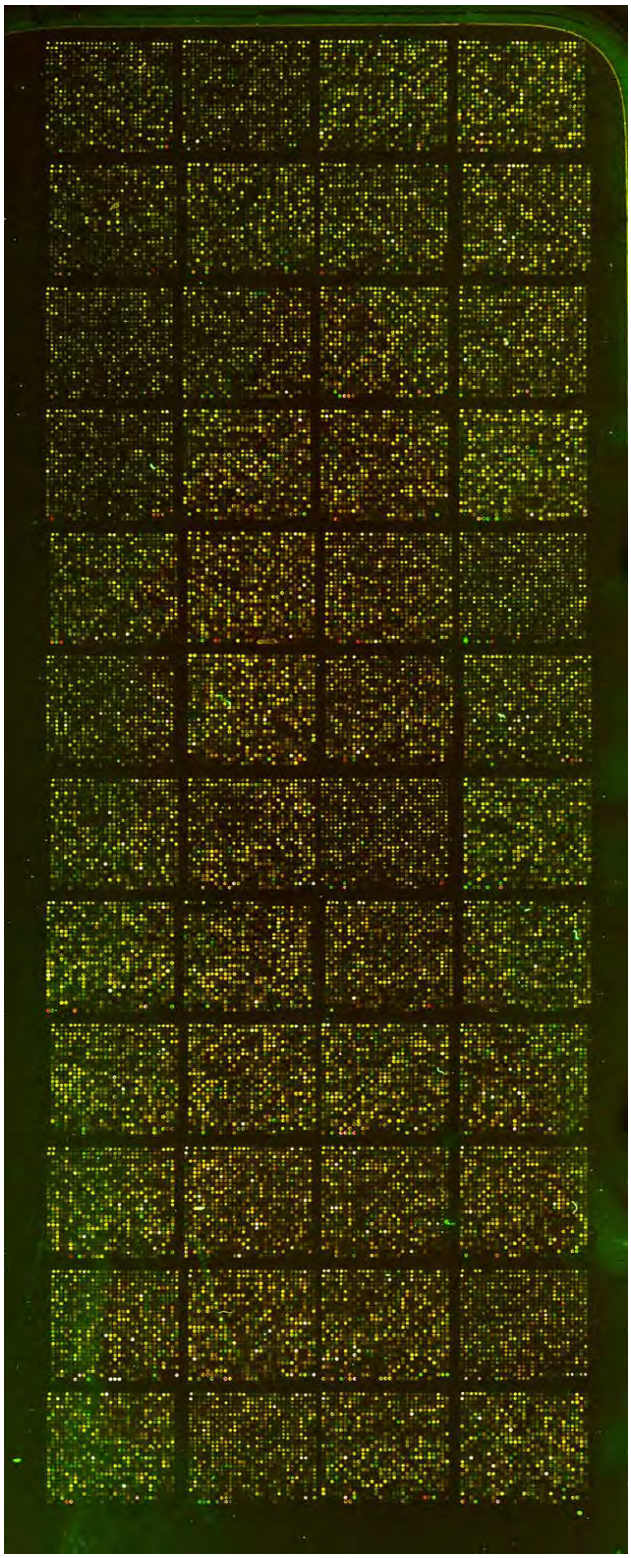

Figure 1B. ↓
Close up image of a single printing field. The printed oligos show uniform size and good circular morphology. The data is from an actual labeled RNA hybridization sample and the variation in intensity corresponds to normal variation in RNA expression.

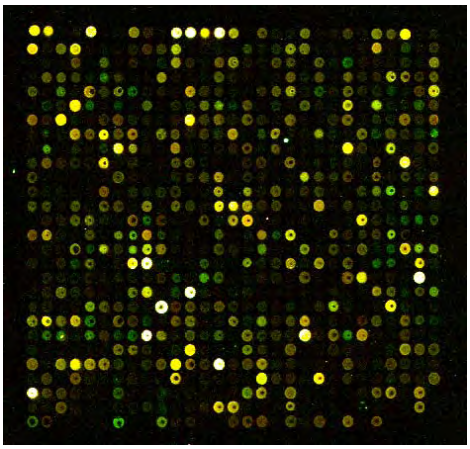

Specific Objective 2. To provide education.

Conferences and Continuing Education

The advances described are developed as a result of learning new methods and technologies from networking and scientific conferences attended by scientists in the MDC. Following is a list of conferences attended and talks given by scientists in the MDC. These conferences led to improvement and incorporations of state of the art technologies in the Microarray Laboratory and Informatics Support Services:

Latest Technologies and Development Conferences attended by Dr. Subburuman Mohan:

- The Endocrine Society, 88th Annual Meeting, June 24-27, 2006, Boston, MA
- American Society for Bone and Mineral Research, 28th Annual Meeting, Sept 15-19, 2006, Philadelphia, PA
- International Congress Of Growth Hormone And Insulin-Like Growth Factor Research Societies, 3rd International Meeting, Nov 11-15, 2006, Kobe, Japan.

Latest Technologies and Development Conferences attended by Dr. Robert Chadwick:

- American Society for Bone and Mineral Research, 28th Annual Meeting, Sept 15-19, 2006, Philadelphia, PA

Latest Technologies and Development Conferences attended by Dr. Hongrun Yu:

- American Society for Bone and Mineral Research, 28th Annual Meeting, Sept 15-19, 2006, Philadelphia, PA

Also, the microarray and informatics support services have trained and assisted multiple investigators in the MDC with their microarray experiments and data analysis.

Technical Objective 3: To update on recent advances.

In past 12 months we have upgraded our microarray analysis software to GeneSpring GX Version 7.3.1. The software allows for faster access to and visualization of biological relevance through the incorporation of full-gene ontology information. This also allows researchers to quickly determine if a gene is a member of a specific molecular pathway, and whether a subset of genes with altered expression are enriched with genes that are in a particular molecular pathway. The new software also provides higher confidence in the microarray expression results through volcano and box plot visualizations. Other new features of the software are an improved error model for two-color microarray hybridization data.

The combination of new pins for spotting of our microarrays and recent software upgrades has led to both improved microarray manufacture and better more reliable microarray data analysis for researchers in the MDC.

Key Research Accomplishments

- Increased the quality of manufactured arrays through the use of 50 micron silicon printing pins.
- Increased oligo library life through the reduction of waste from print blotting and printing to complete dryness with the silicon pins.
- Improved microarray analysis results by the use of GeneSpring GX Version 7.3.1 expression analysis software.
- Trained multiple investigators in informatics and microarray data analysis.

Reportable Outcomes

None.

Conclusions

1) The technical objectives (1) To provide technical service; (2) To provide education; and (3) To update on recent advances have been achieved.

2) The microarray and informatics support services have improved microarray quality and improved microarray analysis results in the Musculoskeletal Disease Center.

3) The improvements made to the microarray and informatics support services will expedite and advance research into gene discovery, function and genetic pathway analysis in the MDC.

PROJECT 12

CO-PRINCIPAL INVESTIGATORS: Kin-Hing William Lau, Ph.D.

Shin-Tai Chen, Ph.D.

TITLE: Vector Support Services

PROJECT 12: VECTOR SUPPORT SERVICE

Introduction

The Vector Support Service Facility is a dynamic resource for materials and technical expertise involving gene transfer and gene therapy. In 2006, we developed and produced viral vectors, especially retroviral vectors that are based on Moloney murine leukemia virus (MLV) and human immunodeficiency virus (HIV) for Investigators working on the projects supported by the Army.

There were three specific objectives for this subproject:

1. To serve as a dynamic resource to construct and provide vectors for delivery and expression of appropriate genes for Investigators supported by the Army grant.
2. To serve as an educational resource, providing technical assistance and training to Investigators in the use of viral and non-viral vector gene delivery and gene expression.
3. To improve and expand vector systems available to Investigators as gene transfer technologies advance.

Body

Specific objectives for the third year of funding period

- **Specific Objective 1: To assist investigators in the design of and to provide with appropriate research-grade viral or plasmid vectors.**

In 2006, the Vector Support Service continues to produce VSV-G pseudotyped MLV-based and HIV-based vectors for various investigators working on projects supported by the Army. Specifically, 1) in collaboration with Dr. Rundle (sub-project 4), the facility generated various batches of concentrated VSV-G pseudotyped MLV vectors expressing different growth factor or control genes that have been used successfully in animal experiments. These growth factor or control genes included β–galactosidase (β-gal), enhances green fluorescent protein (EGFP), bone morphogenetic protein-4 and its derivatives (BMP-2/4), LMP proteins with HA tag (LMPHA), and cyclooxygenase (Cox-2). 2) In support of the sub-project 6, the facility generated three different batches of HIV-based vectors for use in the study of systemic gene therapy of musculoskeletal diseases. These HIV-based vectors contain FGF-2 genes and genes derived from FGF-2. Since the FGF-2 gene can promote cell proliferation, each HIV-based vector was harvested and concentrated, tested for potential contamination of recombination competent retrovirus (RCR) within the preparation. None of these HIV-based vector preparations has shown RCR contamination in our assay system. The results have been submitted to and approved by the Biosafety committee and Animal care and use committee. 3) In support of the sub-project 7, the facility produced different batches of concentrated MLV-based vectors, expressing β–gal, BMP2/4, and Cox-2 genes, respectively. 4) In collaboration with Dr. Strong (sub-project 8), the facility produced several different batches of concentrated VSV-G pseudotyped MLV vectors, expressing β–gal, BMP, Cox-2, LMP-HA, and IGFBP6 for her experiments.

- **Specific objective 2: To provide education, tutorials, practical training, technical assistance, and protocols to Investigators for the experimental use of gene transfer vector.**

Dr. Chen (the director of the Vector Support Service) gave one lectures in J.L.Pettis VAMC, Musculoskeletal Diseases Center during the past year. The lecture was designed to educate and tutor Army projects investigators in viral gene transfer technology, more importantly, to address the safety issues concerning the use of viral vectors in gene transfer and therapy.

- **Specific Objective 3: To evaluate emerging technologies and develop improved viral and plasmid vectors, as appropriate, for more efficient and effective gene transfer**.

a) Development of inducible MLV-based vectors for bone disease gene therapy.

Previously, we have developed a doxycycline inducible retroviral vector, pGYT-EGFP, based on an improved tetracycline induced expression system. We have tested the vector in HT1080, 293T, Rat marrow stromal cells and rat skin fibroblasts and the induction of the marker gene expression is around 10-40 folds dependent on the cell lines used. In this year, we further investigated the induction of the inducible vector in other cell lines.

One of application for the inducible vector is to use it in musculoskeletal cells. Therefore, within this quarter, we tested the expression of the inducible retroviral vector, pGYT-EGFP in human bone cells (HBC), mouse osteoblast cells (MC3T3), Rat marrow stromal cells (RMSC), mouse macrophage cell line (Raw) and mouse muscle stem cell line (C_2C_{12}). We plated the cells in 6 well plates with 1 $X10^5$ cells per well. After over night incubation, 200μl of pGYT-EGFP vectors (viral titer around 1 X 10^7 tfu/ml, MOI around 10) were added to the cells in duplicated wells. After another overnight incubation, the medium of one of the wells was replaced with doxycycline containing medium (1μg/ml). After additional 48 hr of incubation, the cells were harvested and analyzed by flow cytometery. The results are summarized in Table 1.

Table 1

Cell Types	Types of Media	% GFP(+) Cells	Mean Intensity	Fold Induction*
HBC	Regular	52.7	1294	1.0
	+Doxy	83.3	5465	**6.7**
MC3T3	Regular	49.8	295	1.0
	+Doxy	72.3	3975	**19.6**
RMSC	Regular	41.6	464	1.0
	+Doxy	38.0	4063	**8.0**
Raw	Regular	71.2	601	1.0
	+Doxy	99.8	5076	**11.8**
C_2C_{12}	Regular	38.7	607	1.0
	+Doxy	93.3	3259	**12.9**

*Fold induction is calculated by comparing the value of mean intensity multiple by the percentage of the positive cells. We selected the value from regular medium as 1.

From these results we concluded the new tet-on system can be used in all the cells checked. The inductions range from 6.7 to 19.6 folds. Since the MIO used in this experiment in rather high (MOI~10), we expected expression is saturated in some cells. Therefore, the fold induction

may be under estimated. Applications of this vector in bone disease gene therapy are in progress.

In collaboration with Drs. Lau and Hall in MDC, we have demonstrated $Sca1^+$ cells based transplantation strategy with modified FGF-2 gene can induce endosteal trabecular bone formation. However, we also found several adverse effects with high FGF-2 expression. These problems include depletion of serum calcium level, high level of serum PTH and incomplete mineralization of trabecular bone. We hypothesize that the use of an inducible promoter to regular FGF-2 expression in the engrafted cells would optimize the bone formation and minimize the adverse side effects. Within this quarter, we tested the pGYT-EGFP vector in HT1080 cell and $Sca1^+$ cells under a range of doxycycline concentration. We transduced $Sca1^+$ cells with an inducible vector (pGYT-EGFP) or a regular vector (pY-EGFP) with MOI around 6. We also transduced HT1080 cells with same vectors with MOI around 1.5. After the transduction, the cells were exposed to a range of doxycycline (1-2000ng/ml). Seventy-two hours after transduction, the cells were analyzed by flow cytometery. The results were summarized in figure 1.

Figure 1 (A) (B)

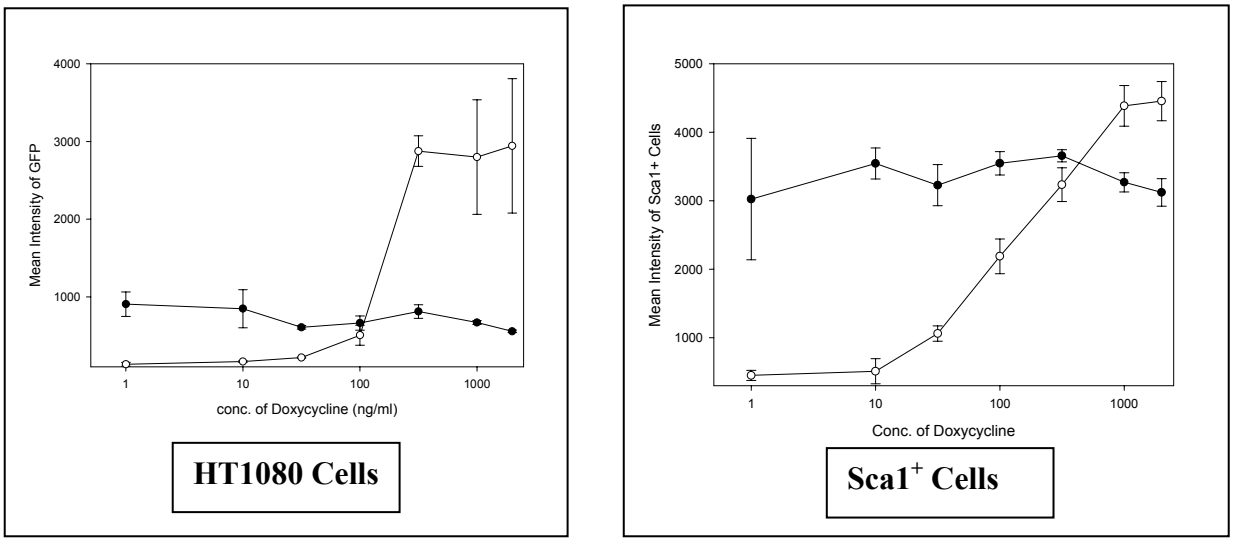

Figure 1 (A) HT1080 cells were transduced with MLV-based vectors containing the GFP gene under the control of either a constitutively expressing promoter (solid dots) or doxycycline inducible promoter (open dots). Cells were cultured in different concentrations of doxycycline (1-2000ng/ml). Seventy-two hours after incubation, the cells were assayed for GFP by flow cytometery. (B) is the same as the part (A) except the $Sca1^+$ cells were used.

As shown in figure 1, the expression of GFP in the doxycycline inducible promoter can reach the full induction under 1000ng/ml of doxycycline. The level of expression of inducible promoter is stronger than the MLV-LTR viral promoter in both HT1080 cells and mouse $Sc1^+$ cells. We also tested a similar construct with modified FGF-2 gene. We found FGF-2 level in the conditioned medium of $Sca1^+$ cells transduced with the modified FGF-2 gene under the control of the doxycycline inducible promoter was 10-fold higher in the present of 1000ng/ml doxycycline (48.3 ± 2.6pg/ml vs. 467.5 ± 71.6 pg/ml). These constructs will be used in the future collaboration with Drs. Lau, and Hall in MDC.

b) Develop inducible HIV based vectors for expression of therapeutic genes for bone formation and bone repair

Previously, we have constructed tetracycline inducible MLV-based and HIV-based vectors. We found tetracycline inducible MLV-based vectors can conditional express the gene of interest. Under inducible condition, the express level is higher than then regular MLV LTR promoter and the expression level is more than 10-fold higher than in the un-inducible condition in the most of cell lines tested. However, under the similar scheme, the gene expression level in HIV-based vectors is much lower and we only can achieve 2-3 fold induction. Within this year we designed a new HIV-based inducible vector for conditional expression gene-of-interest, through different configuration. In our original tet-on HIV-based vector, pHIV-GYT-EGFP, transcriptional factor, GYT and the inducible expression cassette are in the same vector. The functional arrangement of this vector is shown in figure 2. In this vector, CMV promoter drives the transcriptional factor, GYT and it is near to the tetO promoter. This arrangement can have two potential problems. First, the strong enhancer activity of CMV promoter may interfere with TetO promoter and subsequently increases the back ground expression of the gene-of-interest under suppress condition. Second, the strong transcription of CMV promoter may interfere with TetO promoter under inducible condition, since these two transcripts are in the same orientation. The arrangement of the vector doesn't have a transcription stop signal between these two transcripts. Therefore the strong transcription of CMV may suppress the expression of TetO promoter under inducible condition. To test this hypothesis, we separated these two transcripts into two separate vectors. As shown in figure 2, we constructed pHIV-TetO-EGFP contains the tet-on transcriptional unit with the marker gene, EGFP. Additionally, we constructed two viral vectors, pHIV-GYT and pMLV-GYT to express the tet-on transcriptional factor, rtTA-GYT either from a HIV-based vector or a MLV-based vector. After construction of these viral vectors in plasmids, we prepared the VSV-G pseudotyped HIV-based and MLV-based vectors with our standard transient transfection method in 293T cells. The diagrams of these HIV-based and MLV-based vectors are shown in figure 2.

pHIV-9-EGFP

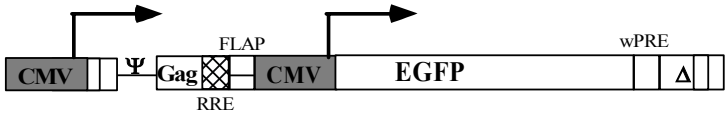

pHIV-GYT-EGFP

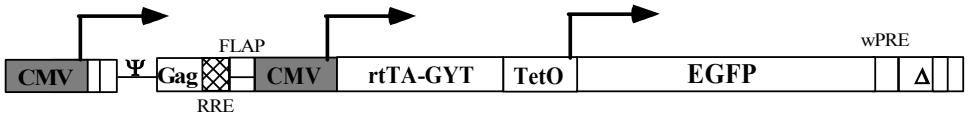

pHIV-TetO-EGFP

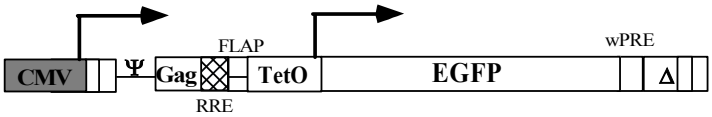

pHIV-GYT

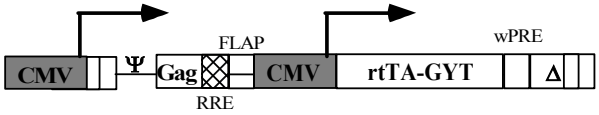

pMLV-GYT

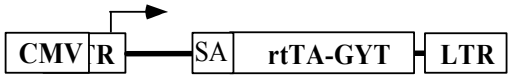

Figure 2: The diagram shows the HIV-based and MLV-based vectors used in this quarter. The pHIV-9-EGFP is the standard HIV-based vector and the EGFP gene is driven by CMV promoter. The pHIV-GYT0EGFP is the original inducible HIV-based vectors, and the EGFP gene is driven by the TetO promoter. The pHIV-TetO-EGFP is derived from pHIV-GYT-EGFP by deleting the CMV promoter and part of rtTA-GYT gene. The pHIV-GYT is the HIV-based vector with rtTA-GYT gene and the pMLV-GYT is the MLV-based vectors with rtTA-GYT. In pHIV-GYT the expression of rtTA-GYT is from CMV promoter and in pMLV-GYT, the expression of rtTA-GYT is from MLV LTR promoter.

Using HT1080 cells, we checked the induction of doxycycline with different combination of these vectors. We first mixed the designated viral vectors and transduced HT1080 cells either in the induction medium (+Dox, 1 μg/ml) or suppression medium (regular medium without doxycycline). Then the viral mixture was added to HT1080 cells in 6-well plates. Forty-eight hours after transduction, the cells were detached and the fluorescent activities were determined by FACS techniques. The results were summarized in the Table 2.

Table 2

Viral Vectors	Types of Media	% of GFP positive cells	Mean Intensity	Fold Induction*
pHIV-9-EGFP 10 μl	Regular	39.46	1694	
	+Doxy	ND**	ND	ND
pHIV-GYT-EGFP 10 μl	Regular	3.08	614	
	+Doxy	5.06	905	2.42
pHIV-tetO-EGFP 10 μl & pHIV-GYT 100 μl	Regular	1.30	188	
	+Doxy	1.54	1926	12.10
pHIV-tetO-EGFP 10 μl & pMLV-GYT 100 μl	Regular	1.94	96	
	+Doxy	30.8	2353	38.73

*Fold induction is calculated by comparing the value of mean intensity multiple by the percentage of the positive cells. We selected the value from regular medium as 1. **ND: Not determined

From these results we found the doxycycline induction is significantly improved in the two vectors system and induction was increase from 2.42 fold to 12.10 fold (GYT-rtTA express by HIV-based vector) and 38.73 fold (GYT-rtTA express by MLV-based vector). To confirm these results, we repeated the experiment with higher amount of the EGFP vectors. The results were summarized in table 3.

Table 3

Viral Vectors	Types of Media	% of GFP positive cells	Mean Intensity	Fold Induction*
pHIV-GYT-EGFP 100 μl	Regular	40.52	277	
	+Doxy	56.74	870	4.40
pHIV-tetO-EGFP 100 μl	Regular	13.38	63	
	+Doxy	15.35	65	1.19
pHIV-tetO-EGFP 100 μl & pHIV-GYT 100 μl	Regular	12.76	75	
	+Doxy	22.26	2159	49.59
pHIV-tetO-EGFP 100 μl & pMLV-GYT 100 μl	Regular	14.67	70	
	+Doxy	33.96	2708	88.37

Concluded from these two experiments, indeed, the two vectors system significantly improved the induction system. The system has several advantages. First, the back ground expression is low (compares mean intensity 63 vs. 277). Second, the expression level is higher under the induction (compares mean intensity 2159 or 2708 vs. 870). Therefore the fold induction is increase from 4.40 to 49.59 or 88.37 in this experiment. One thing is worse notice; the expression level of EGFP in new vector under inducible condition is stronger than the expression level of CMV driven EGFP in pHIV-9-EGFP (1926 or 2353 vs. 1694). This is very unusual since the CMV promoter in HT1080 cells is very strong. Therefore, our new doxycycline inducible HIV-based vector is not only can regulate by ligand, doxycycline, but also can express the gene-of-interest very efficiently under inducible condition. Our next goal will be studying the inducibility of these vectors in our animal models.

c) Develop methods for production of high titer retroviral vectors for bone formation and bone repair.

Concentration of retroviral vectors is one of major challenges for retroviral vector production. Previously, we used ultracentrifugation method to pellet the VSV-G pseudotyped viral particles and then resuspend in smaller volume of the buffer. This type of approach is very simple and easy to scale up. However, it also comes with problems. First, the viral particle may be damaged during the high speed centrifugation, subsequently lower the yield of the recovery. Second, there are many unwanted materials may also be concentrated during the procedures. The desired method for viral particle concentration must preserve its native biological activity upon reconstitution of the precipitate. Since retroviral vector is an envelope virus, the precipitation must not denature the protein nor to disrupt the lipid bilayer. In addition, the procedure shall not add any material that would not be compatible with future applications of viral vectors *in vitro* or *in vivo*. Within this year, we tested a new method to concentrate viral vectors.

One of the other methods for virus purification is polyethylene glycol (PEG) precipitation. PEG is a hydrophilic nonionic polymer which has been used for phase–separation of large molecular out of aqueous solutions. The PEG would not denature proteins at ambient temperature and require relatively low amount (5-10%) for precipitation. Additionally, small amount of residual PEG concentrated in the pellet since most of the PEG is retained in the supernatant. Based on this, we tested the method of concentrating of viral vectors with PEG. First, we prepared 72 ml of viral vectors with marker gene, EGFP. Then, we mixed 36ml of viral vectors with 12ml of PEG solution (40% PEG8000 in PBS) to bring the final concentration of PEG to 10%. After overnight incubation at 4^{o}C, the mixtures were centrifuged at 3000rpm for 30 minutes. A well defined pellet can be seen after the centrifugation. The pellet was resuspended in 1.2ml of 4% lactose in PBS. For the rest of 36ml of viral stock, we precipitated with standard ultra-centrifugation method and also resuspend the pellet in 1 ml of 4%lactose in PBS. The viral titers of viral stocks and concentration viral stocks were determined by end-point dilution in HT1080 cells through flow cytometery. The results were summarized in Table 4.

Table 4

Experiment One	Viral titer before concentration	Viral titer after concentration	% of yield
PEG method	3.57 X10^{7}	1.09X10^{9}	84.8%
Ultra-Ce. Method	3.57 X10^{7}	7.31X10^{8}	56.9%
Experiment Two			
PEG method	7.22 X10^{6}	6.37 X10^{8}	43.0%
Ultra-Ce. Method	7.22 X10^{6}	7.02 X10^{8}	47.4%

Based on these results, we found the PEG method can concentrate the VSV-G pseudotyped MLV-based vectors as efficient as ultra-centrifugation method. The compatibility of the PEG concentrated vector with our *in vivo* and *ex vivo* experiment will be determined in the future experiments.

Key Research Accomplishments:

- Prepared MLV and HIV-based vectors for other sub-projects (sub-projects 4, 6. 7 and 8)
- Developed a new method to concentrate VSV-G pseudotyped retroviral vectors.
- Developed and characterized TET-ON inducible MLV-based and HIV-based retroviral vectors for bone diseases gene therapy and gene transfer.

Reportable Outcomes:

None

Conclusions

c) In collaboration with investigators of other sub-projects of this Army grant, we have generated and provided with the investigators several different batches of MLV and HIV-based vectors for use in their approved projects.

d) We developed a new method for concentrating VSV-G pseudotyped MLV-based and HIV-based vectors.

e) We developed and characterized inducible TET-ON regulatory retroviral vector systems. The gene expression of this vector can be modulated by doxycycline either in MLV-based or HIV-based vectors. This vector system is essential for skeletal gene therapy and for studying function of genes-of-interest during bone repair.

APPENDICES

Project One-

1. **RB Chadwick**, LM Bu, Y Hu, Y Zhu, DJ Baylink, S Mohan. Digit Tip Regrowth and Differential Gene Expression in MRL/Mpj, DBA/2 and C57BL/6 Mice. Wound Repair and Regeneration, in press, 2007.

Project Two-

Abstracts

1. **Srivastava AK**, Mohan S, Baylink DJ. A Sensitized ENU Screening System to Discover Modifier Genes by Utilizing Mouse Models Deficient in Genes Regulating Skeletal Tissues**.** 28th Annual Meeting of American Society for Bone and Mineral Research, 2006.
2. **Srivastava AK**, Mohan S, Baylink DJ. Identification of Mutant with a Large Decrease in Bone Size Identified in a Sensitized ENU Screen using Growth Hormone Deficient 'Little' Mouse. 28th Annual Meeting of American Society for Bone and Mineral Research, 2006.

Project Three-

1. **Xing W**, Baylink D, Kappor A and Mohan S. A platform of high-efficiency non-viral gene transfer in mouse osteoblast cells in vitro. Molecular Biotechnology 34(1):29-35, 2006

2. **Xing W**, Baylink D, Kesavan C and Mohan S. HSV-1 Amplicon-Mediated Transfer of 128-kb BMP-2 Genomic Locus Stimulates Osteoblast Differentiation *in vitro* Biochem Biophys Res Commun 319(3): 781-6, 2004

3. **Xing W**, Baylink D, Kesavan C and Mohan S. Transfer of 128-kb BMP-2 Genomic Locus by HSV-Based Infectious BAC Stimulates Osteoblast Differentiation: A Platform for Functional Genomic Studies. *ASBMR-2004, 19 suppl 1: S150, 2004*

Project Four-

1. Wang, X., **C.H. Rundle,** J. Wergedal, A. Srivastava, S. Mohan and K.H-W. Lau (2007) Loss of sex-specific difference in femoral bone parameters in male leptin knockout mice. Provisionally accepted for publication by *Calcified Tissue International*.

ORIGINAL RESEARCH ARTICLE – REGENERATION SCIENCE

Digit tip regrowth and differential gene expression in MRL/Mpj, DBA/2, and C57BL/6 mice

Robert B. Chadwick, Liming Bu, Hongrun Yu, Yan Hu, Jon E. Wergedal, Subburaman Mohan, David J. Baylink

Musculoskeletal Disease Center, JL Pettis VA Medical Center, Molecular Genetics Division, 11201 Benton Street (151), Loma Linda, California 92357

Reprint requests:
Robert B. Chadwick, Musculoskeletal Disease Center, JL Pettis VA Medical Center, Molecular Genetics Division, 11201 Benton Street (151), Loma Linda, CA 92357.
Tel: +909 825 7084 ext. 1582;
Fax: +909 796 1680;
Email: robert.chadwick@med.va.gov

Manuscript received: February 10, 2006
Accepted in final form: December 13, 2006

DOI:10.1111/j.1524-475X.2007.00216.x

ABSTRACT

MRL/Mpj mice are the only known strain of mouse that can regenerate cardiac lesions and completely heal ear punches without scarring. This study was undertaken to determine if MRL mice also have greater regrowth capabilities in amputated digit tips. Right paw digit tips of neonatal MRL mice were dissected, with the left front paws as uncut controls. Controls used for regrowth comparison were the DBA/2 and C57BL/6 inbred mouse strains. Consecutive x-ray images were captured of front paws at 0, 7, 14, 21, and 28 days postamputation. MRL mouse digit tips were found to distally regrow more quickly and reform nails partially and completely to a greater degree in comparison with DBA and B6 mice ($p < 0.05$). We next undertook microarray expression analysis to identify the genes involved in digit tip regrowth. Four hundred genes out of 15,000 were significantly differentially expressed ($p < 0.05$) in MRL, DBA, and B6 mice at day 4 in comparison with day 0 control tissue. Multiple differences between MRL, DBA, and B6 strains were found in genes that are implicated in the WNT signaling pathway and transcription. We conclude that MRL mice regrow digits distally more rapidly and partially and completely regrow nails to a greater degree than B6 and DBA strains. This enhanced regrowth is likely due to strain-specific increased expression of genes involved in growth and development.

Experiments with amphibian limbs, first undertaken in the 18th century, demonstrate that limb regeneration in vertebrates is possible.[1,2] In amphibians, the first stages of regeneration are initial wound healing by formation of an epidermal layer over the wound, followed by dedifferentiation of cells that cluster under this epidermal layer.[3] These dedifferentiated cells (blastema cells), similar to stem cells, redifferentiate into other cell types including bone, cartilage, and epithelial cells. The genes and genetic pathways that determine how the cells dedifferentiate and redifferentiate into other cell types are not completely understood.

Higher mammals also have marginal abilities to regenerate.[4–8] For example, children and newborn mice will replace digit tips when they are amputated distal to the last interphalangeal joint.[4,5] Another example of regeneration in mammals is the healing of ear holes in rabbits without scarring.[9,10] Recently, we and others have demonstrated that the MRL inbred strain of mouse shows greater regeneration and healing of earhole punches as opposed to several other inbred strains of mice.[11,12] Among inbred mouse strains, the MRL mouse was found to completely heal earhole punches, the DBA strain was found to be an intermediate regenerator, and the B6 strain found to be a poor regenerator of earhole punches.[11] Other studies have found that the MRL mouse is also capable of cardiac muscle regeneration.[13] Thus, the MRL mouse is a unique model to study the genetic mechanisms that regulate wound healing and tissue regeneration. However, to date, the MRL mouse has not been investigated extensively for its abilities to regrow more complex biological structures, such as digit tips. This study examined digit tip regrowth in the MRL, DBA, and B6 inbred strains of mice in order to determine if these mouse strains have similar regenerative capabilities of digit tips as in earhole punches. We also undertook global RNA expression profiling in those strains to identify the genes and genetic pathways responsible for wound healing and digit tip regrowth.

MATERIALS AND METHODS

Mouse surgery

Four-week-old MRL, B6, and DBA mice were obtained from The Jackson Laboratories. The studies were performed with the approval of the animal ethics committee of the Jerry L Pettis Memorial VA Medical Center (Loma Linda, CA). Surgery was conducted on the pup's digit tips within 1 day of birth. The neonatal mice were anesthetized with 5% halothane mixed with O_2 5 L/min. The right front third and fourth digit tips were amputated, with the left side as uncut controls. As the level of amputation is very important to subsequent regrowth capabilities, all surgery was performed under a microscope, and a scalpel was used to dissect the digit tips as accurately as possible at the midpoint of the third phalanges.[6,7] The accuracy of digit tip surgery and amounts of tissue dissected were documented and measured by capturing images of the digits both before and after surgery. The amputated tissues were

Dispatch: 30.1.07 Journal: WRR No. of pages: 10 CE: Pranjal PE: Satish/Gk
Author Received: B 216 Manuscript No. WRR Journal Name
(WUS WRR 216.PDF 30-Jan-07 11:30 677814 Bytes 10 PAGES n operator=mk.gokula)
WRR 216

Q3 collected into RNA later (Ambion), and the tissues from the pups of 1 L were pooled. Both left (uncut) and right (cut) paw x-ray images were taken at 0, 7, 14, 21, and 28 Q4 days postsurgery with a Faxitron MX-20 x-ray. Also, at 4 days postsurgery, mice were sacrificed, regenerating digit tips were collected by surgery, and the tissue was pooled in RNA later and stored at –80 °C for later RNA extraction.

Growth rate measurements

Faxitron x-ray images were measured using the ruler feature of Adobe Photoshop. Three growth amounts were determined: (1) the amount of dissected tissue (A–B in Figure 1); (2) the length of first phalanx of third and fourth fingers of front two paws (C–D in Figure 1); and (3) the length from the bottom of second phalanx to the regenerating tissue edge (C–A in Figure 1). Measurements were made of both left uncut and right cut digits. All measurements were done in duplicate by two different individuals who were blinded to mouse strain. Estimates of errors in measurement were made by capturing 10 consecutive images of the same mouse's digit tips. These error estimates were determined by repositioning a mouse between each image capture to estimate the error in successive weekly image captures. Also, 10 consecutive images were captured with a mouse not repositioned between each image capture to estimate errors in measurements at a particular time point. In order to minimize disruption of mice and mother abandonment of newborn pups, the growth was determined only for 7, 14, 21, and 28 days postsurgery.

Microarray expression analysis

Total RNA was isolated from dissected tissues at days 0 and 4 using the Agilent Total RNA Isolation Kit (Agilent Technologies). For day 0 RNA isolations, digit tip tissue Q5 from 30 MRL, 26 DBA, and 30 B6 mice were, respectively, pooled before processing. For day 4 RNA isolations, digit tip tissue from 15 mice of each respective strain was, respectively, pooled. Tissues were lysed using a Polytron Q6 Generator (Kinemalica AG), and then processed following the manufacturer's protocol (Agilent Technologies). The total RNA concentration was determined by NanoDrop spectrophotometer and RNA quality was determined by 18S/28S ribosomal peak intensity on an Agilent Bioanalyzer. For microarray expression profiling and real-time PCR, RNA samples were used only if they showed little to no degradation. Custom cDNA slides were spotted in duplicate with ~15,000 cDNA clones obtained from the National Institute on Aging (NIA).[14] A Q-Array2 Q7 robot (Genetix) was used for spotting. The arrays were also spotted with Amersham Lucidea Universal Scorecard controls to insure correct gene expression values were obtained from each array. Controls were spotted in duplicate in the first and last PCR plates to insure proper data tracking. Replicate microarrays were run for each RNA sample (10 microarrays each for MRL and DBA, and three microarrays for B6). This number of replicate microarrays is calculated to give 95% power to detect a twofold change in expression between the days 4 and 0 RNA samples and also between MRL and DBA pooled RNA samples at the 0.001 significance level.[15] A total of 250 ng RNA was used to synthesize double-stranded cDNA using the Low RNA Input Fluorescent Linear Application Kit (Agilent Technologies). First-strand cDNA synthesis was primed with T7-(dT24) promoter primer. From the purified cDNA, cRNA was synthesized using transcription master mix and purified. Two hundred and fifty nanograms of purified cRNA was used to reverse transcribe to fluorescent cDNA. Cyanine-3-dCTP and cyanine-5-dCTP were used to label experimental samples (day 4) and control samples (day 0). Dye swaps were also conducted to eliminate potential dye bias effects. Samples were hybridized at 60 °C for 17 hours. The slides were then washed with Solution I (6× SSC, 0.005% Triton X-102) for 10 minutes in the dark and then with Solution II (0.1× SSC, 0.005% Triton X-102) for 5 minutes in the dark. The slides were dried with pressurized nitrogen and immediately scanned using a GSI Lumonics ScanArray 4000 scanner. The signal intensity of all microarray images was determined using ImaGene 5.6 software. Expression analysis of microarray experiments Q8 was performed with GeneSpring 7.1 (Silicon Genetics) using the raw intensity data generated by the ImaGene software. Local background-subtracted median signal intensities were used as intensity measures, and the data were normalized using per spot and per chip LOWESS normalization. The transcripts that passed with flag values present or marginal were targeted for further analyses. The transcripts were then further analyzed by utilizing a one-sample Student's *t*-test to test whether the mean normalized expression level for the gene is statistically different from 1.0. To characterize and classify the function of genes differentially expressed in regenerating digit tip tissue, we used Onto-Express to classify genes according to their biological process Gene-Ontology (GO) category. The number of genes corresponding to GO category among the differentially expressed genes was tallied and compared with the number of genes expected for each GO category

Figure 1. Measurements of digit growth in mice. X-rays were taken at days 0, 7, 14, 21, and 28 postdigit tip dissection. Surgery was performed under a microscope at the middle of the third phalanx (midpoint of A–B). Phalanx and digit tip measurements were determined by the length of first phalanx of third and fourth fingers of both front paws (C–D, measurements used in Figure 2); the length from the bottom of second phalanx to the tissue edge (C–A, measurements used in Figure 3).

based on their representation in the NIA 15K set. Significant differences from the expected were calculated with a two-sided binomial distribution.[16–18]

Confirmation of microarray results by quantitative real time PCR

Reverse transcription of 200 ng of total RNA (days 4 and 0) was carried out in a final volume of 20 μL using a Superscript reverse transcriptase kit according to the manufacturer's instructions (Invitrogen). To prevent 3′ bias of the real-time PCR reactions random decamers (Ambion) were used for priming rather than oligo-dT. Real-time PCR was done using the SYBR Green PCR Core Reagents Kit (Applied Biosystems). Five microliters of cDNA at a concentration of 10 ng/μL and 0.1 μM of each primer in a final volume of 25 μL was used. For statistical significance, each RT-PCR had six replicates. Once the master mix was made, the 25 μL aliquots were transferred into a MicroAmp optical 96-well reaction plate (Applied Biosystems), vortexed, and sealed with an optical adhesive cover (Applied Biosystems). Cycling and signal detection were done using the ABI-7900HT Sequence Detection System with the following cycling conditions: initial activation at 95 °C for 10 minutes, 40 cycles at 95 °C for 15 seconds, and 60 °C for 1 minute. The gene expression level was normalized to housekeeping genes β-actin and TBP5. Subsets of all RT-PCR reactions were sequenced to insure gene specificity for the reactions.

Histology

We examined MRL inbred strains for blastema formation by sacrificing the mice at 1, 4, 7, 14, and 21 days postdigit tip dissection. Dissected paw tissues were stored in 10% formalin until processing. The tissues were fixed in paraffin and 5 μm tissue sections were mounted on to microscope slides. Following hematoxylin and eosin (H&E) staining, the tissues were examined under a microscope.

RESULTS

Amount of dissected tissues in newborn mouse pups

Digit tip dissections were carried out using a scalpel under a microscope on the third and fourth tips of the right paw. The left paw digit tips were not dissected and used as uncut controls. Mice were x-rayed before and after digit tip dissection. The amounts of tissue dissected were calculated by subtracting the after-dissection values from the before-dissection values of the top of the second phalanx to the digit tip edge (Figure 1). The mean amount of tissue dissected in MRL mice was slightly greater (0.14 ± 0.03 mm) than the DBA and B6 mouse strains (0.12 ± 0.02 and 0.11 ± 0.02 mm), though not significantly.

Regrowth results

The strains tested vary in size among each other; thus, it would be expected that normal growth differences among the strains would be found. In order to insure that regrowth results were not influenced by differences in strain

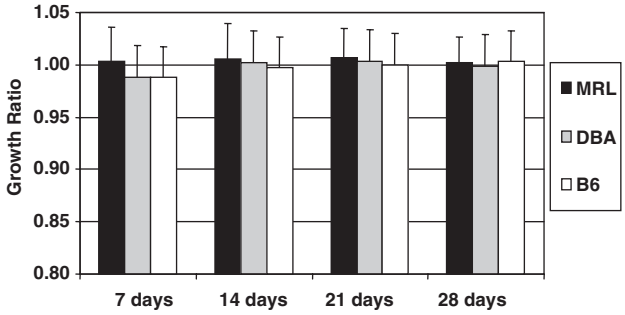

Figure 2. Normalization for strain size. Division of first phalanx right measurements by left measurements gives expected ratios of ~1.00 (mean ± SE). No statistically significant differences between strains are seen in normalized data for the first phalanx growth ratios.

size, the data were normalized by dividing right cut growth measurements by left uncut growth measurements. We tested the validity of this normalization by dividing the right first phalanx measurements by the left first phalanx measurements (Figure 2). These growth ratios do not show significant differences among the mouse strains and give growth ratios of approximately 1.00. As the first phalanges were not dissected, normalizing for strain size by calculating a strain-specific growth ratio is a valid method of correcting for strain growth. This normalization method was utilized for subsequent analysis of regrowth data. Measurement error estimates of 10 x-ray images found that repositioning the mouse between successive measurements give a mean third phalanx length of 1.38 ± 0.10 mm in 3-week-old mice. Ten successive measurements made without mouse repositioning give a mean third phalanx length of 1.34 ± 0.05 mm. As the growth ratio measurements were captured at the same time and did not require repositioning the mice, these measurements should also have less measurement errors than growth rate measurements captured from successive weeks.

Next, we examined the normalized regrowth ratios for dissected digit tips in the mice. As expected, the regrowth ratios are less than 1.0, indicating that growth of dissected digit tips is less than undissected digit tips (Figure 3). However, the MRL mouse regenerates digit tips more quickly than the other mouse strains at days 7, 14, and 21 postdissection. Mice exhibit most of their growth in the first 21 days after birth and this is also when digit tip regrowth in MRL mice is healed more quickly in comparison with the other inbred strains of mice. The degree of regrowth by day 28 was determined by examining mice for the degree of nail regeneration (Table 1). In MRL mice, 90% of mice completely or partially regenerated the nail. In DBA mice and B6, 72.9 and 66.7%, respectively, partially or completely regenerate nails. This difference is significant by chi-squared analysis ($p \leq 0.01$).

Microarray expression results

Four hundred genes out of 15,000 on the microarrays were significantly differentially expressed ($p < 0.05$) in MRL, DBA, and B6 mice at day 4 in comparison with control tissue at day 0 (supplementary table). Of these, 207 genes

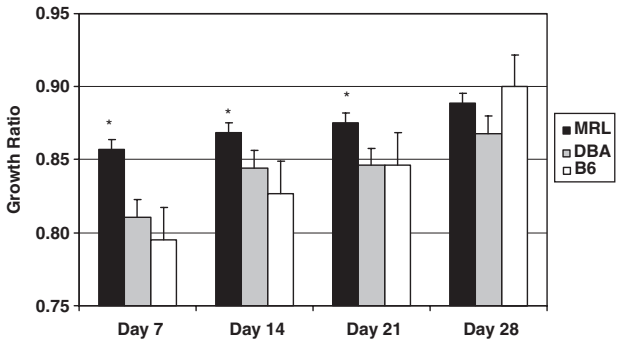

Figure 3. Normalized regrowth of MRL, DBA, and B6 digit tips. Growth ratios of digit tips for 7, 14, 21, and 28 days postdissection (mean ± SE) show that MRL mice regenerate digit tips greater than other strains of mice ($p < 0.05$, marked by * in plot). At day 14, MRL mice regrowth ratios were significant in comparison with B6 mice and approached significance in comparison with DBA mice ($p = 0.089$).

were up-regulated and 193 were down-regulated. About 50% of these genes represent expressed sequence tags (ESTs) and unknown genes. The biological process gene ontology functional classes that are significantly overrepresented in all the strains regenerating digit tips are shown in the supplementary data table. Pathway analysis of these known genes reveals that genes in the IGF and BMP/TGF pathway are differentially expressed in all mouse strains (IGF2, IGF2BP3, IGFBP4, BMP-1, TGFb1i4), thus implicating the IGF and BMP/TGF signaling pathways in regulation of digit tip regrowth. The BMP family of genes has previously been implicated in digit regeneration.[22] Also, several genes involved in cell cycle and growth were found to be differentially expressed in all the strains, including CALM2, NFKB, and Annexin A2. Transcription factors that were found to be differentially expressed in all strains include MYST3, ATRX, SOX13, TCFL4, ANKIB1, TSC22D4, 6030490I01RIK, ZFP110, GATA3, GTF2H3, PHF7, ICSBP1, TRPV2, KLF4, MLL3, ANKRD10, IKBKG, CNOT2, FOXM1, ASH2L, HNRPR, NFE2L1, and ZFP113.

Seventy-five genes and ESTs were significantly differentially expressed only in MRL mice in comparison with DBA and B6 mice (Table 2). Of genes with known function, LRP6, a WNT co-receptor that functions in limb morphogenesis and pattern formation, was found to be differentially expressed. Also FMN2, which functions in cytoskeletal organization and meiosis, is differentially expressed in MRL regenerating digit tips. Transcription factors that were found to be differentially expressed only in MRL regenerating digit tips include SS18L1, NFE2L1, ZFP251, RXRIP110, and TAF5l. Many of the differentially expressed genes are ESTs. This suggests that there are many currently unknown genes and genetic pathways involved in digit tip regrowth.

Confirmation of microarray results was done by real-time PCR of 17 genes (TWSG1, TSC22, TIMP3, TGFBLi4, SMAD4, NET1, MSX2, MMP9, MMP2, MAGED1, FMN2, BMP2, BMP1, B2 M, AK007718, AI987944, ACTR2). RT-PCR results for these genes were consistent with the microarray results and gave correlation coefficients of 0.62, 0.91, and 0.40 for MRL, DBA, and B6 expression results, respectively (Supplementary Figure).

Histology

We examined the histology of regenerating digit tips by sacrificing MRL mice at 1, 4, 7, 14, and 21 days postdigit tip dissection. The formation of an epidermal layer over the wound is seen at 1 day postdissection. At 4 days postdissection, evidence of dedifferentiation of cells and increased proliferation can be seen underneath the wound epithelium (Figure 4A and B). At 7 days postdissection, cartilage has begun to hypertrophy and osteoblasts and osteoclasts begin bone formation and remodeling; by 14 days postdissection, there are fewer undifferentiated cells present underneath the epithelium and the marrow cavity has begun forming (Figure 4B). By 21 days, bone growth continues, the digit tip has nearly completely regrown, and the nail has begun reforming.

DISCUSSION

The salient features of this study are as follows: (1) it provides direct evidence that newborn MRL mice heal digit tips more quickly and regenerate nails to a greater degree than DBA and B6 mice; (2) it provides evidence that the IGF and BMP/TGF pathways are important for digit tip regrowth in all inbred strains of mice tested; (3) it indicates that the improved regenerative capabilities of MRL mice may be due to the genes implicated in the WNT signaling pathway and morphogenesis.

MRL mice have a unique ability to heal and regenerate multiple cell types, including ear tissue and heart tissue. In this study, we find that all strains of mice tested have the capability of regenerating digit tips. However, MRL mice

Table 1. Nail regrowth in MRL, DBA, and B6 mouse strains by 28 days postdissection. Ninety percent of MRL mice regrow nails either partially or completely, in comparison with only about 70% in DBA and B6 mice ($p < 0.01$)

Strain	*N*	None (%)	Partial (%)	Complete (%)	Strain total (%)
MRL	40	10.0	72.5	17.5	100.0
DBA	48	27.1	52.1	20.8	100.0
B6	54	33.3	51.9	14.8	100.0

$\chi^2 = 18.20$.
$p \leq 0.01$.

Table 2. Genes significantly differentially expressed in MRL mouse regenerating digit tips but not in DBA and B6 mice. The LRP6 and FMN2 genes were found to be differentially expressed in MRL mice in comparison with DBA and B6 mice

Gene-Ontology (GO) ID	Gene ontology biological process	# of genes with GO ID differentially expressed in MRL	# of genes with GO ID in NIA15K set	*p*-Value	Accession number	Gene name
GO:0006515	Cell organization and biogenesis	1	4	0.001	AF218940	Fmn2
GO:0006220	Embryonic hindlimb morphogenesis	1	1	0.001	BC056479	Lrp6
GO:0007089	Embryonic forelimb morphogenesis	1	1	0.001	BC056479	Lrp6
GO:0042733	Embryonic digit morphogenesis	1	2	0.001	BC056479	Lrp6
GO:0016043	WNT receptor signaling pathway	1	31	0.028	BC056479	Lrp6
GO:0006826	Anterior/posterior pattern formation	1	15	0.007	BC056479	Lrp6
GO:0006897	Endocytosis	1	58	0.087	BC056479	Lrp6
GO:0016358	Gastrulation	1	11	0.004	BC056479	Lrp6
GO:0010003	Development	2	151	0.138	AF218940; BC056479	Fmn2; Lrp6
GO:0030032	Lamellipodium biogenesis	1	5	0.001	AK083469	Nckap1
GO:0009952	Dendrite morphogenesis	1	7	0.001	BC053087	Ss18l1
GO:0006824	Misfolded protein catabolism	1	2	0.001	AK004024	Clpp
GO:0030163	Protein catabolism	1	21	0.014	BC050902	Mdm2
GO:0015031	Actin filament organization	1	16	0.008	AK078918	Tmod3
GO:0051016	Barbed-end actin filament capping	1	7	0.001	AK078918	Tmod3
GO:0042981	Regulation of apoptosis	1	32	0.030	AK032060	Ank2
GO:0006915	Apoptosis	1	147	0.356	AK032060	Ank2
GO:0035116	Nucleotide biosynthesis	1	9	0.002	AK039066	Dctd
GO:0006260	DNA replication	1	70	0.119	AK051621	Orc4l
GO:0006810	Pyrimidine nucleotide metabolism	1	1	0.001	AK039066	Dctd
GO:0035115	Start control point of mitotic cell cycle	1	7	0.001	BC050902	Mdm2
GO:0007275	Cobalt ion transport	1	3	0.001	AK083478	Slc11a2
GO:0006355	Iron ion homeostasis	1	12	0.004	AK011244	Ftl1

GO:0016055	Iron ion transport	2	15	0.001	AK011244; AK083478	Ftl1; Slc11a2
GO:0006350	Transport	2	635	0.088	AK083478; AK018343	Slc11a2; Syt11
GO:0008283	Calcium ion homeostasis	1	13	0.005	BC008997	Anxa7
GO:0006874	Cell proliferation	1	53	0.075	BC008997	Anxa7
GO:0009165	Intracellular signaling cascade	1	164	0.408	AK049307	2900057D21Rik
GO:0007049	Cell cycle	1	223	0.432	AK049307	2900057D21Rik
GO:0016567	Protein transport	1	255	0.358	BC053504	Tloc1
GO:0006508	Proteolysis and peptidolysis	2	142	0.120	AK004024; AK011589	Clpp; Ctsl
GO:0007015	Protein ubiquitination	1	102	0.215	BC050902	Mdm2
GO:0006512	Ubiquitin cycle	1	237	0.398	BC050902	Mdm2
GO:0008152	Metabolism	1	161	0.399	AK075831	Dbt
GO:0006879	Transcription	3	535	0.328	AK080514; AK087271; AK033477	Zfp251; Rxrip110; Taf5l
GO:0007242	Regulation of transcription	6	709	0.436	BC053087; BC022152; AK080514; AK087271; AK033477	Ss18l1; Nfe2l1; Zfp251; Rxrip110; Taf5l
					AK049010; AK008869;	1700041C02Rik;
					AK075950; AK075950;	2210409E12Rik;
					AK041714; AK014286;	Spbc24; Dhrs4;
					AF104414; AK077025;	Sparc; AW208599;
					AK080723; AK089793;	Slc16a9;
					AK041555; AK034422;	9130404D08Rik;
					BC051459; AK084556;	LOC237749;
					AK122209; AK029139;	C330046E03;
					AK087947; AK086670;	Srrm2;
None	Unknown process	34			AK009347; AK077521;	D13Wsu64e; 2010000I03Rik;

Table 2. Continued.

Gene-Ontology (GO) ID	Gene ontology biological process	# of genes with GO ID differentially expressed in MRL	# of genes with GO ID in NIA15K set	*p*-Value	Accession number	Gene name
					AK077773; AK050612; AK026964; AK027483; AL832193; AK082477; AK036620; AJ272268; AK037650; AK025061; AK085135; AK082946; AK085877; AK044885; AK016563; BC001136	AK122209; Sec24a; 4930438O05Rik; 9430097H08Rik; 2310015A05Rik; 5730436H21Rik; LOC435957; BC057593

can more quickly heal and more completely reform nails of dissected digit tips. The regrowth of digit tips is more complex than simple wound healing of ear punches and cardiac lesions as it involves the regrowth of multiple cell types including bone, cartilage, nervous, and epithelial cells. Similar to stem cells, regenerating digit tips require proper patterning of the regenerating cells to direct their cellular fate. Studies undertaken in axolotls have documented the stages in amphibian limb regeneration.[3] In axolotls, the first stage after amputation involves the formation of wound epithelial cells to cover the wound (http://www.uoguelph.ca/zoology/devobio/210labs/regen1.html). After 2 days, beneath this epithelial layer, cells begin to dedifferentiate and form a blastema. These blastema cells redifferentiate and completely regenerate the amphibian limb within 6 weeks postamputation. In MRL mice, our histology studies find that the early stages of digit tip regrowth are partially similar to that of axolotls (Figure 4). Within 1 day of digit tip amputation epithelial cells have formed over the wound in MRL mice. At 4 days, epithelial cells have completely covered the wound and undifferentiated cells beneath the wound epithelium begin to proliferate. At 7 days osteoblasts are present and have begun to form bone. At 14 days postdissection the cells beneath the wound epithelium are not as dedifferentiated and the bone marrow cavity has begun forming above the third phalange's joint. By 21 days postdissection, the cells have redifferentiated, the nail has begun reforming, and the digit tip has almost completely regenerated. It is interesting that when de- and redifferentiation of cells beneath the wound epithelium is occurring is also when the MRL mouse shows the greatest regenerative capacity. This suggests possible links between the enhanced healing capabilities of MRL mice and the molecular causes of de- and redifferentiation of cells.

The NIA15K cDNA library used to create the microarrays in this study was isolated from developing mouse embryos. Thus, many of these genes are expressed primarily in embryonic development and are a unique source for studies of regrowth. In all the strains examined in this study we found that genes involved in the IGF and BMP/TGF pathways are differentially expressed. This is not unexpected as the IGF and BMP/TGF pathways are known to be critical to limb formation, bone induction, and fracture repair.[19–22] Also, previous studies have reported that high levels of TGFB1 mRNA and/or protein are localized in developing cartilage, bone, and skin, and play a role in the growth and differentiation of these tissues.[21] This study confirms the importance of the IGF1 and TGFB/BMP pathways in regrowth and wound healing and the importance of the BMP family of genes in regulating a regenerative response.[22] Genes involved in cell cycle, transcription, and growth were also found to be differentially expressed in all the strains (CALM2, NFKB, ANXA2, GATA3, RFPL4, KLF4, TCF14, and ZF110).

In only MRL regenerating digit tips, LRP6, SPARC, CTSL, and FMN2 are particularly interesting genes that are differentially expressed. LRP6 and its co-receptor LRP5 are required for WNT/β-catenin–mediated signal transduction.[23] LRP6 knockout mice exhibit severe developmental abnormalities, including the truncation of the axial skeleton, reduced bone mineral density, and limb defects.[24,25] The WNT signaling pathway plays important roles in bone cell function, and LRP6 and LRP5 are essential for proper gastrulation in developing embryos.[25,26] SPARC (osteonectin) is a bone-specific phosphoprotein that accounts for the unique properties of bone collagen to undergo calcification.[27] The absence of SPARC in mice gives rise to alterations in the composition of the extracellular matrix that result in osteopenia and pathological closure of dermal wounds.[28] SPARC regulates the activity of several growth factors including platelet-derived growth factor (PDGF), fibroblast growth factor (FGF), and vascular endothelial growth factor (VEGF). This suggests

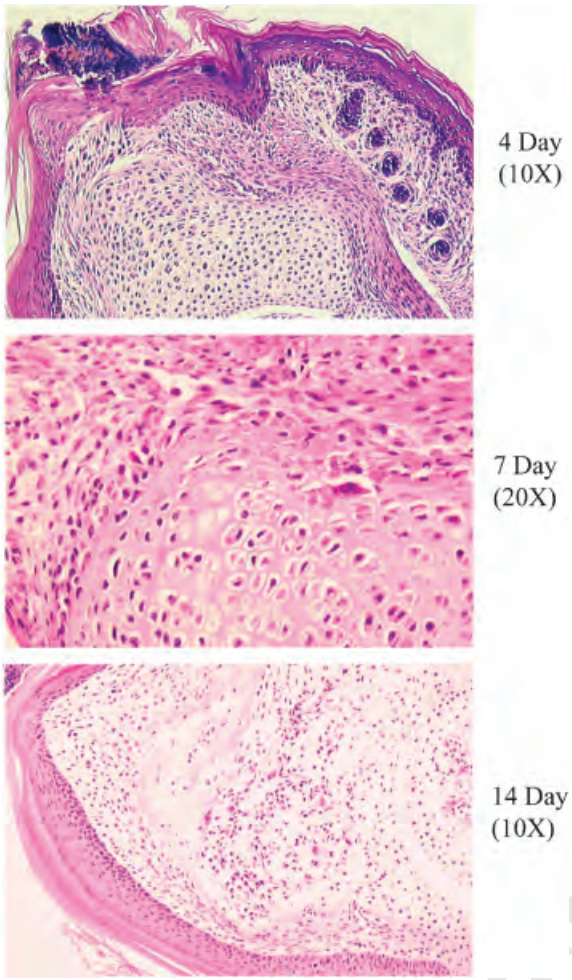

Figure 4. Regeneration histology. At 1 day postdissection a wound epithelial layer has begun to form. By 4 days postdissection the wound epithelial layer has completely covered the tip and beneath this dedifferentiated and proliferating cells are present. At 7 days postdissection bone has begun to form, and by day 14 the marrow cavity is forming above the third phalange's joint. By 21 days, the digit has nearly completed regenerating and the nail has begun reforming. In Figure 4A all images are at ×4, in Figure 4B images are ×10 or ×20.

links between increased expression levels of SPARC in MRL mice and growth factor regulation in regenerating digit tips. Cathepsins are cysteine proteases with essential roles in osteoclast-mediated bone matrix degradation. Cathepsin L acts by integrating endothelial progenitor cells into wounds and is required for neovascularization of ischemic tissue.[29] Also, CTSL knockout mice have impaired healing following limb ischemia.[29] Thus, the increased levels of CTSL in MRL regenerating digit tips may lead to increased regenerative capacity by increasing vascularization of wound tissue.

In only MRL regenerating digit tips, the FMN2 gene is another intriguing gene that is differentially expressed. Mutations in a related formin gene, formin-1, lead to developmental defects in limb formation due to a reduction in the number of bony elements in the fore and hind limbs.[30,31] Formin-1 is thought to act in limb bud polarization through establishment of a SHH/FGF-4 feedback loop.[30] Also, studies in a yeast homologue of formin, forp1, have found that its mutation leads to asymmetric patterns of cell growth.[32] This suggests that formins are critical signaling components of pattern formation and directing cellular fate. Our previous microarray studies of mouse ear punch wound healing found that formin-binding protein 21 is differentially expressed in healing ear tissue.[33] Thus, the formin family of genes is involved in both soft tissue wound healing and digit tip regrowth. This indicates that there are common genetic mechanisms influencing soft tissue wound healing and digit tip regrowth in the MRL super-healer mouse. Members of the formin gene family have been implicated in the WNT signaling pathway.[34] The WNT signaling pathway initiates outgrowth, controls patterning, and regulates cell differentiation in a number of tissues.[35] Also, bone formation has been shown to be activated by WNT signaling in osteoblast stem cells by promoting osteoblastic differentiation.[36] FMN2 has been reported to be highly expressed in both developing and adult central nervous systems.[37] This is intriguing as denervation has been shown to eliminate regeneration capabilities in amphibians.[38] Recently, we have undertaken studies of knockout FMN2 mice and preliminary data find that FMN2 (−/−) mice have significantly reduced femur cortical thickness (unpublished results).

In conclusion, we find that MRL mice show greater regenerative capacities to heal digit tips in comparison with all inbred strains of mice tested. This increased regrowth is seen primarily during the times of greatest growth in mice and during the times of dedifferentiation and redifferentiation of cells in the healing and regrowth process. The determination of the molecular causes of de- and redifferentiation of cells during growth and healing has important implications in stem cell research. The capability of neonatal mammals to regenerate is reduced when they reach adulthood.[39] It is thought that this reduced regenerative capacity is due to a reduction in multipotent cells with age.[39] Future studies will focus on determining whether MRL mice retain more of their regenerative capacity than other strains of mice. The further elucidation of the mechanisms by which genes contribute to regrowth and bone formation will likely lead to new targets and eventually treatments for wound healing, regeneration, and bone diseases.

ACKNOWLEDGMENT

This work was supported by US Army Grant DAMD17-02-1-0685.

REFERENCES

1. Muller TL, Ngo-Muller V, Reginelli A, Taylor G, Anderson R, Muneoka K. Regeneration in higher vertebrates: limb buds and digit tips. *Semin Cell Dev Biol* 1999; 10: 405–13.
2. Brockes JP. Amphibian limb regeneration: rebuilding a complex structure. *Science* 1997; 276: 81–7.

3. Endo T, Bryant SV, Gardiner DM. A stepwise model system for limb regeneration. *Dev Biol* 2004; 270: 135–45.
4. Illingworth CM. Trapped fingers and amputated finger tips in children. *J Pediatr Surg* 1974; 9: 853–8.
5. Borgens RB. Mice regrow the tips of their foretoes. *Science* 1982; 217: 747–50.
6. Neufeld DA, Zhao W. Phalangeal regrowth in rodents: postamputational bone regrowth depends upon the level of amputation. *Prog Clin Biol Res* 1993; 383A: 243–52.
7. Zhao W, Neufeld DA. Bone regrowth in young mice stimulated by nail organ. *J Exp Zool* 1995; 271: 155–9.
8. Reginelli AD, Wang YQ, Sassoon D, Muneoka K. Digit tip regeneration correlates with regions of Msx1 (Hox 7) expression in fetal and newborn mice. *Development* 1995; 121: 1065–76.
9. Goss RJ, Grimes LN. Epidermal downgrowths in regenerating rabbit ear holes. *J Morphol* 1975; 146: 533–42.
10. Joseph J, Dyson M. Effect of anabolic androgens on tissue replacement in the ear of the rabbit. *Nature* 1966; 211: 193–4.
11. Li X, Gu W, Masinde G, Hamilton-Ulland M, Xu S, Mohan S, Baylink DJ. Genetic control of the rate of wound healing in mice. *Heredity* 2001; 86 (Part 6): 668–74.
12. Clark LD, Clark RK, Heber-Katz E. A new murine model for mammalian wound repair and regeneration. *Clin Immunol Immunopathol* 1998; 88: 35–45.
13. Leferovich JM, Bedelbaeva K, Samulewicz S, Zhang XM, Zwas D, Lankford EB, Heber-Katz E. Heart regeneration in adult MRL mice. *Proc Natl Acad Sci USA* 2001; 98: 9830–5.
14. Tanaka TS, Jaradat SA, Lim MK, Kargul GJ, Wang X, Grahovac MJ, Pantano S, Sano Y, Piao Y, Nagaraja R, Doi H, Wood WH III, Becker KG, Ko MS. Genome-wide expression profiling of mid-gestation placenta and embryo using a 15,000 mouse developmental cDNA microarray. *Proc Natl Acad Sci USA* 2000; 97: 9127–32.
15. Shih JH, Michalowska AM, Dobbin K, Ye Y, Qiu TH, Green JE. Effects of pooling mRNA in microarray class comparisons. *Bioinformatics* 2004; 20: 3318–25.
16. Draghici S, Khatri P, Bhavsar P, Shah A, Krawetz S, Tainsky MA. Onto-Tools, The toolkit of the modern biologist: Onto-Express, Onto-Compare, Onto-Design and Onto-Translate. *Nucleic Acids Res* 2003; 31: 3775–81.
17. Draghici S, Khatri P, Shah A, Tainsky MA. Assessing the functional bias of commercial microarrays using the Onto-Compare database. *BioTech Microarrays Cancer Res Appl* 2003.
18. Draghici S, Khatri P, Martins RP, Ostermeier GC, Krawetz SA. Global functional profiling of gene expression. *Genomics* 2003; 81: 98–104.
19. Zuniga A, Haramis AP, McMahon AP, Zeller R. Signal relay by BMP antagonism controls the SHH/FGF4 feedback loop in vertebrate limb buds. *Nature* 1999; 401: 598–602.
20. Cho TJ, Gerstenfeld LC, Einhorn TA. Differential temporal expression of members of the transforming growth factor beta superfamily during murine fracture healing. *J Bone Miner Res* 2002; 17: 513–20.
21. Dickinson ME, Kobrin MS, Silan CM, Kingsley DM, Justice MJ, Miller DA, Ceci JD, Lock LF, Lee A, Buchberg AM, Siracusa LD, Lyons KM, Derync R, Hogan BLM, Copeland NG, Jenkins NA. Chromosomal localization of seven members of the murine TGF-beta superfamily suggests close linkage to several morphogenetic mutant loci. *Genomics* 1990; 6: 505–20.
22. Han M, Yang X, Farrington JE, Muneoka K. Digit regeneration is regulated by Msx1 and BMP4 in fetal mice. *Development* 2003; 130: 5123–32.
23. Tamai K, Semenov M, Kato Y, Spokony R, Liu C, Katsuyama Y, Hess F, Saint-Jeannet JP, He X. LDL-receptor-related proteins in Wnt signal transduction. *Nature* 2000; 407: 530–5.
24. Pinson KI, Brennan J, Monkley S, Avery BJ, Skarnes WC. An LDL-receptor-related protein mediates Wnt signalling in mice. *Nature* 2000; 407: 535–8.
25. Holmen SL, Giambernardi TA, Zylstra CR, Buckner-Berghuis BD, Resau JH, Hess JF, Glatt V, Bouxsein ML, Ai M, Warman ML, Williams BO. Decreased BMD and limb deformities in mice carrying mutations in both Lrp5 and Lrp6. *J Bone Miner Res* 2004; 19: 2033–40.
26. Kelly OG, Pinson KI, Skarnes WC. The Wnt co-receptors Lrp5 and Lrp6 are essential for gastrulation in mice. *Development* 2004; 131: 2803–15.
27. Termine JD, Kleinman HK, Whitson SW, Conn KM, McGarvey ML, Martin GR. Osteonectin, a bone-specific protein linking mineral to collagen. *Cell* 2001; 26: 99–105.
28. Puolakkainen PA, Bradshaw AD, Brekken RA, Reed MJ, Kyriakides T, Funk SE, Gooden MD, Vernon RB, Wight TN, Bornstein P, Sage EH. SPARC-thrombospondin-2-double-null mice exhibit enhanced cutaneous wound healing and increased fibrovascular invasion of subcutaneous polyvinyl alcohol sponges. *J Histochem Cytochem* 2005; 53: 571 –81.
29. Urbich C, Heeschen C, Aicher A, Sasaki K, Bruhl T, Farhadi MR, Vajkoczy P, Hofmann WK, Peters C, Pennacchio LA, Abolmaali ND, Chavakis E, Reinheckel T, Zeiher AM, Dimmeler S. Cathepsin L is required for endothelial progenitor cell-induced neovascularization. *Nat Med* 2005; 11: 206–13.
30. Zeller R, Haramis AG, Zuniga A, McGuigan C, Dono R, Davidson G, Chabanis S, Gibson T. Formin defines a large family of morphoregulatory genes and functions in establishment of the polarising region. *Cell Tissue Res* 1999; 296: 85–93.
31. Leader B, Lim H, Carabatsos MJ, Harrington A, Ecsedy J, Pellman D, Maas R, Leder P. Formin-2, polyploidy, hypofertility and positioning of the meiotic spindle in mouse oocytes. *Nat Cell Biol* 2002; 4: 921–8.
32. Sawin KE. Cell polarity: following formin function. *Curr Biol* 2002; 12: 6–8.
33. Li X, Mohan S, Gu W, Baylink DJ. Analysis of gene expression in the wound repair/regeneration process. *Mamm Genome* 2001; 12: 52–9.
34. Habas R, Kato Y, He X. WNT/Frizzled activation of Rho regulates vertebrate gastrulation and requires a novel Formin homology protein Daam1. *Cell* 2000; 107: 843–54.
35. Church VL, Francis-West P. WNT signalling during limb development. *Int J Dev Biol* 2002; 46: 927–36.
36. Bain G, Muller T, Wang X, Papkoff J. Activated beta-catenin induces osteoblast differentiation of C3H10T1/2 cells and participates in BMP2 mediated signal transduction. *Biochem Biophys Res Commun* 2003; 301: 84–91.
37. Leader B, Leder P. Formin-2, a novel formin homology protein of the cappuccino subfamily, is highly expressed in the developing and adult central nervous system. *Mech Dev* 2000; 93: 221–31.

38. Mullen LM, Bryant SV, Torok MA, Blumberg B, Gardiner DM. Nerve dependency of regeneration: the role of Distal-less and FGF signaling in amphibian limb regeneration. *Development* 1996; 122: 3487–97.
39. Bryant SV, Endo T, Gardiner DM. Vertebrate limb regeneration and the origin of limb stem cells. *Int J Dev Biol* 2002; 46: 887–96.

Q12

Supplementary material

The following supplementary material for this article is available online:

Table S1. Genes Differentially Expressed in MRL, DBA and B6 Mice at Day 4 Post Digit Tip Dissection. About 50% of these genes represent ESTs and unknown genes. Pathway analysis of the known genes reveals that genes in the IGF and BMP/TGF pathway are differentially expressed in all mouse strains (IGF2, IGF2BP3, IGFBP4, BMP-1, TGFb1i4). Also, genes involved in cell cycle regulation and growth (CALM2, NFKB) and transcription (GATA3, RFPL4, KLF4, TCF14, ZF110) are differentially expressed in all strains.

Figure S1. Confirmation of Microarray Expression Results by Real-time PCR. Confirmation of microarray results was done by real-time PCR of 17 genes (TWSG1, TSC22, TIMP3, TGFBLi4, SMAD4, NET1, MSX2, MMP9, MMP2, MAGED1, FMN2, BMP2, BMP1, B2M, AK007718, AI987944, ACTR2). RT-PCR results for these genes were consistent with the microarray results and gave correlation coefficients of 0.62, 0.91 and 0.40 for

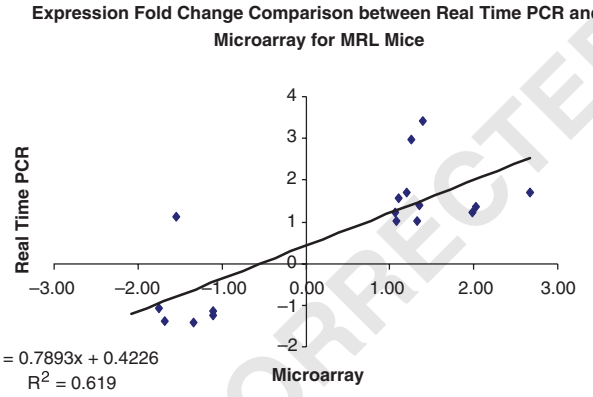

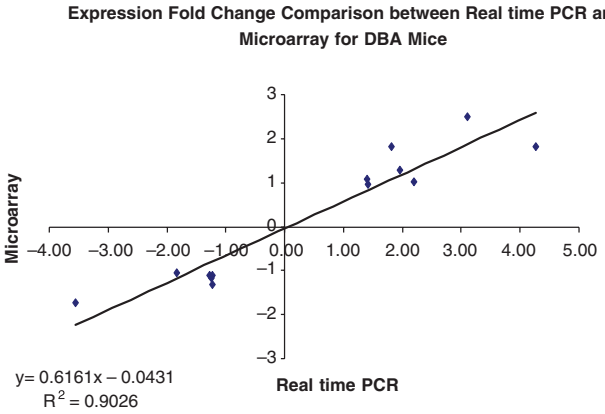

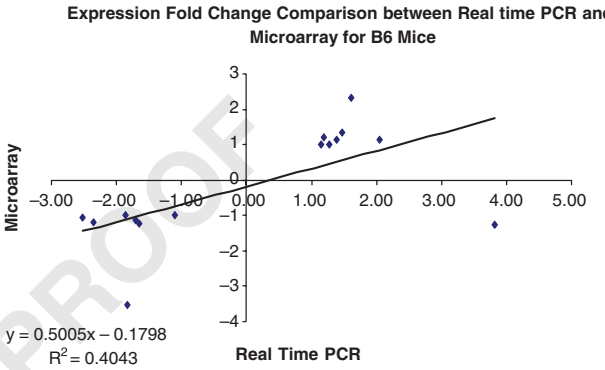

MRL, DBA and B6 expression results respectively.

This material is available as part of the online article from: http://www.blackwell-synergy.com/doi/abs/10.1111/j.1742-4658.2006.00500.x (This link will take you to the article abstract).

Please note: Blackwell Publishing is not responsible for the content or functionality of any supplementary materials supplied by the authors. Any queries (other than missing material) should be directed to the corresponding author for the article.

Author Query Form

Journal	**WRR**
Article	**216**

Dear Author,

During the copy-editing of your paper, the following queries arose. Please respond to these by marking up your proofs with the necessary changes/additions. Please write your answers clearly on the query sheet if there is insufficient space on the page proofs. If returning the proof by fax do not write too close to the paper's edge. Please remember that illegible mark-ups may delay publication.

Query No.	Description	Author Response
Q1	AQ: Please check if the suggested running title is OK.	
Q2	AQ: Please provide the degrees of all the authors in the author group.	
Q3	AQ: Please provide manufacturer information for Ambion: town, state (if USA) and country.	
Q4	AQ: Please provide manufacturer information for Faxitron: company name, town, state (if USA) and country.	
Q5	AQ: Please provide manufacturer information for Agilent Technologies: town, state (if USA) and country.	
Q6	AQ: Please provide manufacturer information for Kinemalica AG: town, state (if USA) and country.	
Q7	AQ: Please provide manufacturer information for Genetix: town, state (if USA) and country.	
Q8	AQ: Please provide manufacturer information for Silicon Genetics: town, state (if USA) and country.	
Q9	AQ: Please provide manufacturer information for Invitrogen: town, state (if USA) and country.	
Q10	AQ: Please provide manufacturer information for Applied Biosystems: town, state (if USA) and country.	
Q11	AQ: Please provide the volume and page numbers for reference [17].	
Q12	PE: Please check if the style followed for Supplementary Material is OK.	

Identification of Mutant with a Large Decrease in Bone Size Identified in a Sensitized ENU Screen using Growth Hormone Deficient 'Little' Mouse

A. K. Srivastava, D. J. Baylink, J. E. Wergedal and S. Mohan
JLP VA Center, Loma Linda, CA 92357 and Dept. Medicine, Loma Linda Univ., Loma Linda, CA 92354.

We have performed a phenotype driven N-ethyl-nitrosourea (ENU) screen in growth hormone (GH) deficient *little* mice (that has point mutation in growth hormone releasing hormone receptor, denoted as *lit* allele) to identify a mutant gene that synergistically interacts with the GH/IGF signaling pathway. In this study, we have characterized a bone size mutant (14104) that was identified as one of the several outliers by breeding ENU injected C57BL/6J male mice with *lit*/+ mice. The 14104 mutant exhibited a 40% decrease in bone cross sectional area (CSA) at the midshaft tibia determined by pQCT at 10 weeks of age. After confirmation of heritability, the 14104 mutant mouse was backcrossed to WT *lit*/+ to generate >75 progeny. As expected for autosomal dominant mutation, about 50% mice were affected. *In-vivo* measurements of tibia midshaft from affected 14104 (n=15-27), non-affected 14104 littermates (n=14-34), and WT *lit*/+ mice (n=5-30) by pQCT show 30-40% lower ($p<0.001$) CSA and 20-30% lower ($p<0.001$) periosteal circumference (PC) in mutant mice (Figure). Tibia and femur length were marginally (2-7%) lower (p=NS) in 14104 mice. Both males and females were affected and phenotypes were confirmed in excised tibia and femur by pQCT and histology. The body weight (BW) of the affected 14104 mice were 10-13% lower ($p<0.05$), but CSA was 20-30% lower even after adjustment for BW. Interestingly, the decrease in CSA was accompanied by a greater (40-50%, $p<0.001$) decrease in endosteal circumference (EC), resulting in a significant decrease in marrow area and, more importantly, a 10-20% increase ($p<0.01$) in volumetric BMD (vBMD). Preliminary histomorphometric studies in female mice revealed an increase in the endocortical bone formation in the mutant mice, leading to increased cortical thickness and vBMD. The changes in the endosteum may reflect a compensatory adaptive mechanism that is a consequence of decreased bone strength caused by a 25% reduction in body weight adjusted CSA in the mutant mice. In conclusion, we report a mutant that affects both embryonic and postnatal development of bone size by interacting with GH/IGF signalling pathway. Thus, the 14104 mice provide a valuable tool to identify a gene involved in periosteal expansion and to discover a molecule that interacts with GH/IGF pathway.

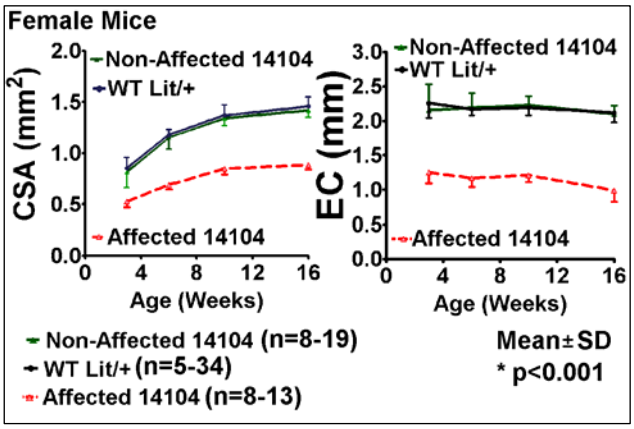

A Sensitized ENU Screening System to Discover Modifier Genes by Utilizing Mouse Models Deficient in Genes Regulating Skeletal Tissues

A. K. Srivastava, S. Mohan, and D. J. Baylink
JLP VA Medical Center, Loma Linda, CA 92357 and Dept. Med., Loma Linda University, Loma Linda, CA 92354.

Abstract

Previously, we demonstrated feasibility of the phenotype driven N-ethylnitrosourea (ENU) mutagenesis approach to isolate mutations affecting skeletal tissues for gene function studies. In this study, we describe a novel ENU screening approach named 'sensitized ENU screen,' which combines gene-based targeting with phenotype-driven ENU mutagenesis. The genes identified in the 'sensitized screen' are often modifier genes; their effects are subtle and hard to detect in commonly employed genetic screens. The presence of an initial mt to isolate in a wild type (WT) background. To accomplish the screen, we utilized two mutant mouse models. The first set of mice carry a mutation in growth hormone (GH) releasing hormone receptor (denoted '*lit*' allele) resulting in GH deficiency, low IGF-I expression, and reduced growth. The second set of mice lack *smad2*, signal transducer for TGF-beta, an important bone growth factor. The *smad2*-/- mice are lethal, but *smad2*-/+ mice exhibit normal growth. We bred lit/+ and *smad2*-/+ with ENU (100 mg/kg) injected males to produce F1 progeny for screening dominant modifiers. DNA from F1 mice was assayed by PCR to identify mice with the *lit*/+ and *smad2*-/+ genotypes. The F1 mice with *lit*/+ or *smad2*-/+ genotype were screened for growth and skeletal phenotypes and an outlier was identified as >2 SD units different from WT control (n=20-30). We screened 105 F1 mice with *lit*/+ and *smad2*-/+ genotypes and identified 9 outliers, out of which three appeared to be heritable (Table-1). Efforts to map these mutant genes are underway. The frequency of outliers for skeletal phenotypes (9%) in sensitized screen using the above two mouse models appears to be greater compared to that obtained in the traditional ENU screen in WT mice (1-5%). In conclusion, our study demonstrates feasibility of a sensitized system of screening mutants with skeletal phenotypes. The discovery of mutants in a selected pathway will provide a valuable tool to not only to discover novel genes involved in a particular process but will also prove useful for the elucidation of the biology of that process.

Table-1. Phenotype of mutants recovered in the sensitized ENU screen.

ID	Genotype	Major Phenotype	Z-Score for Main Phenotype	% Difference from Control Mice
14104	lit/+	Decreased Bone Cross Section Area (and increased volumetric bone density)	-4 to -6	20-30%
1665C	Smad2-/+	Increased Total Body Bone Density (excluding skull area)	+2 to +3	13-14%
1665D	Smad2-/+	Increased Total Body Bone Density (excluding skull area)	+2 to +3	11-13%

Introduction

Our goal in this study is to use a novel approach, namely sensitizer screen, to increase the power of ENU mutagenesis screens [1]. To achieve this, we used mouse strains in which genes that have been previously implicated to play a critical role in the development and maintenance of musculoskeletal tissues have been mutated or knocked-out (KO). By combining the ENU mutagenesis and the KO strains, we propose to sensitize a classical ENU mutagenesis screening system, and thereby increase the recovery of mutants by discovering genes that have subtle effects on musculoskeletal phenotype. The principle for increased sensitivity of recognition is synergism between the unknown ENU mutation and the known knock out gene. Presence of initial (or targeted) mutation renders the screening system highly sensitive to small changes that would be too small to be detected in an otherwise wild-type background. A similar approach has been used in Drosophila to identify novel mutant phenotypes [2, 3]. For example, mutations in a Notch (a receptor for cell-cell interaction mechanism in many metazoan developing tissues) signaling pathway have been used to sensitize mutations in genes regulating many unknown components in bristle development in Drosophila. More recently, the sensitized screen approach have been applied to mouse models with successful identification of mutants in diabetes screen [4].

One of the key requirements for the success of our approach relates to which knockout mouse models are selected for ENU mutagenesis screens. We designed our sensitized screen by utilizing mouse models with deficiency in two signaling pathways, the GH-IGF-I [5] and TGF-β [6] pathways, both of which are critical for the normal development and maintenance of musculoskeletal tissues. Furthermore, both these pathways involve several critical regulatory molecules that regulate growth and development of musculoskeletal tissues and that deficiencies in these two growth factors contribute to impaired growth and maintenance. To study genes involved in the GH-IGF-I pathway, we used a '*little'* mouse strain that has a naturally occurring mutation in growth hormone releasing hormone receptor (GHRHR). The second mutant strain involves mice lacking Smad2, a key intracellular signaling molecule for TGF beta signaling pathway. In this study, we describe mutagenesis screen design and our findings from the sensitized screen.

Methods and Results

Sensitized Screen Design Involving Growth Hormone Pathway

The GHRHR mutant (*little*) mouse is a spontaneous dwarf mouse strain (in 100% C57BL/6J background) with an autosomal recessive GH deficiency (GHD) caused by a missense mutation (D60→G) in the extracellular domain of the GHRH-R that impairs the ability of the receptor to bind to GHRH. Mice that are homozygous for missense mutation (*lit/lit*) has reduced GH secretion, impaired GH-IGF-I axis, and a severe deficiency in bone mass and size. Despite a non-functional GHRHR, the GH receptor works normally in the '*little*' mouse, hence externally administered GH can compensate for the GH deficiency created by impaired GHRHR mutation. To screen for the musculoskeletal mutants, we bred the *lit*/+ mice with ENU injected males and screened *lit*/+ progeny for musculoskeletal defects in haplosufficient (*lit*/+) GHRHR conditions (**Figure-1**). The rationale for screening the mutant in GH haploinsufficiency is based on the observation that mice carrying one copy of '*lit*' mutation have significantly reduced IGF-I levels as compared to the WT levels of IGF-I in B6 mice. This phenomenon is also evident in IGF-I knockout mice where reduced expression of IGF-I in IGF-$I^{+/-}$ mice has a significant effect on prenatal and postnatal bone growth as compared to WT or IGF-$I^{+/-}$ mice. Thus, we anticipated that a reduced dosage of GH would be sufficient to sensitize the screening systems as compared to complete abrogation of GH levels, which causes significantly reduced fertility in *lit*/*lit* males, and therefore will not be feasible for a screening procedure.

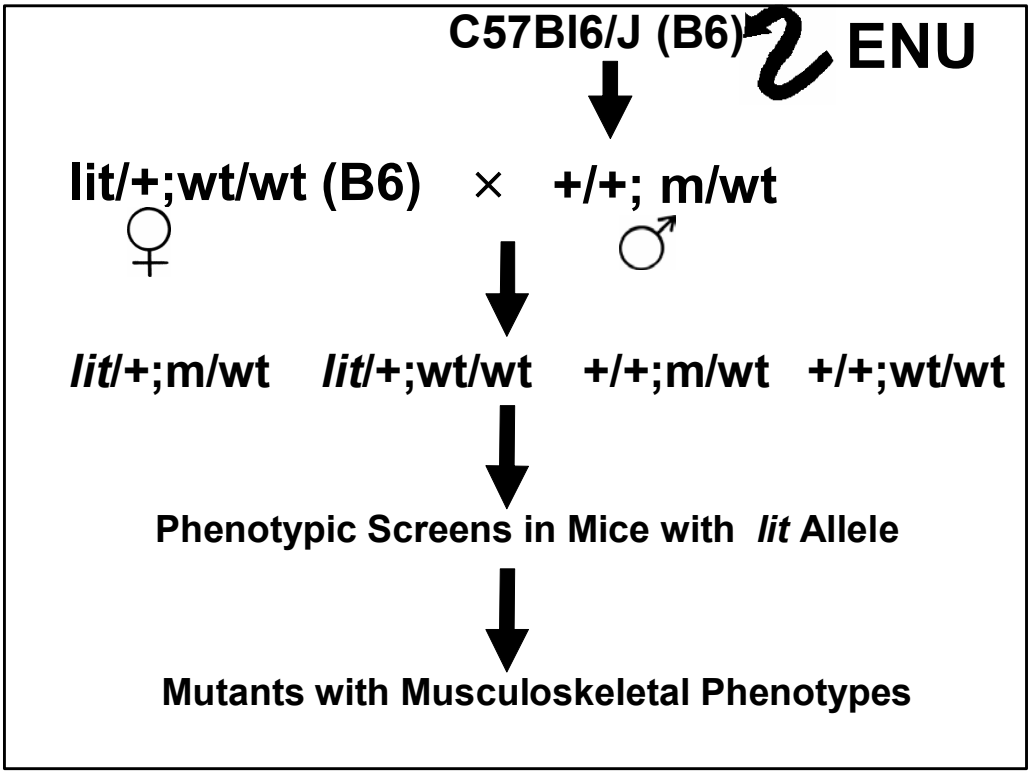

Figure-1. The sensitized screen design to identify mutations affecting growth hormone pathway. The 'lit' allele denotes GHRHR mutant allele and is identified by genotyping the F1 progeny by a RT-PCR based SNP assay. All progeny with lit/+ genotype were candidate for sensitized mutations. For clarity, the wild type alleles are denoted as two separate symbols '+' and 'wt' for 'lit' locus and ENU mutant 'm' locus, respectively.

Sensitized Screen Design Involving TGF-β Pathway

We have chosen Smad2 knockout mice as our second mouse model in the sensitizer screen (**Figure-2**) because of the established role of TGF beta in the regulation of bone formation. It is now fairly well established that TGF beta, like IGF-I, plays a critical role in both bone development and the pathogenesis of bone loss. The biological effects of TGF beta in osteoblasts are known to be mediated by phosphorylation of Smad2/3, which associates with smad4 to cause transcriptional activation of genes in osteoblasts and other cell types. Furthermore, Smad2 has also been shown to be involved in mediating the effects of activins, which are also known to regulate osteoblasts. Thus, inactivation of Smad2 will disrupt the actions of various forms of TGF beta and also activins. Consistent with an important role for Smad2 in mediating the effects of TGF beta family members, recent studies have shown that haploinsufficiency of Smad2 altered TGF-mediated tooth development.

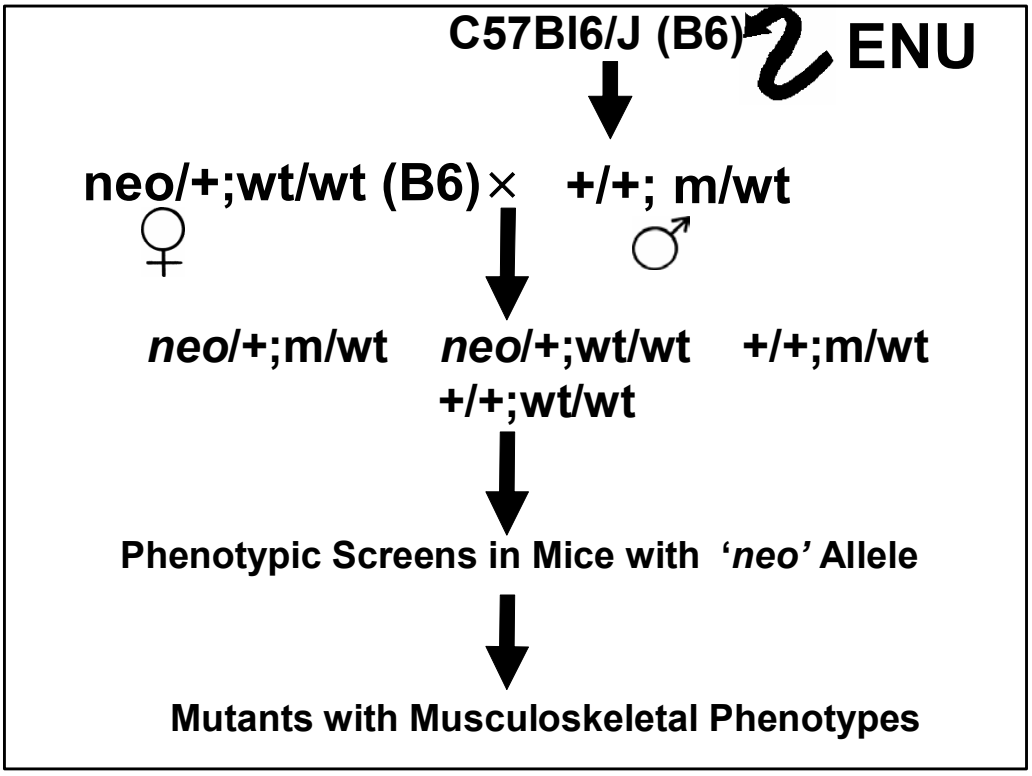

Figure-2. The sensitized ENU screen to identify mutants involved in TGF-β pathway. The 'neo' allele denotes that smad2 gene is absence and is replaced by a neomycin resistant gene cassette. We have designed primers that are specific for the neomycin resistant gene cassette and genotyped all progeny to demonstrate an absence of single copy of smad2. All phenodeviants that have neo/+ background are candidates for sensitized mutations. For clarity, the wild type alleles are denoted as two separate symbols '+' and 'wt' for 'neo' locus and ENU mutant 'm' locus, respectively.

Generation of Mutant Progeny and Screening

The GHRHR mutant '*little*' mouse (*lit*/*lit*) were obtained from The Jackson Laboratory, Maine, and bred in our facility to produce '*lit*/+' heterozygous females. The smad2 knock out mice were obtained from our collaborator, Dr. Michael Weinstein [PNAS, 95, 1998]. Male C57BL/6J (B6) mice were injected with 3×100 mg/kg dose of ENU and subsequently bred with '*lit*/+' heterozygous females. The F1 offspring were screened at 10-weeks through a series of tests, including bone density measurements using PIXImus (Lunar Corporation, Madison, WI) and pQCT (xCT Research M, Norland Medical System, Fort Atkinson, WI), to identify phenodeviants as those with a phenotype difference of >2-3SD units from that of control mice (n=30-40) (Srivastava et al, Bone 2003). Geometrical parameters such as periosteal perimeter, endosteal circumference, and bone area were measured by *in-vivo* pQCT as described previously [7]. Bone size parameters were normalized with body weight. If a phenodeviant was identified in the 10-week screening, measurements were repeated to confirm the phenotype when mice are 16-weeks old. Once a phenotype was confirmed in the 16-week repeat testing, it was bred with '*lit*/+' or 'neo/+' heterozygous male/female mice to determine whether their abnormality is inheritable. All progeny were genotyped for presence of lit or neo mutation by PCR based assays.

Number of Mice Generated and Screened

Table – 1. Number of mice generated, mice screened for various phenotypes, and number of mice introduced to inheritance testing.

Procedure	Number of lit/+ Mice	Number of Smad2/+ Mice
Sensitized ENU Mice Screened for Dominant Mode of Inheritance (F1)	44[a]	61[b]
Abnormal Phenotypes Identified	6	4
Phenotypes Introduced to Progeny Testing	6	3
Mutants Confirmed In Progeny Testing	1	2

[a]The total number of mice produced in the screen was 88 including mice with +/+ genotype. In addition, several mice died before screen.

[b]The total number of mice produced in the screen was 140 including mice with +/+ genotype.

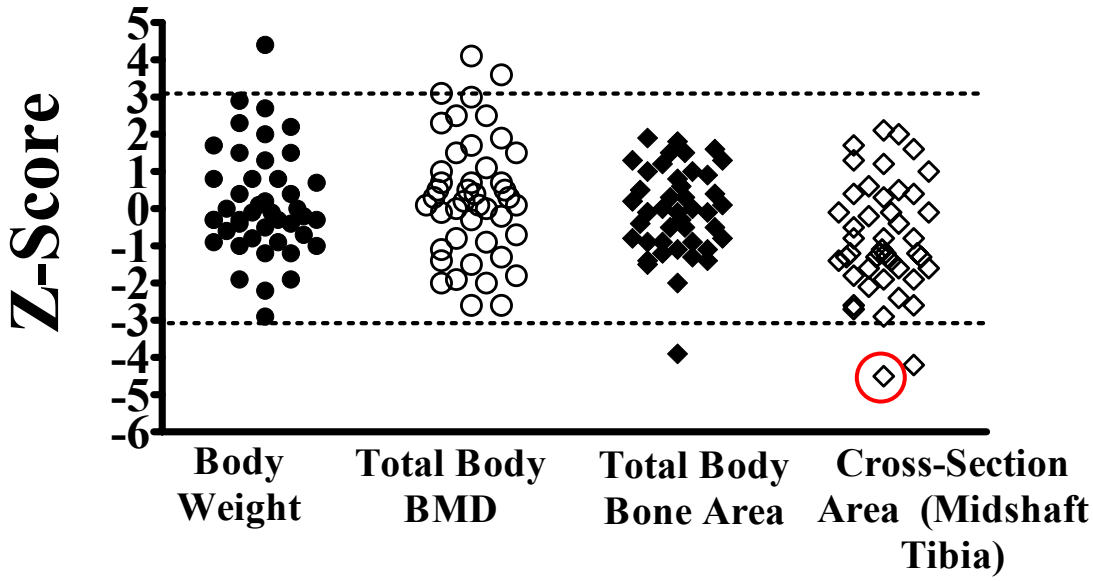

Figure-3. Representative phenotype data for the sensitized screen in *lit*/+ background. The phenotype data is presented as Z-score, which is mutant values expressed as SD unit difference from mean values of wild type control mice. All mice shown in the figure expressed the *lit*/+ genotype. The breeding and generation of these mice is described in Figure-1. The phenodeviant (ID14104) shown in circle showed decreased bone size and was successfully bred for more than three generation to confirm inheritability. The phenotype of the mutant is described in detail in Poster #SU124.

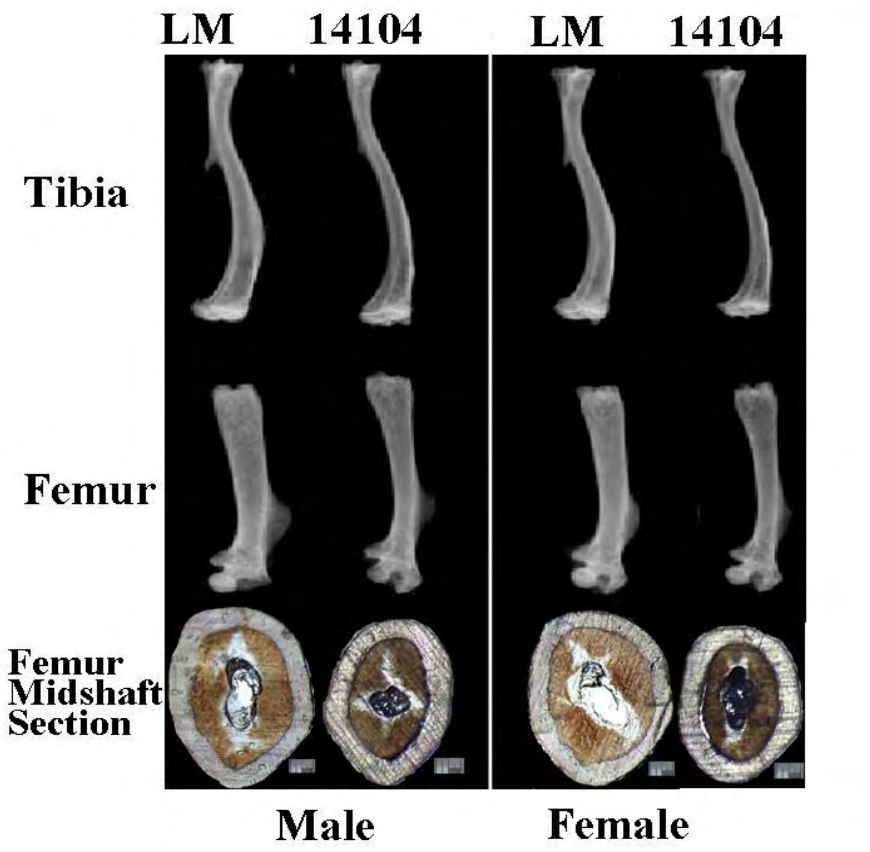

Figure-4. Bone size phenotype of the mutant identified in sensitized screen involving growth hormone deficient lit/- mice. The X-ray images of tibia and femurs from the 12-week old 14104 mutant mice are shown along with their non-affected littermates (LM). The 14104 mice have significantly slender bones with 17-23% lower periosteal circumference and 30-40% lower cross-sectional area ($p<0.001$) as compared to the LM. In mutant mice, the average body weight and bone lengths were marginally lower by 10-12% (Figure-1) and 2-7% (p=NS), respectively. Cross section image of mid-shaft femur is taken from histological analysis.

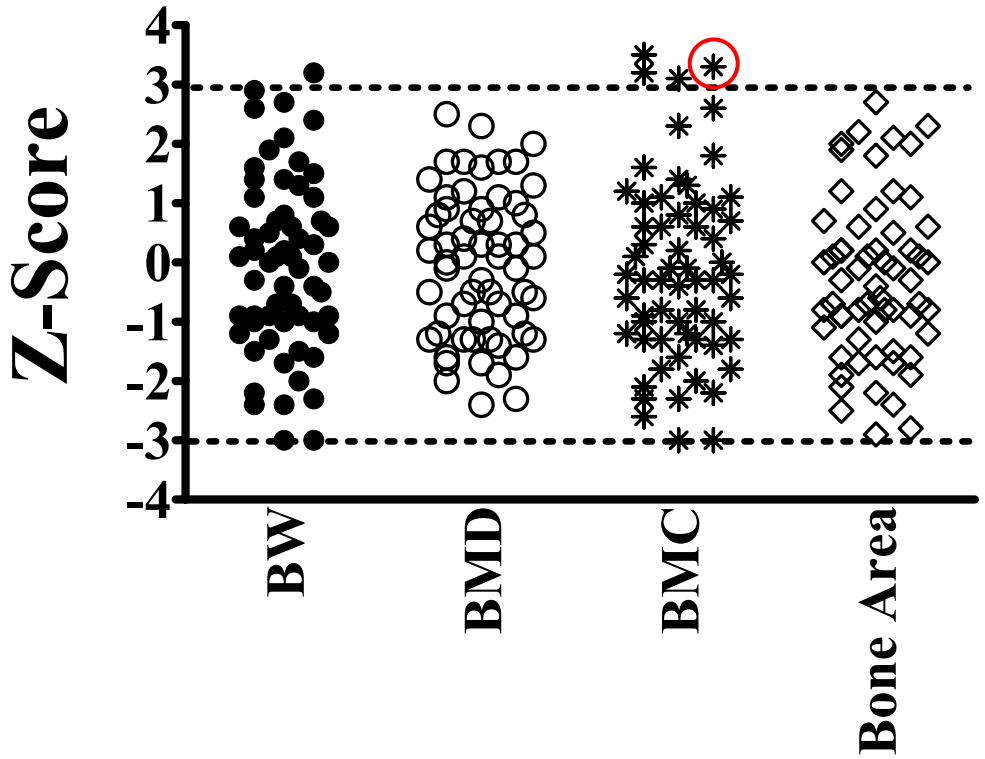

Figure-5. Sensitized ENU mutation screen in Smad2/+ background. Five main phenotypes (body weight, total body bone density, total body bone mineral content, total body bone area, and lean body weight) are shown as Z-Score, which indicates differences in a particular phenotype in terms of SD units from non-mutagenized control mice (in this case, Smad2/+ mice generated from breeding Smad2/+ mice with Smad2/+ or wild type B6 mice). The horizontal lines indicate our cut-off levels for identifying outlier mice. Data points outside 2-3 SD units potentially represent phenodeviants. Several phenodeviants (including one shown in circle) were further followed-up for confirmation of inheritable mutation. BW=Body weight, BMD=Total body bone mineral density, BMC=Total body bone mineral content.

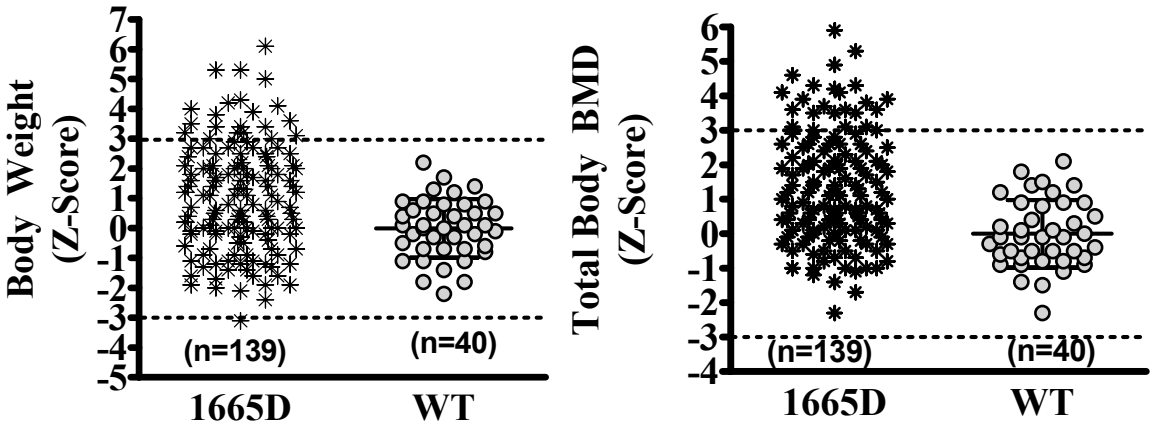

Figure-6. Phenotype data from one of the mutant identified in sensitized screen in Smad2/- background. The mutant mice show increased body weight and total body bone density, which are shown as Z-Score. The WT control mice are Smad2/+ mice generated from breeding Smad2/+ mice with wild type B6 mice. The broken horizontal lines indicate our cut-off levels for identifying outlier mice.

Summary

- We have combined the knockout technique and ENU mutagenesis approach to design a novel procedure of 'sensitized screen' that could uncover genes that have subtle effects on skeletal tissues.

- In the sensitized screen, an ENU-treated male mouse is mated with a female mouse that is deficient in a key signaling molecule critical to the normal development and maintenance of the skeletal phenotype, and the progeny is screened for the abnormal phenotypes. Presence of initial (or targeted) mutation renders the screening system sensitive to small changes that would be too small to be detected in an otherwise wild-type background.

- We used two mouse models for our sensitized screen. The first model involves mice carrying a mutation in growth hormone (GH) releasing hormone receptor (denoted '*lit*' allele) resulting in GH deficiency, low IGF-I expression, and reduced growth. The second mouse model lacked smad2, signal transducer for TGF-beta, an important bone growth factor. The smad2-/- mice are lethal, but smad2-/+ mice exhibit normal growth.

- We screened 105 F1 mice for dominant mutations and identified 9 phenodeviants. We confirmed inheritability of at least three mutants in multiple generation of breeding with WT lit/+ or smad2/- mice. These results indicate a higher recovery of mutation in sensitized screen as compared to classical ENU mutagenesis, which has recovery rate of <1%.

- The results demonstrate feasibility of sensitized screen approach for identifying mutants with skeletal phenotypes.

- The discovery of mutants in a selected pathway will provide a valuable tool to discover novel genes involved in selected pathways.

Conclusion

Our study demonstrates feasibility of a sensitized system of screening mutants with skeletal phenotypes. The discovery of mutants in a selected pathway will provide a valuable tool to not only to discover novel genes involved in a particular process but it will also prove useful for the elucidation of the biology of that process.

References

1. Srivastava AK, Mohan, S, Wergedal JE, Baylink DJ. A Genome-wide Screening of N-Ethyl-N-nitrosourea Mutagenized Mice for Musculoskeletal Phenotypes. Bone, 33, 179-191, 2003.
2. Go MJ and Tsakonas SA. A genetic screen for novel components of the Notch signaling pathway during Drosophila bristle development. Genetics 150:211-220, 1998.

3. Carrera P, Abrell S, Kerber B, Walldorf U, Preiss A, Hoch M, Jackle H. A modifier screen in the eye reveals control genes for Kuüppel activity in the Drosophila embryo. Proc. Natl. Acad. Sci. 95:10779-10784, 1998.
4. Satterthwaite AB, Willis F, Kanchanastit P, Fruman D, Cantley LC, Helgason, Humphries RK, Lowell CA, Simon M, Leitges M, Tarakhovsky A, Tedder TF, Lesche R, Wu H, and Witte ON. A sensitized genetic system for the analysis of murine B lymphocyte signal transduction pathways dependent on Bruton's tyrosine kinase. Proc. Natl. Acad. Sci. 97: 6687-6692, 2000
5. Donahue, L.R. and W.G. Beamer, Growth hormone deficiency in 'little' mice results in aberrant body composition, reduced insulin-like growth factor-I and insulin-like growth factor-binding protein-3 (IGFBP-3), but does not affect IGFBP-2, -1 or -4. J Endocrinol, 136(1): 91-104,1993.
6. Attisano, L. and J.L. Wrana, Signal transduction by the TGF-beta superfamily. Science, 296(5573): 1646-7, 2002.
7. Srivastava AK, Kapur S, Mohan S, Yu H, Kapur S, Wergedal JE and Baylink DJ. Identification of novel genetic loci for bone size and mechanosensitivity in an ENU mutant exhibiting decreased bone size. J Bone & Miner Research, 20 (6), 2005.

.

A Platform of High Efficiency of Non-Viral Gene Transfer in Mouse Osteoblast Cells in Vitro

Weirong Xing[1], David Baylink[1,2], Anil Kapoor[1] and Subburaman Mohan[1,2]

[1] Musculoskeletal Disease Center, JL Pettis Memorial Veterans Administration Medical Center, Loma Linda, CA 92357

[2] Department of Medicine, Loma Linda University, Loma Linda, CA 92357

Running Title: High efficiency of gene transfer in bone cells

Address Correspondence to: Dr. Subburaman Mohan

Musculoskeletal Disease Center

JL Pettis Memorial Veterans Medical Center

Loma Linda, CA 92357

Telephone: 909-825-7084 ext. 2932

Fax: 909-796-1680

E-mail: Subburaman.Mohan@med.va.gov

Abstract

We have previously established mouse genetic models and identified genetic components of quantitative trait loci (QTL) on mouse chromosomes that contribute to phenotypes such as bone size, bone density, and bone anabolic response to mechanical loading. However, these regions contain dozens of unknown genes that are needed for functional testing. In this study, we optimized a protocol of nucleoporation with high efficiency, by utilizing a commercial nucleofection buffer and Gene Pulser, to deliver a test gene into osteoblast cells for functional studies. We cloned an osteoblast differentiation-specific gene osterix (Osx) from a mouse bone cDNA library into a pHGCX expression vector and used nucleoporation to deliver pHGCX/Flag-Osx into the nuclei of MC3T3-E1 cells. We then examined the transfection efficiency, transgene expression, and function. Our results have demonstrated that nucleoporation can deliver a transgene into MC3T3-E1 osteoblast cells with approximately 94% transfection efficiency, and express functional Flag-Osx fusion protein capable of inducing cell differentiation as measured by an increase in alkaline phosphatase (ALP) activity. Therefore, this experimental system provides a rapid, safe, and efficient cell-based model of high-throughput phenotypic screening to identify candidate genes from physically mapped regions that are important for osteoblast differentiation.

Index Entries: Osteoblast, Non-viral, Osterix, Gene Transfer, Electroporation, Nucleofector

Abbreviations: ALP: alkaline phosphatase; BAC: Bacterial artificial chromosomes; CMV: cytomegalovirus; ENU: ethylnitrosourea; FACS: fluorescence-activated cell sorter; GFP: green fluorescent protein; HSV: herpes simplex virus-1; iBAC: infectious BAC; MCS: multiple cloning sites; Osx: osterix; PCR: polymerase chain reaction; QTL: quantitative trait loci.

Introduction

Osteoporosis is a common disease characterized by an age-dependent loss of bone mass and strength, and a microarchitectural deterioration of bone tissue with an increased risk of bone fractures (1). Although environment factors, nutrition, and hormones contribute to the development of osteoporosis, it is clear that genetic factors are the primary determinants for the disease (2-5). In order to localize chromosomal regions and subsequently identify genes responsible for various musculoskeletal phenotypes, we have carried out a genome-wide linkage analyses in several inbred strain F2 crosses and ethylnitrosourea (ENU)-induced mutant mouse strains and discovered quantitative trait loci (QTL) on mouse chromosomes that contribute to bone phenotypes such as size, density, and anabolic response to mechanical loading (6-8). However, these regions contain dozens of genes and are still difficult to clone by more time-consuming, expensive positional cloning strategies. An alternate approach for identifying disease-causing genes that is both feasible and efficient is to transfer the unknown genes from the QTL regions into bone cells in vitro for a high throughput functional screening.

The delivery of candidate genes into bone cells via conventional chemical transfection or electroporation, although possible, renders a poor efficiency of gene transfer and requires drug-selection and identification of stably-integrated transformants for functional testing (9, 10). We and others have previously established a viral gene transfer system of HSV-based amplicon to deliver a bacterial artificial chromosome (BAC) containing a genomic locus as large as 150-kb with a high transduction efficiency in most mammalian cells, including dividing and non-dividing cells for functional studies (10-13). The transgene remains as mini-chromosomes in host cells and expresses protein

of interest at high level in a position-independent manner (13, 14). In this study, we extended our findings and cloned cDNA of candidate genes into the pHGCX expression vector (15). We used this gene transfer strategy for the following reasons: 1) Some of our test genes may contain large introns (>100 kb), such that the size of intact gene including introns and exons could be beyond the limitation of the HSV packaging capacity (e.g. >150 kb); 2) The BAC clone containing the entire candidate gene may be not available in the mouse genome databases; and 3) The BAC clone may encode multiple alternatively spliced variants with diverse functions from a single gene. To overcome these limitations with the BAC clone approach, we utilized the strategy of using HSV amplicon-based plasmid containing cDNA of the test gene for non-viral transfection (10, 15-17). In this regard, we developed an optimal protocol of the "nucleoporation" technique by utilizing a commercial nucleofection buffer and Gene Pulser to make the gene transfer safer, more cost-effective, and feasible. We used the pHGCX expression vector carrying osterix (Osx) cDNA as a model system to test the transfection efficiency, transgene expression, and function. Our results indicated that the nucleoporation of plasmid DNA bearing a test gene could offer a rapid, simple alternative method of gene transfer for functional studies in bone cells.

Materials and Methods

Vector constructs: The DNA construct of pHGCX containing CMV promoter in front of multiple cloning sites (MCS) was kindly provided by Dr. Yoshinaga Saeki (the Ohio State University Medical Center, Columbus, OH). The original construct was modified by inserting a small CMV intron from pmaxGFP (Amaxa Inc., Gaithersburg, MD) into the corresponding sites of SnaB1 and NheI sites of pHGCX to generate a new expression vector driven by CMV promoter/intron (Figure 1). The complete coding sequence of osterix (Osx) was amplified from mouse bone cDNA library by polymerase chain reaction (PCR) using specific primers with an overhang of Flag sequence at the 5' end of the forward primer. The PCR product of Flag-Osx was cloned into pCR2.1 to generate pCR2.1/Flag-Osx using a TA cloning kit (Invitrogen, Carlsbad, CA). The Flag/Osx fusion gene was then released from pCR2.1/Flag-Osx, and subcloned into the BamH1 and XhoI sites of pHGCX to generate pHGCX/Flag-Osx (Figure 1). The sequences of the primers are provided below:

Forward: 5-gccaccatggactacaaagacgatgacgacaaggcgtcctctctgcttgagga-3'

Reverse: 5' ttatcagatctctagcaggttgc-3'

Nucleoporation: MC3T3-E1 cells (10^6) (ATCC, Manassas, VA) were resuspended in 100 μl of Cell Line Nucleofector buffer T (Amaxa Inc.) containing 10 μg of plasmid DNA. The cells were then transferred into a 2-mm gap width electroporation cuvette, and electroporated at 160 V for 15 milliseconds using a Gene Pulser (Bio-Rad, Hercules, CA). After electroporation, the cells were transferred into 3 ml of prewarmed Minimum Essential Medium alpha supplemented with 10 % fetal bovine serum, 2 mM L-glutamine,

100 units/ml penicillin, and 100 μg/ml streptomycin (Invitrogen) in 60-mm plates, and cultured in a humidified 37 ^{0}C incubator with 5% $CO_{2.}$

Western blot and FACS analyses: MC3T3-E1 cells were lysed in a lysis buffer containing 50 mM Tris-HCl (pH8.0), 150 mM NaCl, 0.1% SDS, 1% Triton X-100, 1 x Phosphatase Inhibitor, and 1 x Protease Inhibitor cocktail (Sigma, ST. Louis, MO) 24 hours after transfection. An aliquot of 10-20 μg cellular protein was separated on a 10% SDS-polyacrylamide gel and transferred to nitrocellulose. The membrane was incubated at 4 ^{0}C overnight in a buffer containing 5% dry skim milk, 150 mM NaCl, 50 mM Tris-HCl (pH 8.0), and 0.05% Tween-20. Immunoblotting was performed in the same buffer containing 0.2 μg/ml antibody against Flag (Sigma) or GFP (Santa Cruz, CA) at room temperature for 1 hour. Specific proteins were detected using appropriate secondary antibodies and Enhanced Chemiluminescence's Plus Western blotting detection system (Amersham Pharmacia Biotech UK Limited, Buckinghamshire, England). The cells in a parallel plate were trypsinized 24 hours post transfection and analyzed by fluorescence-activated cell sorter (FACS) (BD Biosciences, San Lose, CA) to assess the transfection efficiency.

Cytochemical staining for alkaline phosphatase: The cytochemical staining for alkaline phosphatase (ALP) was performed according to the protocol described previously (18). Three days after transfection, MC3T3-E1 cells were washed with PBS, and fixed in 0.05% glutaraldehyde at room temperature for 5 minutes. The cells were then incubated at 37 ^{o}C for 30 minutes in a staining buffer containing 50 mM Tris-HCl pH 8.6),100 mM NaCl, 5 mM KCl, 1 mM CaCl2, 1 mM MgCl2, 0.8 mg/ml naphthol AS-

TR phosphate and 0.6 mg/ml fast red violet LB diazonium (Sigma) in dark, followed by two times of washing with PBS and observation without counterstain.

Results and Discussion

In the present study, we cloned cDNA of candidate genes into pHGCX expression vector (15) and established a non-viral gene transfer system for the constructs less than 12 kb in length. We chose the pHGCX as an expression system because it contains a HSV amplicon, which can be used for both viral and a non-viral gene transfer, and a GFP reporter to monitor the efficiency of gene transfer. To improve the expression level, we engineered a CMV small intron at the 5' untranslated region of the Flag-Osx fusion gene. Therefore, the transgene was driven by a CMV promoter/intron (Fig 1). We then utilized a commercial nucleofection buffer and Gene Pulser to deliver the plasmid DNA directly into the nuclei of MC3T3-E1 cells. Twenty-four hours after electroporation, the GFP reporter gene was expressed in most of MC3T3-E1 cells transfected with either pHGCX (Fig 2A) or pHGCX/Flag-Osx (Fig 2B). Flow cytometry analyses revealed more than 94% of the osteoblast cells transfected with the pHGCX or the pGHCX/Flag-Osx plasmid expressed GFP (Fig 2C & D). We have repeated the experiments and found that the efficiency of nucleoporation is reliable. The variation in transfection efficiency was less than 1%, and viability of electroporated cells were more than 90% (data not shown). In comparison with our previous data, the efficiency of gene transfer by nucleoporation was approximately 10% higher than that of a viral deliver system mediated by a HSV-amplicon in mouse preosteoblast cells (10).

The transgene expression of GFP and Flag-Osx was easily detected in the cells transfected with pHGCX/Flag-Osx by utilizing Western blot with specific antibodies against Flag and GFP (Fig 2E). The pHGCX/Flag-Osx transfected cells expressed high level of Flag-Osx fusion protein. As expected, the Flag-Osx fusion protein was

undetectable while the expression of GFP was present in the cells transfected with pHGCX (Fig 2E). To assess osteoblast differentiation in the cells expressing the Osx transgene, we carried out an ALP staining 3 days after transfection (Fig 3). Approximately 20% of the osteoblast cells overexpressing Osx were differentiated and exhibited positive ALP-staining (Fig 3A). In contrast, less than 1% ALP-positive cells were seen in the control cellsoverexpressing GFP only (Fig 3B) .

In this study, we have demonstrated that non-viral gene transfer of nucleoporation can efficiently deliver plasmid DNA directly into the nuclei of preosteoblast cells. The transgene is consistently active and visible for more than 5 days (data not shown), although the intensity of GFP reporter becomes weaker with the culture time. A high level of transgene expression of GFP and Osx in the transfected cells was visual as early as 4 hours after electroporation, and mediated cell differentiation, validating the application of nucleoporation technology for functional studies of candidate genes.

In vivo testing of candidate genes in a transgenic mouse is time-consuming and expensive, requiring the injection of a DNA fragment into fertilized eggs and the examination of mouse phenotypes. Therefore, it would be more efficient to use *in vitro* cell models via viral or non-viral gene transfer approaches to test candidate gene function before initiating *in vivo* transgenic studies. Although infectious viral transduction medicated by HSV amplicon provides an alternative approach, the intensive work of purifying viral particles and potential contamination of viral particles limits its wide use. The studies provided in this manuscript demonstrate that cloning cDNA of an unknown gene into the pHGCX expression vector can be accomplished within a week. By utilizing this approach, a candidate gene search in a QTL region is cheaper, safer, and faster once

an appropriate cell model and end points for candidate gene function are determined. Our data also indicates that it is feasible to use the Gene Pulser for nucleofection once the conditions of voltage and time are optimized. In addition, nucleoporation overcomes the limitation of infectious BAC (iBAC) technology to allow testing of the genes that iBAC cannot apply. In this regard, our data demonstrate that nucleoporation in MC3T3-E1 cells can be used as another gene transfer system for high throughput screening to identify genes important for osteoblast cell differentiation.

Acknowledgments

This work was supported by Assistance Award No. DAMD17-03-2-0021. The U.S. Army Medical Research Acquisition Activity, 820 Chandler Street, Fort Detrick MD 21702-5014, is the awarding and administering acquisition office. The information contained in this publication does not necessarily reflect the position or the policy of the Government, and no official endorsement should be inferred. All work was performed in facilities provided by the Department of Veterans Affairs.

We are grateful to Dr. Yoshinaga Saeki (the Ohio State University Medical Center, Columbus, OH) for providing pHGCX plasmid, and Mr. Sean Belcher for his editorial help.

References

1. Glaser, D. L., and Kaplan, F. S. (1997) Osteoporosis. Definition and clinical presentation. *Spine* 22, 12S-16S
2. Slemenda, C. W., Christian, J. C., Reed, T., Reister, T. K., Williams, C. J., and Johnston, C. C., Jr. (1992) Long-term bone loss in men: effects of genetic and environmental factors. *Ann Intern Med* 117, 286-291
3. Slemenda, C. W., Christian, J. C., Williams, C. J., Norton, J. A., and Johnston, C. C., Jr. (1991) Genetic determinants of bone mass in adult women: a reevaluation of the twin model and the potential importance of gene interaction on heritability estimates. *J Bone Miner Res* 6, 561-567
4. Nicolas, V., Mohan, S., Honda, Y., Prewett, A., Finkelman, R. D., Baylink, D. J., and Farley, J. R. (1995) An age-related decrease in the concentration of insulin-like growth factor binding protein-5 in human cortical bone. *Calcif Tissue Int* 57, 206-212
5. Kesavan, C., Mohan, S., Oberholtzer, S., Wergedal, J. E., and Baylink, D. J. (2005) Mechanical loading induced gene expression and BMD changes are different in two inbred mouse strains. *J Appl Physiol*
6. Masinde, G. L., Wergedal, J., Davidson, H., Mohan, S., Li, R., Li, X., and Baylink, D. J. (2003) Quantitative trait loci for periosteal circumference (PC): identification of single loci and epistatic effects in F2 MRL/SJL mice. *Bone* 32, 554-560
7. Srivastava, A. K., Kapur, S., Mohan, S., Yu, H., Wergedal, J., and Baylink, D. J. (2005) Identification of novel genetic loci for bone size and mechanosensitivity in an ENU mutant exhibiting decreased bone size. *J Bone Miner Res* 20, 1041-1050
8. Kesava, C. M., S.; Yu,H.; Oberholtzer, S.; Wergedal, J.E.;Baylink, D.J.; Mohan, S. (2005) Nove mechanoresponsive BMD and bone size QTL identified in a genome wide linkage study involving C57BL/6J-C3H/HeJ intercross. *J Bone Miner Res* 20, S75
9. Kofron, M. D., and Laurencin, C. T. (2005) Orthopaedic applications of gene therapy. *Curr Gene Ther* 5, 37-61
10. Xing, W., Baylink, D., Kesavan, C., and Mohan, S. (2004) HSV-1 amplicon-mediated transfer of 128-kb BMP-2 genomic locus stimulates osteoblast differentiation in vitro. *Biochem Biophys Res Commun* 319, 781-786
11. Wade-Martins, R., Saeki, Y., and Antonio Chiocca, E. (2003) Infectious delivery of a 135-kb LDLR genomic locus leads to regulated complementation of low-density lipoprotein receptor deficiency in human cells. *Mol Ther*7, 604- 612
12. Wang, Y., Fraefel, C., Protasi, F., Moore, R. A., Fessenden, J. D., Pessah, I. N., DiFrancesco, A., Breakefield, X., and Allen, P. D. (2000) HSV-1 amplicon vectors are a highly efficient gene delivery system for skeletal muscle myoblasts and myotubes. *Am J Physiol Cell Physiol* 278, C619-626
13. Wade-Martins, R., Smith, E. R., Tyminski, E., Chiocca, E. A., and Saeki, Y. (2001) An infectious transfer and expression system for genomic DNA loci in human and mouse cells. *Nat Biotechnol* 19, 1067-1070

14. Saeki, Y., Breakefield, X. O., and Chiocca, E. A. (2003) Improved HSV-1 amplicon packaging system using ICP27-deleted, oversized HSV-1 BAC DNA. *Methods Mol Med* 76, 51-60
15. Cortes, M. L., Bakkenist, C. J., Di Maria, M. V., Kastan, M. B., and Breakefield, X. O. (2003) HSV-1 amplicon vector-mediated expression of ATM cDNA and correction of the ataxia-telangiectasia cellular phenotype. *Gene Ther* 10, 1321-1327
16. Lenz, P., Bacot, S. M., Frazier-Jessen, M. R., and Feldman, G. M. (2003) Nucleoporation of dendritic cells: efficient gene transfer by electroporation into human monocyte-derived dendritic cells. *FEBS Lett* 538, 149-154
17. Iversen, N., Birkenes, B., Torsdalen, K., and Djurovic, S. (2005) Electroporation by nucleofector is the best nonviral transfection technique in human endothelial and smooth muscle cells. *Genet Vaccines Ther* 3, 2
18. Wergedal, J. E., and Baylink, D. J. (1984) Characterization of cells isolated and cultured from human bone. *Proc Soc Exp Biol Med* 176, 60-69

Legends

Figure 1. A schematic diagram of pHGCX/Flag-Osx construction. The PCR product of mouse osterix (Osx) coding sequence tagged with Flag is inserted into BamH1 and XhoI sites downstream of the CMV promoter/intron of pHGCX plasmid to generate an expression vector of pHGCX/Flag-Osx.

Figure 2. Transgene expression in MC3T3-E1 cells transfected by nucleoporation. **A & B**: GPF expression in MC3T3-E1 cells transfected with pHGCX and pHGCX/Flag-Osx respectively; **C & D**: Representative data of flow cytometric analysis in the cells transfected with pHGCX and pHGCX/Flag-Osx respectively; **E**: Flag-Osx and GFP protein expression in MC3T3-E1 cells transfected with pHGCX and pHGCX/Flag-Osx respectively, detected by Western blot.

Figure 3. Alkaline phosphatase (ALP) staining of differentiated MC3T3-E1 cells (x 40 images). MC3T3-E1 cells are subjected for ALP staining 72 hours after transfection. **A**: the cells transfected with pHGCX control plasmid; **B**: the cells transfected with pHGCX/Flag-Osx. Arrows indicate the ALP-positive cells.

Figure 1

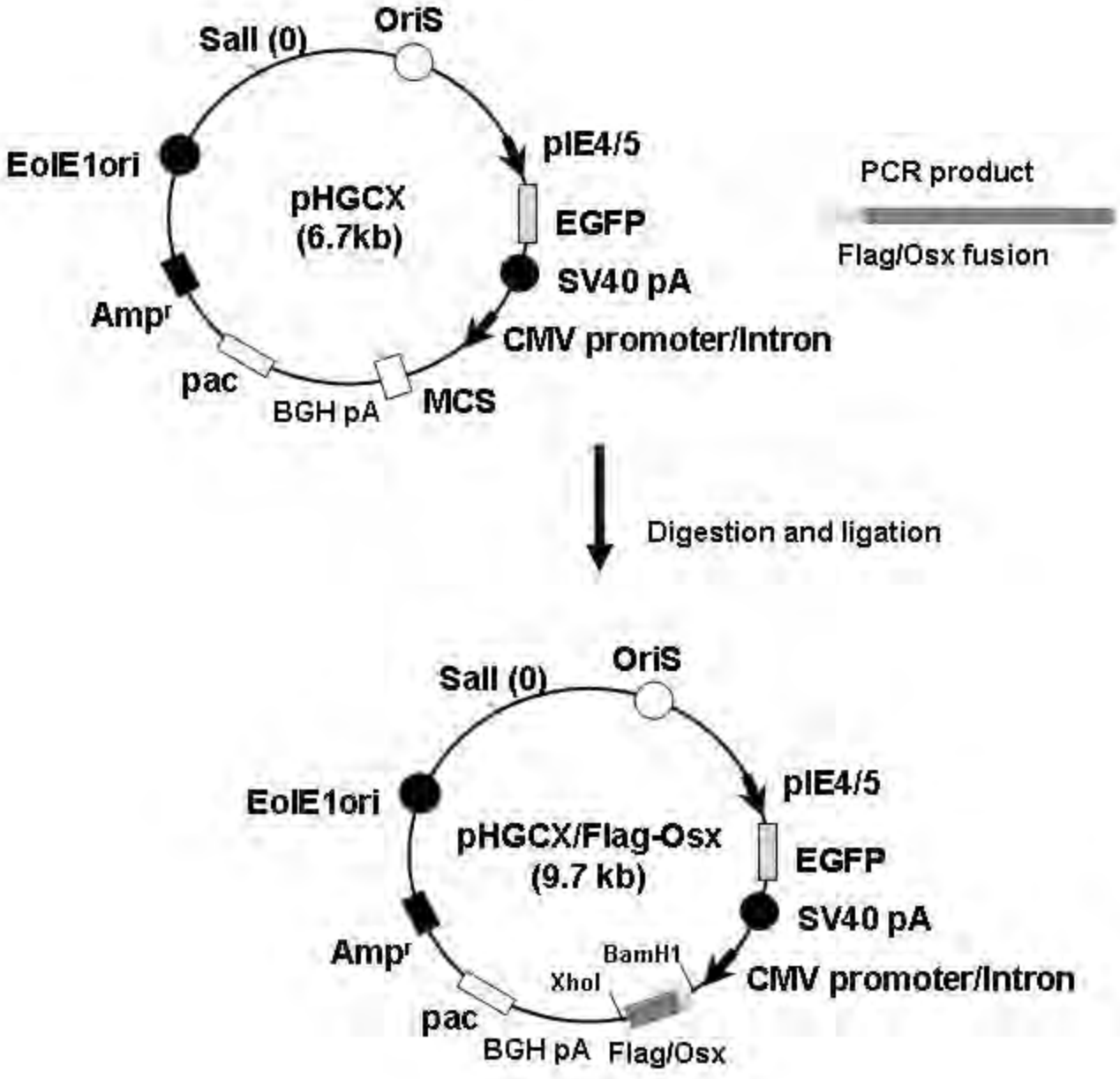
SalI (0)
OriS
pIE4/5
EcoIE1ori
pHGCX
(6.7kb)
EGFP
SV40 pA
Amp^r
CMV promoter/Intron
pac
BGH pA
MCS
PCR product
Flag/Osx fusion
Digestion and ligation
SalI (0)
OriS
pIE4/5
EcoIE1ori
pHGCX/Flag-Osx
(9.7 kb)
EGFP
SV40 pA
Amp^r
BamH1
XhoI
CMV promoter/Intron
pac
BGH pA
Flag/Osx

Figure 2

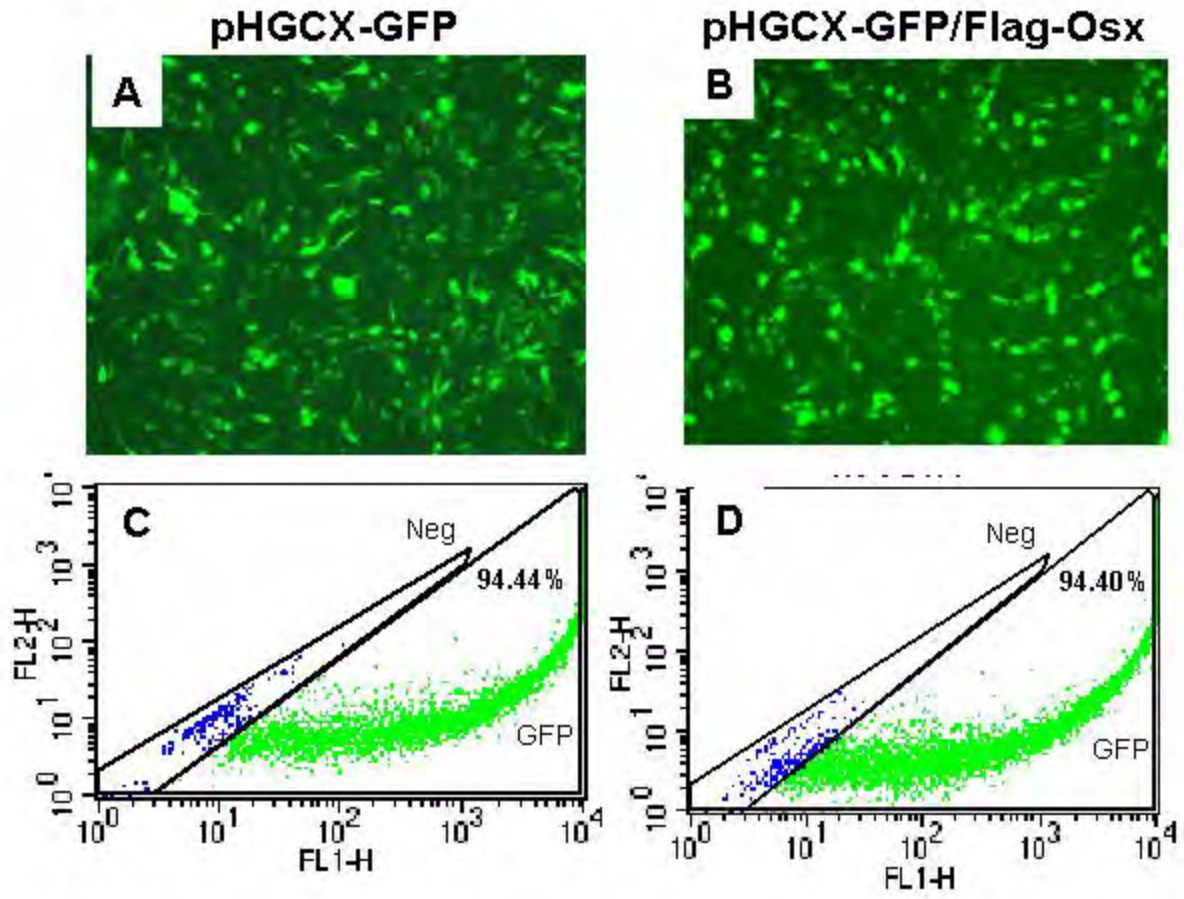
pHGCX-GFP
pHGCX-GFP/Flag-Osx
A
B
C
D
Neg
94.44%
GFP
94.40%
FL2-H
FL1-H

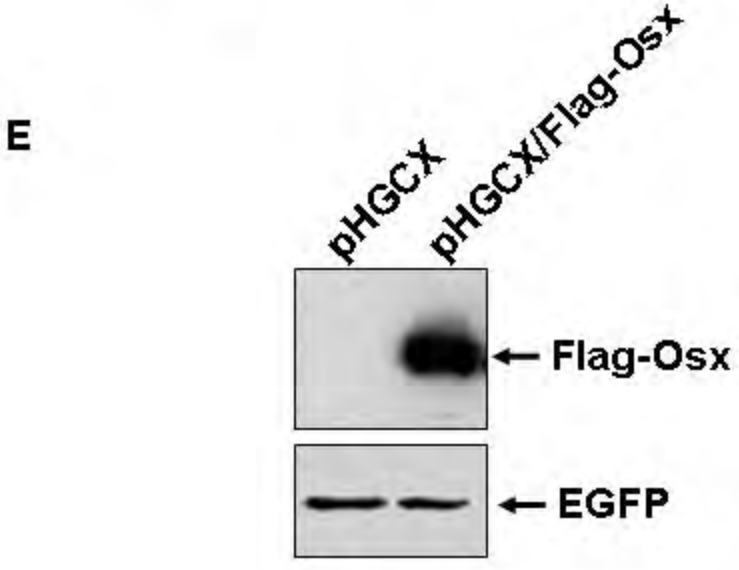
E
pHGCX
pHGCX/Flag-Osx
Flag-Osx
EGFP

Figure 3

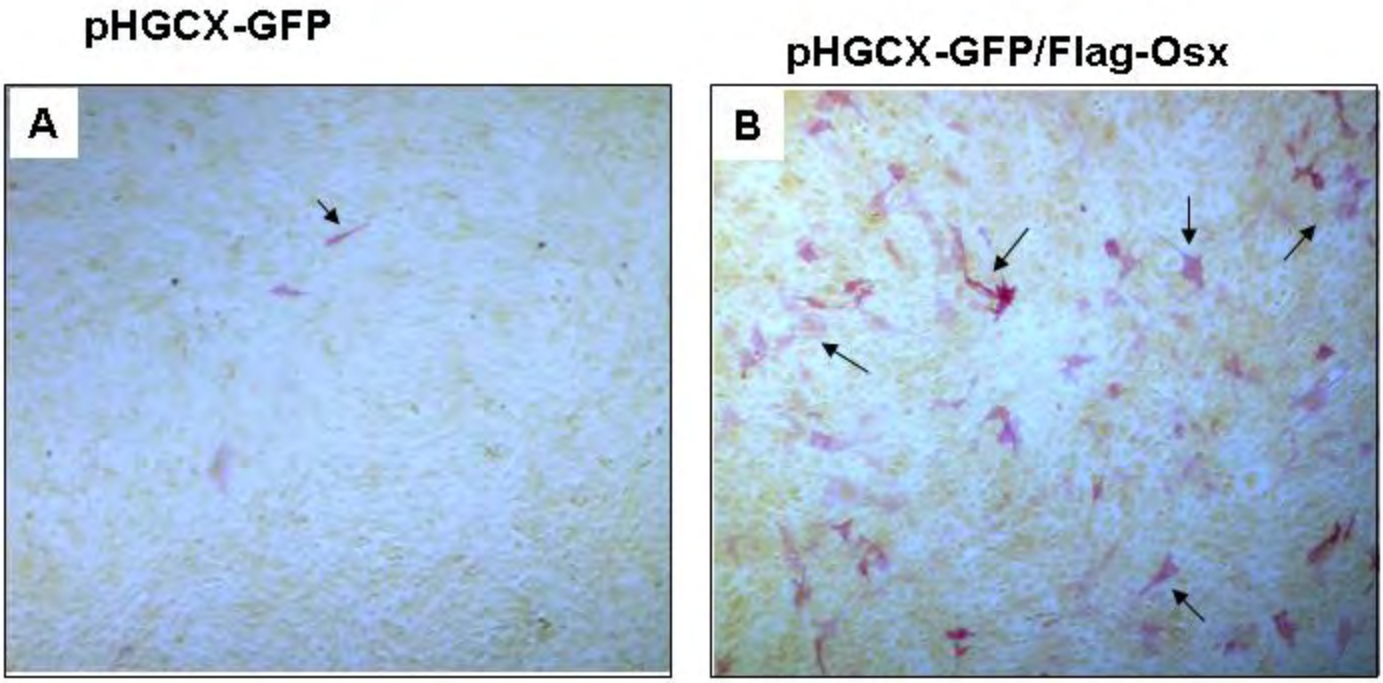

Available online at www.sciencedirect.com
SCIENCE DIRECT®
Biochemical and Biophysical Research Communications 319 (2004) 781–786
BBRC
www.elsevier.com/locate/ybbrc

HSV-1 amplicon-mediated transfer of 128-kb BMP-2 genomic locus stimulates osteoblast differentiation in vitro ☆

Weirong Xing, David Baylink, Chandrasekhar Kesavan, and Subburaman Mohan*

Musculoskeletal Disease Center, JL Pettis Memorial Veterans Administration Medical Center, Loma Linda, CA 92357, USA

Received 5 May 2004
Available online 28 May 2004

Abstract

In previous studies, we developed mouse genetic models and discovered genetic components of quantitative trait loci on mouse chromosomes that contribute to phenotypes such as bone size, bone density, and fracture healing. However, these regions contain dozens of genes in several overlapping bacterial artificial chromosomes (BACs) and are difficult to clone by physical cloning strategies. A feasible and efficient approach of identifying candidate genes is to transfer the genomic loci in BAC clones into mammalian cells for functional studies. In this study, we retrofitted a BAC construct into herpes simplex virus-1 amplicon and packaged it into an infectious BAC (iBAC) to test gene function in a cell-based system, using a 128-kb clone containing the complete bone morphogenetic protein-2 (BMP-2) gene. We transduced MC3T3-E1 cells with the iBAC bearing BMP-2 gene and examined transgene expression and function. Our results have demonstrated that an iBAC can efficiently deliver a BMP-2 genomic locus into preosteoblast cells and express functional BMP-2 protein, inducing a phenotype of cell differentiation, as indicated by an increase in alkaline phosphatase activity. Therefore, this experimental system provides a rapid, efficient cell-based model of high-throughput phenotypic screening to identify the BAC clones from physically mapped regions that are important for osteoblast differentiation. It also illustrates the potential of iBAC technology in functional testing of single nucleotide polymorphisms located in the distal promoter or/and intron regions responsible for low bone density.

Keywords: Osteoblast; HSV-1 amplicon; BMP-2; BAC; Gene transfer; Osteogenesis

Osteoporosis is a common disease characterized by an age-dependent decrease in bone mineral density (BMD) and a microarchitectural deterioration of bone tissue with a consequent increase in the risk of developing fragility fractures of the hip, spine, and other skeletal sites [1]. Although multiple environmental, nutritional, and hormonal factors influence the development of osteoporosis, it is clear that the major determinant for the disease is genetic control of BMD, particularly the achievement of peak bone mass at maturity, bone size and structure, and the subsequent rate of bone turnover [2–5]. Recently, genome-wide linkage analyses have revealed that the genetic components of quantitative trait locus (QTL) on human chromosomes 1q, 2p, 4p, 11q, and 13q are attributed to BMD [6–8], while the loci on chromosomes 17q and 19p are responsible for bone size [9]. However, none of the QTLs reported have actually met criteria for genome-wide significance for linkage, and the results are inconsistent due to the great variation between study groups and populations, as well as the possible involvement of different pathways. To localize chromosomal regions and subsequently identify the genes responsible for skeletal diseases, we have developed mouse genetic models and discovered QTLs on mouse chromosomes that contribute to phenotypes such as bone size, bone density, and fracture healing [10–12]. Subsequent analyses of the

☆ *Abbreviations:* BAC, bacterial artificial chromosomes; iBAC, infectious BAC; PAC, P1 artificial chromosomes; HSV-1, herpes simplex virus-1; ALP, alkaline phosphatase; BMP-2, bone morphogenetic protein-2; QTL, quantitative trait loci; MOI, multiplicity of infection; FACS, fluorescence-activated cell sorter; GFP, green fluorescent protein; EBV, Epstein–Barr virus; PCR, polymerase chain reaction.

* Corresponding author. Fax: 1-909-796-1680.
E-mail address: Subburaman.Mohan@med.va.gov (S. Mohan).

0006-291X/$ - see front matter © 2004 Elsevier Inc. All rights reserved.
doi:10.1016/j.bbrc.2004.05.053

congenic mice further confirmed and narrowed the genes of interest to a 3–12.5 centimorgan (cM) region in mouse chromosome 1 [13,14]. However, these regions contain dozens of genes and are still difficult to clone by time-consuming, expensive position-cloning strategies. However, a feasible and efficient approach for identifying candidate genes is to transfer the genomic loci of overlapping bacterial artificial chromosomes (BACs) or P1 artificial chromosomes (PACs) encompassing the QTL regions into bone cells in vitro for a high-throughput functional screening.

The delivery of large genomic DNA inserts of BACs or PACs into mammalian cells via chemical methods and non-viral vectors, although possible, renders a poor efficiency of gene transfer and requires the drug-selection and identification of stably integrated transformants for functional testing [15–17]. However, the recent advances in infectious BAC (iBAC) technology using the herpes simplex virus type 1 (HSV-1) amplicon in the gene therapy field have made it possible to deliver a genomic locus as large as 150-kb with a high transduction efficiency in most mammalian cells, including dividing and non-dividing cells in vitro and in vivo [18–21]. The improved delivery system of the HSV-1 amplicon also contains an EBNA-1 episomal cassette from the Epstein–Barr virus, (EBV) allowing long-term retention and high level of position-independent expression of BAC transgenes as mini-chromosomes in the host cells [20,21]. Therefore, the iBAC offers a rapid and simple method of BAC DNA transfer for functional genomic studies. This system also allows us to test the functional significance of the large number of gene-associated single nucleotide polymorphisms (SNP) located in the regions of the distal promoter or/and introns that could contribute to low bone density [22,23]. In this study, we chose a BAC clone bearing the bone morphogenetic protein-2 (BMP-2) locus and assembled the genomic DNA as an infectious virion as a model to test the genomic DNA transfer and function. Our results indicated that the iBAC could efficiently deliver a BMP-2 genomic locus and express functional protein promoting osteoblast differentiation.

Materials and methods

Vector constructs. The DNA constructs of pCTP-T, pEBHICP27, pEHHG, and fHSVΔ-pac, Δ-27, 0+ were described in detail elsewhere [20,21], and kindly provided by Dr. Yoshinaga Saeki (Massachusetts General Hospital, Harvard Medical School, MA). A BAC clone, RP23-302H4, containing a complete BMP-2 locus was purchased from Invitrogen Life Technologies (Carlsbad, CA).

Cell culture. Vero 2-2 cells (kindly provided by Dr. Rozanne Sandri-Goldin, University of California, Irvine, CA) were routinely maintained in Dulbecco's modified minimal essential medium (Invitrogen) with 10% fetal bovine serum, 100 U/ml penicillin, 100 μg/ml streptomycin, and G486 (500 μg/ml). MC3T3-E1 cells (ATCC, Manassas, VA) were propagated in alpha minimum essential medium (Invitrogen) supplemented with 10% calf serum, 100 U/ml penicillin, and 100 μg/ml streptomycin. The cells were cultured in a humidified 37 °C incubator with 5% CO_2.

Retrofitting of BAC clone. The retrofitting of BAC clone into HSV-1/EBV amplicons was carried out by Cre-mediated recombination in bacterial cells as described previously [21]. Briefly, an aliquot of 35 μl electro-competent cells containing BAC/BMP-2 (RP23-302H4) was mixed with 10 ng each of pEHHG and pCTP-T plasmid DNA, and the mixture was transferred into 0.1-cm gap width electroporation cuvette (Bio-Rad, Hercules, CA). After 5 min incubation on ice, the cells were electroporated with 25 μF at 1800 V using a Gene Pulser (Bio-Rad), then transferred into a 15-ml conical tube containing 500 μl SOC with 20 μg chlortetracycline (Sigma, St. Louis, MO), and incubated at 30 °C with rigorous shaking for 1 h. An aliquot of 100 μl of the bacterial culture was transferred into a new 15-ml tube containing 20 μg/ml chlortetracycline, 100 μg/ml ampicillin, and 20 μg/ml chloramphenicol in 900 μl SOC, and incubated at 30 °C with shaking for another 3 h. Subsequently, 50–100 μl of the bacterial culture was plated on LB plates containing 100 μg/ml ampicillin and 20 μg/ml chloramphenicol, and incubated overnight at 43 °C. DNA of individual clones was purified and verified by polymerase chain reaction (PCR) using specific primers to BMP-2 (forward: 5′-CCTTCGGAAGACGTCCTCAG and reverse: 5′-TCACTCGATTTCCCTCCAGT) and GFP (forward: 5′-TGCCACCTACGGCAAGCTGA and reverse: 5′-CCATGTGATCG CGCTTCTCG) to confirm the correct retrofitted BAC clone.

Packaging HSV-1 amplicon into virion. HSV-1 amplicon was packaged into infectious virion as described previously [21]. Briefly, Vero 2-2 cells (10^6) were plated in a 60-mm dish. After 18 h, the cells were co-transfected with 2.0 μg pHSV-BAC/BMP-2 or pEHHG, 0.2 μg pEBHICP27, and 2 μg fHSVΔ-pac, Δ-27, 0+ using LipofectAMINE Plus (Invitrogen) for 4 h. The cells were scraped into the supernatant 60 h post-infection, frozen and thawed once, sonicated for 1 min, and centrifuged at 3500 r.p.m. for 15 min. The supernatant was then concentrated through a 25% sucrose by ultracentrifuging, and the amplicon pellet was resuspended in Hanks' buffered salt solution. The purified HSV-1 amplicon was titered in Vero 2-2 cells by counting the number of GFP positive cells after 24 h infection. Typically, the titration of HSV-1 amplicon stocks was around 5×10^6–10^7 GFP transducing units/ml.

HSV-1 virion infection, Western blot and FACS analyses. MC3T3-E1 cells were plated in a 6-well plate at a density of 10^5/well. After 24 h, the cells were infected at a multiplicity of infection (MOI) of 5 with HSV-1 amplicon. After 6 h infection, the medium was removed, and fresh medium was added to the cells. The cells were lysed in a lysis buffer containing 50 mM Tris, pH 8.0, 150 mM NaCl, 0.1% SDS, 1% Triton X-100, and 1× Protease Inhibitor cocktail (Sigma) 24 h after infection. An aliquot of 60 μg cellular protein was electrophoresed on a 15% SDS–polyacrylamide gel and transferred to nitrocellulose. The membrane was incubated at 4 °C overnight in a buffer containing 5% dried skim milk, 150 mM NaCl, 50 mM Tris–HCl (pH 8.0), and 0.05% Tween 20. Immunoblotting was performed in the same buffer containing 0.2 μg/ml antibody against BMP-2 or GFP (Santa Cruz, CA) at room temperature for 1 h. Specific proteins were detected using appropriate secondary antibodies and ECL + plus Western blotting detection system (Amersham–Pharmacia Biotech UK Limited, Buckinghamshire, England). The cells in a parallel well were trypsinized 24 h post-infection and analyzed by fluorescence-activated cell sorter (FACS) (BD Biosciences, San Lose, CA) to assess the transduction efficiency [24].

Cytochemical staining for alkaline phosphatase. The cytochemical staining for alkaline phosphatase (ALP) was performed according to the protocol described previously [25]. Nine days after HSV-1 amplicon infection, the MC3T3-E1 cells were washed with PBS and fixed in 0.05% glutaraldehyde at room temperature for 5 min. The cells were then incubated at 37 °C for 30 min in a staining buffer containing 50 mM Tris–HCl, pH 8.6, 100 mM NaCl, 5 mM KCl, 1 mM $CaCl_2$, 1 mM $MgCl_2$, 0.8 mg/ml naphthol AS-TR phosphate, and 0.6 mg/ml

fast red violet LB diazonium (Sigma) in dark, followed by observation without counterstain.

Results and discussion

We searched the GenBank database and identified a mouse BAC library clone containing a complete 8.7-kb BMP-2 genomic DNA locus driven by a 20.5-kb native promoter within a 128.5-kb insert. We chose this clone because it contains a single BMP-2 gene with most, if not all, of the regulatory elements in the promoter, introns, and 3′ non-coding regions that may regulate a physiological gene expression [26,27]. The length of the BAC clone is also within the size limits that the HSV-1 vector can efficiently package into an iBAC [21]. We used a Cre/loxP-based retrofitting method to convert the BAC/BMP-2 with the pEHHG, consisting of HSV-1 amplicon elements, enhanced green fluorescent protein (GFP), EBV episome retention cassette, R6K bacterial replication origin, and a *loxP* site to generate a 152-kb construct of pHSV-BAC/BMP-2 (Fig. 1A) [20,21]. Subsequently, a PCR with specific primers to BMP-2 and GFP was performed to confirm the presence of two genes within a single pHSV-BAC/BMP-2 construct (Fig. 1B). We then packaged the pHSV-BAC/BMP-2 into the iBAC [21] and infected MC3T3-E1 cells to test the transgenes' function (Fig. 2). Twenty-four hours after infection, the GFP reporter gene was expressed in most of MC3T3-E1 cells transduced with either an HSV-1 mock (Fig. 2C) or an HSV-BAC/BMP-2 amplicon (Fig. 2D). Flow cytometry analyses revealed that 84% of the osteoblast cells transduced with HSV-1 mock amplicon expressed GFP (Fig. 2E) and 77% of the cells infected with HSV-BAC/BMP-2 virion were GFP-positive (Fig. 2F). To compare the efficiencies of transduction and transfection, we also transfected MC3T3-E1 cells with pEHHG and pHSV-BAC/BMP-2 (Fig. 1A) using Lipofectamine-Plus. Only less than 5% of MC3T3-

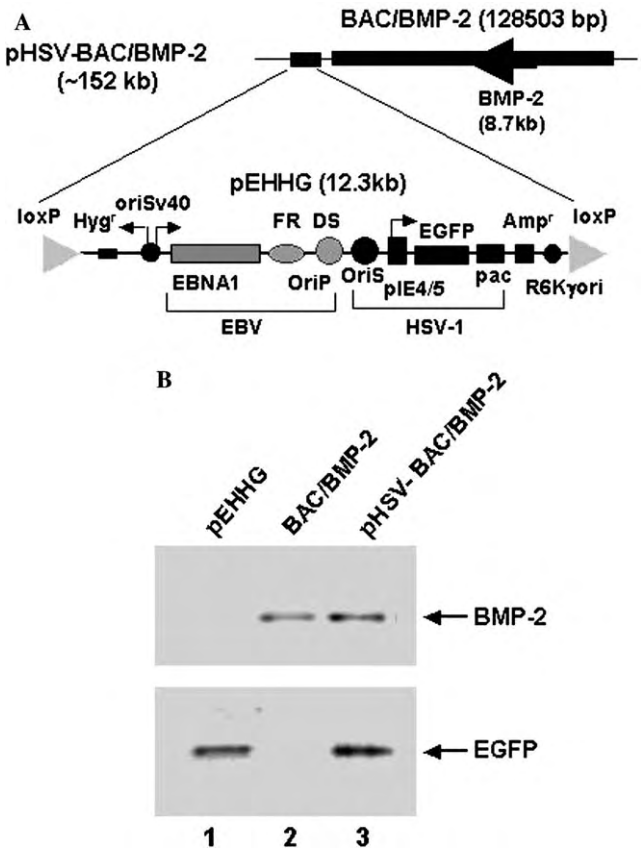

Fig. 1. Schematic diagram of infectious HSV-1/BAC/BMP-2 construct. (A) A detailed structure of retrofitted BAC clone. The retrofitting vector pEHHG containing the HSV-1 amplicon elements (*ori*$_s$ and *pac*) and GFP, the EBV episome retention cassette (*oriP*/*EBNA-1*/*hyg*^{r}), the R6K bacterial replication origin, and a *loxP* site is retrofitted into the BAC clone bearing a complete BMP-2 locus by homologous recombination. The retrofitted BAC contains both GFP reporter and BMP-2 genes. (B) Verification of pHSV-BAC/BMP-2 construct by polymerase chain reaction (PCR). Lane 1: pEHHG control; lane 2: BAC/BMP-2 control; and lane 3: pHSV-BAC/BMP-2 containing both GFP and BMP-2 genes.

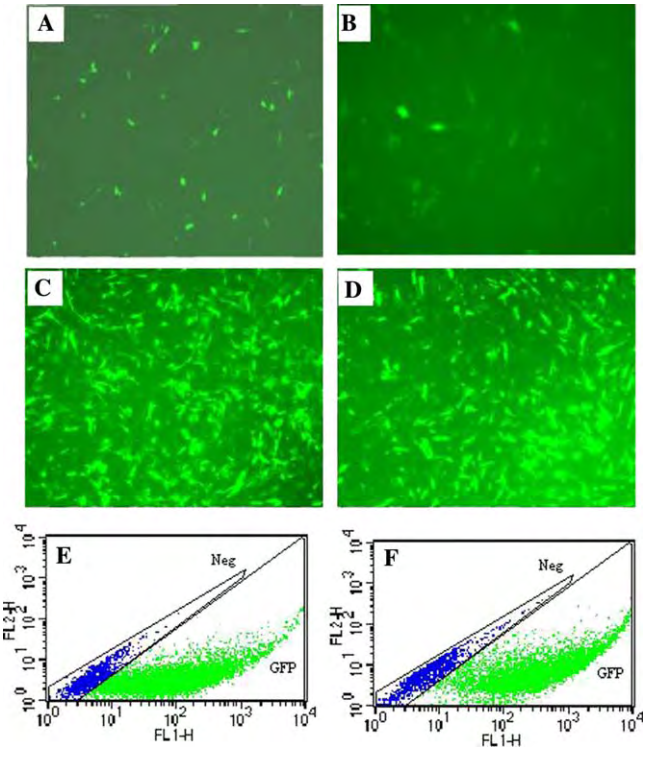

Fig. 2. GFP reporter expression in MC3T3-E1 cells transfected and transduced with HSV-1 amplicon for 24 h (40× images). (A) MC3T3-E1 cells transfected with pEHHG (4 μg) using optimized lipofectamine; (B) MC3T3-E1 cells transfected with pHSV-BAC/BMP-2 (4 μg) using optimized lipofectamine; (C) MC3T3-E1 cells transduced with infectious HSV-1 mock amplicon without BMP-2 genomic locus; (D) MC3T3-E1 cells transduced with infectious HSV-1 amplicon containing a BMP-2 genomic locus; (E) representative data of flow cytometric analysis in MC3T3-E1 cells infected with HSV-1 mock amplicon containing GFP but no BMP-2 genomic locus; and (F) representative data of flow cytometric analysis in MC3T3-E1 cells infected with HSV-1 amplicon containing GFP and a BMP-2 genomic locus.

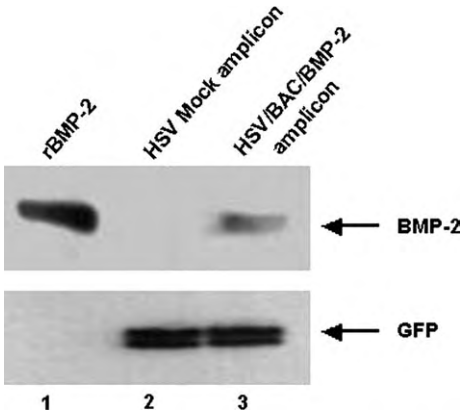

Fig. 3. Western immunoblot analyses of BMP-2 expressed in transduced MC3T3-E1 cells. MC3T3-E1 cells are infected with HSV-1 amplicon for 24 h and harvested for Western blot analysis. An aliquot (60 μg, 10^6 cells) of cellular lysate is separated on 15% SDS–PAGE, transferred to nitrocellulose membranes, and blotted using antibodies against BMP-2 and GFP, respectively. Lane 1: positive control of recombinant BMP-2 (100 ng); lane 2: the cells infected with HSV-1 mock amplicon containing GFP but no BMP-2 genomic locus; and lane 3: the cells infected with HSV-1 amplicon containing GFP and a BMP-2 genomic locus.

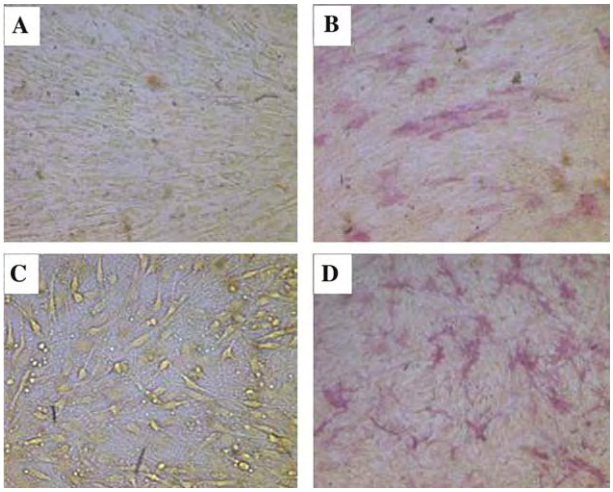

Fig. 4. Alkaline phosphatase (ALP) staining of differentiated MC3T3-E1 cells (40× images). MC3T3-E1 cells are differentiated for 9 days and subjected to ALP staining. (A) The cells infected with HSV-1 mock amplicon without a BMP-2 genomic locus; (B) the cells infected with HSV-1 amplicon containing a BMP-2 genomic locus; (C) negative control of MC3T3-E1 cells treated with vehicle; and (D) positive control of MC3T3-E1 cells treated with recombinant BMP-2 (200 ng/ml).

E1 cells transfected with pHSV-BAC/BMP-2 expressed GFP (Fig. 2A) whereas approximately 10% of the cells transfected with pEHHG turned green (Fig. 2A). Obviously, the efficiency of transduction of BAC-based amplicon was at least 15-fold higher than that of lipid-based transfection (Fig. 2).

The expression of the transgene was examined in cell extract by utilizing Western blot with specific antibodies against BMP-2 and GFP (Fig. 3). The amount of BMP-2 protein was estimated to be 10 ng/10^6 cells based on Western blot analysis (Fig. 3). However, we failed to detect BMP-2 expression in the same number of either native MC3T3-E1 cells or the cells transfected with pHSV-BAC/BMP-2 (Fig. 3 and data not shown). To assess osteoblast phenotype in the cells expressing BMP-2 transgene, we carried out an ALP staining 9 days after transduction (Fig. 4). Like the cells treated with 200 ng/ml recombinant human BMP-2, about 20% of the osteoblast cells were differentiated and exhibited positive ALP-staining (Figs. 4B and D). No ALP-positive cells were seen in the control cells infected with HSV-1 mock amplicon without BMP-2 genomic locus (Fig. 4A) or the cells treated with vehicle alone (Fig. 4C).

In this study, we have demonstrated that the HSV-1 amplicon can efficiently transfer a large piece of genomic locus (Fig. 2), and retain it as episomes in proliferating cells [18]. The GFP gene is consistently active and visible for at least 2 weeks, although the intensity becomes weaker as reported by other investigators [24]. The functional BMP-2 protein in the infected cells was detectable 24 h and even 72 h after infection (Fig. 3 and data not shown) and mediated cell differentiation (Fig. 4) [28]. However, accurate quantification of BMP-2 expression level was impossible because the secreted BMP-2 in the medium was not measured. Nevertheless, the transgene of BMP2 was active and promoted a phenotypic change of targeting cells (Fig. 3, lane 3 and Fig. 4), validating the application of iBAC technology.

In vivo testing of candidate genes in a BAC-based transgenic mouse is time-consuming and expensive, requiring the injection of BAC inserted into fertilized eggs and the examination of mouse phenotypes. Therefore, it would be more efficient to use in vitro cell models via the BAC clone approach to test candidate gene function before introducing in vivo transgenic studies. The studies provided in this manuscript demonstrate that retrofitting of the BAC clone and packaging of the HSV-1 amplicon into infectious virion can be accomplished within 1–2 weeks of work. By utilizing this approach, a candidate gene search in a QTL region is feasible once an appropriate cell model and end points for candidate gene function are determined. In this regard, our data demonstrate that MC3T3-E1 cells can be used as a model for high-throughput phenotypic screening to identify genes important for osteoblast cell differentiation. We have also used this system in C2C12 cells and proved that iBAC containing BMP-2 locus can induce premyoblast dedifferentiation and subsequently commit to osteoblast lineage (data not shown), providing another cell-based model for gene function of dedifferentiation. In addition, BAC or PAC can carry a genomic locus encompassing an intact gene(s) with all regulatory elements including enhancers, suppressors and locus control region that can direct physiological levels of tissue-specific expression for gene therapy. It can also be

manipulated to engineer a deletion, an insertion, and a site-specific mutation in *Escherichia coli* by homologous recombination to mimic natural polymorphisms to test the functional significance of SNPs located in the distal promoter or/and intron regions.

Acknowledgments

This work was supported by Assistance Award No. DAMD17-03-2-0021. The U.S. Army Medical Research Acquisition Activity, 820 Chandler Street, Fort Detrick MD 21702-5014, is the awarding and administering acquisition office. The information contained in this publication does not necessarily reflect the position or the policy of the Government, and no official endorsement should be inferred. All work was performed in facilities provided by the Department of Veterans Affairs. We are grateful to Dr. Yoshinaga Saeki (the Massachusetts General Hospital, Harvard Medical School, MA) for providing HSV-1 amplicon system and his technical assistance, and Dr. Rozanne Sandri-Goldin (the University of California, Irvine, CA) for her generous gift of a Vero 2-2 cell line. We also thank Dr. Shin-Tai Chen, Ms. Mahita Kadmiel, and Mr. Max Davis for their technical assistances of HSV-1 virion purification and FACS analyses (Musculoskeletal Disease Center, JL Pettis Memorial Veterans Medical Center, Loma Linda, CA).

References

[1] D.L. Glaser, F.S. Kaplan, Osteoporosis. Definition and clinical presentation, Spine 22 (1997) 12S–16S.
[2] C.W. Slemenda, J.C. Christian, T. Reed, T.K. Reister, C.J. Williams, C.C. Johnston Jr., Long-term bone loss in men: effects of genetic and environmental factors, Ann. Intern. Med. 117 (1992) 286–291.
[3] C.W. Slemenda, J.C. Christian, C.J. Williams, J.A. Norton, C.C. Johnston Jr., Genetic determinants of bone mass in adult women: a reevaluation of the twin model and the potential importance of gene interaction on heritability estimates, J. Bone Miner. Res. 6 (1991) 561–567.
[4] V. Nicolas, S. Mohan, Y. Honda, A. Prewett, R.D. Finkelman, D.J. Baylink, J.R. Farley, An age-related decrease in the concentration of insulin-like growth factor binding protein-5 in human cortical bone, Calcif. Tissue Int. 57 (1995) 206–212.
[5] D. Baylink, M. Stauffer, J. Wergedal, C. Rich, Formation, mineralization, and resorption of bone in vitamin D-deficient rats, J. Clin. Invest. 49 (1970) 1122–1134.
[6] M.J. Econs, D.L. Koller, S.L. Hui, T. Fishburn, P.M. Conneally, C.C. Johnston Jr., M. Peacock, T.M. Foroud, Confirmation of linkage to chromosome 1q for peak vertebral bone mineral density in premenopausal white women, Am. J. Hum. Genet. 74 (2004) 223–228.
[7] C.M. Kammerer, J.L. Schneider, S.A. Cole, J.E. Hixson, P.B. Samollow, J.R. O'Connell, R. Perez, T.D. Dyer, L. Almasy, J. Blangero, R.L. Bauer, B.D. Mitchell, Quantitative trait loci on chromosomes 2p, 4p, and 13q influence bone mineral density of the forearm and hip in Mexican Americans, J. Bone Miner. Res. 18 (2003) 2245–2252.
[8] F. Wynne, F.J. Drummond, M. Daly, M. Brown, F. Shanahan, M.G. Molloy, K.A. Quane, Suggestive linkage of 2p22-25 and 11q12-13 with low bone mineral density at the lumbar spine in the Irish population, Calcif. Tissue Int. 72 (2003) 651–658.
[9] H.W. Deng, H. Shen, F.H. Xu, H. Deng, T. Conway, Y.J. Liu, Y.Z. Liu, J.L. Li, Q.Y. Huang, K.M. Davies, R.R. Recker, Several genomic regions potentially containing QTLs for bone size variation were identified in a whole-genome linkage scan, Am. J. Med. Genet. 119A (2003) 121–131.
[10] G.L. Masinde, J. Wergedal, H. Davidson, S. Mohan, R. Li, X. Li, D.J. Baylink, Quantitative trait loci for periosteal circumference (PC): identification of single loci and epistatic effects in F2 MRL/SJL mice, Bone 32 (2003) 554–560.
[11] G.L. Masinde, X. Li, W. Gu, J. Wergedal, S. Mohan, D.J. Baylink, Quantitative trait loci for bone density in mice: the genes determining total skeletal density and femur density show little overlap in F2 mice, Calcif. Tissue Int. 71 (2002) 421–428.
[12] W.G. Beamer, C.J. Rosen, R.T. Bronson, W. Gu, L.R. Donahue, D.J. Baylink, C.C. Richardson, G.C. Crawford, J.E. Barker, Spontaneous fracture (sfx): a mouse genetic model of defective peripubertal bone formation, Bone 27 (2000) 619–626.
[13] K.L. Shultz, L.R. Donahue, M.L. Bouxsein, D.J. Baylink, C.J. Rosen, W.G. Beamer, Congenic strains of mice for verification and genetic decomposition of quantitative trait loci for femoral bone mineral density, J. Bone Miner. Res. 18 (2003) 175–185.
[14] W.K. Gu, X.M. Li, B. Edderkaoui, D.D. Strong, K.H. Lau, W.G. Beamer, L.R. Donahue, S. Mohan, D.J. Baylink, Construction of a BAC contig for a 3 cM biologically significant region of mouse chromosome 1, Genetica 114 (2002) 1–9.
[15] R.E. White, R. Wade-Martins, S.L. Hart, J. Frampton, B. Huey, A. Desai-Mehta, K.M. Cerosaletti, P. Concannon, M.R. James, Functional delivery of large genomic DNA to human cells with a peptide-lipid vector, J. Gene. Med. 5 (2003) 883–892.
[16] C. Magin-Lachmann, G. Kotzamanis, L. D'Aiuto, H. Cooke, C. Huxley, E. Wagner, In vitro and in vivo delivery of intact BAC DNA–comparison of different methods, J. Gene. Med. 6 (2004) 195–209.
[17] C. Magin-Lachmann, G. Kotzamanis, L. D'Aiuto, E. Wagner, C. Huxley, Retrofitting BACs with G418 resistance, luciferase, and oriP and EBNA-1-new vectors for in vitro and in vivo delivery, BMC Biotechnol. 3 (2003) 2.
[18] R. Wade-Martins, Y. Saeki, E. Antonio Chiocca, Infectious delivery of a 135-kb LDLR genomic locus leads to regulated complementation of low-density lipoprotein receptor deficiency in human cells, Mol. Ther. 7 (2003) 604–612.
[19] Y. Wang, C. Fraefel, F. Protasi, R.A. Moore, J.D. Fessenden, I.N. Pessah, A. DiFrancesco, X. Breakefield, P.D. Allen, HSV-1 amplicon vectors are a highly efficient gene delivery system for skeletal muscle myoblasts and myotubes, Am. J. Physiol. Cell Physiol. 278 (2000) C619–C626.
[20] R. Wade-Martins, E.R. Smith, E. Tyminski, E.A. Chiocca, Y. Saeki, An infectious transfer and expression system for genomic DNA loci in human and mouse cells, Nat. Biotechnol. 19 (2001) 1067–1070.
[21] Y. Saeki, X.O. Breakefield, E.A. Chiocca, Improved HSV-1 amplicon packaging system using ICP27-deleted, oversized HSV-1 BAC DNA, Methods Mol. Med. 76 (2003) 51–60.
[22] K. Ellnebo-Svedlund, L. Larsson, J. Jonasson, P. Magnusson, Rapid genotyping of the osteoporosis-associated polymorphic transcription factor Sp1 binding site in the COL1A1 gene by pyrosequencing, Mol. Biotechnol. 26 (2004) 87–90.
[23] S.L. Ferrari, D. Karasik, J. Liu, S. Karamohamed, A.G. Herbert, L.A. Cupples, D.P. Kiel, Interactions of interleukin-6 promoter polymorphisms with dietary and lifestyle factors and their association with bone mass in men and women from the Framingham Osteoporosis Study, J. Bone Miner. Res. 19 (2004) 552–559.
[24] R. Nunez, M. Ackermann, Y. Saeki, A. Chiocca, C. Fraefel, Flow cytometric assessment of transduction efficiency and cytotoxicity

of herpes simplex virus type 1-based amplicon vectors, Cytometry 44 (2001) 93–99.

[25] J.E. Wergedal, D.J. Baylink, Characterization of cells isolated and cultured from human bone, Proc. Soc. Exp. Biol. Med. 176 (1984) 60–69.

[26] K.L. Abrams, J. Xu, C. Nativelle-Serpentini, S. Dabirshahsahebi, M.B. Rogers, An evolutionary and molecular analysis of BMP2 expression, J. Biol. Chem. (2004).

[27] L.M. Helvering, R.L. Sharp, X. Ou, A.G. Geiser, Regulation of the promoters for the human bone morphogenetic protein 2 and 4 genes, Gene 256 (2000) 123–138.

[28] D. Noel, D. Gazit, C. Bouquet, F. Apparailly, C. Bony, P. Plence, V. Millet, G. Turgeman, M. Perricaudet, J. Sany, C. Jorgensen, Short-term BMP-2 expression is sufficient for in vivo osteochondral differentiation of mesenchymal stem cells, Stem Cells 22 (2004) 74–85.

Transfer of 128-kb BMP-2 Genomic Locus by HSV-Based Infectious BAC Stimulates Osteoblast Differentiation: A Platform for Functional Genomic Studies

W. Xing, D. J. Baylink, C. Kesavan*, S. Mohan. JLP VAMC/LLU, Loma Linda, CA, USA.

Presentation Number: SA258

In order to localize chromosomal regions and subsequently identify the genes responsible for musculoskeletal diseases, we previously developed mouse genetic models and discovered quantitative trait loci (QTL) in a number of mouse chromosomes that contribute to phenotypes such as bone density, size and strength. Subsequent analyses of the congenic mice further confirmed and narrowed two predominant QTLs that regulate BMD to < 5 cM regions in mouse chromosome 1. However, these regions contain dozens of genes and are still difficult to clone by time-consuming, expensive positional cloning strategies. A feasible and efficient approach for identifying candidate genes is to transfer the genomic loci of overlapping bacterial artificial chromosomes (BACs) or P1 artificial chromosomes (PACs) encompassing the QTL regions into bone cells in vitro for a high throughput functional screening. In this study, we retrofitted a BAC construct into herpes simplex virus-1 (HSV-1) amplicon and packaged it into an infectious BAC (iBAC) to test gene function in a cell-based system, using a 128-kb clone containing the complete bone morphogenetic protein-2 (BMP-2) gene. We transduced MC3T3-E1 cells with the iBAC bearing BMP-2 and examined transduction efficiency, transgene expression and function. Our experiments revealed that approximately 84% of MC3T3-E1 cells were transduced by the iBAC at a multiplicity of infection (MOI) of 5. The amount of BMP-2 protein was estimated to be 10 ng per 10^6 cells 24 hours after infection of HSV amplicon containing BMP-2 genomic locus. Like the cells treated with 200 ng/ml recombinant human BMP-2, about 20% of the osteoblast cells were differentiated and exhibited positive ALP-staining 9 days post-infection. No ALP-positive cells were seen in the control cells infected with HSV-1 mock amplicon without BMP-2 genomic locus. Our results have indicated that an iBAC can efficiently deliver a BMP-2 genomic locus into preosteoblast cells and express functional BMP-2 protein, stimulating a phenotype of cell differentiation. Therefore, this experimental system provides a rapid, efficient cell-based model of high-throughput phenotypic screening to identify the BAC clones from physically mapped regions that are important for osteoblast differentiation. Because multiple copies of BAC clones can be transferred into the target cells depending on the amount of HSV used, the BAC clone approach also provides a sensitive platform for studies on gene function, gene expression and for identification of gene regulatory elements that are located in the intronic regions.

Calcified Tissue International C·T·I· The Official Journal of the European Calcified Tissue Society
Springer

Loss of sex-specific difference in femoral bone parameters in male leptin knockout mice

Journal:	*Calcified Tissue International*
Manuscript ID:	CTI-06-0327.R1
Manuscript Type:	Original Study
Date Submitted by the Author:	n/a
Complete List of Authors:	Rundle, Charles; Jerry L. Pettis Memorial VA Medical Center, Musculoskeletal Disease Center Wang, Xiaoguang; Jerry L. Pettis Memorial VA Medical Center, Musculoskeletal Disease Center Wergedal, Jon; Jerry L. Pettis Memorial VA Medical Center, Musculoskeletal Disease Center Srivastava, Apurva; Jerry L. Pettis Memorial VA Medical Center, Musculoskeletal Disease Center Mohan, Subburaman; Jerry L. Pettis Memorial VA Medical Center, Musculoskeletal Disease Center Lau, K.-H. William; Jerry L. Pettis Memorial VA Medical Center, Musculoskeletal Disease Center
Keywords:	Steroid Hormones: Androgens, Peptide Hormones: Leptin, Osteoporosis: Animal Models, Osteoporosis: Pathogenesis

Loss of sex-specific difference in femoral bone parameters in male leptin knockout mice

Xiaoguang Wang[1,*], Charles H. Rundle[1,2,*], Jon E. Wergedal[1,2,3], Apurva K. Srivastava[1,2], Subburaman Mohan[1,2,3,4], and K.-H. William Lau[1,2,3]

[1]Musculoskeletal Disease Center (151), J.L. Pettis Memorial Veterans Administration Medical Center, 11201 Benton Street, Loma Linda, California, 92357 USA

[2]Department of Medicine,

[3]Department of Biochemistry,

[4]Department of Physiology, Loma Linda University, Loma Linda, California, 92350, USA

* These authors contributed equally to this work.

Address Correspondence to: Charles H. Rundle, Ph.D.

Musculoskeletal Disease Center (151)

J.L. Pettis Memorial Veterans Administration Medical Center

11201 Benton Street

Loma Linda, CA, 92357

Telephone: 909-825-7084 ext. 6149

Fax: 909-796-1680

Email: Charles.Rundle@med.va.gov

Running title: Sex-specific effects of leptin on bone development

Keywords: leptin, sex-related, femur, androgen, mouse.

Number of Figures: 5

Abstract

Sex-dependent differences were identified in the femoral bone parameters of male and female *ob/ob* (leptin knockout) mice as compared with their C57BL/6 wild-type control background strain. Total fat, lean and body weight were not different between adult male and female leptin knockout mice but significantly lower than adult male and female C57BL/6 mice. pQCT measurements at the femoral midshaft revealed that the normal differences in the periosteal circumference, endosteal circumference, total bone mineral content and polar moment of inertia normally observed between adult male and female wild-type mice were lost between adult male and female *ob/ob* mice. Significant reductions in these bone parameters were seen in male *ob/ob* mice as compared to male wild-type mice, but not in female *ob/ob* mice as compared to female wild-type mice. In pre-pubertal mice, there were no differences in phenotype and femoral bone parameters between male and female mice within any strain, suggesting sex hormone functions. Serum free testosterone levels were 5.6-fold higher in adult male *ob/ob* mice than in adult male C57BL/6 wild-type mice, and serum estradiol levels were 1.8 and 1.3-fold greater in adult male and female *ob/ob* mice, respectively, than in their wild-type counterparts. Androgen receptor gene expression was not different in the periosteal cells of male *ob/ob* mice as compared with wild-type mice. The loss of sex-related differences in these bone parameters in adult male *ob/ob* mice might result from deficient signaling in the androgen signaling pathway, and that leptin functions are permissive for androgen effects on bone development.

Introduction

Leptin is a 16 kDa protein expressed predominantly in adipose tissue and functions as a hormone to regulate body fat [1]. Changes in the level of circulating leptin alter feeding behavior, metabolism, and endocrine functions [2]. However, recent data indicate that leptin is also an important regulator of bone mass [3, 4]. Genetic variations in leptin have been associated with bone size and shape [5]. It exerts dual effects on bone formation, depending on the route of administration: when administered through the central nerve system, it produces an anti-osteogenic effect, which appears to be mediated directly through hypothalamic signaling at the sympathetic nervous system [6]. Conversely, when administrated peripherally, leptin stimulates osteoblast differentiation and mineralization of bone matrix, enhancing the development of the periosteal envelope in growing bone during early life [7]. Hamrick et al. [8] showed that leptin deficiency has differential effects on bone mass in the axial and appendicular skeleton, indicating that leptin produces different local effects at different bone sites. Osteoblasts express leptin receptors, which presumably permit leptin to directly stimulate bone metabolism at different skeletal sites [9]. Thus, while it is clear that leptin has a role in regulating bone size, the mechanisms by which leptin regulates bone growth and development at different skeletal sites are complex and remain to be elucidated. It also remains unclear whether the osteogenic effects of leptin are mediated entirely through direct action of leptin on bone, or indirectly, through the systemic functions of other hormones.

Gender-specific effects on bone mass also implicate the sex steroid hormones in bone metabolism [10]; androgen action has been traditionally thought to be primarily anabolic, while the estrogen acts mainly through the suppression of resorption [11]. Estrogen also regulates the closure of the epiphyseal growth plate that affects bone length. The larger bone size in adult

males as compared to females is generally attributed to androgen activity that mediates the periosteal expansion, though aromatization and estrogen can also influence this parameter [see reviews 12, 13]. These observations suggest that the sex steroid effects on bone formation are likely to be complex.

There is also circumstantial evidence that leptin might also regulate sex steroid functions, especially those of testosterone. The receptors for androgen and estrogen have been identified in bone cells [see reviews 14, 15]. Several studies have demonstrated that leptin levels are inversely correlated with testosterone [16, 17], suggesting an interaction between these hormones. However, the potential interactions between the sex hormones and leptin on the regulation of bone metabolism have not been functionally assessed, since previous studies in leptin deficient *(ob/ob)* mice [4, 8, 18] or leptin receptor-deficient (*fa/fa*) rats [19] have examined various bone parameters in one gender, or combined male and female subjects. These approaches yielded valuable information but could not resolve sex-specific differences in bone measurements produced by leptin.

The objective of this study was to evaluate whether interactions between leptin and the sex hormones affect bone formation. Accordingly, male and female leptin knockout (*ob/ob*) and wild type control mice were examined for body and bone size to identify any sex-related effects of leptin on bone development. In this report we show that a comparison of the femurs of male and female mice from the mouse strain with their wild-type counterparts reveals a surprising loss of sex-specific bone characteristics in the male leptin knockout mice. We conclude that leptin is an important modulator of androgen-related functions in bone growth.

Materials and Methods

Mice. Heterozygous male and female leptin knockout (*ob/ob*) mouse (B6.v-Lep^{ob}/J) breeders were obtained from the Jackson Laboratories (Bar Harbor, ME) and maintained at the J.L. Pettis Memorial Veterans Administration Medical Center. Male and female mice of the wild-type background strain C57BL/6 were also obtained from the Jackson Labs. Leptin knockout mice were bred and the homozygous leptin deficient genotype confirmed by PCR as previously described [20]. All animal procedures were approved by the local Institutional Animal Care and Use Committee.

Phenotypic comparison of body characteristics and bone parameters. The body characteristic comparison was performed at 10 weeks of age in groups of 12 male and female mice. Total body fat and total lean body mass (excluding the head) of live mice were determined under general anesthesia by dual energy X-ray absorptiometry (DEXA) using a PIXIMUS system (Lunar Corp., Madison, WI).

Bone parameters were compared in 13 to 14 week-old male and female mice following euthanasia by carbon dioxide inhalation (n=12 each sex). Femurs were collected and fixed in 10% formalin. Femur length and midshaft diameter were manually measured with calipers. Periosteal circumference (PC), endosteal circumference (EC), polar moment of inertia (MOI, a measure of the distribution of material around a given axis), marrow area (MA) and total bone mineral content (BMC) of midshaft of femurs were determined by peripheral quantitative computerized tomography (pQCT, Stratec XCT 960M, Norland Medical Systems, Ft. Atkinson, WI) with the analysis thresholds of 630-630 for cortical bone (PC, EC, MOI) and 570-214 for cancellous bone (MA, total BMC) in adult mice.

In a separate experiment that examined bone parameters prior to the onset of sex hormone function, the femurs of 3 week old pre-pubertal mice in groups of 6 of both sexes were also compared. The thresholds for cortical bone and cancellous bone of pre-pubertal mice were 300-350 and 250-300 respectively, as described by Richman et al. [21] and Taylor et al. [22].

Sex hormone assay. Mouse sera were separated from blood samples collected from the retro-orbital venous plexus of live animals under general anesthesia. Sera were stored frozen at -70^{o}C until assay. Serum testosterone and estradiol levels were determined using the respective radioimmunoassay (RIA) kits obtained from MPBio (Orangeburg, NY), according to the manufacturer's specifications.

Androgen receptor real-time RT-PCR. Expression of the androgen receptor gene in 5 leptin knockout and 5 wild-type male mice was analyzed by real-time PCR. Total RNA was isolated from whole femurs using by Trizol (Invitrogen, Grand Island, NY) extraction, purified using the RNeasy mini kit (Qiagen, Valencia, CA) according to the manufacturers' specifications. RNA integrity was confirmed on the Agilent Bioanalyzer (Agilent, Santa Clara, CA) and reverse-transcribed to cDNA using SuperScript-III kit (Invitrogen) according to the manufacturers' specifications.

Androgen receptor gene expression was normalized to the expression of the cyclophilin-A housekeeping gene. Gene-specific primers were synthesized by IDT (Coralville, IA). The forward 5'-TAC TCT GCC TCC GAA GTG TG-3' and reverse 5'-TCC GTA GTG ACA GCC AGA AG-3', androgen receptor primers, corresponded to bases 1458 to 1477 and 1688 to 1669, respectively, of the mouse androgen receptor gene (Accession #: X53779). The forward 5'-GCA TAC AGG TCC TGG CAT CT-3' and reverse 5'-TCT TGC TGG TCT TGC CAT TC-3' cyclophilin-A primers corresponded to bases 351 to 370 and 544 to 525, respectively, of the

mouse cyclophilin-A gene (Accession #: XR_003025). Real-time RT-PCR was performed in duplicate for each sample on an Opticon thermal cycler (BioRad-MJ Research, Hercules, CA) using the SYBR Green-based Quantitect assay kit (BioRad, Hercules, CA) according to the manufacturer's specifications. Reaction conditions provided the most efficient amplification from either set of primers were 95^{o}C for 45 seconds, 55^{o}C for 45 seconds, and 72^{o}C for 30 seconds for 40 cycles. Androgen receptor gene expression was expressed as fold-activation and calculated from the difference cycle number between androgen receptor and cyclophilin-A genes.

Statistical analysis. Statistical analysis was performed by two-way ANOVA with a post-hoc Newman-Kuels Test for phenotypic comparison of body and skeletal characteristics as well as serum sex hormone comparison. All data are expressed as the Mean ± Standard Error of the Mean (SEM). Differences were deemed significant at $p<0.05$.

Results

Phenotypic comparison of body characteristics in adult male and female leptin knockout and C57BL/6 wild-type mice. Homozygous leptin knockout mice are recognizable by an increased obesity that is evident by 3 weeks of age. As previously reported [21, 22], male wild type C57BL/6 mice, by the age of 10 weeks exhibit significantly higher body weight, greater body fat and greater total lean body mass than females [21, 22]. There was an approximately 2-fold increase in body weight (Fig.1A) and a 6-fold increase in total body fat (Fig.1B), and a significant difference in the total lean body mass (Fig. 1C) in both male and female leptin knockout mice as compared to male and female C57BL/6 wild-type mice. For each of these parameters, the differences between adult C57BL/6 male and female mice were not observed

between the male and female leptin knockout mice, indicating that the sex differences in body weight, body fat and total lean body mass were lost in leptin knockout mice.

Bone parameter comparison in adult male and female leptin knockout and C57BL/6 wild-type mice. Consistent with the previous report that male leptin knockout mice had a shorter femur length than male wild type control mice [8], the femurs of 13 to 14 week-old male and female leptin knockout mice were significantly ($p<0.0002$) shorter than C57BL/6 mice by 9%. There was no significant difference in femur length between males and females of either strain at this age statistically, though male femurs of both strains were longer than the femurs of their females (Fig. 2A).

We next evaluated various bone parameters between the leptin knockout and C57BL/6 strains for sex-related differences in femur size. The bone parameters were examined by pQCT at the midshaft of femur. Cortical periosteal circumference (PC), endosteal circumference (EC) and polar moment of inertia (MOI), as well as marrow area (MA) and total bone mineral content (BMC) were examined at the femoral midshaft. As previously reported [21], adult male C57BL/6 mice have greater femoral PC than female. PC, EC and polar MOI of male C57BL/6 mice were significantly greater than those of male leptin knockout mice (Fig. 2B, C and F). These differences in PC were confirmed by caliper measurement of both the lateral-medial and anterior-posterior diameters of femoral midshaft using calipers (data not shown). Consistent with these data, the MA and total BMC of adult male C57BL/6 mice were significantly greater than the corresponding female mice (Fig. 2D, E). The sex-related differences in these bone parameters seen in C57BL/6 mice were reduced in male *ob/ob* mice to levels similar to those of female *ob/ob* mice, so that there was no significant difference between male and female adult leptin knockout mice in any parameter of femur size (Fig. 2A-E). A closer examination of the PC

and EC values for male leptin knockout mice revealed a slightly thinner cortical bone thickness in the femur as compared with the C57BL/6 mice (Fig. 2B,C), a result consistent with the previous study in male leptin knockout and C57BL/6 mice [8]. Also consistent with that study, male wild-type mice had a greater MA than male leptin knockout mice (Fig. 2D). There was no significant difference in any of the bone size parameters between the females of either strain. These data indicate that the male sex-related increase in bone size is completely lost in leptin knockout mice.

Phenotypic comparison of body characteristics and bone parameters in pre-pubertal male and female leptin knockout and C57BL/6 mice. To demonstrate that the loss of sex-specific skeletal characteristics in male leptin knockout mice may relate with sex hormone biological activity, we compared the basal levels of body characteristics and bone parameters in male and female pre-pubertal mice at 3 weeks of age. In phenotypic comparison, body weight, total body fat and total body lean mass did not significantly differ between male and female mice in either strain (Fig. 3A-C). These observations are consistent with the previous results in C57BL/6 mice [21]. Male C57BL/6 mice have similar body weight, total lean body mass and femur length as those in male leptin knockout mice. There was approximately 2-fold increase in total body fat in leptin knockout mice than that in their corresponding C57BL/6 mice at this age (Fig 3B), suggesting that leptin regulation of body fat is independent of sex steroid effects.

In the comparison of the bone size parameters of these mice (Fig. 4), the length of the femurs in male and female mice was not significantly different in either the leptin knockout or the C57BL/6 mice (Fig. 4A). From a pQCT examination of the femur at midshaft, the bone paramenters, PC, EC, MA, BMC, and polar MOI were also found not to be significantly different among male and female leptin knockout and C57BL/6 mice at the pre-pubertal age. All test bone

parameters in male C57BL/6 and leptin knockout mice were similar to those of their female ones. Therefore, except for the body fat, there were no significant differences in body characteristics and bone parameters between pre-pubertal leptin knockout and C57BL/6 mice, or between males and females of either strain of mouse at this age.

Comparison of serum sex hormone levels in adult male and female leptin knockout and C57BL/6 wild-type mice. To assess whether the loss of the sex-related differences in leptin knockout mice was due to a deficiency in sex-steroids, we next evaluated the serum levels of free testosterone (FT) and estradiol. Male leptin knockout mice had approximately a 5-fold greater serum FT than male C57BL/6 wild-type mice (Fig. 5A). The large variations in the serum FT levels of male leptin knockout mice as compared to male C57BL/6 reflected a greater individual difference in sex hormone levels in male leptin knockout mice. There was no detectable serum FT in either female wild type or female leptin knockout mice.

Male and female leptin knockout mice exhibited no significant differences in serum estradiol, but each was significantly greater than the corresponding C57BL/6 mice (Fig. 5B). There were approximately 1.3-fold and 1.8-fold greater estradiol levels in female and male leptin knockout mice than in the female and male C57BL/6 mice, respectively. These greater serum free testosterone levels in male leptin knockout mice and estradiol levels in both sexes of leptin knockout mice imply that their concentrations should be sufficient to produce a wild-type femur size in each sex. Thus, the functional deficiency in the acquisition of normal bone size in male leptin knockout mice was not the result of insufficient levels of circulating free testosterone. A comparison of the androgen receptor gene expression in male leptin knockout and C57BL/6 mice failed to detect any significant differences in transcript levels (data not shown).

Discussion

Leptin has pleiotropic effects, using multiple pathways to regulate bone formation and balance bone formation with fat production. Previous studies have examined various bone parameters in leptin deficient animals [4, 8, 18, 19], but they have either examined one gender or combined males and females in the same analysis, failing to resolve sex-specific differences in bone measurements. Additionally, different components of the leptin axis have been examined in various studies, including leptin and leptin receptor models in mice and rats. Sex-specific differences in these models have not been well characterized, and to our knowledge this is the first study to identify sex-related differences in bone size in leptin knockout mice.

We compared the femoral parameters of bone size when the usual differences in the lean body mass between male and female wild-type mice were not detected between male and female leptin-deficient mice, despite a doubling in the total body weight observed in the adult leptin knockout mice relative to the wild-type mice (Fig. 1). The reduced lean body mass in male leptin knockout mice suggested a sex hormone interaction with leptin. Because sex hormone effects are also expected to affect bone size, we examined the femur in adult mice, which has been previously established to be shorter in leptin knockout mice than in their wild-type counterparts [8], and would therefore be likely to reveal sex-related differences.

When we compared adult male and female leptin knockout mice at 13 to 14 weeks of age, however, several of the expected sex-related differences in bone parameters were not observed. Specifically, the periosteal and endosteal circumference, as well as trabecular bone mineral content, marrow area and the total bone mineral density in the leptin knockout male mice were all reduced (Fig. 2A-E). Importantly, the polar moment of inertia, a major cross-sectional determinant of torsional bone strength, was not altered between C57BL/6 and leptin knockout

mice (Fig. 2F), which suggests that mechanical loading effects on bone formation did not contribute to the loss of bone size parameters.

These results contrast with the high bone mass phenotype attributed to leptin knockout mice [4]. It is possible that our results vary from previous reports because our measurements were taken at midshaft while previous analyses examined the metaphysis. However, our results largely agree with those of Hamrick et al. [8] who found reduced femur parameters among the 6 month-old male leptin knockout mice. The femurs of the leptin knockout animals are significantly shorter than wild-type mice, an observation reported in that study. Both males and females showed this trait, suggesting that endochondral bone length, at least in the femur, is directly regulated through leptin without sex hormone-related effects. It appears that leptin is permissive for femur length, though other factors, notably estrogen regulation of growth plate chondrocyte proliferation and epiphyseal fusion, also affect femur length [23]. If androgens mediate the periosteal dimensions of the endochondral bones, the reduced femur length in the leptin knockout male mice could compensate such factors as the cortical thinning of leptin knockout mice which might cause an unacceptable loss of bone strength in a femur of normal length.

The effect weight on the mechanical loading on the leptin knockout femur is difficult to determine because the large weight gain renders the animal relatively inactive. The lack of differences in the polar moment of inertia suggests that the increased mechanical loading expected from the greater body weight does not affect bone formation. However, the posture and gait of the animal also appear so altered by the weight mass such that we cannot assume that the different elements of the skeleton will bear the increased weight in the same proportion as they would the normal weight. Hamrick et al. [8] have described muscle atrophy in their male leptin knockout mice, but we do not observe differences in the lean body mass between male and

female leptin knockout mice, which would suggest that the muscle mass is centrally regulated by testosterone and local atrophy is less important. However, our results do agree with the femur analysis of Hamrick et al. [8], who found variations in axial and appendicular bone parameters in male leptin knockout mice. The cortical thinning observed in that study was also observed in this study. These results support a peripheral role for leptin in the regulation of bone size, with leptin expression permissive for the sex hormone functions that affect bone growth. We have not examined other bones and cannot conclude that all skeletal elements of male leptin knockout mice display the loss of sex-related differences in bone size observed in the femur. We cannot discount central regulation of bone size and variable fat content within different skeletal elements that might occur in such an obese animal. To confirm that the loss of sex-related differences in leptin knockout mice was indeed due to sex hormone function, we compared the body characteristics and femur parameters in pre-pubertal wild-type and leptin knockout mice at three weeks of age. This time is prior to the sex hormones that would be expected to affect sex-related functions, including bone development. There were no sex-related differences in body weight, body fat or total lean body mass in pre-pubertal mice (Fig. 3), though both male and female leptin knockout mice exhibited an increase in body fat by this age (Fig. 3B). No differences in any femoral parameters were observed between male and female pre-pubertal mice of either the wild-type or leptin knockout strains (Fig. 4A-F). Taken together, these results confirmed that the loss of differences in femur size between adult male and female leptin knockout mice was related to the sex hormone function.

Surprisingly, adult male leptin knockout mice expressed elevated serum levels of free testosterone, suggesting that the increase in testosterone production may reflect a compensatory mechanism for deficient testosterone function (Fig. 5A). On the other hand, we did not measure

the sex hormone binding globulin (SHBG) level in this study, because assays for murine SHBG are not commercial available. SHBG has been negatively correlated with obesity and insulin resistance [24], which suggests that it might also influence the free testosterone levels in the leptin knockout male mice, although interactions with total testosterone and leptin might be complex. Accordingly, we can not rule out the possibility that the elevated serum testosterone levels might be a consequence of a reduced circulatory SHBG. The leptin knockout males and females also exhibited elevated free serum estrogen (Fig. 5B), consistent with the aromatization of testosterone to estrogen in the males that is also observed in obese human males [25] though the response to aromatase functions could itself also be sex-specific [26]. Although we do not have evidence at this time, the elevated levels of testosterone argue against hypogonadism in leptin knockout males, and the high variation in free serum testosterone between individuals suggests that feedback up-regulation of testosterone is involved. Feedback up-regulation of testosterone, such as that observed in bone cells in vitro [27], is consistent with a defective testosterone signaling mechanism, especially in the absence of transcriptional up-regulation of the androgen receptor that we observed in male leptin knockout mouse femurs. Our future studies will address this possibility. Because testosterone affects the periosteal diameter, it would be expected that androgens would mediate cross-sectional bone size through the periosteal cells. If so, this deficiency appears to reside in the testosterone receptor signaling pathway of leptin knockout cells, as real-time PCR analysis of androgen receptor expression in male leptin knockout and C57BL/6 femurs failed to detect any significant differences in receptor transcript levels. Deficient testosterone signaling in the periosteum might therefore explain the reduction in cross-sectional parameters of bone size in male leptin knockout mice. We continue to investigate the testosterone signaling pathway in male leptin knockout mice.

This study also has not addressed the effects of obesity and leptin deficiency on diabetic hyperinsulinemia and growth hormone regulation of body composition. While the growth hormone (GH)/insulin-like growth factor (IGF) axis is affected by body fat and has been correlated with the leptin levels in normal men and women and leptin and the IGF-1 system did not regulate one another [28], adipose tissue mediation of the GH/IGF system remains poorly understood. Thus, the effects of leptin-deficiency on bone size are affected by multiple hormonal systems that confound interpretations of systemic regulation. Accordingly, we cannot rule out the possibility that the changes in bone size parameters that we have observed might be related to peripheral leptin regulation of osteoblast and adipocyte differentiation [29].

Leptin regulation of bone size parameters would be expected to balance skeletal growth and development with body mass. The loss of sex-specific differences in femur size in the absence of leptin function suggests that leptin is permissive for androgen effects that produce the increased body mass and bone size in males. Such interactions might take place through the any of the several intracellular signaling pathways that mediate leptin receptor signaling [see review 30] and androgen receptor signaling [see review 31]. We propose that in the presence of leptin, normal androgen signaling would be expected to increase bone size to accommodate the increase in body size in males. In the absence of leptin, estrogen might mediate basal bone size parameters while androgen signaling for increased size is impaired in males. Further studies will investigate the mechanism by which leptin mediates sex-specific bone parameters.

Acknowledgements

This work was supported by the U.S. Army Medical Research Acquisition Activity Assistance Award No. DAMD17-03-2-0021. The U.S. Army Medical Research Acquisition Activity, 820

Chandler Street, Fort Detrick MD 21702-5014, is the awarding and administering acquisition office. The information contained in this publication does not necessarily reflect the position or the policy of the Government, and no official endorsement should be inferred. All work was performed in facilities provided by the Department of Veterans Affairs. Preliminary results were presented at the American Society of Bone and Mineral Research, Nashville, Tennessee, USA, September 2005 (abstract # SA508) and at the 52nd Annual Meeting of the Orthopaedic Research Society, Chicago, Illinois, USA, March 2006 (abstract # 188). We are grateful to Mr. Emile Davis and Ms. Jann Smallwood for technical assistance.

References

1. Zhang Y, Proenca R, Maffei M, Barone M, Leopold L, Friedman JM (1994) Positional cloning of the mouse obese gene and its human homologue. Nature 372:425-432.
2. Campfield LA, Smith FJ, Guisez Y, Devos R, Burn R (1995) Recombinant mouse OB protein: evidence for a peripheral signal linking adiposity and central neural networks. Science 269:546-549.
3. Thomas T, Gori F, Khosla S, Jensen MD, Burguera B, Riggs BL (1999) Leptin acts on human marrow stromal cells to enhance differentiation to osteoblasts and to inhibit differentiation to adipocytes. Endocrinology 140:1630-1638.
4. Ducy P, Amling M, Takeda S, Priemel M, Schilling AF, Beil FT, Shen J, Vinson C, Rueger JM, Karsenty G (2000) Leptin inhibits bone formation through a hypothalamic relay: a central control of bone mass. Cell 100:197-207.
5. Livshits G, Pantsulaia I, Trofimov S, Kobyliansky E (2003) Genetic variation of circulating leptin is involved in genetic variation of hand bone size and geometry. Osteoporos Int 14:476-483.
6. Takeda S, Elefteriou F, Levasseur R, Liu X, Zhao L, Parker K, Armstrong D, Ducy P, Karsenty G (2002) Leptin regulates bone formation via the sympathetic nervous system. Cell 111:305-317.

7. Steppan CM, Crawford DT, Chidsey-Frink KL, Ke HZ, Swick AG (2000) Leptin is a potent stimulator of bone growth in *ob/ob* mice. Regul Pept 92:73-78.
8. Hamrick MW, Pennington C, Newton D, Xie D, Isales C (2004) Leptin deficiency produces contrasting phenotypes in bones of the limb and spine. Bone 34:376-383.
9. Iwamoto I, Fujino T, Douchi T (2004) The leptin receptor in human osteoblasts and the direct effect of leptin on bone metabolism. Gynecol Endocrinol 19:97-104.
10. Nelson DA, Simpson PM, Johnson CC, Barondess DA, Kleerekoper M (1997) The accumulation of whole body skeletal mass in third- and fourth-grade children: effects of age, gender, ethnicity, and body composition. Bone 20:73-78.
11. Sims NA, Dupont S, Krust A, Clement-Lacroix P, Minet D, Resche-Rigon M, Gaillard-Kelly M, Baron R (2002) Deletion of estrogen receptors reveals a regulatory role for estrogen receptors-beta in bone remodeling in females but not in males. Bone 30:18-25.
12. Vanderschueren D, Vanderput L, Boonen S, Lindberg MK, Bouillon R, Ohlsson C (2004) Androgens and bone. Endocrine Rev 25:389-425.
13. Vanderschueren D, Venken K, Ophoff J, Bouillon R, Boonen S (2006) Clinical review: Sex steroids and the periosteum - reconsidering the roles of androgens and estrogens in periosteal expansion. J Clin Endocrinol Metab 91:378-382.
14. Vanderschueren D, Bouillon R (1995) Androgens and bone. Calcif Tissue Int 56:341-346.
15. Compston JE (2001) Sex steroids and bone. Physiol Rev 81:419-447.
16. Luukkaa V, Pesonen U, Huhtaniemi I, Lehtonen A, Tilvis R, Tuomilehto J, Koulu M, Huupponen R (1998) Inverse correlation between serum testosterone and leptin in men. J Clin Endocrinol Metab 83:3243-3246.
17. Wabitsch M, Blum WF, Muche R, Braun M, Hube F, Rascher W, Heinze E, Teller W, Hauner H (1997) Contribution of androgens to the gender difference in leptin production in obese children and adolescents. J Clin Invest 100:808-813.
18. Hamrick MW, Della-Fera MA, Choi YH, Pennington C, Hartzell D, Baile CA (2005) Leptin treatment induces loss of bone marrow adipocytes and increases bone formation in leptin-deficient ob/ob mice. J Bone Miner Res 20:994-1001.
19. Tamasi JA, Arey BJ, Bertolini DR, Feyen JH (2003) Characterization of bone structure in leptin receptor-deficient Zucker (*fa/fa*) rats. J Bone Miner Res 18:1605-1611.

20. Namae M, Mori Y, Yasuda K, Kadowaki T, Kanazawa Y, Komeda K (1998) New method for genotyping the mouse Lep(ob) mutation, using a polymerase chain reaction assay. Lab Anim Sci 48:103-104.
21. Richman C, Kutilek S, Miyakoshi N, Srivastava AK, Beamer WG, Donahue LR, Rosen CJ, Wergedal JE, Baylink DJ, Mohan S (2001) Postnatal and pubertal skeletal changes contribute predominantly to the differences in peak bone density between C3H/HeJ and C57BL/6J mice. J Bone Miner Res 16:386-397.
22. Taylor BA, Tarantino LM, Phillips SJ (1999) Gender-influenced obesity QTLs identified in a cross involving the KK type II diabetes-prone mouse strain. Mamm Genome 10:963-968.
23. Weise M, De-Levi S., Barnes KM, Gafni RI, Abad V, Baron J (2001) Effects of estrogen on growth plate senescence and epiphyseal fusion. Proc Natl Acad Sci USA 98:6871-6876.
24. Osuna JA, Gomez-Perez R, Arata-Bellabarba G, Villaroel V (2006) Relationship between BMI, total testosterone, sex-hormone-binding-globulin, leptin, insulin and insulin resistance in obese men. Arch Androl 52:355-361.
25. Kley HK, Deselaers T, Peerenboom H, Kruskemper HL (1980) Enhanced conversion of androstenedione to estrogens in obese males. J Clin Endocrinol Metab 51:1128-1132.
26. Oz OK, Zerwekh JE, Fisher C, Graves K, Nanu L, Millsaps R, Simpson ER (2000) Bone has a sexually dimorphic response to aromatase deficiency. J Bone Miner Res 15:507-514.
27. Wiren KM, Zhang X, Chang C, Keenan E, Orwoll ES (1997) Transcriptional up-regulation of the human androgen receptor by androgen in bone cells. Endocrinology 138:2291-2300.
28. Gomez JM, Maravall FJ, Gomez N, Navarro MA, Casamitjana R and Soler J (2003) Interactions between serum leptin, the insulin-like growth factor-1 system, and sex, age anthropometric and body composition variables in a healthy population randomly selected. Clin Endocrinol 58:213-219.
29. Martin A, de Vittoris R, David V, Moraes R, Begeot M, Lafage-Proust M-H, Alexandre C, Vico L, Thomas T (2005) Leptin modulates both resorption and formation while preventing disuse-induced bone loss in tail-suspended female rats. Endocrinology 146:3652-3659.
30. Fruhbeck G (2006) Intracellular pathways activated by leptin. Biochem J 393:7-20.
31. Culig Z (2004) Androgen receptor cross-talk with cell signaling pathways. Growth Factors 22:179-184.

Figure Legends

Fig. 1. Comparison of body characteristics in adult C57BL/6 and leptin knockout mice. Each group contained 12 mice at 10 weeks of age. (A) body weight; (B) total body fat; (C) total lean body mass. Results are expressed as mean ± standard error of mean (SEM).

Fig. 2. Comparison of bone parameters in adult C57BL/6 and leptin knockout mice. (A) femur length, (B) periosteal circumference, (C) endosteal circumference, (D) marrow area, (E) total bone mineral content, (F) polar moment of inertia. Each group contained 12 mice at 13 to 14 weeks of age. Results are expressed as mean ± standard error of mean (SEM).

Fig. 3. Comparison of body characteristics in pre-pubertal C57BL/6 and leptin knockout mice. (A) body weight, (B) total body fat, (C) total lean body mass. Each group contained 6 mice at 3 weeks of age. Results are expressed as mean ± standard error of mean (SEM).

Fig. 4. Comparison of bone parameters of pre-pubertal C57BL/6 and leptin knockout mice. (A) femur length, (B) periosteal circumference, (C) endosteal circumference, (D) marrow area, (E) total bone mineral content, (F) polar moment of inertia. Each group contained 6 mice at 3 weeks of age. Results are expressed as mean ± standard error of mean (SEM).

Fig. 5. Comparison of serum sex hormone levels in male and female leptin knockout and C57BL/6 wild type mice. Each group contained 15 mice at 10 weeks of age. Results are expressed as mean ± standard error of mean (SEM).

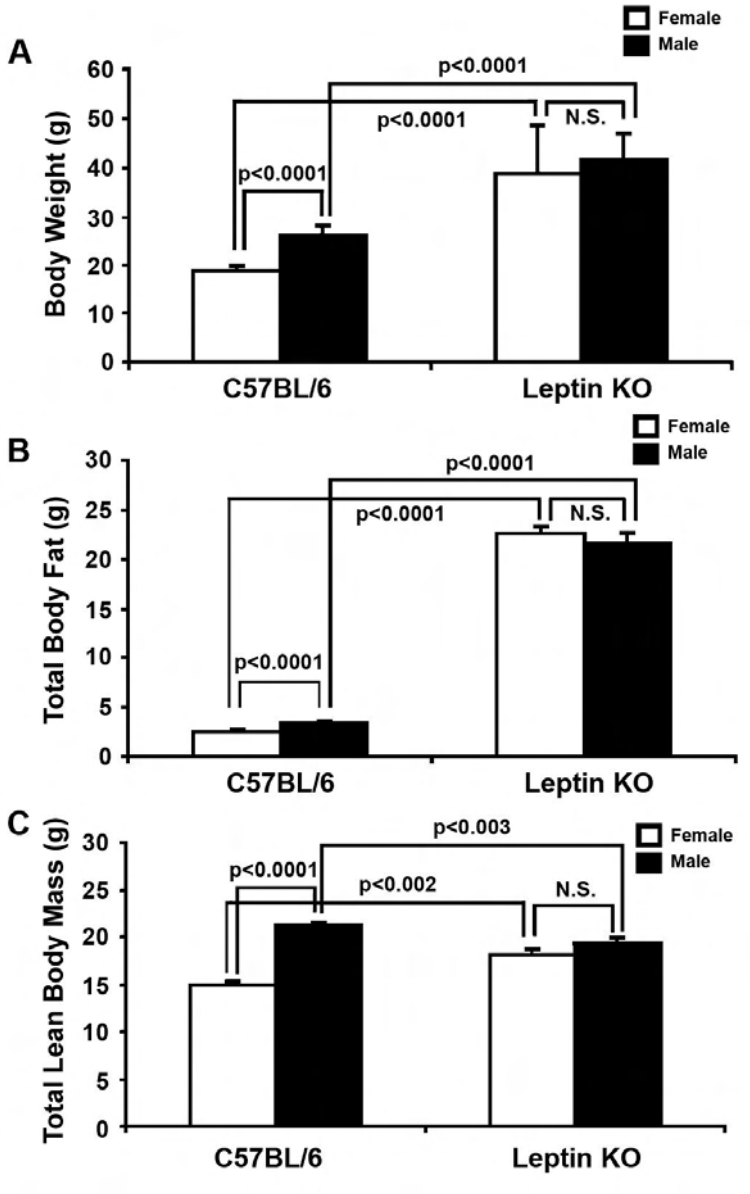

Fig. 1. Comparison of body characteristics in adult C57BL/6 and leptin knockout mice. Each group contained 12 mice at 10 weeks of age. (A) body weight; (B) total body fat; (C) total lean body mass. Results are expressed as mean ± standard error of mean (SEM).

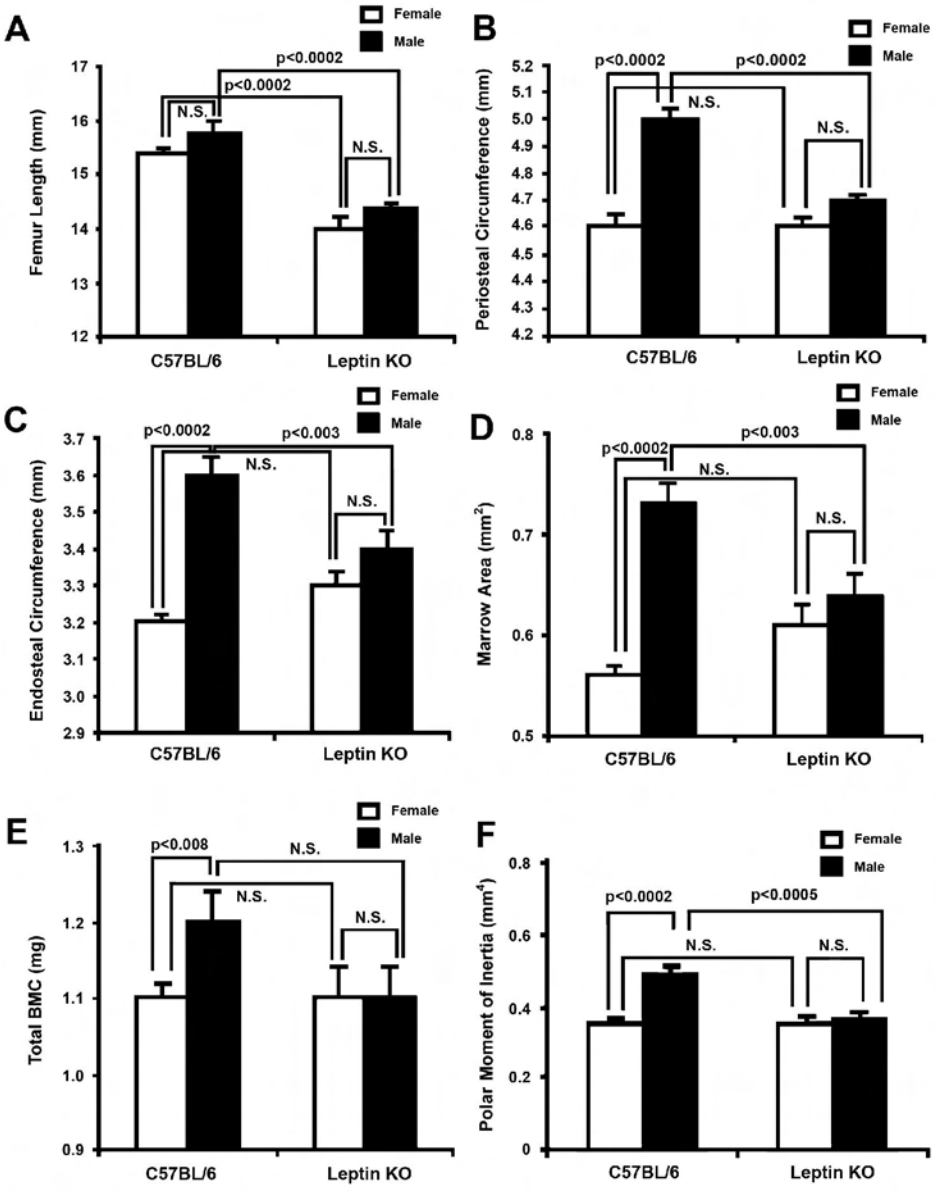

Fig. 2. Comparison of bone parameters in adult C57BL/6 and leptin knockout mice. (A) femur length, (B) periosteal circumference, (C) endosteal circumference, (D) marrow area, (E) total bone mineral content, (F) polar moment of inertia. Each group contained 12 mice at 13 to 14 weeks of age. Results are expressed as mean ± standard error of mean (SEM).

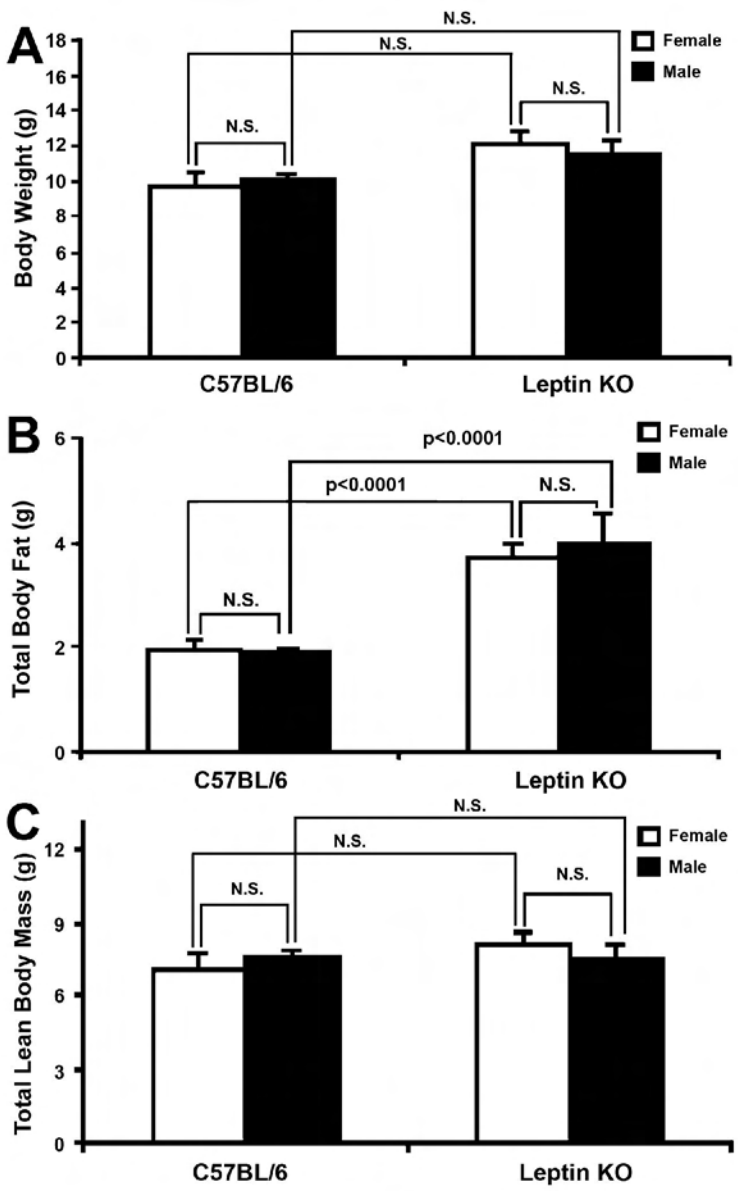

Fig. 3. Comparison of body characteristics in pre-pubertal C57BL/6 and leptin knockout mice. (A) body weight, (B) total body fat, (C) total lean body mass. Each group contained 6 mice at 3 weeks of age. Results are expressed as mean ± standard error of mean (SEM).

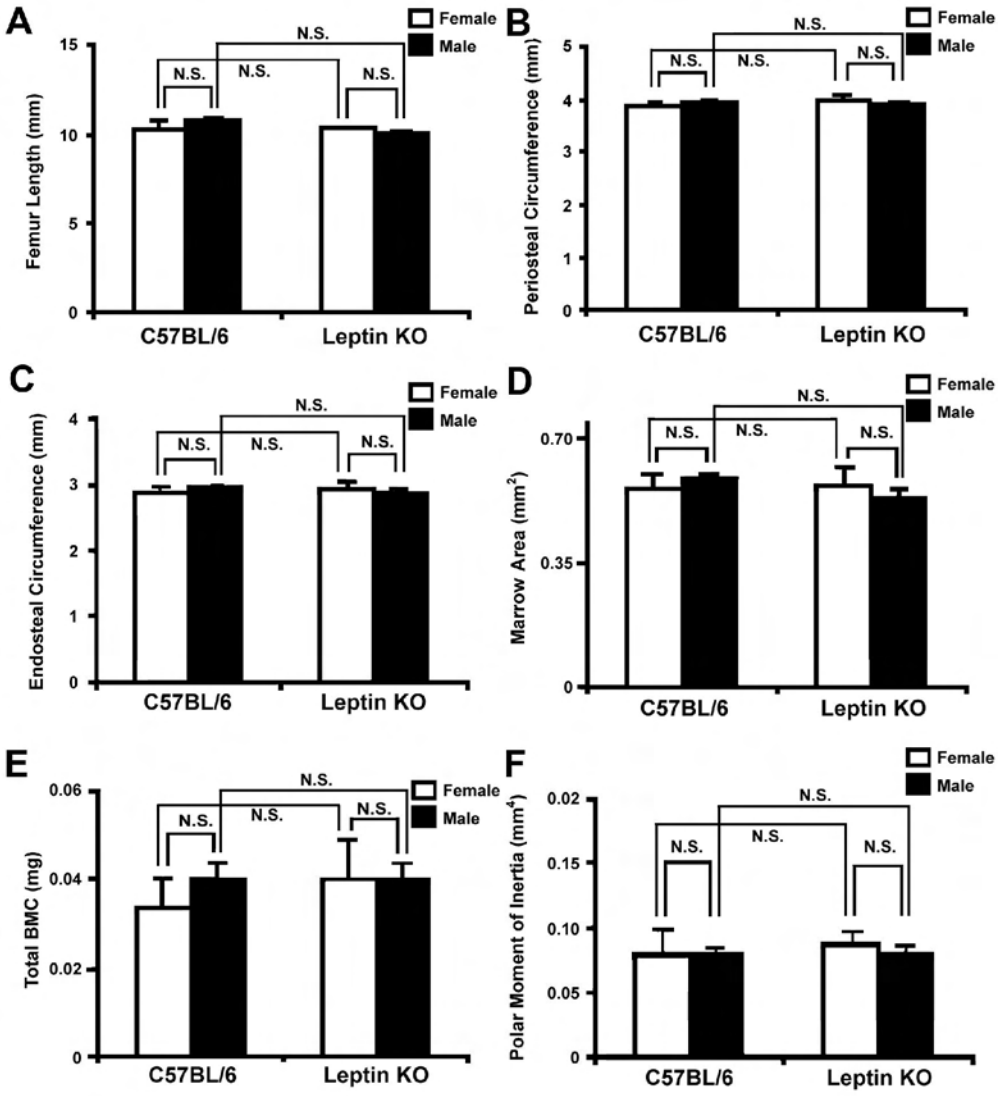

Fig. 4. Comparison of bone parameters of pre-pubertal C57BL/6 and leptin knockout mice. (A) femur length, (B) periosteal circumference, (C) endosteal circumference, (D) marrow area, (E) total bone mineral content, (F) polar moment of inertia. Each group contained 6 mice at 3 weeks of age. Results are expressed as mean ± standard error of mean (SEM).

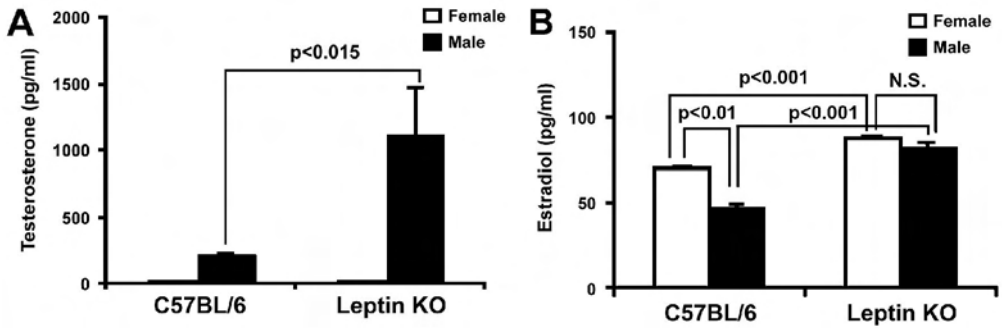

Fig. 5. Comparison of serum sex hormone levels in male and female leptin knockout and C57BL/6 wild type mice. Each group contained 15 mice at 10 weeks of age. Results are expressed as mean ± standard error of mean (SEM).

VA LOMA LINDA
HEALTHCARE SYSTEM
A Division of VA Desert Pacific Healthcare Network

VA Loma Linda Healthcare System
11201 Benton Street
Loma Linda, CA 92357
1 (800) 741-8387 - (909) 825-7084 - (909) 796-9573
www.lom.med.va.gov

In Reply Refer To 151)

February 28, 2007

Juanita Livingston
U.S. Army Medical Research and Material Command
ATTN: MCMR-RMI-S
504 Scott Street
Fort Detrick, Maryland 21702-5012

RE: Annual Report for Award Number DAMD17-03-2-0021

Dear Madam:

Enclosed is copy of our annual report for the grant award entitled "Molecular Genetic and Gene Therapy Studies of the Musculoskeletal System." The report covers the period of September 9, 2005 – January 31, 2007.

This progress report does not contain any unpublished data that is proprietary.

If you have any questions regarding any of the information in the progress report, please feel free to contact me.

Sincerely

Subburaman Mohan, PhD
Senior Scientist
Musculoskeletal Disease Center
VA Loma Linda Healthcare System
Research Professor of Medicine, Biochemistry and Physiology
Loma Linda University
11201 Benton Street
Loma Linda, CA 92357
(909) 825-7084 ext. 2932
E-mail: subburaman.mohan@va.gov

CC:
Eva Lai, Ph.D.
USAMRMC/TATRC
301-619-2751 (Office Direct)
301-619-7041 (Office Fax)

Jerry L. Pettis Memorial VA Medical Center
11201 Benton Street
Loma Linda, CA 92357
(909) 825-7084

Corona VA Clinic
800 Magnolia Ave. #101
Corona, CA 92879
(951) 817-8820

Palm Desert VA Clinic
41-865 Boardwalk, #103
Palm Desert, CA 92211
(760) 341-5570

Sun City VA Clinic
28125 Bradley Road #130
Sun City, CA 92586
(951) 672-1931

Victorville VA Clinic 12138
Industrial Blvd., #120
Victorville, CA 92392
(760) 951-2599

Upland VA Clinic
1238 E. Arrow Hwy. #100
Upland, CA 91786
(909) 946-5348